



UNIVERSITAT DE  
BARCELONA

## The role of RANK pathway in the intestinal epithelium, breast cancer and tumor immune modulation

Clara Gómez Aleza

**ADVERTIMENT.** La consulta d'aquesta tesi queda condicionada a l'acceptació de les següents condicions d'ús: La difusió d'aquesta tesi per mitjà del servei TDX ([www.tdx.cat](http://www.tdx.cat)) i a través del Dipòsit Digital de la UB ([diposit.ub.edu](http://diposit.ub.edu)) ha estat autoritzada pels titulars dels drets de propietat intel·lectual únicament per a usos privats emmarcats en activitats d'investigació i docència. No s'autoritza la seva reproducció amb finalitats de lucre ni la seva difusió i posada a disposició des d'un lloc aliè al servei TDX ni al Dipòsit Digital de la UB. No s'autoritza la presentació del seu contingut en una finestra o marc aliè a TDX o al Dipòsit Digital de la UB (framing). Aquesta reserva de drets afecta tant al resum de presentació de la tesi com als seus continguts. En la utilització o cita de parts de la tesi és obligat indicar el nom de la persona autora.

**ADVERTENCIA.** La consulta de esta tesis queda condicionada a la aceptación de las siguientes condiciones de uso: La difusión de esta tesis por medio del servicio TDR ([www.tdx.cat](http://www.tdx.cat)) y a través del Repositorio Digital de la UB ([diposit.ub.edu](http://diposit.ub.edu)) ha sido autorizada por los titulares de los derechos de propiedad intelectual únicamente para usos privados enmarcados en actividades de investigación y docencia. No se autoriza su reproducción con finalidades de lucro ni su difusión y puesta a disposición desde un sitio ajeno al servicio TDR o al Repositorio Digital de la UB. No se autoriza la presentación de su contenido en una ventana o marco ajeno a TDR o al Repositorio Digital de la UB (framing). Esta reserva de derechos afecta tanto al resumen de presentación de la tesis como a sus contenidos. En la utilización o cita de partes de la tesis es obligado indicar el nombre de la persona autora.

**WARNING.** On having consulted this thesis you're accepting the following use conditions: Spreading this thesis by the TDX ([www.tdx.cat](http://www.tdx.cat)) service and by the UB Digital Repository ([diposit.ub.edu](http://diposit.ub.edu)) has been authorized by the titular of the intellectual property rights only for private uses placed in investigation and teaching activities. Reproduction with lucrative aims is not authorized nor its spreading and availability from a site foreign to the TDX service or to the UB Digital Repository. Introducing its content in a window or frame foreign to the TDX service or to the UB Digital Repository is not authorized (framing). Those rights affect to the presentation summary of the thesis as well as to its contents. In the using or citation of parts of the thesis it's obliged to indicate the name of the author.

University of Barcelona  
Faculty of Medicine  
Biomedicine PhD Program  
(Programa de Doctorado en Biomedicina)



# The role of RANK pathway in the intestinal epithelium, breast cancer and tumor immune modulation

Doctoral Thesis performed at:  
Institut d'Investigació Biomèdica de Bellvitge (IDIBELL).  
L'Hospitalet d'Llobregat

PhD Candidate: Clara Gómez Aleza

Thesis Supervisor: Eva González Suárez

Thesis Tutor: Francesc Viñals

Clara Gómez Aleza. Barcelona, 2021





A mi familia





# INDEX

ABBREVIATIONS LIST .....	9
INTRODUCTION .....	13
RANK as a member of the TNFRSF.....	15
RANK signaling in detail: the bone as model system.....	19
Intestinal/colon epithelia and RANK pathway.....	23
RANK in the mammary gland .....	27
The immune system and RANK pathway.....	30
Lymphoid lineage .....	31
T cells .....	31
B cells.....	35
NK cells .....	35
Innate Lymphoid Cells (ILCs).....	36
Myeloid lineage .....	37
Dendritic cells .....	37
Monocyte/Macrophages .....	38
Granulocytes-Neutrophils .....	40
Lymphoid organs: Lymph nodes and Thymus .....	41
RANK in human breast cancer .....	43
RANK in models of mammary gland tumorigenesis .....	44
Clinical Trials with Denosumab in Breast Cancer.....	47
RANK in colorectal cancer .....	48
Tumor Immunology .....	49
RANK in tumor immunology.....	55
MMTV-PyMT as a model for breast cancer tumor immunology .....	56
OBJECTIVES .....	61
METHODS .....	65
Mouse transgenic models .....	67
Mouse treatments.....	68
Tissue collection and processing .....	69
Mouse tumor-cell isolation, tumor-initiation assays and <i>in vitro</i> culture .....	69

Mouse intestinal organoid purification and <i>in vitro</i> culture.....	70
Flow cytometry.....	71
Immunostaining in mouse tumor tissues .....	72
Real-time PCR .....	73
Mouse RNA labeling and hybridization to Agilent microarrays.....	75
RNA sequencing.....	75
Tumor acini and mouse serum cytokine array .....	76
Cell line culture and lentiviral transduction .....	76
Human neutrophil and T cell isolation and culture .....	77
Clinical trial design and patient characteristics .....	77
Pathological assessment and immunohistochemical staining of human tumor samples .....	79
RNA extraction from human samples and RNA sequencing.....	80
Bioinformatic analyses .....	81
Statistical analyses.....	82
RESULTS.....	85
Chapter 1: Inhibition of RANK signaling in breast cancer induces an anti-tumor immune response orchestrated by CD8+ T cells .....	87
1.1 Loss of RANK in tumor cells leads to increased lymphocyte infiltration .....	89
1.2 T cells mediate the longer tumor latency of RANK <sup>-/-</sup> tumors .....	89
1.3 CD8 <sup>+</sup> T cell depletion rescues the delay in tumor onset of RANK <sup>-/-</sup> tumors .....	92
1.4 RANK <sup>+</sup> tumor cells promote immunosuppression through neutrophils .....	94
1.5 RL inhibition in tumor cells increases responsiveness to immunotherapy.....	97
1.6 A short course of denosumab treatment in early-stage BC increased TILs .....	99
Supplementary Figures.....	107
Supplementary Data.....	125
Appendix: RNAseq data analysis from RANK <sup>+/+</sup> and RANK <sup>-/-</sup> tumor transplants.....	145
The potential effects of immunoediting in gene expression changes between RANK <sup>+/+</sup> and RANK <sup>-/-</sup> tumors .....	147
Effects of RANK depletion in tumor cells, CD8 and CD4 T cells. ....	152
Chapter 2: Characterization of an inducible, tissue-specific RANK depletion model of mammary gland tumorigenesis .....	159
2.1 The K8-PyMT model allows RANK depletion in luminal MG epithelium at different stages during tumorigenesis.....	161

2.2 RANK depletion is achieved in luminal-like tumor cell populations but is avoided in undifferentiated or basal-like areas. ....	165
2.3 RANK depletion during late tumorigenesis affects tumor initiation.....	167
2.4 Late RANK depletion reduces the number of microscopic metastatic lung nodules.....	170
2.5 RANK depletion alters immune infiltration in MMTV_PyMT primary tumors.....	172
2.6 RANK depletion affects several proteins found in mice serum .....	174
2.7 RANK depletion delays growth of tumor transplants from certain primary tumors in immunodeficient mice.....	179
2.8 The primary tumor of origin could influence the impact of RANK depletion on tumor transplants in immunodeficient hosts.....	180
2.9 Combined RANK depletion and aRL treatment could have a beneficial impact on lung metastasis reduction. ....	182
2.10 Exploring RANK depletion in K8+ organs from host mice in tumor transplant models..	184
Chapter 3: Rank Pathway in Intestinal Epithelium .....	187
3.1 RANK expression is higher on differentiated intestinal epithelium.....	189
3.2 RANK loss has no evident effect on intestinal epithelium homeostasis <i>in vivo</i> and <i>in vitro</i> . ....	189
3.3 RANKL induces M cell differentiation <i>in vitro</i> but high doses disrupt intestinal organoid maintenance.....	192
3.4 Loss of RANK in the intestinal epithelia or myeloid cells does not affect the development of colorectal adenomas in mice under the AOM/DSS protocol .....	198
3.5 High RANK expression in colorectal adenomas is found on differentiated epithelium....	201
DISCUSSION .....	203
Discussion Chapter 1: Inhibition of RANK signaling in breast cancer induces an anti-tumor immune response orchestrated by CD8 <sup>+</sup> T cells. ....	205
Discussion Chapter 2: Characterization of an inducible, tissue-specific RANK depletion model of mammary gland tumorigenesis.....	209
Discussion Chapter 3: RANK pathway in intestinal epithelium. ....	223
CONCLUSIONS .....	227
ACKNOWLEDGEMENTS.....	231
BIBLIOGRAPHY .....	235





# **ABBREVIATIONS LIST**





## Abbreviation List

ADAM10	A disintegrin and metalloproteinase domain-containing protein 10
AKT/PKB	Ak strain transforming/Protein Kinase B
APC	Antigen presenting cell
AML	Acute myeloid leukemia
Bcl-2	B-cell lymphoma 2
Bcl-xL	B-cell lymphoma extra large
BM	Bone marrow
cDC	Classical Dendritic cell
cTEC	Cortical thymic epithelial cell
DC	Dendritic cell
DD	Death Domain
Dmab	Denosumab
DMBA	7,12-dimethylbenz[a]anthracene
DN	Double-negative
DP	Double-positive
DSS	Dextran Sulfate Sodium
ERK	Extracellular Signal-Regulated Kinase
FADD	Fas-associated Death Domain protein
FAE	Follicle-associated epithelium
FcγR	Fc receptor-γ
FOXP3	Forkhead box P3
GALT	Gut-associated lymphoid tissue
GMP	Granulocyte-macrophage progenitors
HER2	Human epidermal growth factor receptor 2
Ig	Immunoglobulin
IKK	IκB kinase
IL	Interleukin
iNOS	inducible nitric oxide synthase
ITIM	Immunoreceptor tyrosine-based inhibitory motif
IκB	Inhibitor of κB
JNK	Jun N-terminal Kinase
LGR4	Leucine-rich repeat-containing G-protein coupled receptor 4
LN	Lymph node
LT-HSC	Long-term hematopoietic stem cells
LTi	Lymphoid Tissue inducer
LTo	Lymphoid Tissue organicer
LTα1β2	Lymphotoxin α1β2
LTβR	Lymphotoxin α1β2 receptor
Ly6C	Lymphocyte antigen 6 complex locus C1
M cell	Microfold cell

MaSC	Mammary stem cells
MCP-1	<i>monocyte chemotactic protein-1</i>
mDC	Monocyte-derived dendritic cell
MDP	Monocyte-macrophage/dendritic lineage-restricted progenitors
MDSC	Myeloid-derived suppressor cell
MHC-I and MHC-II	Major histocompatibility complex I and II
MIN	Mammary intraepithelial neoplasias
MMP	Matrix metalloproteinase
MMTV	Mouse mammary tumor virus
MPA	Medroxyprogesterone acetate
mTECs	Medullary thymic epithelial cell
NCR	Natural cytotoxicity receptor
NFκB	Nuclear factor κB
NK	Natural killer
NKG2D	Natural-killer group 2, member D
OPG	Osteoprotegerin
pDC	Plasmacytoid Dendritic Cell
PDX	Patient Derived Xenograft
PP2A	Protein phosphatase 2A
PTHrP	Parathyroid hormone-related protein
PyMT	Polyomavirus middle T antigen
RANK	Receptor activator of nuclear factor-κB
RANKL	Receptor activator of nuclear factor-κB ligand
RSPO1	R-spondin 1
snN	Synovial fluid neutrophils
TACE	TNFα-converting enzyme
TAM	Tumor-associated macrophage
TCR	T-cell receptor
TEB	Terminal End Bud
Th	T helper (CD4+ T cell)
TNF	Tumor necrosis factor
TNFRSF	Tumor necrosis factor receptor superfamily
TNFSF	Tumor necrosis factor superfamily
TNFα	tumor necrosis factor α
TRADD	TNFR-associated Death Domain protein
TRAF	TNF receptor-associated factor
TRAIL	TNF-related apoptosis-inducing ligand
TRAP	Tartrate-resistant acid phosphatase
Treg	T regulatory cell
WNT	Wingless-related integration site

# **INTRODUCTION**

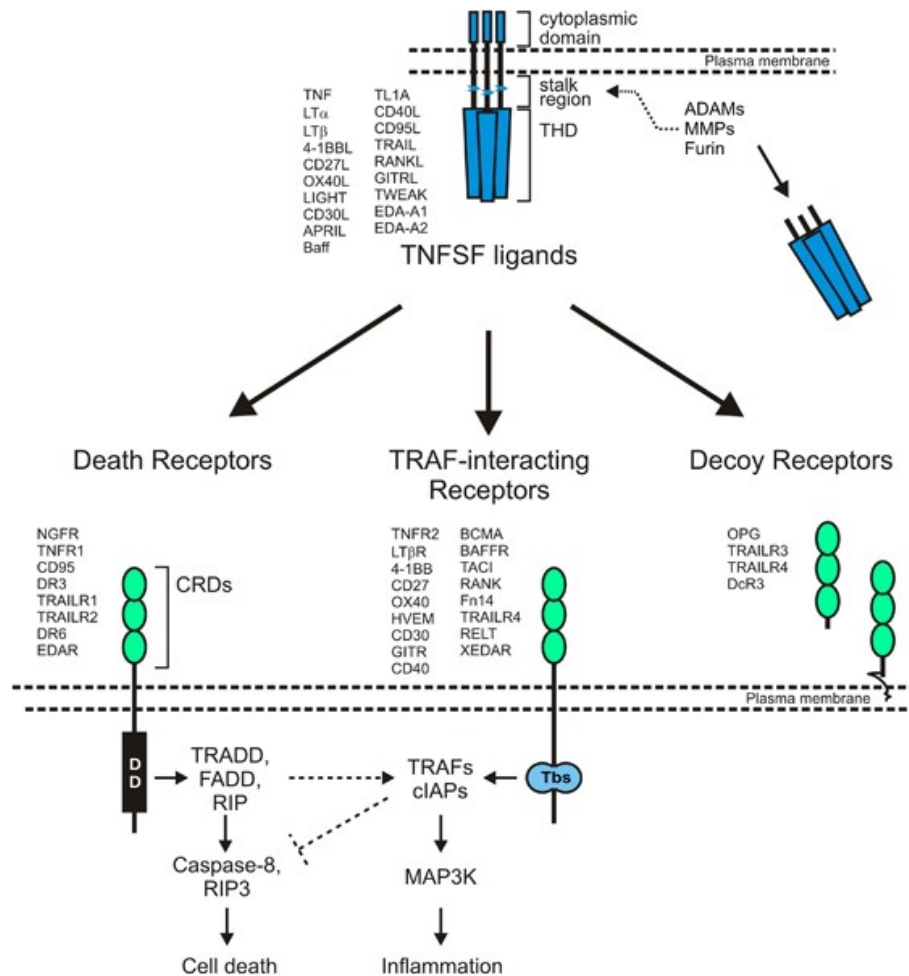


Receptor activator of nuclear factor- $\kappa$ B ligand (RANKL), its signaling receptor RANK, and its natural decoy receptor, Osteoprotegerin (OPG) are members of the tumor necrosis factor (TNF) and TNF receptor superfamily (González-Suárez and Sanz-Moreno, 2016). RANK and RANKL are classically known for their essential role in bone remodelling<sup>2</sup> and an anti-RANKL antibody (Denosumab) is currently used in the clinic to treat osteoporosis and skeletal related events such as bone metastasis<sup>1</sup>. RANK signaling is also crucial for mammary epithelial stem cell homeostasis, mammary gland development and function (Asselin-Labat et al., 2010; Beleut et al., 2010; Duheron et al., 2011; Fata et al., 2000a; Gonzalez-Suarez et al., 2010; Joshi et al., 2010; Schramek et al., 2010; Tanos et al., 2013a). Additionally, RANK pathway has been described to play a role in the immune system, where it participates in the development and functioning of the thymus, the lymph nodes and intestinal Peyers Patches (Akiyama et al., 2008; Baik et al., 2016; Dougall et al., 1999a; Knoop et al., 2009; Onder et al., 2017; Rios et al., 2016; Roberts et al., 2012; Rossi et al., 2007), as well as other tissues (Duheron et al., 2011; Loser et al., 2006; Shimamura et al., 2014).

This highly versatile and complex signaling pathway is the core of this doctoral thesis, where RANK will be studied in the mammary and colorectal epithelia, with a special focus in cancer and the crosstalk between tumor cells and their immune microenvironment.

## **RANK as a member of the TNFRSF**

The TNF receptor and ligand superfamilies (TNFRSF and TNFSF) are formed by a group of proteins characterized by their conserved structural domains, which allow them to form homo- or heterotrimers to activate downstream signaling pathways (Locksley et al., 2001). TNFSF ligands are type II transmembrane proteins, with the only exception of Lymphotoxin  $\alpha$  (LT $\alpha$ ). They are characterized by their C-terminal extracellular TNF-homology domain (THD), which allows them to trimerize using non-covalent bonds. Ligands can be solubilized by being translated from transcripts derived from alternative splicing or via enzymatic cleavage from the transmembrane protein form (**Figure 1**) (Lang et al., 2016; Locksley et al., 2001; Medler et al., 2019). Interestingly, some TNFRSF receptors respond differently depending on the soluble or transmembrane status of ligand trimers, being able to activate different downstream signaling pathways, with variable strength (Locksley et al., 2001; Medler et al., 2019; Wajant, 2015).



**Figure 1. RANK within the TNRSF.** The TNFSF ligands consist of several protein members characterized by their C-terminal TDH domain, which allows them to trimerize with each other. TNFSF are type II membrane proteins (except for LT $\alpha$ ) and can be cleaved and solubilized by enzymes such as ADAM and MMPs. The TNFRSF can be divided on three subtypes based on their cytoplasmic domains: Death receptors, which bind adaptor proteins which lead to caspase activation and apoptosis; TRAF-interacting receptors, which lack “death domains” and instead bind TRAF adaptor proteins, activating diverse downstream kinase activity; and Decoy receptors, which lack a cytoplasmic domain and can be soluble, capturing TNFSF ligands. Figure from H Wajant, 2015 (Wajant, 2015).

In the case of RANKL, three alternative splicing isoforms have been described: RANKL-1, corresponding to the full-length transmembrane protein; RANKL-2, which presents a shorter intracellular domain; and RANKL-3, which lacks the transmembrane and intracellular domains, thus being soluble in the cytoplasm (Ikeda et al., 2001). Additionally, RANKL transmembrane isoforms can be cleaved and solubilized by TNF $\alpha$ -converting enzyme (TACE), matrix metalloproteinase (MMP)-7, MMP-14, or a disintegrin and metalloproteinase domain-containing protein 10 (ADAM10) in different contexts (Hikita et al., 2006; Kanzaki et al., 2016). In fact, it has been suggested that membrane-bound RANKL presents a stronger

activation of RANK pathway in bone osteoclasts with MMP-14 downregulation (Hikita et al., 2006). More elegant murine models with cleavage-resistant RANKL show that soluble RANKL is dispensable for several of the well-characterized RANK-dependent roles in bone, mammary gland, intestine and lymphoid organs, although it does partially affect osteoclast numbers *in vivo* (Asano et al., 2019; Nagashima et al., 2017; Xiong et al., 2018).

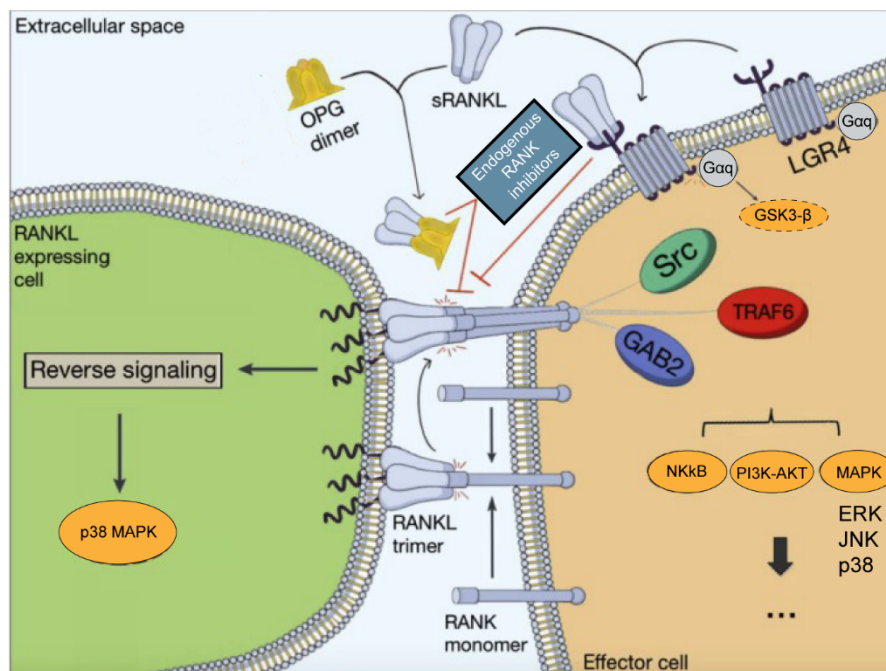
After binding the ligand trimers, TNFRSF members have been described to require the association of several receptor-ligand trimers to effectively activate certain pathways (Medler et al., 2019). This secondary clustering of receptor trimers might be dependent on the density of receptors within a specific membrane area. In fact, several TNFRSF receptors have been described to trimerize with low affinity in the absence of ligands. This process is termed “pre-ligand assembly” and it has been described to facilitate the recognition of ligand trimers (Chan, 2007). These associations have even been proposed as necessary for initial ligand binding, since a TNFSF receptor alone may not have the required affinity to stabilize ligand-receptor interactions (Wajant, 2015). An especially relevant example would be the Fas receptor in activated CD4 T cells. Upon T cell activation, Fas receptors are redistributed to lipid rafts, thus locally increasing receptor density, allowing for ligand-independent receptor clustering to occur. This redistribution of receptors specifically sensitizes activated T cells to Fas-ligand-induced cell death (Chan, 2007; Muppidi and Siegel, 2004).

The domains necessary for this receptor preassembly have been identified for RANK in the cytoplasmic region, (position 534-I-I-V-V-Y-V-539 in the mouse protein)(Kanazawa and Kudo, 2005). RANK has been observed to associate with itself, and in an overexpression context is able to activate downstream pathways in absence of RANKL (Das et al., 2014; Kanazawa and Kudo, 2005; Palafox et al., 2012a). Missense mutations in this domain affect the ligand-independent receptor clustering, both in the murine and human protein, delaying the formation of trimers even in the presence of RANKL, thus affecting the activation of downstream pathways (Das et al., 2014).

Beside their interactions during the pre-ligand assembly, TNFRSF receptors rely on several conserved cysteine-rich-domains (CRD) in their extracellular region to stabilize their trimerization. The highly conserved cysteines create disulphide bonds, which in turn induce conformational changes in the intracellular domains of TNFRs (Chan et al., 2000; Locksley et al., 2001). These changes in conformation expose their relatively short cytoplasmic domains, which depending on the specific protein, would be TRAF (TNF receptor-associated factor)-binding motifs or death domains (DDs) (Figure 1).

DDs recruit adaptor proteins such as Fas-associated DD protein (FADD) and TNFR-associated DD protein (TRADD) which lead to the activation of caspases, resulting in apoptosis and cell death. TRAF binding motifs recruit TRAF proteins, which mediate the activation of a broad list of downstream kinases.

RANK belongs to TNFRSF members which lack DDs. After binding RANKL, RANK has been described to gain the ability to interact with TRAF1, 2, 3, 5 and 6. These TRAF proteins have variable binding affinities for specific intracellular domains of RANK, and will activate different downstream pathways in a context-dependent manner (Darnay et al., 1998, 1999; Kadono et al., 2005; Walsh and Choi, 2014).



**Figure 2. Scheme depicting RANK pathway downstream signaling.** Upon ligand binding, thus stabilizing receptor trimerization, RANK recruits several adaptor proteins and kinases (TRAFs, Src, GAB2) depending on the cellular context. These act as mediators, recruiting kinases, which activate downstream pathways, namely NFκB, PI3K-Akt-mTOR and MAPK pathways (JNK, ERK, and p38). Membrane bound RANKL has also been described to transduce reverse signaling after binding to the receptor, leading to p38 activation. RANKL can be solubilized and captured by the decoy receptor OPG, and it has also been reported to bind to LGR4, activating GSK3β. Figure adapted from Van Dam P.A. *et al*, 2019(van Dam et al., 2019).

TRAF6 was identified as the main protein adaptor responsible for activation protein pathways downstream of RANK (Darnay et al., 1999). TRAF6 has been reported to recruit other adaptor proteins and protein kinases, leading to the activation of a broad range of downstream pathways (Arron et al., 2001; González-Suárez and Sanz-Moreno, 2016; Mizukami et al., 2002; Walsh and Choi, 2014; Wong et al., 1999). The most characterized



pathway downstream RANK activation is NFκB, further discussed in the next section. Moreover, RANK-associated TRAF6 has been described to interact with TGF-beta-activated kinase 1 (TAB2), which promotes the activation of members of the mitogen-activated protein kinases (MAPKs), such as TAK1, which in turn can activate several downstream kinases: JNK, p38 and IκB kinases (Chaisson et al., 2004; Kadono et al., 2005; Mizukami et al., 2002; Walsh and Choi, 2014). TRAF6 is also a mediator of PI3K-AKT-ERK pathway when interacting with Cbl and Src family kinases (Arron et al., 2001; Wong et al., 1999) (**Figure 2**). Further regulation of RANK downstream pathway activation relies on other adaptor proteins, such as TRAF2, which also activates JNK and NFκB pathways (Darnay et al., 1998, 1999), or TRAF3 and TANK, which act as negative regulator of NFκB activation (Maruyama et al., 2012; Xiu et al., 2014).

Other RANK regulatory mechanisms act through the crosstalk with other pathways. For instance, interferon gamma (IFNγ) signaling will trigger the ubiquitination and proteasomal degradation of TRAF6, suppressing the activation of downstream signals even in the presence of RANKL (Takayanagi et al., 2000).

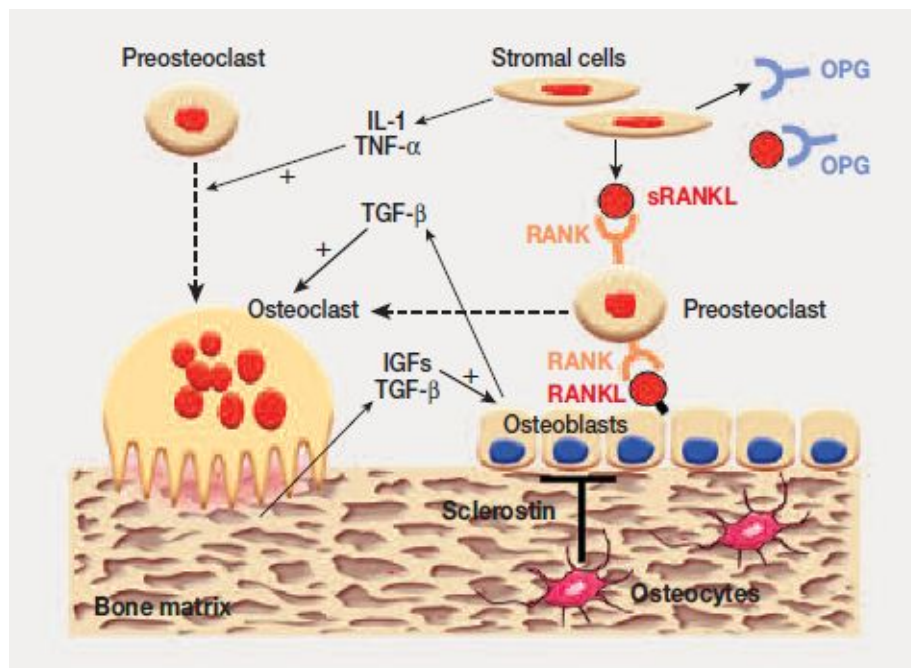
Finally, RANK pathway is also regulated by the expression of different RANK isoforms, first described by Papanastasiou *et al.* RANK alternative splicing results into 5 different variants of RANK (Papanastasiou et al., 2012). RANK-c isoform, which lacks exons 7-9 (spanning over the transmembrane domain), was described to act as a dominant-negative regulator of RANK pathway. RANK-c interacted with other RANK isoforms, which then bound TRAF2 instead of TRAF6, ultimately decreasing the activation of NFκB and AKT downstream pathways (Papanastasiou et al., 2012; Sirinian et al., 2018). RANK-c has also been described to interact with EGFR, reducing the phosphorylation of the receptor (Sirinian et al., 2018).

To sum up, mounting evidence regarding RANK and other TNFRSF members depicts the complex regulation layers that determine which specific pathways are triggered after the activation of the receptor, ultimately dictating the phenotypic changes that RANK signaling will have in each cell context.

## **RANK signaling in detail: the bone as model system**

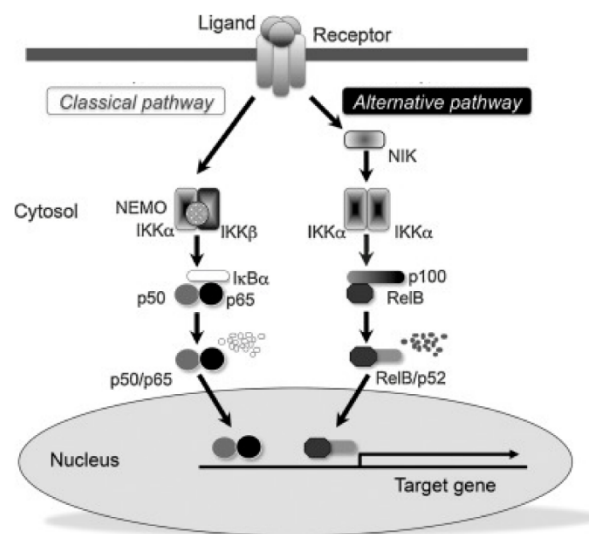
RANK pathway has been extensively characterized in the bone, where it plays a fundamental role in the balance between bone formation and resorption. This fact was evident with murine full-body knockouts of RANK or RANKL, which presented severe

osteopetrosis, as inferred from their aberrantly short and dense bones (Dougall et al., 1999b; Kong et al., 1999). Overexpression of OPG, the decoy receptor which binds RANKL and prevents RANK activation, also results in severe osteopetrosis in murine models (Simonet et al., 1997). In the bone, the main two populations mediating bone formation and resorption are osteoblasts and osteoclasts (Dougall et al., 1999b; Fata et al., 2000b; González-Suárez and Sanz-Moreno, 2016; Kong et al., 1999). Osteoblasts, which can further differentiate into osteocytes, are mesenchymal cells which secrete the main components of the bone (collagens, hydroxylapatite, osteocalcin, etc) (Kong et al., 1999). Osteocytes are the main source of RANKL in the bone (Nakashima et al., 2011). Osteoclasts are RANK+ cells which derive from hematopoietic precursors within the bone marrow. Upon RANK activation, they reabsorb bone tissue, liberating calcium and participating in homeostatic bone remodeling processes (see Figure 3) (Dougall et al., 1999b; Fata et al., 2000b; González-Suárez and Sanz-Moreno, 2016; Kong et al., 1999). Classical *in vitro* functional studies of RANK pathway often show the ability of RANKL (directly added to the culture or derived from osteoblasts in co-culture) to differentiate bone-marrow precursors into osteoclasts, which are characterized by the detection of tartrate-resistant acid phosphatase (TRAP) (Cenci et al., 2000; Dougall et al., 1999b; Fata et al., 2000b; Ju et al., 2008; Kong et al., 1999; Nakamura et al., 2006; Takayanagi et al., 2000).



**Figure 3. Osteoblast-osteoclast communication through RANK pathway during bone remodeling.** Picture obtained from Marie P.J, 2012.

Mice with osteoclast-specific IKK dominant negative overexpression or double p52-p50 knockout, which would inactivate both canonical and non-canonical NFκB pathways, present evident defects on bone resorption *in vivo* and *in vitro* (Chang et al., 2009; Franzoso et al., 1997), while other RANK downstream pathways such as JNK and p38 were not diminished (Chang et al., 2009). Knockout mouse models of key members of the non-canonical NFκB pathway (NIK, p100 and RelB) do not present an osteopetrotic phenotype (Boyce et al., 2015). Interestingly, *in vitro* studies with genetic models of IKKα loss determined that bone-marrow derived cells were unable to differentiate into osteoclasts upon RANKL stimulation (Chaisson et al., 2004; Ruocco et al., 2005). The lack of osteopetrosis found *in vivo* was attributed to osteoblast-derived factors (IL-1 and TNFα), which allowed IKKα-deficient osteoclast precursor cells to differentiation *in vitro* (Ruocco et al., 2005). These data suggest canonical NFκB pathway is the main mediator of osteoclast differentiation and function, while non-canonical NFκB pathway has redundant effects to those of other inflammatory pathways and may play alternative regulatory functions in bone homeostasis.



**Figure 4. Scheme depicting NFκB pathway.** Upon ligand binding (for instance RANKL-RANK interactions), TRAF adaptor proteins bind to cytoplasmic regions of the receptor, where they recruit and activate different kinases in a context-dependent manner. In case of canonical (or classical) NFκB pathway, the IKK complex; formed by three subunits: IKKα and IKKβ and IKKγ/NEMO, phosphorylates and triggers the degradation of IκBα, liberating NFκB dimers formed by p65-p50 (also called RelA-p50). Through the non-canonical (alternate) pathway, NIK activates IKKα dimers, which processes p100 from RelB/p100 dimers into its mature form: RelB/p52. Both p65/p50 and RelB/p52 are then able to migrate to the nucleus, where they trigger the transcription of target genes. Figure from Jimi E., *et al.*, 2016(Jimi et al., 2016).

Studies with osteoclasts revealed that can activate both canonical and non-canonical NFκB pathway, which are the main downstream effectors of RANK-mediated bone resorption

(Boyce et al., 2015; Locksley et al., 2001; Wada et al., 2006). NF $\kappa$ B is sequestered in the cytoplasm, bound to I $\kappa$ Bs (inhibitors of  $\kappa$ B). Its nuclear translocation requires the phosphorylation and degradation of these I $\kappa$ Bs by the I $\kappa$ B kinase complex (IKK; formed by three subunits: IKK $\alpha$  and IKK $\beta$  and IKK $\gamma$ /NEMO). Through the canonical pathway, the IKK $\beta$  subunit mediates the phosphorylation and subsequent degradation of I $\kappa$ B $\alpha$ , liberating NF $\kappa$ B dimers formed by p65-p50 (also called RelA-p50). The non-canonical pathway involves the activation of IKK $\alpha$  homodimers by NF- $\kappa$ B-inducing kinase (NIK). IKK $\alpha$  processes p100 into the p52 mature form, mediating the switch from RelB-p100 to RelB-p52 heterodimers (**Figure 4**)(Boyce et al., 2015; Chaisson et al., 2004; Chang et al., 2009; Novack et al., 2003).

As an additional regulation mechanism, OPG is expressed in osteoblasts in response to several cytokines and growth factors such as Wnt, TGF $\beta$  and INF $\gamma$ (Glass et al., 2005; Theoleyre et al., 2004). OPG binds to RANKL with higher affinity than RANK (Nelson et al., 2012), therefore acting as a robust inhibitor of the RANK pathway. The ectodomain of RANK has also been described to be released by TACE-mediated proteasomal activity, acting as a negative regulator of the pathway (Hakozaki et al., 2010). Thus, RANK pathway in the bone is tightly regulated by several feedback loops to maintain the balance between bone resorption and formation.

In fact, RANK secreted in extracellular vesicles from osteoclasts has been described to activate reverse-signaling through membrane-bound RANKL in osteoblasts (Ikebuchi et al., 2018; Ma et al., 2019). Depending on the timing of the stimuli, the outcome varies. During early osteoblast differentiation, RANKL reverse signaling results in an upregulation of osteoblast differentiation markers and an increase in their mineralization activity. However, in later timepoints, activation of RANKL reverse signaling induces the suppression of osteoblast activity. Ikebuchi Y. *et al* claimed that RANKL reverse signaling can be activated by trimerized anti-RANKL molecules or membrane-bound RANK, but not by soluble RANK or OPG. Its activation relies on the proline-rich motifs in the cytoplasmic tail, where Src kinases can bind through their SH3 domains, ultimately inducing the activation of the PI3K–Akt–mTORC1 pathway (**Figure 2**). In other publications, though, mineralization in E1 cells could be induced by the addition of a soluble RANK fragment (Zhang et al., 2017) or a peptide which was designed to bind and block TNF- $\alpha$  (W9) and also binds and inhibits RANKL signaling through RANK (Furuya et al., 2013), both identifying p38 as a downstream pathway of RANKL reverse signaling (Furuya et al., 2013; Zhang et al., 2017).

This reverse signaling could play a role in bone homeostasis, as shown by the impaired bone formation *in vivo* due to a single point mutation in RANKL proline-29, key for its reverse signaling (Ikebuchi et al., 2018), and may also be important in other unexplored physiological settings. RANKL reverse signaling has also been described in B-cell lymphoma and acute myeloid lymphoma (AML) cells, where immobilized RANK-Fc triggered IL-8 release in a dose-dependent manner (Schmiedel et al., 2013; Secchiero et al., 2006), as well as additional cytokines in AML (TNF, IL-6, and IL-10), whose release was blocked in the presence of denosumab (Schmiedel et al., 2013).

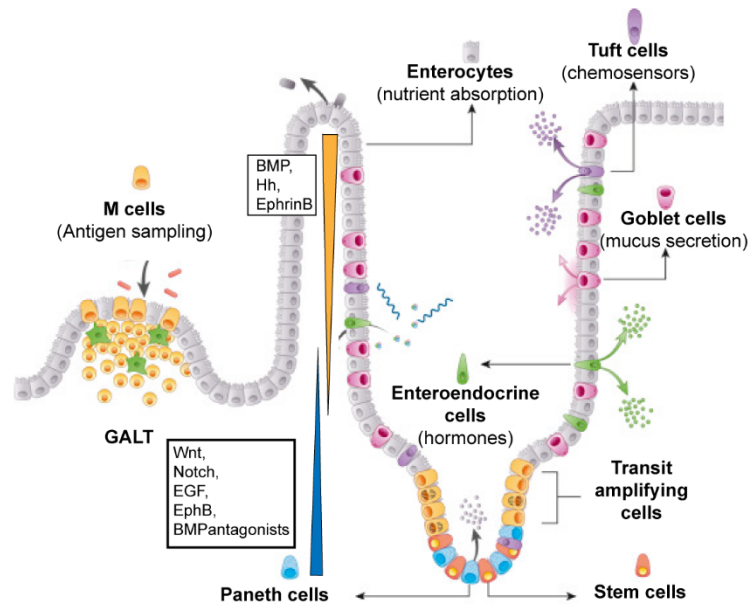
Another ramification of RANKL effects in the bone was described by Luo J. *et al*, who identified Leucine-rich repeat-containing G-protein coupled receptor 4 (LGR4) as an alternative receptor for RANKL. The ligand binds LGR4 using different domains than for its interaction with RANK and activates the Gq protein alpha subunit ( $G_q\alpha$ ), which triggers intracellular calcium release, resulting in NFATc1 inhibition. LGR4 competes with RANK for RANKL in the bone and therefore affects osteoclast differentiation and survival (Luo et al., 2016a). However, this observation has not been further explored in other tissues and contexts.

## **Intestinal/colon epithelia and RANK pathway**

The intestinal and colon epithelia undergo rapid renewal, with a complete regeneration occurring every 5 days. This is due to the continuous proliferation and subsequent differentiation of cells derived from stem cells within the epithelial monolayer which separates the lumen of the digestive tract from the stromal cell layers below. In the small intestine, epithelium organizes in a series of invaginations (crypts) and protrusions (villi) to maximize the absorptive area, whereas the colon presents only crypts. Intestinal stem cells reside at the bottom of the crypts and give rise to all other epithelial cells which differentiate as they get positioned in the crypt-villi axis, where they will be exposed to different gradients of signaling molecules which will define their final lineage differentiation (Spit et al., 2018).

At the bottom of the crypt, LGR5+ cells have been identified as the stem cell population, with a subpopulation cycling as fast as once every 24h and other, termed “label-retaining-cells”, remaining quiescent. This latter subpopulation has been proposed to act as “stem cell reservoir” upon tissue damage. These cells give rise to a pool of “transit amplifying cells”, which give rise to the rest of epithelial populations (Clevers, 2013; Spit et al., 2018).

To maintain the proliferation and de-differentiated status of stem cell populations, subepithelial mesenchymal cells at the bottom of the crypt provide WNT ligands and co-activators (R-spondins), epidermal growth factor (EGF) and inhibitors of bone morphogenetic protein (BMP) pathway: Gremlin 1/2 and Noggin (Clevers, 2013; Spit et al., 2018). The concentration of these molecules is thus maintained higher at the base of the crypt, gradually diminishing for cells positioned further across the crypt-villi axis.



**Figure 5. Intestinal epithelium cell subpopulations and signal gradients.** Intestinal stem cells give rise to the different intestinal epithelial cells. Wnt and EGF signals derived from Paneth cells and surrounding stroma at the crypts maintain the stem cell niche. Notch signaling blocks the differentiation into Goblet cells, specialized cells which form intestinal mucus. Notch signaling will commit cell differentiation into enterocytes, the nutrient absorbing cells. Proliferation drives epithelial cells away from the crypt bottom, where cells start expressing EphrinB, a repulsive ligand which further prompts their migration away from the EphB-high crypt. Hh is expressed by villi epithelia, inducing BMP expression on surrounding stroma. BMP blocks proliferation and gradients of BMP antagonists are secreted at the crypt to allow controlled proliferation. Epithelial cells which migrate over GALT regions will be exposed to RANKL, which will trigger their differentiation into M cells, specialized in antigen sampling. Image adapted from Williams, Ifor R. and Owen, Robert L., 2015 (Williams and Owen, 2015).

Wnt pathway activates the expression of ephrins (EphB2 and EphB3) and inhibits the transcription of the repulsive ligand ephrin-B1, which will start to be expressed in cells excluded from the base of the crypt, further promoting their migration towards the villi tips. Villi epithelial cells secrete Hedgehog (Hh), which activates the expression of BMP proteins on mesenchymal cells in their proximity. Therefore, a gradient of BMP from villi to crypt

epithelium is established, blocking proliferation and inducing differentiation of epithelial cells (**Figure 5**) (Clevers, 2013; Spit et al., 2018).

Additionally, Notch signaling prevents cells to commit into the secretory lineage fate. Paneth cells, specialized in secreting antimicrobial agents and localized at the bottom of small intestine crypts, express Notch ligands. Paneth cells are also a source of Wnt ligands and EGF, which further maintain the stem cell niche. Lack of Notch signaling on cells at the crypt prompts their differentiation into Goblet cells, which are characterized by their production of the components of the luminal mucosal layer. Expression of Notch ligands in these cells will stochastically prevent the commitment of other differentiating cells into the secretory lineage. These cells will then become enterocytes, cells specialized in the absorption of nutrients from the intestinal lumen (Clevers, 2013; Spit et al., 2018).

Other less abundant epithelial cell populations include enteroendocrine cells, Tuft cells and microfold (M) cells. Enteroendocrine cells secrete hormones and signaling molecules systemically, to activate nervous responses. Tuft cells are very scarce in the intestinal epithelium and act as chemical sensors (Clevers, 2013; Spit et al., 2018).

M cells are antigen-sampling cells positioned on the follicle associated epithelium (FAE). This area of epithelium lacks villi and covers organized lymphoid tissue structures which collectively are referred to as the gut-associated lymphoid epithelium (GALT) (**Figure 5**) (Kimura et al., 2015a, 2020; Knoop et al., 2009). M cells are crucial for the formation and function of the germinal centers within the GALT, which are needed to establish mucosal tolerance towards commensal microorganisms and trigger efficient immune responses against pathogens (Kimura et al., 2015a). Mature M cells are characterized by the expression of glycoprotein 2 (GP2), which acts as an uptake receptor for the translocation of bacteria to the germinal centers for the immune system to detect (Kanaya et al., 2012; Kimura et al., 2015a, 2020; Knoop et al., 2009; Rios et al., 2016). This translocation of microorganisms and proteins from the intestinal lumen is necessary for antigens to be accessible to immune cells. However, this mechanism is also an entry form for some specialized pathogens and, thus, M cell numbers are tightly regulated (Kimura et al., 2020).

In the intestine, most of the research regarding RANK pathway has focused on the differentiation of microfold (M) cells (Kanaya et al., 2012; Kimura et al., 2015a, 2020; Knoop et al., 2009; Rios et al., 2016). RANKL-null and RANK conditional intestinal knockout mice have a dramatic decrease of functionally mature M cells. RANKL neutralization reduces

functional M cells, as measured by bead uptake, while RANKL administration restores M cell numbers and function in RANKL knockouts in 7 days, demonstrating that M cell development is a dynamic process during adult life (Knoop et al., 2009). RANK has been reported to be expressed throughout the intestinal and colon epithelium, while RANKL is restricted to cells within the GALT which are positioned immediately below the FAE (Kanaya et al., 2012; Kimura et al., 2015a, 2020; Knoop et al., 2009; Rios et al., 2016). In particular, RANKL is expressed in group 3 innate lymphoid cells (ILC3s), T cells and mesenchymal cells. Tissue-specific deletion of RANKL and expression of uncleavable forms of RANKL identified membrane-bound mesenchymal RANKL as the main effector of M cell differentiation (Nagashima et al., 2017).

At the molecular level, the activation of RANK pathway in intestinal epithelium triggers the activation of NF $\kappa$ B pathway through TRAF6, as illustrated by the lack of M cell differentiation after RANKL addition in a context of I $\kappa$ B kinase- $\beta$  inhibition or in TRAF6 knockouts (Kanaya et al., 2018). Activation of canonical NF $\kappa$ B (p52/RelA) induces the expression of RelB, switching towards non-canonical NF $\kappa$ B (p52/RelB) activation, which triggers the expression of classical M cell markers such as (*Tnfrsf25* and *Ccl19*) and crucial transcription factors for M cell differentiation such as *SpiB* and *Sox8* (Kanaya et al., 2012, 2018; Kimura et al., 2019a). These transcription factors activate the expression of functional proteins such as GP2, which is a *bona fide* marker of mature M cells (Kimura et al., 2015a, 2019a, 2020).

Importantly, when RANKL is injected intraperitoneally, M cells develop in ectopic regions of the intestinal epithelium, such as the villi, suggesting that RANK pathway is regulated by the spatial restriction of RANKL within the lymphoid secondary structures surrounded by the FAE (Kimura et al., 2015a; Knoop et al., 2009). As an additional mechanism to avoid the complete differentiation of the FAE into M cells, it has been proposed that OPG acts to block RANKL signaling locally. OPG levels are significantly higher in FAE as compared to villus epithelium, probably as part of a molecular mechanism for RANK pathway modulation as seen in the bone. The protein is detected in RL<sup>+</sup> reticular cells in the GALT but its transcription has been described to happen only in SPIB<sup>+</sup> cells in the FAE. OPG detected in reticular cells would then be secreted by M cells and would block RANKL sources (Kimura et al., 2020). Indeed, OPG knockout mice present higher levels of M cells, especially in the cecum and colon, where B cell numbers and subsequently IgA production were also increased (Kanaya et al., 2018). This publication complements studies on RANK intestinal epithelial knockout and RL full-body knockout mice, where germinal centers present



dampened B cell activation and therefore less IgA production due to defective M cell development (Knoop et al., 2009; Rios et al., 2016). Interestingly, RANKL in other mucosal-associated lymphoid tissues also induces epithelial cell differentiation into M cells. This is the case in the larynx, the trachea (Kimura et al., 2019b) and in the nasal cavity (Mutoh et al., 2016). Similar M-cell like populations exist in other mucosal-associated tissue, where the role of RANK pathway remains to be explored (Brandtzaeg et al., 2008; Kimura et al., 2015b).

## **RANK in the mammary gland**

The mammary gland is an organ formed by adipose tissue (fat pad) and an epithelial ductal tree composed by a bilayer of epithelial cells: a layer of luminal cells, surrounded by a layer of basal cells. Luminal cells are distinguished by the expression of cytokeratin 8 (K8), and they produce milk during pregnancy and lactation. Basal cells have a myoepithelial phenotype and express cytokeratin 14 (K14) and 5 (K5). Basal cells separate the mammary epithelium from the surrounding stroma and, through their contractile ability, aid milk secretion from the lumen of the mammary duct during lactation (Fu et al., 2020; Pellegrini et al., 2013). This epithelial structure is common for other secretory glands in mammals such as prostate, salivary and sweat glands. The two mammary epithelial subpopulations can also be distinguished by the expression of CD24 and CD49f, with luminal cells presenting CD24<sup>+</sup>CD49f<sup>low</sup> expression and basal cells CD24<sup>+</sup>CD49f<sup>hi</sup> staining by flow cytometry (Fu et al., 2020; Pellegrini et al., 2013).

At birth, mice have a rudimental small branched ductal tree connected to the nipple. The mammary epithelium remains quiescent until puberty, when the ductal tree elongates responding to estrogen signals until it completely invades the fat pad. This process occurs due to proliferation of specialized cells at the terminal end buds (TEBs), which are structures localized at the tips of the ducts. Proliferation is coordinated with apoptosis to guarantee the formation of a luminal space within the ducts. At adulthood, progesterone foments branching and the mammary epithelium from virgin female mice is subjected to changes depending on hormonal levels during the estrous cycles and upon pregnancy (Briskin and Ataca, 2015; Fu et al., 2020). During pregnancy, luminal epithelial cells undergo a first phase of proliferation in response to high levels of progesterone, followed by a phase of differentiation into a secretory phenotype and an organization in milk-secreting alveoli orchestrated by both progesterone and prolactin. After the pups are weaned, the mammary gland undergoes

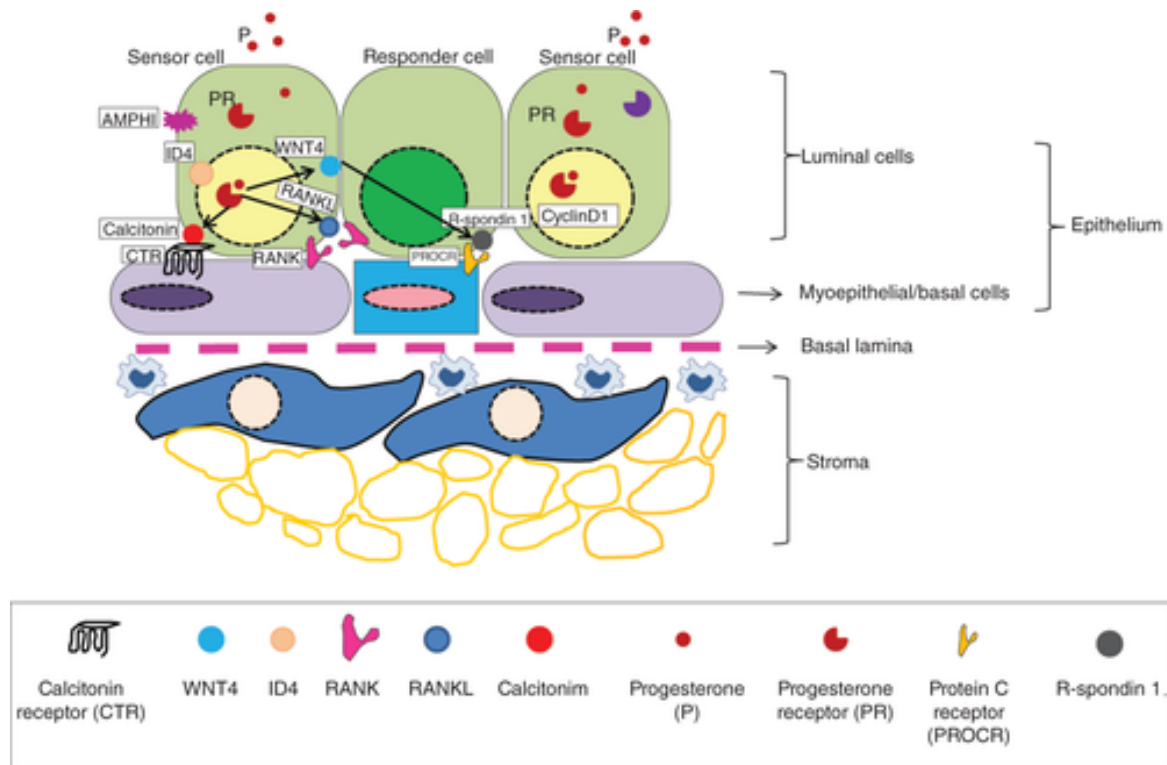
dramatic remodeling (involution), and most of the epithelial cells die in a coordinated process triggered by local and systemic signals (Fu et al., 2020).

This high rearrangement capacity of the adult mammary gland epithelium prompted the investigation of putative populations of stem or progenitor cells within the different epithelial subpopulations. Transplantation and *in vitro* culture experiments highlighted the capacity of basal cells to give rise to both luminal and basal lineages, while luminal cells remain lineage-restricted (Fu et al., 2020). Basal cells give rise to luminal cells during embryogenesis, however, unbiased lineage tracing experiments have not identified any switch between basal and luminal lineages in physiological conditions after birth (Davis et al., 2016; Scheele et al., 2017), suggesting that the bipotency of basal cells is limited to embryonic development, situations where luminal cells are artificially removed or upon tissue damage (Centonze et al., 2020; Fu et al., 2020).

In the luminal compartment, progenitor cells were identified as CD61<sup>+</sup> cells (Lin<sup>-</sup>CD24<sup>+</sup>CD29<sup>low</sup>CD61<sup>+</sup>), with high expression of alveolar cell-fate determinant Elf5 and lack of estrogen receptor (ER) expression (Fu et al., 2020; Van Keymeulen et al., 2017). A minor subset of ER<sup>+</sup> luminal progenitors has also been proposed to contribute to the formation of the hormone-receptor-positive populations within the luminal layer. ER<sup>+</sup> and ER<sup>-</sup> luminal progenitors can be also distinguished by the expression of other markers, ER<sup>+</sup> being Sca1<sup>+</sup>CD49b<sup>+</sup> and ER<sup>-</sup> corresponding to Sca1<sup>-</sup>CD49b<sup>+</sup> cells (Fu et al., 2020; Van Keymeulen et al., 2017). Indeed, Sca1<sup>-</sup> cell populations were early identified as potential luminal progenitors with higher colony-forming ability, compared to Sca1<sup>+</sup> cells, associated with the ER<sup>+</sup> mature luminal compartment (Sleeman et al., 2007).

RANK pathway has been extensively studied in the mammary gland, where it plays a crucial role, especially during pregnancy (Fata et al., 2000a). In murine virgin mammary gland, RANK expression is maintained relatively low, with small variations during the estrous cycle (Gonzalez-Suarez et al., 2007; Joshi et al., 2010). Progesterone peaks, which happen during the luteal diestrus phase of murine menstrual cycle and pregnancy (Joshi et al., 2010), induce RANKL expression in progesterone-receptor-positive (PR<sup>+</sup>) luminal cells (Srivastava et al., 2003). Progesterone induces a first wave of proliferation in PR<sup>+</sup> luminal cells, as well as an upregulation of Wnt4 and RL (Joshi et al., 2010, 2015b). These ligands then act as a paracrine signals, inducing proliferation on neighbor PR-negative luminal cells (Beleut et al., 2010; Joshi et al., 2010, 2015b). Luminal cells will only be responsive to Wnt signalling when RANK pathway is activated, since it upregulates the expression of Wnt co-

receptor LRP5 and R-spondin 1 (RSPO1), an essential molecule for Wnt pathway activation (Joshi et al., 2015b). Basal cells in the dioestrus phase were reported to significantly upregulate RANK expression and increase cyclinD2 levels (Joshi et al., 2010), but this observation was not validated in subsequent studies (Joshi et al., 2015b) (**Figure 6**).



**Figure 6. RANK in mammary gland epithelium.** The mammary gland epithelium consists of two layers of cells (luminal and basal) surrounded by an adipose stroma. During the peaks of progesterone at menstrual cycles or pregnancy, PR+ luminal cell populations undergo a first cycle of proliferation orchestrated by CyclinD and secrete RANKL and WNT4. RANKL binds to RANK+ luminal and basal cells, triggering a second wave of proliferation, accompanied by RSPO1 secretion to sustain Wnt signaling. Figure from Briskin C. and Ataca D., 2015(Briskin and Ataca, 2015).

The progesterone-driven expansion of the luminal epithelium observed during the menstrual cycle is also essential for the alveologenesis process during pregnancy and lactation (Fata et al., 2000a; Gonzalez-Suarez et al., 2007). RANK expression greatly increases at day 15.5 of pregnancy, gradually downregulates thereafter and maintains at the lobulo-alveolar structures and branching areas within the ducts throughout the pregnancy (Gonzalez-Suarez et al., 2007). RANKL expression is induced by progesterone. The effects of impaired proliferation and alveologenesis observed in PR-null mice can be rescued by RANKL injection, depicting the essential role of RANK pathway as an amplifier of progesterone signals during pregnancy (Beleut et al., 2010). Interestingly, overexpression of RANK in the

mammary gland is sufficient to induce proliferation and the appearance of small alveoli-like structures, also preventing the differentiation of luminal cells into functional secretory cells during pregnancy and lactation *in vivo* and *in vitro* (Cordero et al., 2016; Gonzalez-Suarez et al., 2007; Pellegrini et al., 2013). This impairment in lactogenic differentiation has also been observed in gestation mammary gland epithelium acini treated with RANKL, which prevents Stat5 phosphorylation in response to prolactin, while RANKL inhibition at mid-gestation induced precocious lactogenesis in pregnant mice (Cordero et al., 2016).

Importantly, some of these observations in mouse models have been validated in human samples. Using tissue derived from reduction mammoplasty, Tanos T. *et al.* verified that RANKL expression on the mammary gland was only found in PR+ cells from patients which presented high progesterone serum levels. Furthermore, primary mammary epithelial cells cultured *in vitro* upregulated RANKL upon PR activation, followed by a RANKL-dependent increase in proliferation (Tanos et al., 2013b). Another study using healthy and malignant tissue from breast cancer patients also identified that pregnancy, where progesterone levels are high, associated with higher levels of RL (Azim et al., 2015).

## **The immune system and RANK pathway**

Full-body RANKL or RANK knockouts revealed that RANK pathway is crucial for the correct functioning of the immune system. RANK or RANKL loss resulted in abnormal bone marrow hematopoietic compartmentalization (probably due to the osteopetrosis phenotype), with defects in B cell development, lack of LN formation and blocked T cell thymic development (Dougall et al., 1999a; Kong et al., 1999). These dramatic phenotypes, together with several other functional assays, prompted further investigation of RANK pathway in the different compartments of the immune system.

The immune system comprises of multiple specialized cells and organs. Immune cells all derive from long-term hematopoietic stem cells (LT-HSC) in bone marrow (BM). These cells give rise to more differentiated, lineage-committed progenitors: monocyte and lymphoid progenitors. Lymphoid progenitors give rise to T cells, B cells and innate lymphoid cells (ILCs). Common monocyte progenitors can give rise to: megakaryocytes (which give rise to platelets), erythroid progenitors, granulocyte-macrophage progenitors (GMP) or to monocyte-macrophage/dendritic lineage-restricted progenitors (MDP). GMP can then differentiate into granulocytes (neutrophils, eosinophils, basophils) or neutrophil-like

inflammatory monocytes. MDP give rise to monocytes, macrophages and dendritic cells (**Figure 7**) (Fang et al., 2018).

Studies with bone marrow and peripheral blood human samples revealed that RANK is expressed in monocytes (CD14<sup>+</sup>), Natural Killer cells (CD56<sup>+</sup>CD3<sup>-</sup>), B cells (CD19<sup>+</sup>) and erythrocyte progenitors (glycophorin A<sup>+</sup>), while T cells (CD3<sup>+</sup>) showed no staining (Atkins et al., 2006). The immune populations which are of particular relevance to this doctoral thesis, and in which RANK pathway has been described to play a role, will be discussed below (**Figure 7**).

## **Lymphoid lineage**

### **T cells**

T cell differentiation from lymphoid progenitors takes place in the thymus. Each T cell rearranges its DNA to create a unique T cell receptor (TCR) and then undergoes a series of controls to verify proper TCR expression and lack of self-antigen recognition (Smith-Garvin et al., 2009; Wei et al., 2018).

The TCR is a specialized protein which detects peptides presented by major histocompatibility complex (MHC) molecules. Each cell in the body degrades its proteins into peptides and loads them onto the MHC, which will then be localized at the membrane surface. MHC-I will load peptides produced by the cell which presents them, and MHC-II will load peptides from proteins uptaken from the extracellular environment. T cells which show affinity to MHC-I would become CD8<sup>+</sup> cells and those with affinity to MHC-II would become CD4<sup>+</sup> T cells (also known as T helper cells- Th) (Fang et al., 2018; Smith-Garvin et al., 2009; Wei et al., 2018).

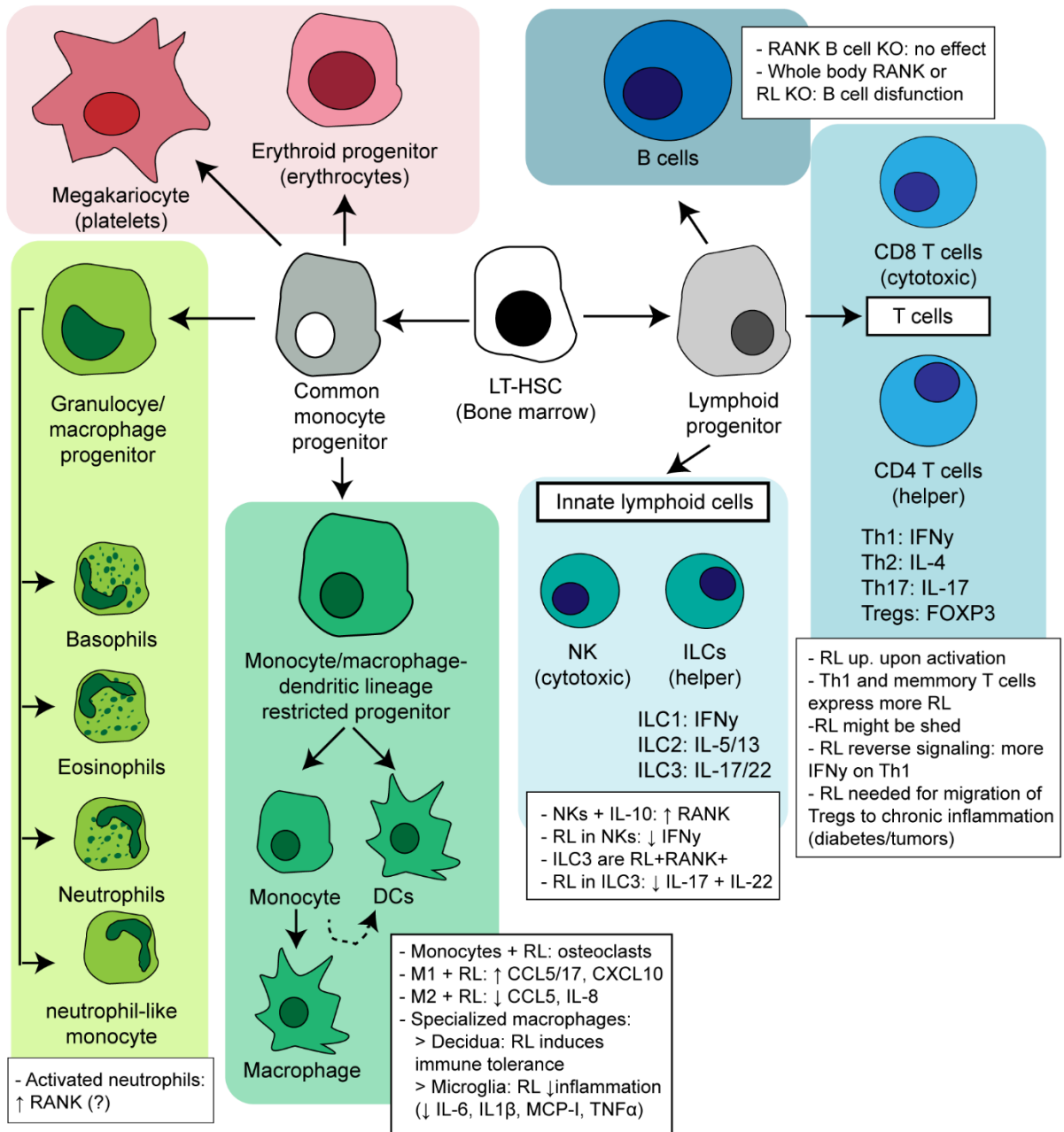
CD4 T cells can further differentiate into different subtypes when encountering specific cytokine stimuli. The main subtypes are four:

- Th1. Pro-inflammatory, they secrete INF $\gamma$  and TNF- $\beta$  to activate CD8 T cell cytotoxicity and macrophage/monocyte phagocytosis.
- Th2. They activate B cells, eosinophils and mast cells by secreting cytokines such as interleukin (IL)-4, 5, 6, 9, 10 and 13.
- Th17. They secrete mainly IL-17, a pro-inflammatory molecule.
- T regulatory cells (Tregs). They express forkhead box P3 (FOXP3) and suppress T cell activity.

The transformation of naïve CD4<sup>+</sup> cells into one of the subtypes depends on the cytokine cocktail they are exposed to, and a high plasticity regarding the transition between Th2, Th17 and Treg status has been described (Fang et al., 2018). Th1 cells are primed by IL-12, released by active antigen-presenting cells (APC), which triggers IFN $\gamma$  secretion and thus aids in the activation of the immune response. By contrast, IL-4 is the main driver of Th2 differentiation. Th17 arise after the combined effects of IL-6 and TGF- $\beta$ , which activate Stat3, resulting in the upregulation of ROR $\gamma$ t, a transcription factor essential for IL-17 production. Tregs arise after TGF- $\beta$  and IL-2 signaling, which upregulate FOXP3 expression (Fang et al., 2018).

All T cells need to encounter an antigen presented in MHC molecules to trigger their activation, which varies depending on their subtype, as briefly explained above. The first encounter, termed “T cell priming”, can happen in peripheral tissues or secondary lymphoid organs (such as lymph nodes), where antigens are presented by APC (Smith-Garvin et al., 2009; Wei et al., 2018). Upon binding MHC molecules with their TCR-CD3 complex, T cells trigger the activation of several downstream signals, including intracellular calcium release, to trigger their different effector functions (cytokine secretion, cytoskeleton rearrangements, cytotoxic granule release, etc). However, the activation of T cells is tightly regulated. If only the TCR is stimulated, T cells go into an anergy state, where they will be refractory to stimulation. For a successful T cell activation, certain co-stimulatory receptors should be stimulated. This is the case of CD28, which upon binding of CD80 or CD86 (B7 ligands) on APCs triggers PI3K-Akt, NF $\kappa$ B, JNK, and p38 MAPK signaling, which ultimately results in the expression of anti-apoptotic genes and the production of IL2, essential for T cell survival. Other less potent costimulatory signals in T cells are triggered by ICOS and TNFRs (OX40 and 4-1BB), and they are suggested to play a role in maintaining an attenuated T cell activation after a first TCR stimulation (Smith-Garvin et al., 2009).

In order to limit T cell activity, regulatory mechanisms are triggered after T cell activation, including the upregulation of immune checkpoint molecules: cytotoxic T-lymphocyte-associated protein 4 (CTLA-4) and programmed death receptor 1 (PD-1)(Smith-Garvin et al., 2009; Wei et al., 2018). CTLA-4 expression peaks 2-3 days after T cell activation. CTLA-4 and competes with CD28, binding CD80 and CD86 ligands. PD-1 binds PD-L1 and PD-L2, which are found on APC or epithelial cells.



**Figure 7. RANK in immune cell subpopulations.** Scheme summarizing reported roles for RANK pathway on the different immune subpopulations, divided according to their lineage. Long-term hematopoietic stem cells (LT-HSC) in bone marrow (BM) give rise to common monocyte and lymphoid progenitors (CMP). CMP give rise to megakaryocytes (precursor of platelets), erythroid cells, granulocyte/macrophage progenitors (GMPs) and monocyte/macrophage-dendritic lineage restricted progenitors (MDPs). GMPs give rise to basophils, eosinophils, neutrophils and neutrophil-like monocytes. MDPs give rise to DCs and monocytes, which can also give rise to macrophages and DC subpopulations. Lymphoid progenitors can give rise to B cells (antibody-producing cells), T cells (CD8 or CD4, further subdivided into Th1, Th2, Th17 and Tregs) and innate lymphoid cells (NKs, ILC1, ILC2 or ILC3)(Fang et al., 2018).

cells which have been exposed to inflammatory signals such as IFN $\gamma$ . PD-1 recruits dephosphorylases which directly block CD28 downstream signaling. Activated PD-1 also drives metabolic restriction, which limits T cell proliferation and, when expressed together with LAG3 and TIM3, is a marker of T cell exhaustion (Wei et al., 2018).

Low RANK expression was reported in early studies with human T cells, cultured in activating conditions (Anderson et al., 1997; Josien et al., 1999). IL4 and TGF $\beta$  were described to increase RANK expression on peripheral blood T cells (Anderson et al., 1997) but these observations were not confirmed by following studies (Josien et al., 1999). However, treating T cells with recombinant-RL activates JNK pathway (Wong et al., 1997a) and RANKL treatment has been reported to increase the number of viable T cells found after 6 days in culture (Anderson et al., 1997).

T cells have been described to upregulate RANKL upon TCR activation, especially during a re-stimulation (Bachmann et al., 1999; Josien et al., 1999; Wang et al., 2002; Wong et al., 1997a), as a direct consequence of Ca<sup>2+</sup> mobilization occurring downstream TCR activation, which activates calcium-dependent kinases such as calcineurin (Wang et al., 2002; Wong et al., 1997a). Memory T cells (CD44<sup>+</sup>) express basal levels of RANKL and greatly increase its expression upon stimulation (Josien et al., 1999). Interestingly, activated Th1 CD4 T cells present stronger RL upregulation than Th2 T cells and IL-4 treatment partially inhibits the increase in RANKL expression (Josien et al., 1999). It has been suggested that RANKL is normally shed from T cells by protease cleavage after activation (Kanamaru et al., 2004).

The upregulation of RANKL on activated T cells rose the question of whether RANK pathway was playing a role in the modulation of T cell function, as it is the case with other TNFRSF members (Smith-Garvin et al., 2009). During viral infection, systemic RANKL inhibition had only an effect in the activation of CD4 T cells of CD40 knockout models and not in wildtype controls, suggesting a redundant or co-stimulatory function for RANK signaling (Bachmann et al., 1999). *In vitro* models of CD4 T cell activation and re-stimulation revealed that reverse signaling through RANKL, in a p38, MAPK dependent manner, augments the production of IFN $\gamma$  in Th1 T cells without affecting IL-4 secretion in Th2 cells (Chen et al., 2001). Most studies on T cell-derived RANKL, though, focus on its role as source for RANK activation. In models of bone inflammation, RANKL expressed in CD4 T cells themselves was sufficient to induce osteoclastogenesis (Ju et al., 2008). Others argue that RANKL levels in T cells are not enough to explain this phenotype and suggest that RANKL expression in mesenchymal cells and osteoblasts is potently induced by IL-17 released by Th17 cells.



Th17 cells would be maintained by the high levels of IL-23 in the inflamed joint. This higher local production of RANKL, regardless of the source, would exacerbate bone resorption in diseases such as rheumatoid arthritis (Sato et al., 2006). In models of diabetes driven by CD8-mediated pancreatic islet destruction, a systemic blockade of RANK signaling accelerated the onset of diabetes, suggesting a role for RANK pathway in the modulation of autoreactive CD8 activity. The effect was due to a subset of immunosuppressive CD4 T cells, whose accumulation in the pancreas required RANKL activity. Importantly, RANK-Fc exposure impaired the ability of these CD4 T cells to delay diabetes onset when transplanted into recipient diabetic-prone mice (Green et al., 2002).

Thus, RANKL in T cells might play a role in regulating T cell responses, either directly through reverse signaling, or acting as a paracrine signal in other immune populations.

### **B cells**

Like T cells, B cells also undergo DNA rearrangement to express antigen-detecting molecules. In B cells, the rearrangement occurs in the immunoglobulin (Ig) gene regions, producing a unique B-cell receptor (BCR) per B cell. In the bone marrow, B cells undergo a selection process to avoid self-reactive Ig expression. B cells then migrate to the spleen and lymph nodes where, upon encounter with a compatible antigen, they will secrete high levels of Ig, while proliferating and rearranging their BCR to achieve the highest antigen-binding affinity Ig (LeBien and Tedder, 2008).

Despite the defects on B cell phenotypes observed on full-body RANK or RANKL knockouts (Dougall et al., 1999a; Kong et al., 1999), an extensive analysis performed on a B-cell specific RANK depletion model reports no differences on secondary/tertiary lymphoid organ formation, B cell development or B cell activity (Perlot and Penninger, 2012). This observation suggests that B cells do not directly rely on RANK signaling but are affected by the lack of RANK signaling on other cell populations, which indeed affects important organs for B cell development such as lymph nodes and bone. Interestingly, although naïve B cells do not express RANKL, a study with B-cell lymphoma patients showed malignant B cells present elevated levels of RANKL, which triggered IL-8 release when activated through RANK-mediated reverse signaling (Secchiero et al., 2006).

### **NK cells**

Natural Killer (NK) cells are derived from lymphoid progenitors but, unlike T and B cells, are part of the innate immune system since their activation does not rely on the encounter of a

particular antigen. Their activation depends on a delicate signaling balance between activating and inhibitory receptors expressed on their cell membrane. The most characteristic NK inhibitory receptor is Ly49 (the human homologue being killer cell immunoglobulin-like receptor -KIR-), which binds to MHC-I molecules, irrespective of the presented peptide. Using immunoreceptor tyrosine-based inhibitory motifs (ITIMs), Ly49 recruits phosphatases which block activating NK signals. Besides lack of MHC-I on the target cells, NK need to integrate several signals to trigger cytotoxic granule and cytokine release. Some of the activating receptors are natural-killer group 2, member D (NKG2D), Natural cytotoxicity receptors (NCRs), CD44, CD16 and CD38. These proteins bind a broad number of activating ligands, ranging from viral/bacterial particles to proteins expressed in target cells as a result of DNA-damage or inflammation signals, together with certain cytokines such as IL-2, IL-12, IL-15 or IL-18 (Paul and Lal, 2017).

NKs derived from bone marrow and blood have been described to express RANK (Atkins et al., 2006), and subsequent studies demonstrated that RANK was upregulated upon exposure of NK to immunosuppressive cytokines such as IL-10. Importantly, NKs cocultured with RANKL-expressing AML cells present reduced IFN $\gamma$  release and cytotoxicity, which is recovered when denosumab is added (Schmiedel et al., 2013). These observations suggest that RANK could be an additional inhibitory receptor of NK activity.

### **Innate Lymphoid Cells (ILCs)**

Beside NK cells, additional subsets of ILC have begun to be characterized. NK are often termed as “cytotoxic” ILC and ILC type 1, 2 and 3 cells are considered “helper” ILCs, similar to the classification of CD8 and CD4 T cells, based on their function (Eberl et al., 2015). Helper ILCs rely on the expression of GATA-3 for the differentiation from lymphoid precursors. ILC-1 are characterized by the expression of IL-7 receptor and T-bet transcription factor. They secrete IFN $\gamma$  and induce apoptosis in target cells through TRAIL pathway. ILC-2 are found in adipose tissues and the lung, where they secrete IL-5- and IL-13 to resolve parasitic and viral infections or tissue damage, also promoting CD4 Th2 differentiation (Eberl et al., 2015). ILC-3 are identified by the expression of ROR $\gamma$ t transcription factor. They are best characterized in the intestinal lamina propria, where they remain inactive due to signals derived from the microbiota. Upon infection or tissue damage, ILC-3 will secrete IL-22 to resolve the infection or repair the affected tissue. However, ILC-3 can prolong and worsen chronic inflammation through the secretion of high levels of IL-17 and IL-22 (Eberl et al., 2015; Luci et al., 2009; Sawa et al., 2010).

ILC-3 have been described to present both RANKL and RANK expression levels (Bando et al., 2018; Luci et al., 2009). In a very elegant study, Bando J. *et al* identified RANK pathway as a suppressor of ILC-3 activity in the lamina propria. Using RANKL or RANK genetic depletion under the ROR $\gamma$ t promoter and *in vitro* assays with RANKL or anti-RL treatments, they observed that blockage of RANK pathway results in higher proliferation and secretion of IL-17A and IL-23 cytokines by CCR6<sup>+</sup> ILC-3, leading to an hyper-responsiveness of these cell population to bacterial infection (Bando et al., 2018). Thus, RANK pathway in this ILC-3 population dampens immune reactivity.

## **Myeloid lineage**

### **Dendritic cells**

Dendritic cells (DCs) are often referred as “professional” APCs since they are the main stimulators of T cell activity in an antigen-dependent manner. There are three distinct subtypes of DCs, which derive from different bone marrow precursors: monocyte-derived, plasmacytoid and classical DCs (mDC, pDC, and cDC respectively). mDCs differentiate from monocytes after being exposed to certain cytokines (Fang et al., 2018; Wacleche et al., 2018) and both pDCs and cDCs derive from the dendritic cell progenitor in the bone marrow. cDCs are further subdivided into CD103<sup>+</sup> and CD11b<sup>+</sup> cDCs (Broz et al., 2014).

DCs located in peripheral tissues remain in a highly phagocytic immature state, which allows them to accumulate circulating antigens. Only when receiving inflammatory signals will they evolve to a more mature status and migrate to secondary lymphoid organs to activate T cells. Indeed, tissue-resident DCs have the relatively long lifespan of weeks, while those in lymphoid organs have a high turnout rate (Cremer et al., 2002).

The first observations regarding RANK pathway in DCs were made in culture models. Bone-marrow derived DCs were found to express RANK (Anderson et al., 1997; Wong et al., 1997b), and upregulation of the protein has been described upon DC activation with CD40L (Anderson et al., 1997). Spleen-derived DC expressed RANK after one day in culture and changed their cytokine secretion patterns upon RANKL treatment (Bachmann et al., 1999; Wong et al., 1997b). As observed also with CD40L, RANKL treatment greatly increased the survival and clustering of mature DCs growing *in vitro* (Anderson et al., 1997; Wong et al., 1997b), maybe due to the downregulation of pro-apoptotic B-cell lymphoma 2 (Bcl-2) and the upregulation of anti-apoptotic B-cell lymphoma-extra large (Bcl-xL) proteins (Wong et al., 1997b). However, RANKL did not increase antigen presentation or the expression of

adhesion proteins necessary for DC-mediated T cell activation (Anderson et al., 1997; Wong et al., 1997b). There was thus no increase on T cell proliferation *in vitro* when the same number of DCs were compared. Accordingly, the survival of bone-marrow monocyte progenitors primed *in vitro* towards a DC lineage is greatly reduced when cultured in presence of RANK-Fc, and increased in *opg*<sup>-/-</sup> DCs (Chino et al., 2009; Cremer et al., 2002), suggesting a role for auto/paracrine RANK signaling in immature DC survival. Interestingly, the increase in DC survival presents a major advantage to establish a longer and stronger T cell stimulation when antigen-loaded DCs are re-injected *in vivo* (Josien et al., 2000).

In models of skin inflammation, RANKL is greatly upregulated in keratinocytes. Models of keratinocyte RANKL overexpression mimicking this observation resulted in a switch towards an immunosuppressive phenotype of epidermis-resident DCs (Langerhans cells). The secretion of cytokines such as IL-6, IL-10 and TNF $\alpha$ , together with the upregulation of CD86 and CD205 resulted in the expansion of the Treg population, which was able to block autoimmunity in CD40-overexpression mouse models (Loser et al., 2006). Interestingly, upon an LPS-driven inflammation mDCs derived from CD16<sup>-</sup> (but not CD16<sup>+</sup>) monocytes were described to upregulate RANK (Wacleche et al., 2018), maybe reflecting a compensatory mechanism to prime DCs to receiving immunomodulatory signals via RANKL.

Overall, extensive data identified RANK pathway to promote DC survival. However, models of acute and chronic inflammation suggest that RANKL stimulation may promote a switch in DCs towards an immunomodulatory APC phenotype, which will ultimately dampen immune responses.

### **Monocyte/Macrophages**

Monocytes are released from the bone marrow into the blood stream. In humans, they are subclassified depending on their CD16 expression level into classical monocytes (CD16<sup>-</sup>), the most abundant in human blood; intermediate monocytes (CD16<sup>low</sup>), and non-classical monocytes, which perform a patrolling function. (CD16<sup>hi</sup>) (Fang et al., 2018; Wacleche et al., 2018). In mice, lymphocyte antigen 6 complex locus C1 (Ly6C) is used as a monocyte marker. Upon inflammatory signals, monocytes migrate into the affected tissue and differentiate into different macrophage (M $\phi$ ) subsets or into DCs, depending on the cytokine environment (Fang et al., 2018; Wacleche et al., 2018). For instance, a combination of GM-CSF and IL-4 is able to differentiate both CD16<sup>+</sup> and CD16<sup>-</sup> monocytes to DCs *in vitro* (Wacleche et al., 2018).

M $\phi$  transit between different polarization states depending on signals from their microenvironment. A simplistic subclassification divides M $\phi$  into M1 (pro-inflammatory) and M2 (anti-inflammatory) subtypes. M1 phenotype is reached through exposure to hypoxia, IFN $\gamma$  and active NF $\kappa$ B signaling; and is characterized by production of IL-12, type I interferons, CXCL9 and CXCL10. M2 macrophages usually secrete IL-10 and are differentiated by IL-4, IL-13 and Fc receptor- $\gamma$  (Fc $\gamma$ R) signaling. However, M $\phi$  have been described to have high plasticity and probably transit through a gradient of phenotypes between M1 and M2, depending on the signals received.

RANK pathway's effects in monocyte/macrophage polarization and function is probably context dependent. *In vitro*, studies with bone-marrow-derived and peritoneal macrophages describe how treatment with RANKL attenuates the production of pro-inflammatory cytokines upon LPS stimulation (Maruyama et al., 2006). However, RANKL-mediated osteoclast differentiation might be influencing the results (Nakamura et al., 2006). OPG and RANKL serum levels were found to be regulated *in vivo* upon an LPS challenge; with a higher expression of pro-inflammatory cytokines on RL-/- and lower in OPG-/- mice (Maruyama et al., 2006). These observations imply that RANK signaling might indeed play role on controlling systemic inflammation.

In another study using human monocytes polarized either to M1 or M2-like macrophage phenotype, RANKL treatment was reported to induce abundant cytokine expression changes in M2 macrophages, while only decreasing CCL5 and IL8 expression in M1 macrophages. Cytokine release was validated on the targets identified on M2 macrophages and CCL5, CCL17 and CXCL10 production was greatly increased upon RANKL stimulation (Fujimura et al., 2016). CCL17 in these macrophage's supernatant was described to act as a CD4 T cell chemoattractant in *in vitro* assays (Fujimura et al., 2015). In a model of RANK overexpression driven by the S100A8 promoter, active in macrophages, a higher proportion of myeloid cells were found in LNs, spleen and bone marrow, although the cause was not further explored (Hess et al., 2012).

At the decidua, the mucus membrane in the uterus located between maternal and fetal tissues, RANK signaling in macrophages was described to play an essential role in establishing immune tolerance to fetal proteins. RANKL expressed by stromal cells in trophoblasts from the placenta triggered M2 polarization in decidual macrophages, which causes a switch from a Th1 to an immunosuppressed Th2 phenotype in infiltrating CD4 T

cells. This observation was validated in mice, where RANKL knockouts were observed to have more embryonic losses than wildtype littermates (Meng et al., 2017).

A similar immunomodulatory role was described for RANK pathway in monocytic populations of the brain, where active RANK signaling was associated with better prognosis in ischemia models. An increase in RANK signaling in macrophages/microglia which surround the damaged area in early stages resulted in lower inflammatory cytokine expression, namely IL-6, IL-1 $\beta$ , monocyte chemoattractant protein-1 (MCP-1), and tumor necrosis factor  $\alpha$  (TNF $\alpha$ ). This reduction of inflammation reduced the neuronal damage in these ischemia models (Shimamura et al., 2014).

Overall, most studies of RANK pathway in monocytes and macrophages suggest that the activation of the pathway plays a role in controlling exacerbated inflammatory responses and promoting immune tolerance.

### **Granulocytes-Neutrophils**

The most abundant populations rising from granulocytic progenitors in the bone marrow are neutrophils. These cells accumulate in sequential differentiation stages within the bone marrow and are released in a controlled manner to reach adequate levels in circulation. Classically, neutrophil function was defined as being the first immune cells to invade a damaged tissue, where they display high phagocytic activity, release cytotoxic granules and chemoattractants to recruit other immune cells. Neutrophils then undergo quick apoptosis, although a certain subset of ICAM<sup>hi</sup>CXCR1<sup>lo</sup> neutrophils have been observed to return to circulation (Nicolás-Ávila et al., 2017).

A small study on blood from healthy donors described that RANK is found in polymorphonuclear neutrophils at variable levels, which are increased upon sample manipulation (i.e after neutrophil purification) or activation, as happens with other dynamic markers such as CD11b. Interestingly, RANKL was described to act as a chemoattractant for the neutrophils of some of the donors (Riegel et al., 2012).

In contrast, other studies report lack of RANK mRNA in neutrophils from peripheral blood, while the expression is detected in neutrophils extracted from synovial fluids from patients with rheumatoid arthritis. OPG follows a similar pattern, with a strong expression in these populations. Interestingly, when culturing blood neutrophils with synovial fluid (depleted from cells), RANK and OPG were strongly upregulated (Poubelle et al., 2007). These might

indicate that RANK expression in neutrophils is induced upon receiving inflammatory signals.

### **Lymphoid organs: Lymph nodes and Thymus**

RANK pathway is necessary to form lymphoid structures early during development. In particular, RANK and RANKL control lymph node formation (Dougall et al., 1999a; Onder et al., 2017), the correct function of intestinal mucosal immune responses (Knoop et al., 2009; Rios et al., 2016) and thymus (Akiyama et al., 2008; Baik et al., 2016; Roberts et al., 2012; Rossi et al., 2007). Lack of RANK, RANKL or OPG results in absence of lymph node formation (Fata et al., 2000a; Kim et al., 2000), defective secretion of antibodies and antigen sampling at the GALT (Kanaya et al., 2018; Knoop et al., 2009; Rios et al., 2016) and a lack of negative selection in the thymus (Haljasorg et al., 2015; Hikosaka et al., 2008b, 2008a; Josien et al., 1999; McCarthy et al., 2015), which results in incomplete T cell development.

Lymph node formation has its origin at embryonic stages in an organized manner. First, mesenchymal fibroblasts and endothelial cells called Lymphoid Tissue organizers (LTo), produce CXCL13, a chemokine that binds CXCR5 and thus attracts a specific subtype ILC-3 (Zeng et al., 2019): the Lymphoid Tissue inducer (LTi) cells. LTi cells then cluster around LTo, producing lymphotoxin (LT) $\alpha_1\beta_2$ , which binds to its receptor (LT $\beta$ R) in LTo, triggering non-canonical NF $\kappa$ B pathway activation, which leads to the release of attracting chemokines which bind CCR7 and CXCR5 receptors on T cells and B cells, recruiting them to the newly forming lymph node (Mueller and Hess, 2012; Onder et al., 2017). RANK-Fc administration during development resulted in a reduction in LTi numbers during lymph node formation (Eberl et al., 2004), and RANKL administration to fetal LTi cells induced the expression of LT $\alpha_1\beta_2$  (Yoshida et al., 2002). Studies of RANK and RANKL specific deletion on ROR $\gamma$ t+ cells identified that RANK on these ILC-3 and T cell subsets was necessary for lymphogenesis, while RANKL specific depletion had no effect on lymphogenesis (Bando et al., 2018). Additionally, RANK overexpression on T cells was able to partially rescue LN formation in RANKL $^{-/-}$  mice but not on LT $\alpha$  deficient mice (Kim et al., 2000). Overall, these data suggest a role for RANK pathway in amplifying the signal to recruit immune cells to an emerging lymph node. Targeted RANKL depletion on LTo cells did not impair LN formation (Camara et al., 2019), implying that LTo are not the main RANKL source during lymphogenesis.

In established LN, RANKL has been described to partially regulate the expression of integrin  $\alpha 2b$  and to regulate LN size through its activity in stromal compartments, although probably other signals also contribute to lymph node dynamics (Cordeiro et al., 2016; Hess et al., 2012). RANKL expression on sinusoidal macrophages was crucial for their maintenance and function in murine LNs. This source of RANKL was described to be essential during early age or after activation of innate immunity to activate RANK in the lymphatic endothelial cells, which create an appropriate microenvironment for sinusoidal macrophage recruitment and development (Camara et al., 2019).

In the thymus, RANK pathway has been described to play a crucial role in establishing immune tolerance. Lymphoid progenitors which have correctly rearranged their TCR (immature thymocytes) interact with MHC molecules of thymic epithelial cells and APCs within the inner cortex of the thymus in a process called “positive selection”(Fang et al., 2018). Thymocytes which undergo positive selection in the inner cortex of the thymus upregulate RL (Hikosaka et al., 2008a; Josien et al., 1999), which is indispensable for the proliferation and maturation of medullary thymic epithelial cells (mTECs) and, thus, to the formation of the thymic medulla (Hikosaka et al., 2008b). RANK is expressed in a subset of mTECs (McCarthy et al., 2015) and its activation leads to downstream NF $\kappa$ B activity, which results in expression of Aire, a transcription factor which triggers the promiscuous transcription of all available genes, which will be processed into peptides and presented on MHC molecules (Haljasorg et al., 2015). Additionally, OPG expressed by a subset of MHCII<sup>hi</sup>Aire<sup>+</sup> mTECs regulates the expansion of this cell population (Hikosaka et al., 2008b; McCarthy et al., 2015). This population is thus crucial for thymic “negative selection”, where thymocytes which recognize self-peptides with high affinity undergo apoptosis to avoid autoimmune responses (Fang et al., 2018; Haljasorg et al., 2015).

It should be noted that, although CD8 T cell development relies on mTEC positive selection in the thymic medulla, CD4 T cell development has been reported to happen in an mTEC-independent manner (Cowan et al., 2013). A noteworthy exception are naïve Tregs, which rely on mTECs to generate FoxP3+CD25+ subsets. Surprisingly, despite the increased number of mTECs in OPG knockout models, the generation of new CD4 Tregs is decreased, although Treg recirculation into the thymus increases (McCarthy et al., 2015).

Interestingly, Aire-expressing cells are not only expressed in the thymus and are encountered in secondary lymphoid organs such as LN and the spleen, where they play a role in establishing peripheral immune tolerance (Gardner et al., 2008).



## RANK in human breast cancer

Breast cancer has benefited over the last years from the development of targeted therapies, which rely on the subclassification of the tumors depending on their molecular and histological characteristics. Global gene expression data from extensive breast cancer patient cohorts was used to identify distinct breast cancer subtypes (Rakha and Green, 2017; Russnes et al., 2017). Due to cost-effectiveness, current routine clinical identification of breast cancer subtype is based on the immunohistochemical detection of hormone receptors (progesterone receptor -PR- and estrogen receptor -ER-), human epidermal growth factor receptor 2 (HER2) and cell proliferation, using ki67 as marker (**Table 1**) (Goldhirsch et al., 2011).

	Luminal A	Luminal B	HER2-enriched	Triple-negative
IHC markers	ER+PR+HER2- ki67-low	ER+PR+/-HER2+/- ki67-high	ER-PR-HER2+	ER-PR-HER2-
Most common therapy	Hormonal therapy	Anthracyclines and taxanes	Trastuzumab (+chemotherapy)	Anthracyclines, taxanes and alkylating agents
Prognosis	Good	Bad	Bad	Worst

**Table 1. Table summarizing breast cancer subtypes.** Histological markers, most common therapy and clinical prognosis are specified for each breast cancer subtype (Goldhirsch et al., 2011).

Luminal-A tumors are ER+PR+HER2- and typically present low tumor proliferation. These are the tumors with best prognosis and respond better to hormonal therapy than to chemotherapy. Luminal B-tumors are ER+ and can have positive staining for PR or HER2. They are highly proliferative, have bad prognosis and present a poor response to hormonal therapy and chemotherapy, although anthracyclines and taxanes in combination with endocrine therapy are the main recommended treatment. HER2-enriched subtype is characterized by lack of ER and PR staining and being presenting HER2 overexpression or *HER2* gene amplification. They have bad prognosis but respond to chemotherapy and HER2-targeted therapy (i.e trastuzumab), a combination recommended in the adjuvant setting. Finally, triple-negative breast cancer (TNBC) is a heterogeneous group, with tumors lacking ER, PR and HER2 expression. These tumors present the worst prognosis, lack targeted therapies and the recommended treatments include anthracyclines, taxanes and alkylating agents (**Table 1**) (Goldhirsch et al., 2011; Rakha and Green, 2017). Gene

expression data, can further subdivide TNBC into three subtypes: basal-like (with genes common to basal epithelial cells), normal-like (with gene expression reminiscent of a normal mammary gland) and claudin-low (Coates et al., 2015). However, the normal-like breast cancer subtype is thought to potentially be a sampling artifact due to contamination with normal breast epithelia (Yersal and Barutca, 2014).

Palafox *et al.* described that RANK expression was found in 18% of luminal (ER+PR+) and 50% of ER-PR- tumors breast cancer tumors. This and several other studies identified ER-PR- or TNBC as the breast tumor subgroups with the highest probability of expressing RANK (Palafox et al., 2012a; Reyes et al., 2017; Santini et al., 2011). Accordingly to its more frequent expression in TNBC, the subtype with worst prognosis, high RANK expression in breast tumors correlated with worse disease-free survival, overall survival (Park et al., 2014; Pfitzner et al., 2014) and a shorter distant-metastasis free survival (Santini et al., 2011) in breast cancer patients. In a different study, higher RL/OPG ratio in patient serum showed a correlation with the development of distant bone metastasis (Rachner et al., 2019). Moreover, RANK levels were found to be higher in the mammary gland and breast tumors from BRCA1-mutation carriers (Bonifaci et al., 2011; Nolan et al., 2016), where RANKL was shown to increase proliferation and DNA damage (Nolan et al., 2016). Interestingly, the expression of a dominant-negative RANK isoform (RANK-c) was found to inversely correlate with tumor grade, proliferative index and presence of lung metastasis in the TCGA breast cancer cohort (Papanastasiou et al., 2012; Sirinian et al., 2018).

## **RANK in models of mammary gland tumorigenesis**

Studies with preclinical models manifested that RANK plays a key role in tumor initiation in both genetic and carcinogen + hormonal-induced murine tumor models (Gonzalez-Suarez et al., 2010; Schramek et al., 2010; Yoldi et al., 2016). Tumor latency was longer upon RANKL pharmacological inhibition and after genetic loss of either RANK or RANKL in several models of tumorigenesis (Gonzalez-Suarez et al., 2010; Nolan et al., 2016; Schramek et al., 2010; Sigl et al., 2016; Yoldi et al., 2016).

RANK overexpression under a mammary-gland specific promoter results in faster and more aggressive tumor development after treatment with a carcinogenic agent (7,12-dimethylbenz[a]anthracene -DMBA-) together with a progesterone-analog (medroxyprogesterone acetate -MPA-) (Gonzalez-Suarez et al., 2010). This observation illustrated a potential mechanism of RANK pathway's involvement in breast cancer initiation,

due to the known RANK-driven proliferation signal orchestrated by progesterone in mammary gland epithelium (Beleut et al., 2010; Joshi et al., 2010, 2015b). Importantly, tumor formation was prevented with RANK-Fc treatment in wildtype mice or delayed in RANK-overexpressing mice (Gonzalez-Suarez et al., 2010). Accordingly, RANK deletion in mammary epithelia induced by cre expression under a mammary-gland specific promoter resulted in decreased tumor formation and longer tumor latency after MPA/DMBA treatment. In addition to its role as mediator of progesterone-driven proliferation, RANK activation was reported to foment anchor-independent growth and protection from cell apoptosis triggered after  $\gamma$ -irradiation (Schramek et al., 2010).

In murine breast tumor models driven by the overexpression of a constantly-active rat homologue of HER2 (also called NeuT), depletion of RANK in mammary epithelium did not prevent tumor initiation or development (Schramek et al., 2010). This might be because progesterone-driven proliferation is not as crucial for tumor initiation in the context of a constantly-active HER2-driven proliferative signaling or due to the fast tumor onset in this aggressive tumor model. Additionally, an incomplete RANK depletion due to cre expression depending on the MMTV promoter might explain the lack of effects of RANK loss. A different study with a HER2 overexpression model also reports no differences in tumor initiation when mice were treated with RANK-Fc at 5 months of age, before tumors are palpable. However, RANK-Fc treatment did result in a lower tumor and metastatic burden, suggesting a possible effect for RANK pathway inhibition in delaying tumor growth and metastatic ability in this HER2+ breast cancer model (Gonzalez-Suarez et al., 2010). Differences between genetic and pharmacological approaches or additional systemic effects of RANK-Fc may also explain the differences observed between the two studies. In a whole-body RANK knockout mouse model, tumors driven by Polyoma middle-T expression in the mammary gland showed significantly lower tumor initiating and metastatic ability, in part due to a reduction in the Sca1- tumor cell population, which is enriched in tumor-initiating cells (Yoldi et al., 2016).

Nolan et. al observed that RANKL inhibition in MMTV-cre BRCA-1<sup>fl/fl</sup> p53<sup>-/+</sup> models delayed tumor appearance, also showing tumorigenesis prevention upon transplantation of mammary glands from these transgenic models into immunodeficient hosts treated with OPG-Fc. The same study showed that in human BRCA-1-deficient tumors, RANK+ cells had increased DNA damage and progesterone treatment increased tumor cell proliferation. These effects were blocked by denosumab (Nolan et al., 2016). Other groups further

validated the role of RANK in models of BRCA1-mutant breast cancer, in combination with p53 loss. RANK knockout in the mammary gland resulted in delayed tumor latency and the development of lower-grade tumors (Sigl et al., 2016). Importantly, RANK-Fc treatment was reported to prevent tumor formation almost completely in tumor models induced solely by BRCA-1 loss (Sigl et al., 2016), showing thus a similar tumor-preventing efficacy as that reported using the MPA/DMPA breast cancer models (Gonzalez-Suarez et al., 2010). A clinical trial is currently ongoing to test the preventive potential of denosumab in BRCA-mutated patients (BRCA-D: ACTRN12614000694617). Overall, inhibition of RANK pathway through either RANK genetic depletion or RANKL pharmacological inhibition has shown its potential in preventing breast cancer development on several mouse models (Gonzalez-Suarez et al., 2010; Nolan et al., 2016; Schramek et al., 2010; Sigl et al., 2016; Yoldi et al., 2016).

Yoldi *et al.* also reported an effect for RANK loss in delaying tumor onset and the tumor and metastasis initiating potential after transplantation of mammary tumor cells (Yoldi et al., 2016), thus presenting it as a potential target for breast cancer treatment. RANK loss or RANKL blockade in tumor transplants from this model induce tumor cell differentiation, as implied by the upregulation of lactogenic proteins, which resulted in reduced tumor initiating ability (Yoldi et al., 2016). Tumor transplant models are a tool to study the effects of RANK depletion or inhibition in advanced tumors, a setting more relevant to evaluate RANK pathway inhibition as a therapeutic (instead of preventive) treatment, which is of higher relevance in the clinic. In this work, RANKL treatment induced the de-differentiation of established tumors from the MMTV-PyMT mouse model, as well as promoting the growth of tumor transplants in syngenic hosts. RANK-Fc partially attenuated tumor transplant growth and diminished the tumor-initiating ability of transplanted carcinoma cells. Indeed, mammary tumor cells treated with RANK-Fc showed less stemness ability through colony-forming assays and were enriched in populations showing a differentiated phenotype, enriched in milk proteins (Yoldi et al., 2016). As these tumor cells lack expression of progesterone receptor and RANKL, a progesterone-independent mechanism of action could be causing these RANK-driven effects.

RANK pathway has also been described to induce epithelial-to-mesenchymal transition in human breast cancer cell lines overexpressing the receptor or which receive RANKL treatment (Palafox et al., 2012a; Tsubaki et al., 2013). Early reports also identified RANKL signaling to trigger epithelial cell migration in normal mammary epithelial mouse cells and

breast cancer human cell lines, as well as in a melanoma cell line (Jones et al., 2006). Interestingly, administration of OPG *in vivo* strongly reduced melanoma cell line bone metastasis (Jones et al., 2006). Additionally, studies with dominant-negative RANK-c showed that breast cancer cells diminished their migration and colony-forming ability when expressing this RANK isoform (Papanastasiou et al., 2012; Sirinian et al., 2018):

Together, these results suggest that RANKL inhibitors such as denosumab, could reduce reduced recurrence and metastasis in the clinical setting.

### **Clinical Trials with Denosumab in Breast Cancer**

In the clinic, Denosumab (anti-RANKL humanized monoclonal antibody) is administered to breast cancer patients to treat skeletal related events, such as bone metastasis, due to its known role in bone remodelling (Infante et al., 2019). Its effects as adjuvant treatment on breast cancer outcome in terms of overall survival (OS), disease-free survival (DFS), bone metastasis- or distant-metastasis-free survival (BMFS, DMFS) were studied in two phase III clinical trials, which reached conflicting results: ABCSG-18 and D-CARE clinical trials (Coleman et al., 2020; Gnant et al., 2015). D-CARE included 4509 pre- and post-menopausal patients which were randomized to receive placebo or high dose Denosumab (120 mg) every month for 6 months and thereafter quarterly for 5 years (Coleman et al., 2020). ABCSG-18 randomized 3420 post-menopausal hormone-positive breast cancer patient between placebo and Denosumab, which was administered in 60 mg doses every 6 months until the end of the study (Gnant et al., 2015). Patients from D-CARE had or were receiving chemotherapy and hormonal therapy, and most had grade II or III tumors with LN metastases, while ABCSG-18 patients were receiving aromatase inhibitors, with a quarter having received previous chemotherapy, and consisted mainly of grade II tumors (Coleman et al., 2020; Gnant et al., 2015). The radically different patient cohorts and/or the different Denosumab treatment schedules might explain the differences observed in clinical trial outcomes. ABCSG-18 met its primary endpoint, concluding that Denosumab succeeded in reducing the rate of clinical fractures by increasing bone mineral density(Gnant et al., 2015). Additionally, a moderate increase in DFS was reported in those patients receiving denosumab (Cairns and Curigliano, 2016; Gnant et al., 2015, 2019). D-CARE however, reported no added benefit of Denosumab regarding OS, DFS or BMFS, regardless of menopausal status (Coleman et al., 2020, 2018). Another clinical trial with denosumab recruiting a high number of breast cancer patients was GeparX (NCT02682693). This trial evaluates the addition of denosumab in a neoadjuvant setting (120 mg every 4 weeks for 6

cycles) in hormone-receptor-negative breast cancer patients. The neoadjuvant therapeutic combinations where denosumab's added benefit is evaluated were: two different Paclitaxel regimens in combination with either Trastuzumab and Pertuzumab (for HER2+ patients) or Carboplatin (for TNBC patients), and a Epirubicin + Cyclophosphamide regimen (also combined with the HER2 inhibitors for HER2+ cases). However, the primary endpoint was not met, since denosumab had no effect on pathologic complete response (pCR) when given in combination with paclitaxel (Kummel et al., 2018).

## **RANK in colorectal cancer**

In contrast with the abundant information in breast cancer, the role of RANK in colorectal tumorigenesis has not been addressed yet. RANK mRNA and protein levels were reported to be variable between stage II colorectal cancer patients and between different areas of the same tumor, but no association was found with tumor relapse (Gröne et al., 2011). In a small study in patients with rectal cancer, RANK was found to be upregulated in tumor biopsies after receiving radiotherapy (Supiot et al., 2013). Inhibition of RANK in a modest study using a colorectal PDX model was reported to diminish tumor growth (Wei et al., 2017). Overall, studies of RANK pathway and clinical trials with denosumab (as treatment for skeletal afflictions) on colorectal cancer patients is scarce and anecdotal.

However, chronic inflammation is one of the early associated events leading to colorectal cancer (CRC) (Lasry et al., 2016) and NF $\kappa$ B pathway has been associated with colorectal tumorigenesis, as a mediator of colitis-associated CRC (CAC) (Greten et al., 2004; Schwitalla et al., 2013; Shaked et al., 2012). Constitutive NF $\kappa$ B activation through overexpression of IKK $\beta$  in intestinal epithelial cells caused the spontaneous appearance of adenomas without nuclear  $\beta$ -catenin in aged mice and accelerates tumor onset in APC<sup>min/+</sup> mice (Shaked et al., 2012). The mechanism involved upregulated iNOS expression which resulted in high levels of reactive nitric oxide (NO), which induced high levels of DNA damage (Shaked et al., 2012). Accordingly, IKK $\beta$  depletion results in partial prevention of adenoma formation in mice under the carcinogen + inflammation AOM/DSS tumorigenesis protocol by increasing epithelial apoptosis during early tumorigenesis (Greten et al., 2004). When depleted in the myeloid compartment using the LysM-cre transgene, IKK $\beta$  loss also resulted in attenuated adenoma number and size in the colon from AOM/DSS-treated mice by attenuation of pro-tumorigenic inflammatory cytokine expression (Greten et al., 2004). NF $\kappa$ B pathway has also been described to be activated in AOM-induced tumor models as a result of p53 loss (Schwitalla et al., 2013), which is one of the common sequential mutations

described during CRC development (Fearon, 2011). Importantly, simultaneous p53 and IKK $\beta$  genetic deletion after AOM treatment resulted in reduced adenoma invasiveness, further confirming the relevance of NF $\kappa$ B in colon tumorigenesis (Schwitalla et al., 2013).

Interestingly, RANK pathway has also proven to be critically involved in chronic intestinal inflammation, recognized as a driver of colon cancer (Ashcroft et al., 2003; Kanaya et al., 2018; Moschen et al., 2005). OPG knockout mice presented less severe symptoms under a colitis-induction protocol using dextran sulfate sodium (DSS), in terms of less body weight loss, colon length, stool score and splenomegaly. This effect might be due to the increased number of M cells present in the intestinal and colon epithelium from these mice, which in turn promote higher production of pathogen-neutralizing IgA (Kanaya et al., 2018). In agreement with this observation, RANK intestinal epithelia knockout and RANKL full-body knockout mice present less IgA production, derived from the impaired M cell development (Knoop et al., 2009; Rios et al., 2016). In agreement with the preclinical data, in a study with patients of Chron's disease or Ulcerative colitis, OPG serum levels were elevated as compared with controls, while RANKL levels were comparable (Moschen et al., 2005). Colonic explant cultures confirmed that OPG release was higher in tissues from patients compared with controls, thus proposing the colon as the source responsible for the OPG increase in circulation. Further analysis identified infiltrating macrophages and DCs as main sources of OPG (Moschen et al., 2005).

Therefore, RANK activation of NF $\kappa$ B pathway could be playing a role during colitis-associated CRC development and it would be worth exploring the role of RANK pathway in this setting.

## **Tumor Immunology**

The tumor microenvironment has been gaining attention over the years, as increasing evidence indicated that tumor cells often rely on their interactions with endothelial cells, fibroblasts and infiltrating immune cells to survive and proliferate. Recently, the field of oncoimmunology has become especially popular due to the remarkable success of cancer immunotherapies.

The immune system has been described to detect tumor cells early during the tumorigenic process. Mutations in proteins that give rise to aberrantly proliferative cells are sensed by the adaptive immune system. These mutated proteins (neoantigens) can be uptaken by APCs at affected tissues or in secondary lymphoid organs, where APCs ultimately migrate

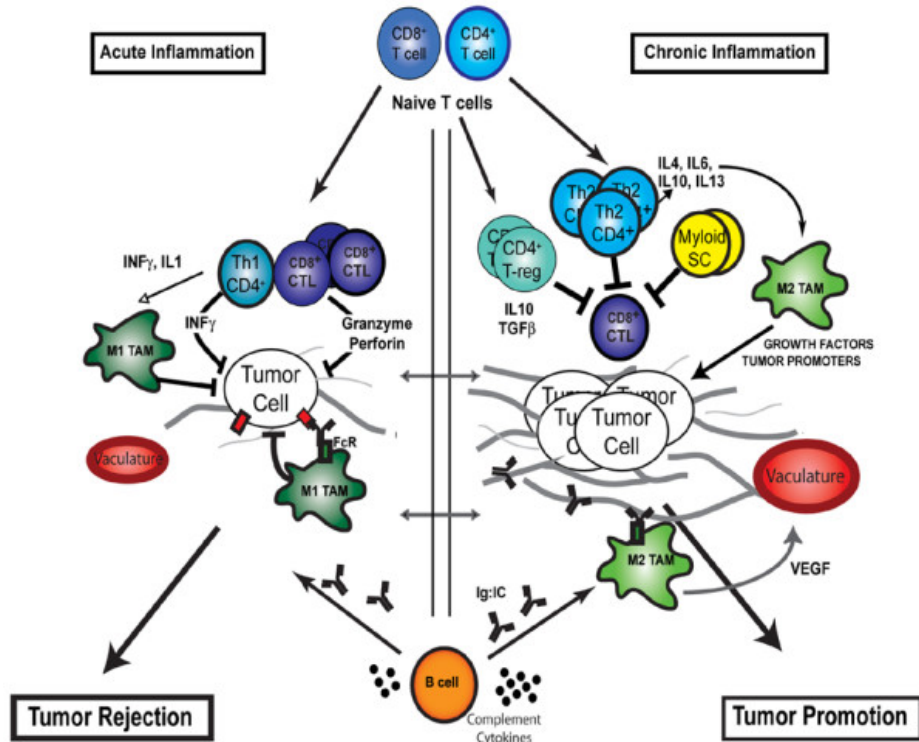
to present the antigen on MHC-II molecules to activate CD8 T cells, B cells and CD4 T cells, to trigger the immune response (Mardis, 2019; Vesely et al., 2011). All proteins within a cell, including neoantigens, are processed into peptides and loaded onto the cell's MHC-I molecules. MHC-I loaded with neoantigen peptides would then be exposed in the membrane of tumor cells and will be detected by the compatible TCR of a CD8 T cell. CD8 T cells previously activated by APCs will then release cytotoxic granules, killing the targeted tumor cell (**Figure 8**).

Indeed, tumors with higher mutational load generate more neoantigens, thus being more readily detected and cleared by the immune system (Germano et al., 2017; Mardis, 2019). Consequently, an impaired immune response has been reported to accelerate tumor onset on several models of tumorigenesis (Gross et al., 2017; Kaplan et al., 1998; Shankaran et al., 2001; Swann et al., 2008a).

This mechanism of mutation detection by the immune system acts as an evolutionary pressure on tumor cells. Immune cells thus shape the pool of tumor cells, progressively selecting the less immunogenic clones, which together with immune-suppressive mechanisms, will allow tumor cells to evade the immune surveillance and grow (Gonzalez et al., 2018; Gross et al., 2017; Shankaran et al., 2001). This process is called immunoediting, and its importance in tumor progression is patent when transplanting tumor cells growing in immunodeficient mice into an immunocompetent host. As compared with tumors transplanted from syngeneic hosts, tumors which had not been exposed to an active immune system fail or are less competent to grow, since the more immunogenic clones have not been yet eliminated (Gross et al., 2017; Shankaran et al., 2001).

The tumor cells which survive the initial elimination by immune cells are described to present several mechanisms to dampen an active immune response. Tumor cells may decrease their MHC-I antigen presentation by downregulating MHC-I itself or members of the antigen-presentation machinery. They have also been described to suppress the production of signals which prompt DC maturation or NK activation, or to upregulate anti-apoptotic proteins to avoid death signals. Tumor cells can also upregulate proteins such as PD-L1 or histocompatibility antigens G and E, which trigger immunosuppressive signals in T and NK cells (Gonzalez et al., 2018; Gross et al., 2017; Shankaran et al., 2001).





**Figure 8. Tumor interactions with immune populations.** During the first stages of tumorigenesis, immune surveillance will detect tumor neoantigens and build an immune response, with APCs (TAMs and DCs), triggering the activation of the adaptive immune response. B cells will mature and produce anti-tumor IgG, aiding macrophage phagocytosis. CD4 Th1 cells will secrete cytokines to further increase the secretion of cytotoxic granules by CD8 T cells, which target tumor cells presenting neoantigen peptides on their MHC-I. If the tumor is not rejected, the immune infiltrates will switch towards tumor-promoting phenotypes. Macrophages will limit their phagocytic ability and secrete angiogenic and growth factors, CD4 Treg and Th2 cells will be recruited, secreting immunosuppressive molecules which restrict TAM phagocytosis and CD8 T cell cytotoxic ability, thus establishing a local chronic inflammation which aids tumor growth. Figure from De Nardo D. *et al.*, 2007(DeNardo and Coussens, 2007).

An immunosuppressive environment can also be locally established by tumor cells and the infiltrating stroma. The tumor microenvironment can be enriched in molecules which impair DC antigen-presentation and migration abilities; cytokines, such as TGF $\beta$  and IL10, which polarize immune cells towards an immunoregulatory phenotype (Tregs or M2 macrophages); and even in enzymes which affect nutrient availability to avoid T cell proliferation, such as IDO. Additionally, secretion of molecules such as GM-CSF, IL-1 $\beta$ , vascular endothelial growth factor (VEGF), and prostaglandin E2 would increase the infiltration of monocytes and neutrophils, often referred to as myeloid-derived suppressor cells (MDSCs), into the tumor, which further contribute to establish an immunosuppressive, pro-tumorigenic environment (Figure 8) (Coffelt *et al.*, 2015; Vesely *et al.*, 2011).

Prostaglandin E2 has even been described to exclude antitumorigenic NK and professional APC from the tumor core (Böttcher et al., 2018).

Recruited Tregs have been shown to dampen T cell responses by engaging them with suppressive membrane proteins such as PDL-1, LAG-3, CD39/73 and CTLA-4 or through secretion of immunosuppressive molecules such as TGF $\beta$ , IL10, prostaglandin E2, adenosine, and galectin-1 (Figure 8) (Böttcher et al., 2018).

Monocytes, TAMs and neutrophils have been described to be highly pro-tumorigenic in advanced cancers, with higher TAM and neutrophil infiltration correlating with worse prognosis (Gonzalez et al., 2018). TAMs can remodel the extracellular matrix and stimulate neo-angiogenesis, promoting tumor cell extravasation and metastasis. They have also been described to secrete immunosuppressive molecules which limit DC maturation and T cell cytotoxic activity, and also promote tumor cell survival acting as source of growth factors such as EGF (Gonzalez et al., 2018). Although most myeloid populations have been described as pro-tumorigenic, monocytes and macrophages have very plastic phenotypes and different subsets can have anti-tumorigenic roles. For instance, patrolling monocytes have been described to greatly prevent lung metastasis in several tumor models. Upregulation of CX3CL1 by endothelial cells in the tumor extravasation sites acts as a chemoattractant for patrolling monocytes, which engulf tumor-derived particles and secrete molecules to recruit and activate NK cells (Hanna et al., 2015).

These mechanisms of tumor immune evasion result in the presence of abundant tumor immune infiltration without tumor resolution capacity, ultimately leading to chronic inflammation, which is one of the hallmarks of cancer (Hanahan et al., 2011), and is even essential for the development of certain tumors (Gonzalez et al., 2018; Swann et al., 2008b; Vesely et al., 2011). Inflammatory cells have been described to secrete factors which promote genomic instability, tumor proliferation and angiogenesis, which ultimately benefit tumor development (Hanahan and Coussens, 2012; Hanahan et al., 2011; Vesely et al., 2011). For instance, tumor-infiltrating immune cells have been reported to act as source of epidermal growth factor (EGF), TGF- $\beta$ , TNF- $\alpha$ , fibroblast growth factors (FGFs) and Vascular Endothelial Growth Factor (VEGF), which contribute to tumor growth and angiogenesis (Figure 8) (DeNardo and Coussens, 2007; Hanahan and Coussens, 2012). Also, TAMs have been described to promote adhesion-free survival and motility of metastatic cells by binding integrins in their surface and secreting proteases which remodel the extracellular matrix (Hanahan and Coussens, 2012).

Therefore, current immunotherapies focus on reactivating a suppressed immune activity or in diminishing the tumor-promoting inflammatory signals. The most successful of these approaches have been the immune-checkpoint inhibitors: humanized antibodies targeting the co-inhibitory signals of T cell activation triggered by CTLA-4 (Ipilimumab, Tremelimumab) and PD-1/PD-L1 (Pembrolizumab, Nivolumab, Cemiplimab or Atezolizumab, Avelumab, Durvalumab) molecules (Wei et al., 2018). The mechanisms of action of these proteins were discussed in the section about T cells above.

However, not all patients are benefiting from these immunotherapies and increasing efforts are being made to further understand tumor immunology, aiming to identify response biomarkers or to increase the therapeutic effects in unresponsive patients.

Tumors with a high mutational burden, such as melanoma and lung cancer, which are often developed due to DNA damage induced by UV-light or smoking respectively, present a high immune infiltration and better response to immunotherapy (Rizvi et al., 2015; Thorsson et al., 2018). Compared to melanoma and lung tumors, breast cancer has been traditionally considered “immune-cold” due to its lower immune infiltration (Gatti-Mays et al., 2019). However, a recent study with TCGA data aiming to identify immune subtypes across different tumors showed that breast tumors grouped into several of their cohorts, with none identifying as “immunologically quiet” (Gatti-Mays et al., 2019; Thorsson et al., 2018). The types of immune infiltration had variable proportions depending on the breast cancer subtype and were able to predict prognosis, with those tumors with an active adaptive immune response, enriched in Th1 genes and predominantly M1 phenotype in macrophages having the best prognosis (Thorsson et al., 2018).

Levels of tumor-infiltrating lymphocytes (TILs) have been extensively studied for their prognostic value (Salgado et al., 2015). TILs accumulate in stromal sections of the tumor and higher levels generally associate with better prognosis, in terms of disease-free and overall survival for HER2+ and TNBC (Denkert et al., 2018; Loi et al., 2019; Luen et al., 2017). However, there are differences when breast tumors are stratified by subtype. Surprisingly, a recent retrospective study identified reduced TILs with better overall survival in HER2-negative luminal tumors (Denkert et al., 2018). This highlights the differences between the immune microenvironment of different breast cancer subtypes also described in deconvolution analysis from TCGA gene expression data (Thorsson et al., 2018). In fact, TIL identification often relies on morphological differences assessed by pathologists without additional markers and thus, the type of lymphocyte is unknown. The importance of this

characterization is highlighted by the fact that higher Treg infiltration associate with poor prognosis in ER+ breast cancer patients (Bates et al., 2006; Liu et al., 2014), while correlating with better prognosis in the HER2+ patients, but only in the presence of CD8+ T cell infiltration (Liu et al., 2014). NK cells have also associated with increased overall and disease-free survival of HER2+ breast cancer patients (Muntasell et al., 2019).

It has been described that metastatic BC presents lower immune infiltration and markers of response to immunotherapy than early BC (Hutchinson et al., 2020; Szekely et al., 2018), which partly explains the rationale behind testing immunotherapy in clinical trials not only for heavily pre-treated BC patients, but also as the first therapeutic line (Franzoi et al., 2021). Most of these trials currently ongoing occur in the neoadjuvant setting and involve PD1 or PDL1 inhibition in combination with other therapeutic agents, with TNBC being the subtype with the highest representation (Franzoi et al., 2021), probably due to the lack of targeted therapies available. Additionally, TNBC are more commonly PDL1+ (Mittendorf et al., 2014) and present more TILs than other subtypes (Denkert et al., 2018). In fact PD-L1+ TNBC patients showed a significantly better response to anti-PDL1 monotherapy (Emens et al., 2019), and the combination of anti-PDL1 with chemotherapy in patients with these characteristics was approved due to clinically meaningful differences in OS (Emens et al., 2020). These results have been corroborated by other clinical trials with first line anti-PDL1 + chemotherapy combinations (Cortes et al., 2020; Franzoi et al., 2021). For HR+ BC, which commonly show lower expression of biomarkers associated with response to immunotherapy (tumor mutation burden, TILs and PDL1 expression), clinical trials are also combining PD1/PDL1 inhibition with chemotherapy. GIADA and I-SPY2 Phase II clinical trials have concluded that there might be an opportunity for these combinations in the first line neoadjuvant HR+ BC setting (Dieci et al., 2020; Yee et al., 2020) and clinical significance will be further evaluated in ongoing Phase III trials: Keynote756 ([NCT03725059](https://clinicaltrials.gov/ct2/show/study/NCT03725059)) and Checkmate7FL ([NCT04109066](https://clinicaltrials.gov/ct2/show/study/NCT04109066)) (Franzoi et al., 2021). Importantly, the line of therapy or tumor stage might be critical for the effectiveness of immunotherapy regimens, since trials in heavily pretreated patients show overall worse response to the selected combinations (Franzoi et al., 2021; Tolaney et al., 2020).

In conclusion, immune infiltration has been gaining special attention in basic research and in the clinic, even in tumors which were considered “immune-cold” in the past, such as breast cancer, where immunotherapy might still reach the effectivity observed for other solid tumors.

## **RANK in tumor immunology**

The abundant reports of the role of RANK pathway in several aspects of immune cell and immune organ function and development, combined with its importance in mammary gland biology and breast cancer, prompted the investigation of the pathway in the crosstalk between cancer cells and tumor immune infiltrates.

Tan W. *et al* described that Tregs were responsible of promoting breast tumor metastasis by activating RANK pathway in tumor cells (Tan et al., 2011). However, functional assays were performed with CD4 T cells positive for CD25, which is a marker of Tregs but also of general T cell activation. Therefore, results might be extended to activated CD4 T cells, which have been described to upregulate RANKL as compared with naïve stage (Bachmann et al., 1999; Josien et al., 1999; Wang et al., 2002; Wong et al., 1997a). Using a model of HER2+ breast cancer, the MMTV-ErbB2, loss of only one *Rank* allele resulted in less metastatic nodules in the lung, while RANKL treatment increased them. Silencing RANK or treating with RANK-Fc also greatly reduced lung metastasis in a transplant tumor model. RANKL promoted the survival of tumor cells *in vitro* and *in vivo*, and the main physiological source of RANKL in the tumor microenvironment was identified to be CD4 T cells. Importantly, lack of CD4 T cells (and not CD8 T cells) resulted in decreased lung metastasis. RANKL inoculation or transplant of CD4+CD25+ T cells rescued the metastatic potential of tumor cells, but RANK-Fc blocked this effect (Tan et al., 2011).

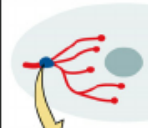
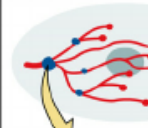
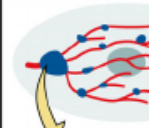
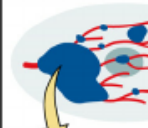
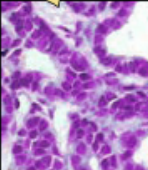
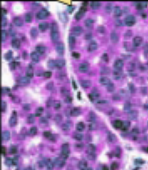
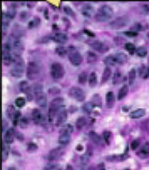
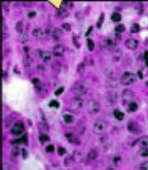
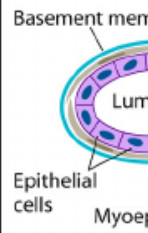
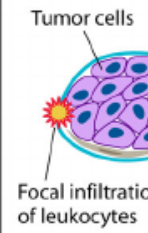

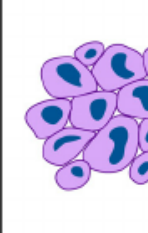
The combination of anti-RL treatments with immune checkpoint inhibitors, namely anti-PDL1, anti-PD1 or anti-CTLA-4, has been reported to diminish metastasis and tumor growth in several colorectal, prostate and melanoma cancer cell line transplantation models, as compared to immune checkpoint therapy alone (Ahern et al., 2017, 2018). The cell lines used in these studies are known to lack RANK expression, so the effects are likely due to systemic effects. The therapeutic effect of the triple combination of anti-CTLA-4, anti-PD1 and anti-RL is lost upon T cell or NK depletion and IFN $\gamma$  blockade (Ahern et al., 2018), but the studies did not compare these effects on tumors receiving immunotherapy alone. However, addition of anti-RL to anti-CTLA-4 + anti-PD1 treatments *in vivo* did prime tumor T cells to a stronger *in vitro* restimulation (Ahern et al., 2018). Indeed, the combination of anti-RL to anti-CTLA-4 in melanoma B16 cell line transplant models promoted a higher TIL infiltration, enriched in proliferating CD8 T cells which presented higher secretion of antitumorigenic cytokines such as IFN $\gamma$ , TNF $\alpha$  and IL-2 (Ahern et al., 2017).

Given these promising effects in tumor growth when combining immunotherapy with RANKL blockade, a Phase I clinical trial (POPCORN; ACTRN12618001121257) was recently initiated to explore the pharmacodynamic and therapeutic effects of combining denosumab to anti-PD1 therapy in NSCLC. Additionally, the CHARLI trial (NCT03161756) will evaluate the combination of denosumab with anti-PD1 (nivolumab) with or without the addition of anti-CTLA4 (ipilimumab) in melanoma. Clinical trials evaluating the immunomodulatory effects of denosumab in breast cancer have also been launched. D-BEYOND (NCT01864798), analyzed paired biopsy and surgery samples of premenopausal breast cancer patients which received denosumab between the two interventions. The trial was terminated due to poor recruitment, but the observations derived from data collected from the 27 patients which enrolled will be discussed in the results section. Our own group has an ongoing clinical trial, D-BIOMARK (NCT03691311), where the effects of denosumab are explored in a similar setting, but also including postmenopausal patients. PERIDENO (NCT03532087) was a clinical trial also designed to explore the effects of denosumab in the immune system of HER2- breast cancer patients, but it was recently withdrawn.

## **MMTV-PyMT as a model for breast cancer tumor immunology**

The MMTV\_PyMT transgenic mice, used in this doctoral thesis as breast cancer model, rely on the mammary-gland-specific overexpression of the polyomavirus middle T antigen (PyMT) oncogene. The expression of PyMT is driven by a promoter from the mouse mammary tumor virus (MMTV), whose activation is triggered by glucocorticoids and pregnancy hormones like progesterone and is thus mainly active in the mammary epithelium (Günzburg and Salmons, 1992; Guy et al., 1992). The PyMT activates several members of the tyrosine kinase pathway by binding Protein phosphatase 2A (PP2A), members from the c-Src and the ShcA families, PI3K and PLC- $\gamma$  (Fluck and Schaffhausen, 2009). However, the high variability in the development of lesions within the mammary gland epithelia suggests that the tumorigenesis process driven by this oncogene relies on additional context-dependent events (Fluck and Schaffhausen, 2009). This model is considered a Luminal breast cancer tumor model, based on molecular and histological analyses. However, broad transcriptional analysis comparing MMTV\_PyMT tumors with samples from the TCGA database showed that the mouse model mirrors the heterogeneity of human breast tumors. Different MMTV\_PyMT tumor groups

clustered with basal breast cancer, Her2-enriched, or with each other (Rennhack et al., 2019). The genetic alterations were significantly lower in the mouse model as compared to the human tumors. Interestingly, mutations in *Ptprh* gene (a suppressor of EGFR phosphorylation) were found in 80% of the tumors (Rennhack et al., 2019).

Stage	Hyperplasia	Adenoma/MIN	Early carcinoma	Late carcinoma
Gross				
H&E				
Cellular morphology				
Biomarkers	ER++ PR+ Neu (T/D) ~ 1 Cyclin D1 + Integrin β ±	ER+++ PR++ Neu (T/D) ↑ Cyclin D1 + Integrin β ±	ER++ PR± Neu (T/D) ↑↑ Cyclin D1 ++ Integrin β -	ER± PR- Neu (T/D) ↑↑↑ Cyclin D1 +++ Integrin β -

**Figure 9. MMTV-PyMT mouse model tumor progression (FVB genetic background).** Table summarizing the gradual stages of tumorigenesis observed in the MMTV-PyMT multifocal mammary gland tumor model. Including histological markers, tissue and cellular morphology. Figure from Fluck M. M. and Schaffhausen B. S., 2009(Fluck and Schaffhausen, 2009).

Tumor onset in MMTV\_PyMT transgenic mice is highly dependent on the genetic background (Davie et al., 2007), with neoplasias appearing as early as 4-5 weeks of age and tumors palpable at 7 weeks of age in mice with pure FVB or C3H/B6 × FVB mixed background (Davie et al., 2007; Guy et al., 1992; Lin et al., 2003; Maglione et al., 2001) and palpable tumors being detected at 13-14 weeks in mice with C57/BI6 background (Davie et al., 2007; Gross et al., 2017; Yoldi et al., 2016). Regardless of the latency to tumor onset, expression of PyMT leads to a gradual transformation of the mammary gland epithelia, similar to that observed in human breast cancer. An increase in proliferation causes the formation of early hyperplastic lesions, which evolve into adenomas/mammary intraepithelial neoplasias (MINs), leading to noninvasive focal lesions and ultimately to carcinomas which

can give rise to lung metastasis (Figure 9) (Guy et al., 1992; Lin et al., 2003; Yoldi et al., 2016).

Epithelial expression of progesterone and estrogen receptor (PR and ER) is higher in the adenomas, and gets gradually lost during tumor progression (Lin et al., 2003; Maglione et al., 2001; Yoldi et al., 2016), while HER2 expression has been described to be maintained high throughout all stages at the transformed epithelia (Lin et al., 2003). RANK expression peaks during the earlier stages of tumorigenesis and then maintained high during the carcinoma stages. Epithelial RANKL is lost at the carcinoma stage (Yoldi et al., 2016). Basal cells (SMA+ or K14+) are gradually reduced and carcinomas are mostly formed by K8+ luminal cells (Maglione et al., 2001; Yoldi et al., 2016).

The effects of the anti-tumor immune response in this genetic model have been investigated both in FVB/NJ and C57/Bl6 genetic background. Interestingly, the fast growing MMTV\_PyMT primary tumors in the FVB-NJ background were unaffected by loss of B and T cell activity by genetic or pharmacological methods (DeNardo et al., 2009; Gross et al., 2017). However, in the slower-growing tumors in the C57/Bl6 background, the same approaches accelerated tumor onset, and further studies with tumor transplants suggested that slower-growth allows tumors to be detected and affected by the immune system (Gross et al., 2017).

Interestingly, using a combination of genetic and pharmacological depletion of key immune populations in the FVB/NJ MMTV\_PyMT tumor model, DeNardo *et al.* identified that CD4 T cells infiltrating these tumors have a Th2-like phenotype. The IL-4 secreted by these T cells maintains TAMs in a pro-tumorigenic state. TAMs then support migration and survival of epithelial tumor cells, increasing the lung metastatic burden (DeNardo and Coussens, 2007). Indeed, studies blocking macrophage/monocyte infiltration through colony stimulating factor 1 receptor (CSF1R), CSF1R pharmacological inhibition or CSF1 genetic loss showed that lung metastasis are inhibited in the absence of these cell populations in the primary tumor (Lin et al., 2001; Lohela et al., 2014). TAMs and monocytes have been described to promote lung metastasis by the secretion of survival proteins such as EGF (DeNardo and Coussens, 2007), by presenting MMPs activity remodeling the extracellular matrix (Lohela et al., 2014) and by aiding extravasation in the lungs, being recruited by CCL2(Qian et al., 2011). Neutrophils have also been described to play a key role in MMTV\_PyMT models, where neutrophil abundance in bone marrow, blood and spleen is greatly increased compared to wildtype mice (Wculek and Malanchi, 2015). Neutrophil production in the bone marrow is



exacerbated and neutrophils infiltrate early into the lung premetastatic niche (Casbon et al., 2015; Wculek and Malanchi, 2015). Neutrophils have been described to secrete several factors which contribute to induce a pro-metastatic phenotype in MMTV\_PyMT tumor cells (Wculek and Malanchi, 2015). Additionally, neutrophils in MMTV\_PyMT models present an immunosuppressive phenotype driven by tumor-derived G-CSF, which allows them to strongly inhibit T cell proliferation *in vitro* through the high production of reactive oxygen species (ROS) (Casbon et al., 2015). However, contradicting reports have been published using MMTV\_PyMT tumor models and murine and human breast cancer cell lines, where depletion of neutrophils diminishes primary tumor growth and metastatic load due to their high cytotoxicity against tumor cells (Granot et al., 2011). These results were corroborated with neutrophils extracted from breast cancer patients (Granot et al., 2011). Therefore, the plasticity of neutrophils might allow them to switch between different phenotypes, playing different roles during tumorigenesis, in a time- and context-dependent manner.

DC populations have also been described to play a role in the MMTV\_PyMT model. In the primary tumor microenvironment, most of the immune cells which uptake tumor antigens are CD11c+Gr1- and F4/80+MHCII<sup>hi</sup>, corresponding to DC and TAM populations respectively (Engelhardt et al., 2012). *In vivo* imaging revealed that tumor antigen uptake by CD11c+ cells happens preferably in tumor margins and that interaction with T cells is longer and more frequent in that location (Engelhardt et al., 2012). This observation might be limited by the technique, which might fail to detect populations deeper within the tumor, but exclusion of anti-tumorigenic populations has indeed been described as a key immunosuppressive mechanism (Böttcher et al., 2018). DCs have the strongest ability to cross-present tumor neoantigens and activate naïve T cells, but only a subset of phagocytic, mature, CD103+ DCs is able to re-stimulate a previously activated T cell *in vitro* (Broz et al., 2014; Engelhardt et al., 2012).

These numerous reports highlight the suitability of the MMTV\_PyMT model to study breast cancer and the interaction of tumor cells with the immune system.



# **OBJECTIVES**



The overall objectives of this doctoral thesis are:

**1. To Investigate RANK pathway in immune-tumor crosstalk**

- 1.1 Functionally characterize changes in tumor immune infiltration upon RANK loss using genetic models.
- 1.2 Identify mechanisms by which RANK influences tumor immune infiltrates.
- 1.3 Investigate the therapeutic effects of RL inhibition, with a special focus in its immunomodulatory effects.

**2. To determine the role of RANK pathway in the Intestine/Colon epithelium**

- 1.4 Determine whether RANK is implicated in intestinal homeostasis, with special focus on the stem cell compartment.
- 1.5 Evaluate the role of intestinal RANK expression during inflammation-driven tumorigenesis.



# **METHODS**



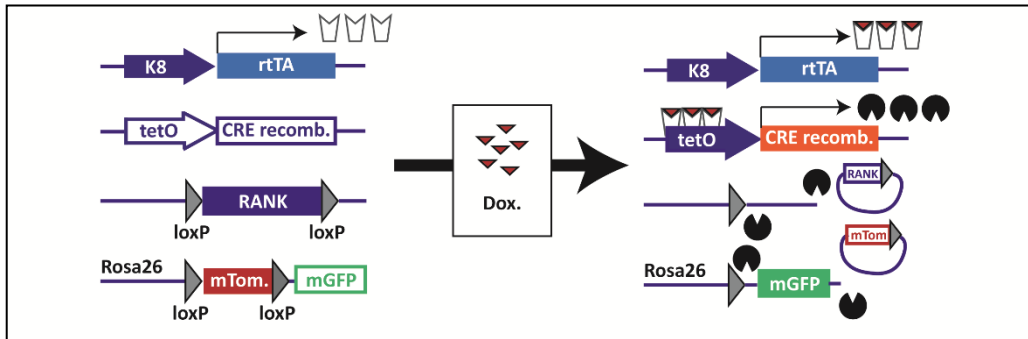


## **Mouse transgenic models**

All research involving animals was performed at the IDIBELL animal facility in compliance with protocols approved by the IDIBELL Committee on Animal Care and following national and European Union regulations. Mice were kept in individually ventilated and open cages and food and water were provided ad libitum.

The athymic nude *Foxn1<sup>nu</sup>* mice were obtained from Envigo. Nod.Scid (NOD.CB17-Prkdc<sup>scid</sup>/NCrHsdNSG) and NSG<sup>TM</sup> (NOD.Cg-Prkdcscid; Il2rgtm1Wjl/SzJ) immunodeficient mice are bred at IDIBELL's animal facility. MMTV-PyMT (FVB/N-Tg(MMTV-PyVT)634Mul) were acquired from the Jackson Laboratory (Guy et al., 1992), and RANK+/- (C57Bl/6) mice from Amgen Inc (Dougall et al., 1999a). MMTV-PyMT-/+; RANK-/- mice were obtained by backcrossing the MMTV-PyMT (FvB/N) strain with RANK+/- mice into the C57Bl/6 background for at least ten generations. RANK<sup>fllox/fllox</sup> mice (MGI: 4415802) in C57Bl/6 background were provided by Dr. J. Penninger (Hanada et al., 2009). When the cre-recombinase is active in RANK<sup>fllox/fllox</sup> mice, the loxP-flanked *Tnfrsf11a* exon 2 and 3 are excised resulting on a frame shift which leads to a premature stop codon. LysM-cre mice (MGI: 1934631) and Villin-cre mice (MGI: 3053819) in C57Bl/6 were received from A. Nebreda. Villin-cre mice present a single transgene copy consisting of a 9 kB regulatory region from the *Villin* promoter followed by the cre recombinase coding sequence. K8-rtTA (Watson et al., 2015) and TetOCre (Perl et al., 2002) mice in mixed background were donated by C. Blanpain's group and ROSA26-mTmG mice (MGI: 3716464) were obtained from M. Graupera. K8-rtTA mice present transgene constructs with a fraction of murine cytokeratin 8 (K8) promoter followed by the reverse tetracycline transactivator (rtTA) (Watson et al., 2015). TetOCre mice present transgenes with cre recombinase under TetO promoter sequences. When doxycycline (dox) is administered, it binds rtTA, allowing it to bind to the TetO promoter (Perl et al., 2002), thus inducing cre recombinase activity in K8+ cells. ROSA26-mTmG mice (mTmG) have a knock-in transgene on the Rosa26 locus, consisting of a CMV enhancer/chicken beta-actin core promoter (pCA), which drives the expression of membrane tdTomato. tdTomato sequence is flanked by loxP sites and immediately followed by a membrane-tagged, enhanced green fluorescent protein (EGFP) sequence. The ROSA26-mTmG construct serves thus as a fluorescent reporter for cre recombinase activity. When crossed with RANK<sup>fllox/fllox</sup> mice, dox administration in K8-rtTA: TetOCre: RANK<sup>fllox/fllox</sup>: mTmG mice induces a switch from tdTomato to EGFP expression together with *Rank* depletion in K8+ tissues (see Figure 10). These mice were additionally crossed with MMTV-

PyMT transgenic mice (hereafter referred to as  $RANK^{\Delta K8}$ ) to obtain a luminal tumor model with inducible RANK depletion.



**Figure 10. Scheme showing inducible depletion of RANK in the  $RANK^{\Delta K8}$  model.** K8-rtTA transgene expresses rtTA under the control of a K8 promoter fragment (luminal cell marker). When dox is administered, it binds rtTA, allowing it to activate the tetO promoter, leading to Cre-recombinase expression. Cre recombinase deletes exons 2-3 from *rank* gene, resulting in a reading frame shift and the appearance of a premature stop codon. Additionally, the model includes the mTom reporter in the Rosa26 locus. All cells will express membrane tdTomato which after the action of recombinase will be excised switching the expression to membrane EGFP.

## Mouse treatments

Therapeutic anti-RANKL (clone IK22/5), anti-CTLA4 (clone 9D9), anti-PD-L1 (clone 10F.9G2) and isotype control rat IgG2A (clone 2A3) and mouse IgG2b (clone MCP-11) were obtained from BioXCell and 200  $\mu$ g were administered intraperitoneally twice per week, for treatments starting 72 h after tumor cell injection, or three times per week for treatments of established tumors (size > 0.09 cm<sup>2</sup>). For depletion experiments, anti-CD8 (300  $\mu$ g, clone 53-5.8), anti-NK1.1 (200  $\mu$ g, clone PK136), anti-Ly6G (first injection 400  $\mu$ g, 100  $\mu$ g thereafter, clone 1A8), and isotype controls mouse IgG2a (clone C1.18.4) and rat IgG1 (clone TNP6A7) were injected intraperitoneally. Treatment was administered on days -1, 0, 3, and 7 after tumor cell injection, and then once per week until sacrifice for CD8 and NK depletion. For neutrophil depletion, anti-Ly6G was injected on day -1 and thereafter, three times weekly. In all cases, mice were sacrificed before tumors exceeded 10 mm in any dimension. Euthanasia by CO<sub>2</sub> inhalation was performed. Blood samples were taken for flow cytometry analyses to check the depletion 7-10 days and 14-20 days after the first injection.

RANK depletion in K8-PyMT mice was induced by administering 10mg/ml doxycycline in drinking water, together with 2% sucrose to reduce sourness, for four weeks. Depletion was induced “early” during tumorigenesis (when tumors no larger than 3x3 mm were palpated) or “late” (when at least one tumor had reached 5x5 mm). Mice which lacked one of the

transgenes necessary for full RANK depletion treated with doxycycline were used as controls. Mice were euthanized by CO<sub>2</sub> inhalation once a tumor exceeded 10x10 mm dimensions.

To induce colorectal tumors, the carcinogen azoxymethane (AOM; A5486, Sigma) was injected intraperitoneally at 10 mg/kg in 8-10 weeks old Villin-cre RANK<sup>flox/flox</sup> mice and control littermates. Five days after, 3% Dextran Sodium Sulfate (DSS; 160110, MP Biochemicals) was delivered through drinking water for five days, followed by 14 days of recovery with pure drinking water. After three cycles of DSS + recovery, mice are kept for 63 additional days to allow tumors to form. Mice are thus euthanized 120 days after the AOM injection. Mouse weight loss is monitored during the duration of the experiment every 2-3 days.

## **Tissue collection and processing**

Tissue pieces are snap-frozen freshly upon collection and stored at -80 °C for further analysis. For histological samples, tissue is fixed over-night in 37% formaldehyde or for 6 h in 4% paraformaldehyde at 4 °C. Samples are then gradually dehydrated by subsequent immersion in 70, 80, 96 and 100% ethanol, followed by 1 h incubation in xylol to be finally embedded in paraffin.

Blood is collected by intracardiac puncture at endpoint or from the submandibular vein by cheek punch at experimental midpoints.

## **Mouse tumor-cell isolation, tumor-initiation assays and *in vitro* culture**

Draining lymph nodes were removed and fresh tissues were mechanically dissected with a McIlwain tissue chopper and enzymatically digested with appropriate medium (DMEM F-12, 0.3% collagenase A, 2.5 U/mL dispase, 20 mM HEPES and antibiotics) for 40 min at 37°C. Samples were washed with Leibowitz L15 medium containing 10% fetal bovine serum (FBS) between each step. Erythrocytes were eliminated by treating samples with hypotonic lysis buffer (Lonza Iberica). Single cells were isolated by treating with trypsin (PAA Laboratories) for 2 min at 37°C. Cell aggregates were removed by filtering the cell suspension with a 70-µm filter and counted. For orthotopic transplants and tumor-limiting dilution assays tumor cells isolated from MMTV-PyMT;RANK<sup>+/+</sup> (C57BL/6) or MMTV-PyMT;RANK<sup>-/-</sup> (C57BL/6) mice were mixed 1:1 with Matrigel matrix (BD Biosciences) and orthotopically implanted in

the inguinal mammary gland of 6-12-week-old syngeneic females or immunodeficient *Foxn1<sup>nu</sup>*, NSG or Nod.Scid females. Mammary tumor growth was monitored by palpation and caliper measurements three times per week. Lymph nodes were treated with hypotonic lysis buffer and then mashed through a 70- $\mu$ m cell strainer to isolate single cells.

For *in vitro* assays, isolated tumor cells were either seeded in 3D, on top of growth factor-reduced matrigel (1 million cells/well in 6-well plates) in growth medium (DMEM-F12, 5% FBS, 10 ng/mL of EGF, 100 ng/mL cholera toxin, 5  $\mu$ g/mL insulin and 1x penicillin/streptomycin); or plated in 2D in DMEM-F12 containing 1x Insulin-transferrin-sodium selenite media supplement (ITS, I3146, Sigma), and 1x penicillin/streptomycin.

For RANK depletion in the MMTV-PyMT-/+ RANK<sup>fl/fl</sup> tumors, cells were plated *in vitro* and infected with lentivirus produced in HEK293T cells. Lentiviral packaging plasmids psPAX2 (Adgene, 12260) and pMD2.G (Adgene, 12259), with either control pLVX-IRES-ZsGreen1 vector (Adgene, 632187) or pLVX-Cre-IRES-ZsGreen1, kindly provided by Dr. Alejandro Vaquero, were used, following Adgene's recommended protocol for lentiviral production. Tumor cells were cultured for 16 hours with 1:3 virus-containing medium and 72 h later, infected cells were FACS-sorted for ZsGreen expression before being injected into syngeneic hosts.

## **Mouse intestinal organoid purification and *in vitro* culture**

A proximal small intestine section is longitudinally opened, villi are scraped gently with a razor and the remaining tissue is digested for 5 min on ice in 5 mM EDTA/HBSS. After vigorous shaking, the tissue is washed with PBS to remove remaining villi and incubated for 15 min in 5 mM EDTA/HBSS in ice. After vigorous shaking, the remaining tissue piece is discarded and crypts in suspension are centrifuged and resuspended in PBS to be passed through a 70  $\mu$ m filter. Crypts are counted and resuspended in an appropriate volume of growth factor-reduced Matrigel which is allowed to solidify for 20 min before adding organoid culture medium. The medium consists of DMEM-F12 (L0093-500, Biowest) supplemented with 1x Glutamax, non-essential amino acids, Sodium Pyruvate, Glutamax<sup>TM</sup> (35050-061, Life Technologies), B27 (17504044, Life Technologies) and Normocin (ANT-NR-1, Nucliber), all diluted to 1; and 0.05 ng/ml EGF (E9644, Sigma), 0.1 mg/ul Noggin (250-38, PreproTech), 0.5 ng/ml RSPO1 (120-38, PeproTech) and 10  $\mu$ M Rock inhibitor (HY-10583, MedChem Express).

Medium was refreshed every 2-3 days. When specified, RL is added to the medium at either 100 or 1000 ng/ml and WNT3a (315-20, PeproTech) is added at 100 ng/ml. For downstream analysis or organoid passage, Matrisperse (354253, Corning) was used to dissolve Matrigel following manufacturer's instructions.

## **Flow cytometry**

Single cells from tumors or lymph nodes were resuspended and blocked with PBS 2% FBS and blocked with FcR blocking reagent (Mylteni Biotec) for 10 min on ice and incubated for 30 min on ice with the corresponding surface antibodies: CD45-APCCy7 (0.125 µg/mL; 30-F11), CD11b-APC (2.5 µg/mL; M1/70), CD11b-PECy7 (2.5 µg/mL; M1/70), CD8-PE (1 µg/mL; 53-6.7), CD8-FITC (8 µg/mL; 53-6.7), CD4-PE-Cy7 (2 µg/mL; RM4-5), CD25-APC (2 µg/mL; PC61), Ly6C-FITC (1.25 µg/mL; HK1.4), Gr1-FITC (2 µg/mL; RB6-8C5), Ly6G-PECy7 (1.25 µg/mL; 1A8), F4/80-PE (1.25 µg/mL; BM8), CD3-PerCPCy5.5 (3.2 µg/mL; 145-2C11), CD3-APC (3.2 µg/mL; 145-2C11), Siglec-F- PerCP-Cy™5.5 (4 µg/mL, E50-2440), CD19-PE (2.5 µg/mL, 6D5), NK1.1-PE (2.5 µg/mL; PK136), PD-1-PE (10 µg/mL; 29F.1A12), PD-L1-PECy7 (1.25 µg/mL; 10F.9G2) and anti-human CD11b-PECy7 (0.8 µg/mL; M1/70) from BioLegend. Apoptosis and necrosis were evaluated using the Annexin AV Apoptosis Detection Kit (640930, BioLegend). 7AAD or LIVE/DEAD™ Fixable Green Dead Cell Stain Kit (488nm) from ThermoFisher was added in the various antibody combinations to remove dead cells. The following antibodies were used for intracellular staining: IFNγ-PE (2 µg/mL; XMG1.2); CTLA4-PerCPCy5.5 (10 µg/mL; UC10-4B9), CTLA4-PECy7 (5 µg/mL; UC10-4B9) from BioLegend, and FOXP3-FITC (10 µg/mL; FJK-16s), IL-12-FITC (2 µg/mL; C17.8) from eBioscience. Single-cell suspensions were stimulated in Leibowitz L15 medium containing 10% FBS, 10 ng/mL PMA, 1 µg/mL ionomycin and 5 µg/mL brefeldin A (for IFNγ and CTLA4) or just 5 µg/mL brefeldin A (for IL-12) for 4 h at 37°C. Surface antibodies were stained first, then fixed with PFA 4% (in the case of cytokines) or Fixation Reagent of the Foxp3/Transcription Factor Staining Buffer Set from eBioscience (in the case of FOXP3), and permeabilized using Permeabilization Buffer of the Foxp3/Transcription Factor Staining Buffer Set from eBioscience. The intracellular proteins were then stained. FACS analysis was performed using FACS Canto and Diva software. Cells were sorted using MoFlo (Beckman Coulter) at 25 psi with a 100-µm tip.

Blood samples were collected in tubes containing heparin and stained with CD45-APC-Cy7 (0.125 µg/mL; 30-F11), CD11b-APC (2.5 µg/mL; M1/70), CD3-PerCPCy5.5 (3.2 µg/mL; 145-2C11), CD8-PE (1 µg/mL; 53-6.7), NK1.1-PE (2.5 µg/mL; PK136), Ly6G-PECy7 (1.25

µg/mL; 1A8) and Gr1-FITC (2 µg/mL; RB6-8C5) for 30 min at RT in the dark. Versalyse (Beckman Coulter) containing 0.1% paraformaldehyde (PFA) was added to the samples and incubated for 10 min at RT in the dark before passing them through the cytometer.

## **Immunostaining in mouse tumor tissues**

3-µm sections were cut for histological analysis and stained with hematoxylin and eosin. Masson's and Alcian blue + Nuclear fast red stainings were performed at the Pathology Department of Bellvitge's Hospital.

3-µm tissue sections were used for immunostaining. Samples were deparaffinized with xylol and gradually rehydrated in descending ethanol concentrations. Antigen pressure-heat retrieval with citrate buffer (pH 6) in a pressure cooker for 20 minutes was routinely used. RANK and RL staining require alternative antigen retrieval. For RANK detection 5-minute treatment with Protease type XXIV (P8038, Sigma) was used, and for RL detection, pressure-heat retrieval was limited to 2 min at maximum pressure, followed by 5 min incubation with Pronase (P8811, Sigma). Primary antibody incubation was performed at 4°C over-night and 0.01% Tween/PBS was employed for washes between steps. A list of primary and secondary antibodies is provided at Methods Tables 1 and 2, below.

Primary Antibody	Concentration	Reference
Goat anti-mRANK	1:200	AF692, R&D
Goat anti-mRL	1:200	AF462, R&D
Rabbit anti-ki67	1:500	RM9106S1, Thermo Scientific
Rat anti-Keratin 8	1:200	DSHB, TROMA
Rabbit anti-Keratin 14	1:500	PRB-155P, Covance
Chicken anti-GFP	1:1000	AB13970, Abcam
Mouse anti-β Catenin	1:150	610154, Becton Dickinson

Methods Table 1. Primary antibodies employed.

Immunohistochemistry		Immunofluorescence	
Antibody	Reference	Antibody	Reference
Donkey anti-chicken	703-065-155, Jackson ImmunoResearch	Donkey anti-chicken A647	703-605-155, Jackson ImmunoResearch
Goat anti-rat	BA-9400, VECTOR	Goat anti-rat A546	A11081, Life Technologies
Goat anti-rabbit	BA-1000, VECTOR	Donkey anti-rabbit A488	A31556, Life Technologies
Goat anti-mouse	BA-9200, VECTOR		
Horse anti-goat	BA-9500, VECTOR		

Methods Table 2. Secondary antibodies employed.

For immunohistochemical detection, endogenous peroxidase was blocked with 3% hydrogen peroxide (EMD Millipore), avidin and biotin were blocked using DAKO's commercial kit (X0590) and protein block was performed with 5% donkey, goat or horse serum, depending on the source of the secondary antibody, for 40 min at room temperature. Biotinylated secondary antibodies were added at a 1:1000 concentration for 1 hour at RT and were detected with streptavidin horseradish peroxidase kit (Vector) and DAB substrate (DAKO). Slides were counterstained with hematoxylin.

For immunofluorescence, protein was blocked using 1% bovine serum albumin (BSA), 5% donkey serum, 0.1% TritonX. Fluorochrome-tagged secondary antibodies were used at a 1:400 concentration for 1 hour at RT. DAPI was added 1:1000 to stain nuclei. A list of primary and secondary antibodies is provided at Methods Tables 1 and 2, above.

CD3, FoxP3 and CD8 immunostaining was performed in the Histopathology Core Unit of the Spanish National Cancer Research Centre (CNIO, Madrid, Spain), using antibodies CD3 (clone M20 from Santa Cruz Biotechnology), CD8 (clone 94A from the Monoclonal Antibodies Core Unit of the CNIO) and FoxP3 (clone 221D from the Monoclonal Antibodies Core Unit of the CNIO).

## **Real-time PCR**

Total RNA was extracted with Tripure Isolation Reagent (Roche) or Maxwell RSC Simply RNA Tissue kit (AS1340, Promega). Frozen tissues were fractionated using glass beads

(Sigma-Aldrich) and the Precellys® 24 tissue homogenizer (Berting Technologies) and Polytron PT 1200e (Kinematica). cDNA was produced by reverse transcription using 1 µg of RNA in a 35-µL reaction with random hexamers following the kit instructions (Applied Biosystems).

<b>Gene</b>	<b>Forward Primer</b>	<b>Reverse Primer</b>
<i>Hprt1</i>	TCAGTCAACGGGGGACATAAA	GGGGCTGTACTGCTTAACCAG
<i>Rank</i>	AGAGGCATTATGAGCATCTCG	CAGACTTTATGCAGCAAGCA
<i>Rl</i>	CCCACAATGTGTTGCAGTTC	TCCTGAGACTCCATGAAAACG
<i>Spib</i>	CGTCTTCCAGTTCTCCTCCA	GGTGAGTTTGCGTTTGACCT
<i>Axin2</i>	TTCTGTGCTGTCCCAGTGAG	TGAAGAAAACCCCTTGTGCT
<i>Lgr5</i>	AGCAGACTACGCCTTTGGAA	TCCCAGGGAGTGGATTCTATTA
<i>Lgr4</i>	GGACTTGAATTATAATAACTTGG ATGA	TACAAATGGATAGTTCTTAGCAG TGG
<i>Opg</i>	GAGACACAGCTCACAAGAGCAA	GCTTTCACAGAGGTCAATGTCTT
<i>Trail</i>	ATGGAGAGCTGGTCATCGAG	ATGAGCACTATGGGATCCGG
<i>Icam1</i>	AAGATGACCTGCAGACGGAA	ATAAGAGGCTGCCATCACGA
<i>E-cadherin</i>	AGAGAAGCCATTGCCAAGTAC	AACGAATCCCTCAAAGACCG
<i>Nos2</i>	TTCTGTGCTGTCCCAGTGAG	TGAAGAAAACCCCTTGTGCT
<i>Vimentin</i>	CATTGAGATCGCCACCTACAG	AGGAGTGTTCTTTTGGAGTGG
<i>Gp2</i>	TGACTGTTGATGTGGACGGA	GTGGCATAGCAGTTGGTCAG
<i>Prf1</i>	CTGGATGTGAACCCTAGGCC	GCGAAAACCTGTACATGCGAC
<i>Ifny</i>	CACGGCACAGTCATTGAAAG	CCATCCTTTTGCCAGTTCCTC
<i>Il-1β</i>	CAACCAACAAGTGATATTCTCCA TG	GATCCACACTCTCCAGCTGCA
<i>Casp4</i>	AATTGCCACTGTCCAGGTCT	CTCTGCACAACCTGGGGTTTT
<i>S100a9</i>	TCAGACAAATGGTGGGAAGCA	GTCCTGGTTTGTGTCCAGGT

Methods Table 3. Primer sequences for murine genes detected by RT-qPCR.

<b>Gene</b>	<b>Forward primer</b>	<b>Reverse primer</b>
<i>PPIA</i>	GGGCCTGGATACCAAGAAGT	TCTGCTGTCTTTGGGACCTT
<i>BIRC3</i>	GGTAACAGTGATGATGTCAAATG	TAAGTGGCTTGAACCTGACG
<i>ICAM1</i>	AACTGACACCTTTGTTAGCCACCTC	CCCAGTGAAATGCAAACAGGAC
<i>NFκB2</i>	GGCGGGCGTCTAAAATTCTG	TCCAGACCTGGGTTGTAGCA
<i>RELB</i>	TGTGGTGAGGATCTGCTTCCAG	TCGGCAAATCCGCAGCTCTGAT

Methods Table 4. Primer sequences for human genes detected by RT-qPCR.

In the case of sorted cells, RNA was retrotranscribed with Superscript II Reverse Transcriptase in a 20-µL reaction carried out according to manufacturer's instructions (ThermoFisher). 20 ng/well of cDNA for whole tumors were analyzed by SYBR green real-



time PCR with 10- $\mu$ M primers using a LightCycler® 480 thermocycler (Roche). Analyses were performed in triplicate. *Hprt1* was used as the reference gene. The following primer sequences used for each gene are listed at the Methods Tables 3 and 4 above.

## **Mouse RNA labeling and hybridization to Agilent microarrays**

Hybridization to the SurePrint G3 Mouse Gene Expression Microarray (ID G4852A, Agilent Technologies) was conducted following the manufacturer's two-color protocol (Two-Color Microarray-Based Gene Expression Analysis v. 6.5, Agilent Technologies). Dye swaps (Cy3 and Cy5) were performed on RNA amplified from each sample. Microarray chips were then washed and immediately scanned using a DNA Microarray Scanner (Model G2505C, Agilent Technologies).

## **RNA sequencing**

Tumor cell populations (CD45-CD31-CD24+), CD8 T cells (CD8+CD3+CD11b-CD45+) and CD4 T cells (CD8+CD3+CD11b-CD45+) were FACs-sorted from RANK+/+ or RANK-/- tumor transplants and RNA extracted with RNAeasy micro and mini kits (Qiagen, 74004) on the same day following manufacturer's protocol.

Raw sequencing reads in the fastq files were mapped with STAR version 2.6.1b (Dobin et al., 2013) to the Gencode release 17 based on the GRCm38.p6 reference genome and the corresponding GTF file. The table of counts was obtained with FeatureCounts function in the package subread, version 1.5 (Liao et al., 2014). The differential expression gene analysis (DEG) was assessed with voom+limma in the limma package version 3.40.6 (Liao et al., 2014) and R version 3.6.0. Gene having less than 10 counts in at least 3 samples were excluded from the analysis. Raw library size differences between samples were treated with the weighted "trimmed mean method" TMM (Robinson and Oshlack, 2010) implemented in the edgeR package (Robinson et al., 2009). The normalized counts were used in order to make unsupervised analysis, PCA and clusters. For the differential expression (DE) analysis, read counts were converted to log<sub>2</sub>-counts-per-million (logCPM) and the mean-variance relationship was modelled with precision weights using voom approach in limma package

Pre-Ranked Gene Set Enrichment Analysis (GSEA) (GSEA 2017) was used in order to retrieve functional pathways. The ranked list of genes was generated using the-

$\log(p.val) * \text{signFC}$  for each gene from the statistics obtained in the DE analysis with limma (Robinson and Oshlack, 2010). Functional annotation was obtained based on the enrichment of gene sets belonging to gene set collections (MSigDB 2017). The collections used in this project are: c2.all, gene sets collected from various sources such as online pathway databases, publications in PubMed, and knowledge of domain experts; c5.bp, gene sets derived from the Biological Process Gene Ontology (GO) and Hall, Hallmark gene sets. Coherently expressed signatures derived by aggregating many MSigDB gene sets to represent well-defined biological states or processes

## **Tumor acini and mouse serum cytokine array**

Multiplex quantification of cytokines and chemokines of supernatants collected from 3D acinar cultures or mouse sera was performed using the Mouse Cytokine Array C1000 (RayBiotech) following manufacturer's instruction and using the recommended ImageJ plugin and provided excel analysis tool. Cytokines secreted from tumor acini growing *in vitro* were detected in tumor supernatants collected 72h after plating. A pool of three supernatants derived from three independent tumor transplants and primary tumors was used for the analyses. To detect genes affected by RANK activation, 1  $\mu\text{g}/\text{mL}$  RANKL was added 24 h after tumor plating. RNA was extracted 24 hours after RANKL stimulation for hybridization to a gene expression microarray, as previously described. For murine blood serum, blood was extracted by intracardiac puncture immediately after euthanasia. Blood was centrifuged at maximum speed on a tabletop centrifuge and the top-fraction (serum) was stored at  $-80$  until analysis. Three sera from each experimental conditioned were pooled together to incubate with the cytokine array membranes.

## **Cell line culture and lentiviral transduction**

The human breast cancer cell lines MCF-7 and HCC1954 were purchased from the American Type Culture Collection (ATCC). ATCC provides molecular authentication in support of their collection through their genomics, immunology, and proteomic cores, as described, by using DNA barcoding and species identification, quantitative gene expression, and transcriptomic analyses (ATCC Bulletin, 2010). Cells were grown in DMEM and RPMI 1640 medium, respectively, supplemented with 10% fetal bovine serum (FBS) and 1% penicillin-streptomycin solution (all from Gibco). The cells were grown at  $37^{\circ}\text{C}$  in the presence of 5%  $\text{CO}_2$  in humidified incubators and were tested for absence of mycoplasma.

To ectopically express GFP (control) or RANK (*TNFRSF11A*), the corresponding genes were cloned in the lentiviral vector pSD-69 (PGK promoter, generously donated by S Duss and M Bentires-Alj) following Gateway cloning protocols. To knock down the expression of endogenous RANK we used the lenti-viral vector pGIPZ clones V3LHS\_307325 and V3LHS\_400741 with RANK specific shRNA expression (Dharmacon). As a control (ctrl) we used a verified non-targeting clone (Dharmacon). Lentiviruses were prepared in HEK293T cells with packaging and envelope plasmids psPAX2 and pMD2.G (AdGene). Transduced cells were selected with 1.5 µg/ml puromycin, starting 3 days after infection.

## **Human neutrophil and T cell isolation and culture**

Peripheral blood was provided by the “Banc de Sang I Teixits” (Hospital Universitari de Bellvitge). Mononuclear cells were isolated from buffy coats using Ficoll-plus gradient (GE Healthcare Bio-Sciences). Neutrophils were isolated from the red fraction, then purified by dextran sedimentation. Purified cells were resuspended at 5 x 10<sup>6</sup> cells/mL in RPMI supplemented with 10% of FBS and 50 U/mL streptomycin and penicillin. FACS analysis was performed to detect CD66b (G10F5, BD Bioscience) to confirm purity (98% average).

Neutrophil apoptosis and activation were analyzed culturing 10<sup>4</sup> neutrophils per well in 96-well plates over 24 h in the indicated medium or CM. Apoptosis was measured using the Annexin AV Apoptosis Detection Kit (640930, BioLegend) and activation was detected by staining for CD11b following the previously described flow cytometry staining protocol.

## **Clinical trial design and patient characteristics**

Twenty-seven patients were enrolled in the D-BEYOND trial: first patient enrolled 2nd October 2013; last patient enrolled 9th June 2016. D-BEYOND was a prospective, single arm, multi-center, open label, preoperative “window-of-opportunity” phase IIa trial (NCT01864798). All patients received two injections of denosumab 120 mg subcutaneously, administered 7 to 12 days apart, prior to surgical intervention. Surgery was performed 10-21 days after the first dose of denosumab (median, 13 days). Post-study treatment was at the discretion of the investigator. Snap-frozen and formalin-fixed, paraffin-embedded (FFPE) tumor and normal tissues were collected at baseline (pre-treatment) and at surgery (post-treatment). Normal tissues (snap-frozen and FFPE) were defined as being at least 1cm away from tumor, another quadrant or contralateral breast biopsies. All samples (including normal) were reviewed by a pathologist to assess epithelial content. Eligible patients were premenopausal women with histologically confirmed newly diagnosed

operable primary invasive carcinoma of the breast who had not undergone previous treatment for invasive breast cancer. Other key eligibility criteria included a tumor size > 1.5 cm, any nodal status, and known estrogen receptor (ER), progesterone receptor (PR), human epidermal growth factor receptor 2 (HER2) status. Key exclusion criteria included bilateral invasive tumors, current or previous osteonecrosis or osteomyelitis of the jaw, and known hypersensitivity to denosumab. Evaluation of conventional breast cancer markers including ER, PR, HER2 and Ki-67 were centrally performed at the Institut Jules Bordet (IJB). ER and PR status were defined according to ASCO-CAP guidelines. Breast cancer subtypes were defined according to the St Gallen 2015 Consensus Meetings (Coates et al., 2015) using immunohistochemical surrogates as follows: Luminal A: ER and/or PR(+), HER2(-), Ki-67 < 20%; Luminal B: ER and/or PR(+), HER2(-), Ki-67 ≥ 20; Basal: ER(-), PR(-) and HER2(-), irrespective of Ki-67 score; and HER2: HER2(+), irrespective of ER, PR or Ki-67. All 4 HER2+ patients included in the study were ER+ PR+. The full study protocol is available as Supplementary Note 1 in the Supplementary Information file.

Serious and non-serious adverse events (AEs) were collected from the day of signed informed consent until one month after the final administration of the study drug, except for the project-specific AEs, for which the reporting was extended to 3 months after the final dose of denosumab. Safety data were evaluated using the National Cancer Institute Common Terminology Criteria for Adverse Events (NCI-CTCAE v 4.0). AEs were coded according to the Medical Dictionary for Regulatory Activities (version 20.1). All non-serious AEs are summarized in Supplementary Data 6, the most frequent one being arthralgia (4/27, 14.8%). This study was approved by the Ethics Committee of the trial sponsor; the Medical Ethics Committee of the Institute Jules Bordet (IJB N°: 2064) and the Melbourne Health Human Research Ethics Committee. All patients provided written informed consent prior to study entry.

One patient was excluded because she had a ductal *in situ* carcinoma and two patients were excluded because of lack of available tumor tissue. Another patient was excluded from TIL evaluation due to tissue exhaustion. The primary study endpoint was a geometric mean decrease in the percentage of Ki-67-positive cells assessed by immunohistochemistry (IHC). Key secondary endpoints included absolute Ki-67 responders (defined as < 2.7% Ki-67 IHC staining in the post-treatment tumor tissue), decrease in serum C-terminal telopeptide (CTX) levels measured by ELISA, increase in apoptosis as detected by cleaved caspase-3 or TUNEL assays, evaluate the tolerability of a short-course of denosumab and observe changes in TIL percentage in tumor tissue evaluated on hematoxylin and eosin (HE) slides.

Changes in the infiltration of immune populations as measured by IHC were also performed. Paired samples of breast tumor and normal tissue at baseline and at surgery were required. The limited epithelial content precluded analyses of changes in the paired normal tissues. Gene expression analyses in paired tumor and normal tissue at baseline and at surgery was performed for patients with enough epithelial content. Additional secondary endpoints include: change in RANK/RANKL gene expression and signaling, change in tumor proliferation rates using gene expression, change in expression levels from genes corresponding to mammary progenitor populations, estrogen pathways, immune pathways, and gene expression changes in the paired samples of surrounding normal tissue when available. All primary, secondary and exploratory endpoints performed are summarized in Supplementary Data 17.

## **Pathological assessment and immunohistochemical staining of human tumor samples**

Tumor cellularity was centrally assessed on hematoxylin and eosin-stained (HE) tissue sections from FFPE and frozen human tumor samples. For patients with multiple samples, the sample with the highest tumor content was chosen for further analyses. The percentage of intratumoral and stromal TILs was independently evaluated by two trained pathologists (R.S. and G.V.D.E.) who were blinded to the clinical and experimental data on the HE slides, following the International TIL Working Group 2014 methodology, as described elsewhere (Salgado et al., 2015). Median tumor cellularity ranged between 35 and 90%. TIL proliferation was assessed as the percentage of Ki67<sup>+</sup> TILs among all TILs.

Tissue sections (4 µm) from FFPE tissues of human primary breast tissue were used to assess RANK and RANKL. For each patient, representative unstained slides of the primary tumor were shipped to NeoGenomics Laboratories (California, USA) for immunohistochemical staining of RANK (N1H8, Amgen) RANKL (M366, Amgen), blinded to clinical information. The percentage of stained cells and their intensity (0, negative; 1<sup>+</sup>, weak; 2<sup>+</sup>, moderate; and 3<sup>+</sup>, strong) were recorded as described previously<sup>26</sup>.

An H-score was calculated using the following formula:  $H = (\% \text{ of cells of weak intensity} \times 1) + (\% \text{ of cells with moderate staining} \times 2) + (\% \text{ of cells of strong staining} \times 3)$ . The maximum possible H-score is 300, corresponding to 100% of cells with strong intensity.

Serial FFPE tissue sections (4 µm) were immunohistochemically stained for CD3/CD20, CD4/CD8, and FOXP3/CD4 dual-staining as well as single Ki-67 and cleaved caspase-3 staining on a Ventana Benchmark XT automated staining instrument (Ventana Medical

Systems)(Buisseret et al., 2017). The antibodies used for dual IHC are: CD3 (IR503, polyclonal), CD8 (C8/144B, IR623) and CD20 (L26, IR604) from Dako, CD4 (RBT-CD4, BSB5150) from BioSB and FOXP3 (236A/E7, 14-4777-82) from E-Bioscience, Ki-67 (Clone MIB-1) from Dako and cleaved caspase-3 (ab2302) from Abcam. T cells were quantified by CD3 protein expression, B cells by CD20 protein expression, cytotoxic T cells by CD4 negative and CD8 positive expression, and T regulatory cells by simultaneous CD4 and FOXP3 expression. Scoring was defined as the percentage of immune-positive cells among stromal and tumoral area.

For multiplex IHC (mIHC), FFPE tissue sections (4 µm) were processed manually. Briefly, slides were heated at 37°C overnight, deparaffinized and then fixed in neutral-buffered 10% formalin. The presence of helper T cells (CD4), cytotoxic T cells (CD8), B cells (CD20), regulatory T cells (FOXP3), macrophages (CD68), cancer cells (pan-cytokeratin) and cell nuclei (DAPI) was assessed using a serial same-species fluorescence-labeling approach that employs tyramide signal amplification and microwave-based antigen retrieval and antibody stripping in accordance with the manufacturer's instructions (Opal Multiplex IHC, Perkin Elmer). Staining was visualized on a Zeiss LSM 710 confocal microscope equipped with PMT spectral 34-Channel QUASAR (Carl Zeiss). All IHC slides were centrally reviewed by a breast pathologist (R.S.).

## **RNA extraction from human samples and RNA sequencing**

RNA was extracted from frozen tumor and normal tissue using the AllPrep DNA/RNA Mini kit (Qiagen, Germany) according to the manufacturer's instructions. RNA quality was assessed using a Bioanalyzer 2100 (Agilent Technologies). A total of 22 patients had sufficient tumor RNA quantity from both pre- and post- treatment timepoints. A total of 11 patients had sufficient RNA quantity in normal tissue samples from both pre- and post-treatment timepoints. Among the patients without enough RNA quantity in normal tissue, six had biopsies containing mainly fatty tissue without any epithelial cell. Indexed cDNA libraries were obtained using the TruSeq Stranded Total RNA Kit (Illumina) following the manufacturer's recommendations. The multiplexed libraries were loaded onto a NovaSeq 6000 apparatus (Illumina) using a S2 flow cell, and sequences were produced using a 200 Cycle Kit (Illumina).

## **Bioinformatic analyses**

RNA-sequencing read pairs from the D-BEYOND samples were trimmed using Trimmomatic(Bolger et al., 2014). Alignment was performed using STAR<sup>31</sup>. The number of reads mapping to each gene was assessed with the Rsamtools package in the R environment. Since gene expression profiles of tissues taken at biopsy and surgery are known to be sensitive to differences in tissue-handling procedures (López-Knowles et al., 2016), we used a publicly available dataset from the no-treatment arm of The Peri Operative Endocrine Therapy - Individualizing Care (POETIC) study to filter-out differentially expressed genes. This study included 57 pairs of samples from untreated patients taken at diagnosis (baseline) and surgery (GEO ID: GSE73235(López-Knowles et al., 2016)). We filtered out 3270/21.931 (14.9%) genes that were differentially expressed between diagnosis and surgery by using a strict cut-off of a raw value of  $P < 0.05$  from a non-parametric Mann–Whitney U test. Differential expression was analyzed with DESeq2 v.1.14.1 R/Bioconductor package(Love et al., 2014) using raw count data. Significantly differentially expressed genes were selected if they had a  $qval$  of  $< 0.05$  and an absolute  $\log_2$ -fold change of  $> 0.5$ . We used the GAGE v.2.24.0 R/Bioconductor package(Luo et al., 2009) to identify significantly enriched biological processes from the Biological Process from Gene Ontology database. CIBERSORT software was used (Newman et al., 2015a) to refine the subsets of immune cells present in each sample. RPKM expression data were uploaded to [www.cibersort.stanford.edu](http://www.cibersort.stanford.edu) and CIBERSORT was run using LM22 as a reference matrix and, as recommended for RNA-seq data, quantile normalization was disabled. All other parameters were set to default values. Output files were downloaded as tab-delimited text files and immune cell subsets that were present in fewer than 10 samples were discarded.

We reported the 10 aggregates as described before [PMID: 29628290]:

T.cells.CD8 = T.cells.CD8,

T.cells.CD4 = T.CD4.naive + T.CD4.memory.resting + T.CD4.memory.activated,

T.reg = T.cells.regulatory.Tregs.

B.cells = B.cells.naive + B.cells.memory,

NK.cells = NK.cells.resting+NK.cells.activated,

Macrophage = Macrophages.M0 + Macrophages.M1 + Macrophages.M2,

Dendritic.cells = Dendritic.cells.resting + Dendritic.cells.activated,

Mast.cells = Mast.cells.resting + Mast.cells.activated,

Neutrophils = Neutrophils,

Eosinophils = Eosinophils

RNAseq data have been deposited under EGA accession number EGAS00001003252 as a fastq file (available on request from the IJB Data Access Committee).

The prototype-based co-expression module score for *TNFRSF11A* (RANK metagene) and *TNFSF11* (RANKL metagene) was computed for each sample as;  $module\ score = \sum_{i=1}^{100} w_i x_i$ . Where  $x_i$  is the expression of the top 100 genes positively correlated with *TNFRSF11A* or *TNFSF11* at baseline (before treatment) and  $w_i$  is the Pearson correlation coefficient between  $x_i$  and *TNFRSF11A* or *TNFSF11*.

The public signatures of RANK/NF $\kappa$ B were retrieved from MSigDB (Liberzon et al., 2015) (Cell Systems, PMID:26771021) and computed using the geometric mean and then scaling. RANKL-induced genes in mouse mammary epithelial cells (MECs) (WT and Rank overexpression) were retrieved from publicly available GEO dataset: GSE66174.

Mouse microarray data were feature-extracted using Agilent's Feature Extraction Software (v. 10.7), using the default variable values.

Outlier features in the arrays were flagged by the same software package. Data were analyzed using the *Bioconductor* package in the R environment. Data preprocessing and differential expression analysis were performed using the *limma* and *RankProd* packages, and the most recently available gene annotations were used. Raw feature intensities were background-corrected using the *normexp* background-correction algorithm. Within-array normalization was done using spatial and intensity-dependent *loess*. *Aquantile* normalization was used to normalize between arrays. The expression of each gene was reported as the base 2 logarithm of the ratio of the value obtained for each condition relative to the control condition. A gene was considered differentially expressed if it displayed a *pfp* (proportion of false positives) < 0.05, as determined by a non-parametric test. Raw microarray data have been deposited in GEO, access number GSE119464.

## **Statistical analyses**

All statistical tests comparing pre- and post-treatment paired values were done using the sign test or Student's paired samples t-test. All IHC values were log-transformed to give values of  $\log_{10}(x + 1)$ , thereby overcoming the problem of some raw variable values being zero. To compare non-responders and responders, the Mann-Whitney U and Fisher's exact tests were used for continuous and categorical variables, respectively. All correlations were measured using the Spearman's non-parametric *rho* coefficient. All reported P-values were two-tailed. All analyses were performed using R version 3.3.3 (available at [www.r-project.org](http://www.r-project.org)).



project.org) and Bioconductor version 3.6. No correction was made for multiple testing for exploratory analyses, except for the gene expression analysis, for which the false discovery rate (FDR) was used.

Mouse experimental data were analyzed using GraphPad Prism version 5. Differences were analyzed with a two-tailed Student's t-test, an F-test or an unpaired-samples t-test against a reference value of 1. Tumor growth curves were compared using two-way analysis of variance. Frequency of tumor initiation was estimated using the extreme limiting dilution assay (ELDA) (<http://bioinf.wehi.edu.au/software/elda/>). Regression analysis of the growth curves' mean for the anti-CTLA4, anti-RANKL, and anti-PD-L1 treatments was performed, and 2 x 2 chi-square contingency tables (two-tailed probabilities) were used to evaluate responses. The statistical significance of group differences is expressed by asterisks: \*,  $p < 0.05$ ; \*\*,  $p < 0.01$ ; \*\*\*,  $p < 0.0001$ ; \*\*\*\*,  $p < 0.0001$ ).



# RESULTS



## CHAPTER 1

# **Inhibition of RANK signaling in breast cancer induces an anti-tumor immune response orchestrated by CD8+ T cells**

Chapter associated with the work published at: Nat Commun 11, 6335 (2020).  
<https://doi.org/10.1038/s41467-020-20138-8>



## 1.1 Loss of RANK in tumor cells leads to increased lymphocyte infiltration

We hypothesized that, beyond its tumor cell-intrinsic effects (Yoldi et al., 2016), inhibition of RANK signaling pathway may enhance immune activation in BC. To test this hypothesis, we undertook genetic approaches using the PyMT luminal tumor mouse model. First, we tested whether loss of RANK signaling in myeloid cells could induce changes in immune infiltration, by using LysM-cre/RANK<sup>flox/flox</sup> mice. Expression of Cre driven by LysM deletes RANK in the myeloid compartment (RANK MC<sup>-/-</sup>) (Clausen et al., 1999). As expected, lower levels of *Rank* mRNA were found in peritoneal macrophages from RANK MC<sup>-/-</sup> mice (Figure 1A). PyMT RANK<sup>+/+</sup> (RANK<sup>+/+</sup>) tumors were orthotopically transplanted in RANK MC<sup>-/-</sup> mice and corresponding controls (RANK MC<sup>+/+</sup>) (Figure 1A). Analyses of the tumor immune infiltrates revealed no changes in immune infiltration, leukocytes (CD45<sup>+</sup>), lymphocytes (CD11b<sup>-</sup> within CD45<sup>+</sup>), TAMs (F4/80<sup>+</sup>CD11b<sup>+</sup> within CD45<sup>+</sup>) or TANs (Ly6G<sup>+</sup> CD11b<sup>+</sup> within CD45<sup>+</sup>) between genotypes (Figure 1B, Supplementary Figure 1A-B). The frequencies of infiltrating CD8<sup>+</sup> T cells (CD11b<sup>-</sup> CD3<sup>+</sup> CD8<sup>+</sup>), CD4<sup>+</sup> T cells (CD11b<sup>-</sup> CD3<sup>+</sup> CD8<sup>-</sup>), and the CD4/CD8 ratio were also similar in RANK<sup>+/+</sup> tumors growing in RANK MC<sup>-/-</sup> or RANK MC<sup>+/+</sup> mice (Supplementary Figure 1A-B).

We next tested whether RANK loss exclusively in tumor cells could alter tumor immune infiltration: tumors derived from PyMT/RANK<sup>-/-</sup> mice (RANK<sup>-/-</sup> tumors) were orthotopically transplanted in syngeneic C57Bl6 mice and compared with RANK<sup>+/+</sup> tumor transplants (Figure 1C). RANK<sup>-/-</sup> tumors showed greater infiltration by leukocytes, lymphocytes and CD8<sup>+</sup> T cells compared with RANK<sup>+/+</sup> tumors of similar size (Supplementary Figure 1A, 1C). Together these results demonstrate that loss of RANK in tumor cells, but not in myeloid cells, induces an increase in tumor-immune infiltrates, TILs and CD8<sup>+</sup> T cells.

## 1.2 T cells mediate the longer tumor latency of RANK<sup>-/-</sup> tumors

The increase in TILs observed after loss of RANK in tumor cells, prompted us to investigate the functional contribution of this immune population. To this end, RANK<sup>+/+</sup> and RANK<sup>-/-</sup> tumor cells were transplanted in parallel in syngeneic mice and in T cell-deficient *Foxp1<sup>nu</sup>* mice (Figure 1C). We had previously demonstrated that, compared with RANK<sup>+/+</sup>, RANK<sup>-/-</sup> tumor cells display prolonged latency to tumor formation, increased apoptosis and a lower frequency of tumor-initiating cells when transplanted in syngeneic mice (Yoldi et al., 2016). Strikingly, when transplanted in T cell-deficient *Foxp1<sup>nu</sup>* mice, no differences in latency to tumor onset were observed between RANK<sup>+/+</sup> and RANK<sup>-/-</sup> tumor transplants, while the same tumors transplanted in syngeneic C57BL/6 mice corroborated previous results (Figure 1D

and Supplementary Figure 2A)(Yoldi et al., 2016). Additionally, limiting dilution assays in *Foxn1<sup>nu</sup>* mice showed no differences in the ability of RANK<sup>+/+</sup> and RANK<sup>-/-</sup> tumor cells to initiate tumors (Figure 1E). Further characterization of the tumors revealed that RANK<sup>-/-</sup> tumor transplants growing in syngeneic hosts contained more apoptotic and necrotic cells than did their RANK<sup>+/+</sup> counterparts (Supplementary Figure 2B), corroborating previous findings (Yoldi et al., 2016). However, the frequency of apoptotic cells was similar in RANK<sup>-/-</sup> and RANK<sup>+/+</sup> tumor cells growing in *Foxn1<sup>nu</sup>* mice. Differences in late apoptosis/necrosis (7AAD<sup>+</sup>/Annexin V<sup>+</sup> cells) between RANK<sup>+/+</sup> and RANK<sup>-/-</sup> tumor cells were observed in both syngeneic and *Foxn1<sup>nu</sup>* recipients but were less marked in T cell-deficient mice (Supplementary Figure 2B). These observations suggest that the increased tumor cell death rate in the absence of RANK is due to a combination of tumor cell-intrinsic and T cell-mediated effects, whereas T cells are responsible for the delayed tumor onset and the reduced tumor-initiating ability of RANK-null tumor cells.

Analyses of RANK<sup>+/+</sup> and RANK<sup>-/-</sup> tumors confirmed the higher frequency of leukocytes and the enrichment in TILs in RANK<sup>-/-</sup> compared with RANK<sup>+/+</sup> tumors (Figure 1F-G; Supplementary Figure 1C). In contrast, the relative frequency of TAMs and TANs was higher in RANK<sup>+/+</sup> than in RANK<sup>-/-</sup> tumors (Figure 1F-G, Supplementary Figure 1C). These differences were no longer observed in *Foxn1<sup>nu</sup>* transplants (Figure 1F-G).

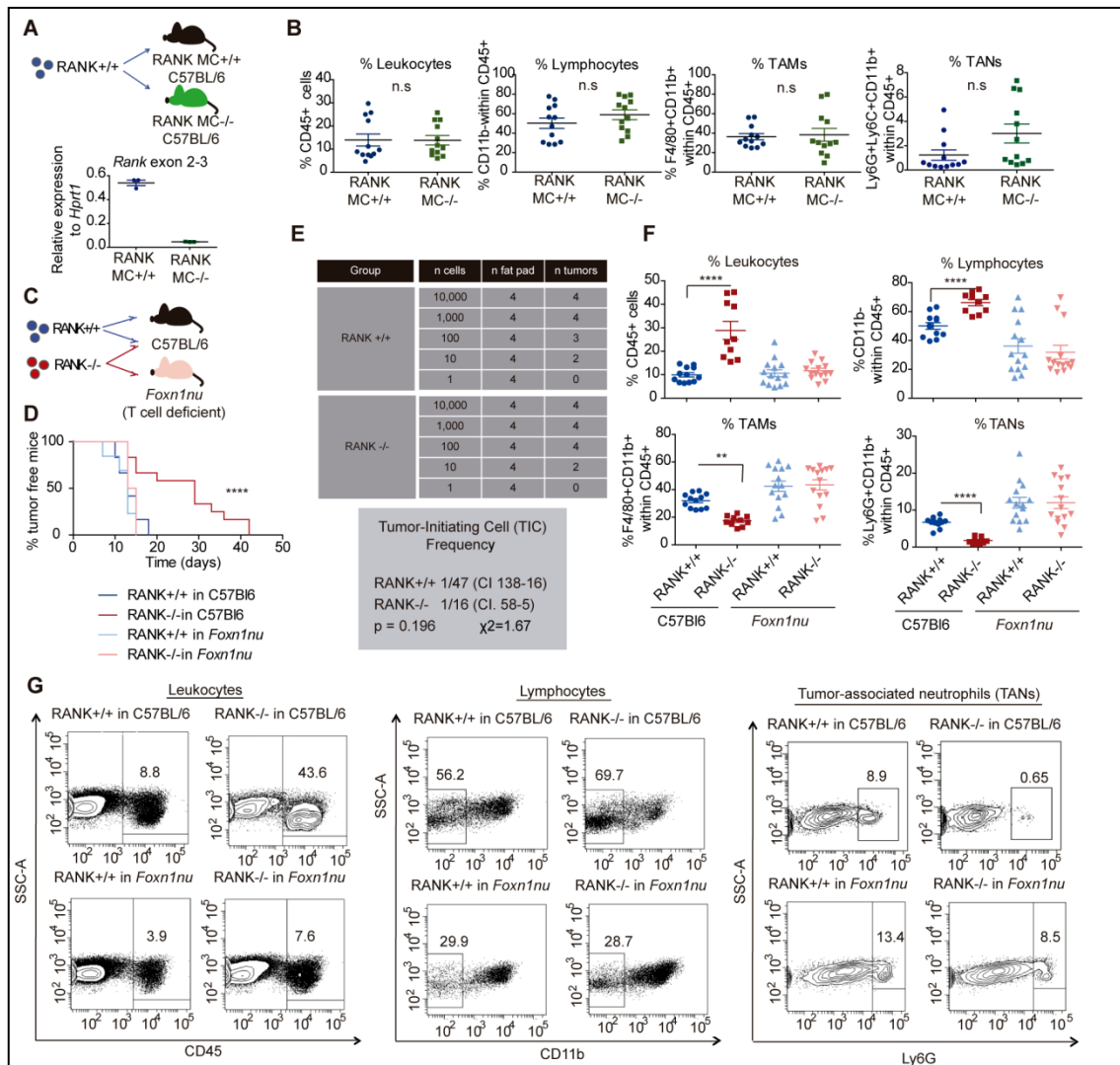
To rule out the possibility that immune cells transplanted along with tumor cells were responsible for the observed changes, the CD45<sup>-</sup> population (tumor cell-enriched) was sorted and transplanted into syngeneic hosts. The longer tumor latency observed in RANK<sup>-/-</sup> was exacerbated when sorted CD45<sup>-</sup> cells were injected compared with whole tumor transplants (Supplementary Figure 2C). Accordingly, differences in immune infiltration were also observed between tumors derived from sorted CD45<sup>-</sup> RANK<sup>+/+</sup> and CD45<sup>-</sup> RANK<sup>-/-</sup> cells and those derived from whole tumor transplants (Supplementary Figure 2D).

To confirm that our findings are not affected by differences other than RANK status between RANK<sup>+/+</sup> and RANK<sup>-/-</sup> tumors, we infected PyMT/RANK<sup>flox/flox</sup> tumors with pLVX-Cre-IRES-zsGreen or control lentivirus. Infected tumor populations were FACS-sorted and orthotopically transplanted into C57BL/6 mice. RANK depletion was confirmed by RT-PCR and IHC (Supplementary Figure 2e). RANK-depleted tumors showed lower tumor growth rate (Supplementary Figure 2f) and greater infiltration of leukocytes, lymphocytes, and T cells (CD3<sup>+</sup> CD11b<sup>-</sup> CD45<sup>+</sup>), corroborating previous findings (Supplementary Figure 2G). CD8<sup>+</sup> T cells were more abundant, and TANs were reduced in RANK-depleted tumors,



although the differences were not significant (Supplementary Figure 2G). Thus, RANK loss in tumor cells leads to a significant increase in TILs.

Together, these results demonstrate that RANK loss in tumor cells leads to a significant increase in TILs that restrict RANK<sup>-/-</sup> tumor cell growth. Reciprocally, they indicate that RANK expression in tumor cells induces an immunosuppressive microenvironment enriched in TAMs and TANs, allowing tumor cells to escape T cell immune surveillance.

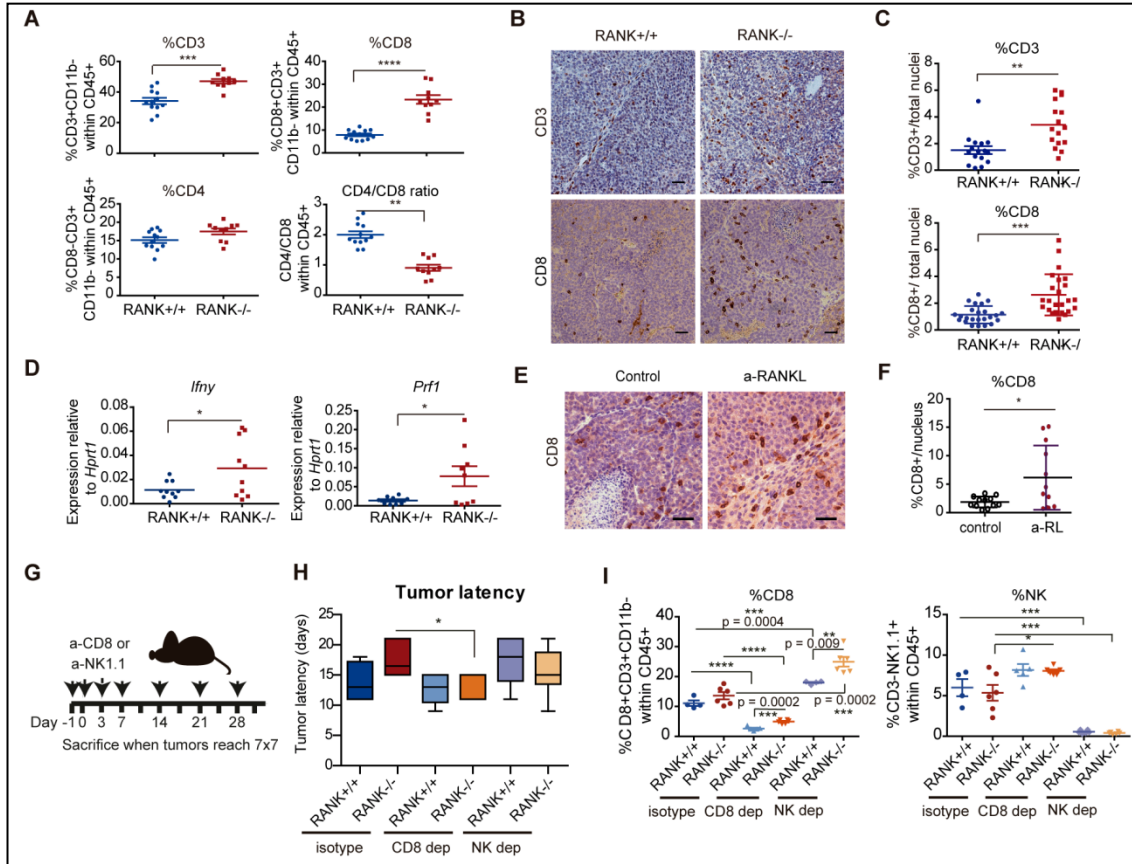


**Figure 1. Loss of RANK in tumor cells, but not in myeloid cells, leads to increased TIL frequency, and T cells drive the delayed tumor formation and the reduced tumor-initiating ability of RANK-null tumor cells.** A, Top panel: Injection scheme showing the implantation of PyMT RANK<sup>+/+</sup> (RANK<sup>+/+</sup>) tumors in LysM-Cre RANK<sup>fl/fl</sup> mice (RANK MC<sup>-/-</sup>) and WT (RANK MC<sup>+/+</sup>) (C57BL/6); Bottom panel: *Rank* mRNA expression levels relative to *Hprt1* in peritoneal macrophages of RANK MC<sup>-/-</sup> and RANK MC<sup>+/+</sup> mice (n=3). Mean +/-SEM is shown. B, Graphs showing the percentages of tumor-infiltrating leukocytes (CD45<sup>+</sup>), lymphocytes (CD11b<sup>-</sup> within CD45<sup>+</sup>), tumor-associated macrophages (TAMs) (F4/80<sup>+</sup>CD11b<sup>+</sup> within CD45<sup>+</sup>) and tumor-associated neutrophils (TANs) (Ly6G<sup>+</sup>Ly6C<sup>+</sup>CD11b<sup>+</sup> within CD45<sup>+</sup>) in RANK<sup>+/+</sup> tumor transplants in RANK MC<sup>-/-</sup> and RANK MC<sup>+/+</sup> mice (n=12 tumors). Mean, SEM shown. t-test and p-values were calculated. C, Injection

scheme showing the implantation of PyMT RANK<sup>+/+</sup> and PyMT RANK<sup>-/-</sup> tumors in C57BL/6 WT animals and *Foxn1<sup>nu</sup>* mice. D, Kinetics of palpable tumor onset (left) after tumor transplantation of RANK<sup>+/+</sup> and RANK<sup>-/-</sup> tumor cells in syngeneic C57BL/6 (n=6) and *Foxn1<sup>nu</sup>* mice (n=7). Log-rank test performed with two-tailed p value (\*\*\*\*, p = 0.005). One representative experiment out of two is shown. E, Tumor-initiating frequencies as calculated by ELDA. Cells isolated from RANK<sup>+/+</sup> and RANK<sup>-/-</sup> tumors were injected in *Foxn1<sup>nu</sup>* mice in limiting dilutions. WEHI's online ELDA-software (<http://bioinf.wehi.edu.au/software/elda/>) was used to calculate the chi-square ( $\chi^2$ ) values with 95% confidence interval. F, Graphs showing the percentages tumor-infiltrating leukocytes (CD45<sup>+</sup>; \*\*\*\* p<0.0001), lymphocytes (CD11b<sup>-</sup> within CD45<sup>+</sup>; \*\*\*\* p<0.0001), TAMs (F4/80<sup>+</sup>CD11b<sup>+</sup> within CD45<sup>+</sup>; \*\*\*\* p<0.0001), TANs (Ly6G<sup>+</sup>CD11b<sup>+</sup> within CD45<sup>+</sup>; \*\*\*\* p<0.0001) in RANK<sup>+/+</sup> or RANK<sup>-/-</sup> tumor transplants in syngeneic C57BL/6 and *Foxn1<sup>nu</sup>* mice (n= 12 RANK<sup>+/+</sup> tumors, n=10 RANK<sup>-/-</sup> tumors in C57BL/6 hosts; n=14 RANK<sup>+/+</sup> or RANK<sup>-/-</sup> tumors in *Foxn1<sup>nu</sup>* hosts). Tumors were analyzed at endpoint (>0.2 cm<sup>2</sup>). Mean, SEM and t-test two-tailed p-values are shown. Two representative primary tumors were used in these experiments. G, Representative dot blots of leukocytes (CD45<sup>+</sup>) gated in live cells (7AAD<sup>-</sup>) and lymphocytes (CD11b<sup>-</sup>) gated on CD45<sup>+</sup>.

### 1.3 CD8<sup>+</sup> T cell depletion rescues the delay in tumor onset of RANK<sup>-/-</sup> tumors

Further characterization of TIL subsets from syngeneic transplants (Supplementary Figure 1A), revealed a significant increase in the percentage of CD3<sup>+</sup> T lymphocytes and CD8<sup>+</sup> T cells in RANK<sup>-/-</sup> tumors and a lower CD4<sup>+</sup>/CD8<sup>+</sup> ratio in RANK<sup>-/-</sup> compared with the RANK<sup>+/+</sup> tumors (Figure 2A). There were no significant differences between the two groups in the frequencies of NK cells (NK1.1<sup>+</sup> CD3<sup>-</sup>), B cells (CD19<sup>+</sup> CD3<sup>-</sup> CD11b<sup>-</sup>) or levels of IFN $\gamma$  production by tumor-infiltrating CD4<sup>+</sup> and CD8<sup>+</sup> T cells (Supplementary Figure 3A). However, TAMs that infiltrated RANK<sup>-/-</sup> tumors expressed higher levels of IL12/IL23, indicative of an anti-tumor M1 response (Supplementary Figure 3A). Increased CD3<sup>+</sup> T lymphocyte and CD8<sup>+</sup> T cell tumor infiltration in RANK<sup>-/-</sup> tumors compared with RANK<sup>+/+</sup> was confirmed by IHC (Figure 2B-C) and the mRNA levels of the cytotoxicity markers, namely interferon gamma (*Ifn $\gamma$* ) and perforin (*Prf1*) were higher in RANK<sup>-/-</sup> tumors (Figure 2D). Gene expression analysis comparing sorted CD45<sup>-</sup> cells (tumor cell-enriched) isolated from RANK<sup>+/+</sup> versus RANK<sup>-/-</sup> tumor transplants revealed 604 differentially expressed genes (Supplementary Data 1). Gene Ontology (GO) and Generally Applicable Gene Set Enrichment (GAGE) analyses revealed that RANK<sup>-/-</sup> tumor cells overexpressed a subset of genes related to the “intrinsic apoptotic signaling pathway”, “antigen processing and presentation” and “positive regulation of T cell-mediated cytotoxicity” (Supplementary Data 2-4). Similar frequencies of CD3<sup>+</sup>, CD4<sup>+</sup> and CD8<sup>+</sup> cells were found in draining lymph nodes from RANK<sup>+/+</sup> and RANK<sup>-/-</sup> tumor transplants, but a moderate increase in IFN $\gamma$  production in the lymph node T cells was observed in the RANK<sup>-/-</sup> tumor transplants (Supplementary Figure 3B).



**Figure 2. RANK loss in tumor cells leads to increased CD8<sup>+</sup> T cell tumor infiltration that mediates the delayed tumor latency of RANK<sup>-/-</sup> tumors.** A, Graphs showing the percentage of T cells (CD3<sup>+</sup>CD11b<sup>-</sup> within CD45<sup>+</sup>; \*\*\* p = 0.0001), CD8 (CD8<sup>+</sup>CD3<sup>+</sup>CD11b<sup>-</sup> within CD45<sup>+</sup>; \*\*\*\* p < 0.0001), CD4 (CD8-CD3<sup>+</sup>CD11b<sup>-</sup> within CD45<sup>+</sup>; p = 0.0503) and the CD4/CD8 ratio (\*\*\*\* p < 0.0001) in RANK<sup>+/+</sup> (n=12) or RANK<sup>-/-</sup> (n=10) tumor cells injected in syngeneic C57BL/6 mice<sup>#</sup>. B-C, Representative images (B) and quantification (C) of CD3<sup>+</sup> (n = 4 tumors, \*\*\* p = 0.0009) and CD8<sup>+</sup> cells (n = 6 tumors, \*\*\* p = 0.0001) in RANK<sup>+/+</sup> and RANK<sup>-/-</sup> tumor transplants as assessed by IHC. Scale = 25  $\mu$ m. Tumors derived from three independent primary tumors were used. Each dot represents one picture<sup>#</sup>. D, *Prf1* and *Ifny* mRNA levels relative to *Hprt1* of whole tumors from RANK<sup>+/+</sup> and RANK<sup>-/-</sup> transplants in syngeneic C57BL/6 mice (n=10; *Prf1* \* p = 0.0286, *Ifny* \* p = 0.0360)<sup>#</sup>. E-F, Representative images (E) and quantification (F) of CD8<sup>+</sup> cells in RANK<sup>+/+</sup> control and anti-RL-treated tumors from second transplants as assessed by IHC. Scale= 25  $\mu$ m. Each dot represents one picture (n=12 pictures, n=3 tumors, \* p = 0.0168)<sup>#</sup>. G, Schematic overview of CD8 (300 $\mu$ g, clone 53-5.8) and NK1.1 (200 $\mu$ g, clone PK136) treatments in orthotopic RANK<sup>+/+</sup> and RANK<sup>-/-</sup> tumor transplants. Animals were treated i.p. on days -1, 0, 3 and 7 after tumor cell injection, and then once per week until the day of sacrifice, when tumors were > 0.5 cm<sup>2</sup>. H, Latency to tumor onset of RANK<sup>+/+</sup> and RANK<sup>-/-</sup> tumor cells implanted in syngeneic C57BL/6 animals and treated with anti-CD8 or anti-NK1.1 depletion antibodies (n=6) or corresponding isotype control (n=4 for RANK<sup>+/+</sup> and n=6 for RANK<sup>-/-</sup>). Box and whisker plots (box represents the median and the 25th and 75th percentiles, whiskers show the largest and smallest values) and significant t test two-tailed p values are shown (\*, p = 0.05). I, Graphs showing the percentage of infiltrating CD8 T cells (CD8<sup>+</sup>CD3<sup>+</sup>CD11b<sup>-</sup> within CD45<sup>+</sup>) and NK (NK1.1<sup>+</sup>CD3<sup>-</sup> within CD45<sup>+</sup>). Each dot represents one tumor (n=4 control and NK-depleted RANK<sup>+/+</sup> tumors; n=5 CD8-depleted RANK<sup>+/+</sup> tumors and n=6 RANK<sup>-/-</sup> control, NK- and CD8-depleted tumors)<sup>#</sup>. ; <sup>#</sup>Mean, SEM and t test two-tailed p-values are shown. (\*, p < 0.05; \*\*, 0.001 < p < 0.01; \*\*\*, 0.001 < p < 0.0001; \*\*\*\*, p < 0.0001). For panels a and d, each dot represents one tumor analyzed at the endpoint (> 0.2 cm<sup>2</sup>). Data for tumor transplants derived from two representative primary tumors in two independent experiments.

Next, we investigated the effects on the tumor immune infiltrate after systemic pharmacological inhibition of RL (RL) (RANK-Fc treatment 10 mg/kg three times per week, for 4 weeks) in serial tumor transplants from PyMT mice (Supplementary Figure 3C)(Yoldi et al., 2016). No significant changes in the total number of TILs upon RL inhibition were observed (Supplementary Figure 3D-E). However, after RL inhibition, the frequency of infiltrating CD8<sup>+</sup> T cells increased (Supplementary Figure 3D) and CD4<sup>+</sup> T cells decreased (Supplementary Figure 3e), leading to a lower CD4<sup>+</sup>/CD8<sup>+</sup> ratio (Supplementary Figure 3D-E). An increased infiltration by CD8<sup>+</sup> T cells in tumors continuously treated with RL inhibitor was also observed by IHC (Figure 2E-F). Together, these evidences demonstrate that genetic or pharmacologic inhibition of RANK signaling increases CD8<sup>+</sup> T cell tumor infiltration.

CD8<sup>+</sup> T and NK cells have been shown to drive tumor cell cytotoxicity(DeNardo and Coussens, 2007), therefore depletion experiments were performed in RANK<sup>+/+</sup> and RANK<sup>-/-</sup> tumor transplants to confirm their involvement (Figure 2G). Depletion of CD8<sup>+</sup> T cells, but not of NK cells, rescued the delayed tumor formation observed in RANK<sup>-/-</sup> transplants with minor effects on RANK<sup>+/+</sup> transplants (Figure 2H). CD8<sup>+</sup> T and NK cell depletions were corroborated in blood samples and tumor infiltrates (Supplementary Figure 4A-B). CD8<sup>+</sup> T cell depletion resulted in increased NK cell frequency in tumors and, conversely, NK cell depletion led to increased CD8<sup>+</sup> T cell infiltration (Figure 2I). These results suggest that CD8<sup>+</sup> T cells mediate the anti-tumorigenic response induced by RANK loss in tumor cells and that the exacerbated T cell response in RANK<sup>-/-</sup> tumors is responsible for the delay in tumor formation.

#### **1.4 RANK+ tumor cells promote immunosuppression through neutrophils**

To clarify the intercellular crosstalk involved in the observed phenotypes we cultured 3D tumor acini from RANK<sup>+/+</sup> and RANK<sup>-/-</sup> tumor transplants for 72 h and measured the levels of cytokines and chemokines in the culture supernatants (Supplementary Data 5). Fewer cytokines/chemokines were more abundant in RANK<sup>-/-</sup> than RANK<sup>+/+</sup> tumor supernatants, and included eotaxin 1, which is involved in eosinophil recruitment, CD40, which enhances T cell responses, and BLC, which controls B cell trafficking (Griffith et al., 2014) (Figure 3A). However, no significant differences in the frequencies of eosinophils or B cells were found in RANK<sup>-/-</sup> as compared to RANK<sup>+/+</sup> tumor transplants (Supplementary Figure 3A). In supernatants derived from RANK<sup>+/+</sup> tumor acini many cytokines were upregulated including SDF-1 $\alpha$ , MIP-1 $\alpha$ , IL-1 $\alpha$ , SCF, TNF $\alpha$ , IL-13, M-CSF, IL-10, IL-4, IL-17 and IL-1 $\beta$  (Supplementary Data 5, Figure 3A). These various cytokines/chemokines are characteristic

of an immunosuppressive microenvironment and have a wide-ranging actions, including myeloid cell recruitment (Griffith et al., 2014). The mRNA expression levels of *Il-1 $\beta$*  and *Caspase-4*, which mediates the activation of pre-IL1- $\beta$  in the inflammasome (Guo et al., 2015) were also higher in RANK<sup>+/+</sup> tumors, while *s100a9*, a gene related to neutrophil stimulation and migration, showed a tendency to increase (Ryckman et al., 2003), (Figure 3B). These changes may contribute to the increased infiltration of TANs observed in RANK<sup>+/+</sup> tumors (Figure 1F-G, Supplementary Figure 1C and 2D) and the suppression of T cell immunity as previously reported (Coffelt et al., 2016; Youn et al., 2008). In fact, the percentage of TANs (Ly6G<sup>+</sup>) and that of CD8<sup>+</sup> T cells were negatively correlated in the mouse tumors (Figure 3C).

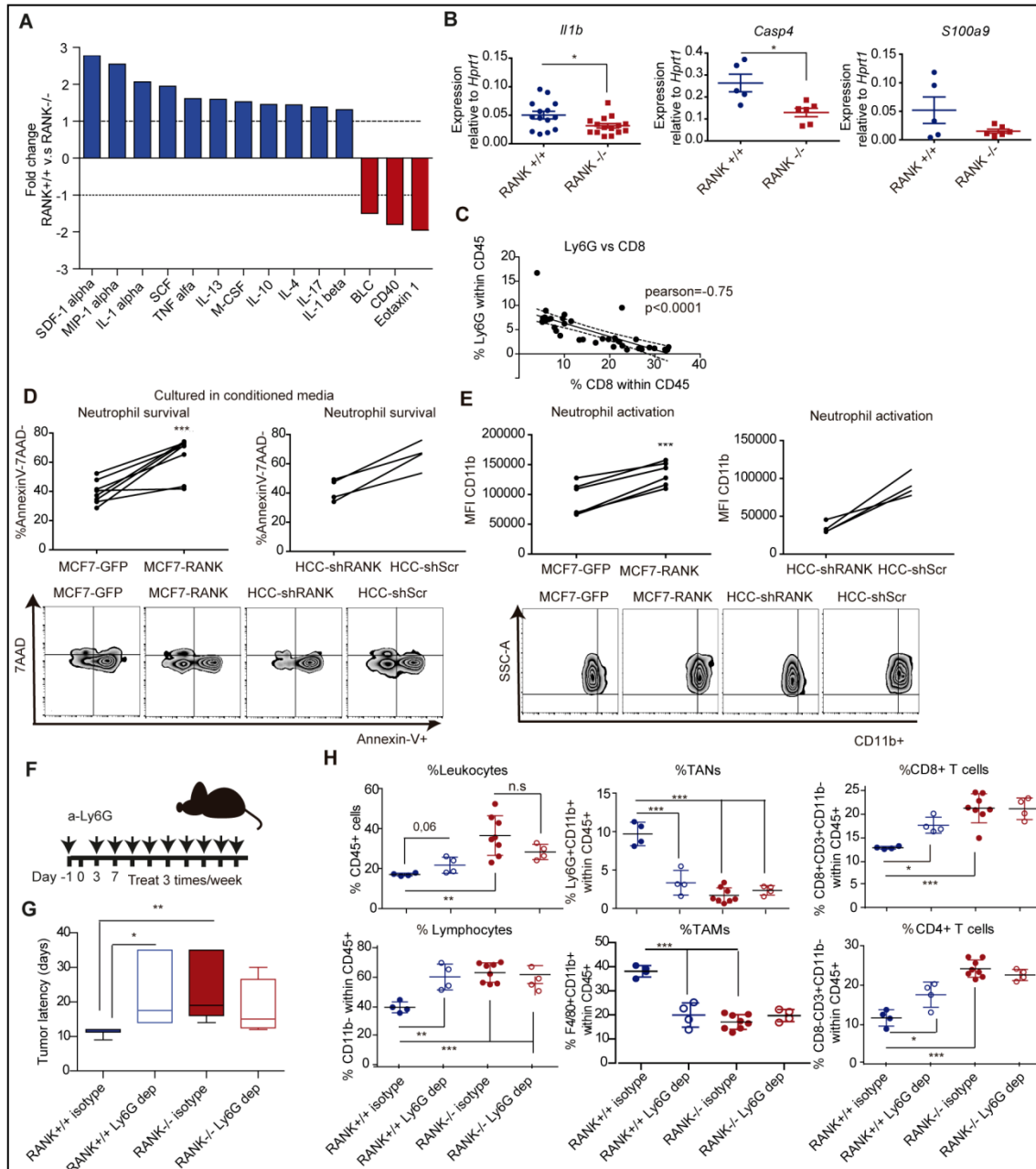
To confirm the crosstalk between RANK activation in BC cells and neutrophils, we adopted an independent experimental approach by modulating RANK expression levels in human BC cells and directly testing in co-culture assays whether this influenced neutrophil survival and activation. MCF7 luminal BC cells that had undetectable RANK expression and were unresponsive to RL stimulation, were infected with RANK-overexpressing vectors (Supplementary Figure 4C). Conversely, HCC1954 basal-like, HER2<sup>+</sup> cells, which, despite the low levels of RANK expression, are responsive to RL stimulation, were infected with short-hairpin RNAs to downregulate RANK (Supplementary Figure 4C). Changes in RANK expression and downstream targets (*BIRC3*, *ICAM1*, *NF $\kappa$ B2*, *RELB*) were confirmed by RT-PCR (Supplementary Figure 4C).

BC cells were stimulated with RL for one hour before co-culturing with neutrophils, isolated from blood of healthy human donors (Supplementary Figure 4D). MCF7-RANK tumor cells and HCC1954-shSCR cells increased neutrophil survival more than their corresponding tumor cells lacking RANK did (Supplementary Figure 4E). Conditioned medium (CM) from BC cells with higher level of RANK expression and activation was enough to increase the survival of neutrophils significantly more than CM from control cells (Figure 3D). These neutrophils also presented a more mature/active phenotype based on the increased CD11b levels (Figure 3E)(Shaul and Fridlender, 2018).

Finally, to confirm whether neutrophils are involved in the observed differences in latency between RANK<sup>+/+</sup> and RANK<sup>-/-</sup> tumor transplants and the crosstalk with T cells, Ly6G depletion assays were performed (Figure 3F). Neutrophil depletion significantly delayed tumor appearance in RANK<sup>+/+</sup> transplants with no effects in RANK<sup>-/-</sup> transplants (Figure 3G). Neutrophil depletion was confirmed in blood samples (Supplementary Figure 4F-G). The frequency of TANs after depletion was reduced in RANK<sup>+/+</sup> but not in RANK<sup>-/-</sup> tumor



transplants, in which TAN infiltration was much lower (Figure 3H). Neutrophil depletion led to a significant increase in TILs, CD4<sup>+</sup> and CD8<sup>+</sup> T cells, and to a decrease in the frequency of TAMs infiltrating RANK<sup>+/+</sup> transplants to levels comparable with those found in RANK<sup>-/-</sup> transplants (Figure 3H). A trend to increased levels of total leukocyte infiltration was also observed after neutrophil depletion ( $p = 0.06$ , Figure 3H).



**Figure 3. Neutrophils recruited by the proinflammatory cytokine/chemokine milieu driven by RANK restrict T cell immunity.** A, Cytokines/chemokines in the supernatant of RANK<sup>+/+</sup> and RANK<sup>-/-</sup> tumor 3D acini cultured during 72 h, expressed as the magnitude of change between RANK<sup>+/+</sup> and RANK<sup>-/-</sup> tumor acini (pool of 3 tumors, n=1). See also Supplementary Data 5. B, *Il1b*, *Casp4* and *S100a9* mRNA levels relative to *Hprt1* of whole tumors from RANK<sup>+/+</sup> and RANK<sup>-/-</sup> transplants in

syngeneic C57BL/6 mice (n=14 for *Il1b*, \* p = 0.005; n=5 RANK<sup>+/+</sup> tumors n=6 RANK<sup>-/-</sup> tumors for *Casp4*, p = 0.011, and *S100a9*, p = 0.12). Two representative primary tumors of two independent experiments were used<sup>#</sup>. C, Correlation between the frequency of TANs (Ly6G<sup>+</sup> Ly6C<sup>+</sup> CD11b<sup>+</sup>) and CD8<sup>+</sup> T cells (CD8<sup>+</sup> CD3<sup>+</sup> CD11b<sup>-</sup>) infiltrates in tumor transplants. Pearson correlation coefficients (r) associated probabilities are shown (p < 0.0001). D, Percentage of Annexin-V<sup>-</sup>7AAD<sup>-</sup> neutrophils (n = 5, 2 healthy donors) cultured with conditioned media (CM) from the indicated RL-treated tumor cells. CM was added (1:1) to human neutrophil cultures for 24 h. Paired t-test with one-tailed p value is shown (\*\*\* p = 0.0002, \*\* p = 0.009). E, Mean fluorescence intensity (MFI) of CD11b<sup>+</sup> neutrophils (n=4, 2 healthy donors) cultured in CM from the indicated RL-treated tumor cells. CM was added (1:1) to human neutrophils cultures for 24 h. Paired t-test with one-tailed p value is shown (\*\*\* p = 0.0004, \* p = 0.01). F, Schematic overview of TAN (Ly6G<sup>+</sup>) depletion experiments in orthotopic RANK<sup>+/+</sup> and RANK<sup>-/-</sup> tumor transplants. Anti-Ly6G (clone 1A8) was administered i.p. before tumor cell injection (400 µg), and then once per week (100 µg) until the day of sacrifice. G, Latency to tumor formation of RANK<sup>+/+</sup> and RANK<sup>-/-</sup> tumor cells orthotopically implanted in syngeneic C57BL/6 animals and treated with anti-Ly6G depletion antibody or isotype control (n=4 control and neutrophil-depleted RANK<sup>+/+</sup> tumors, n= 8 control RANK<sup>-/-</sup> tumors, n=4 neutrophil-depleted RANK<sup>-/-</sup> tumors). Box and whisker plots (box represents the median and the 25th and 75th percentiles, whiskers show the largest and smallest values) and t test two-tailed p-values are shown. (\*, p = 0.028; \*\*, p = 0.007). H, Graphs showing the percentage of TANs (Ly6G<sup>+</sup> CD11b<sup>+</sup>, \*\* p = 0.0012; \*\*\* p = 0.0003; \*\*\*\* p < 0.0001), leukocytes (CD45<sup>+</sup>, \*\* p = 0.034), lymphocytes (CD11b<sup>-</sup>, \*\* p = 0.048; \*\*\* p = 0.0008; \*\*\*\* p < 0.0001), TAMs (F4/80<sup>+</sup> CD11b<sup>+</sup>, \*\* p = 0.0019; \*\*\*\* p < 0.0001), CD8<sup>+</sup> (CD8<sup>+</sup> CD3<sup>+</sup> CD11b<sup>-</sup>, \*\*\* p = 0.0003, \*\* p = 0.0014) and CD4<sup>+</sup> T cells (CD8<sup>-</sup> CD3<sup>+</sup> CD11b<sup>-</sup>, \* p = 0.0213, \*\*\* p = 0.001; \*\*\*\* p < 0.0001) (n=4 control and neutrophil-depleted RANK<sup>+/+</sup> tumors, n= 8 control RANK<sup>-/-</sup> tumors, n=4 neutrophil-depleted RANK<sup>-/-</sup> tumors)<sup>#</sup>.

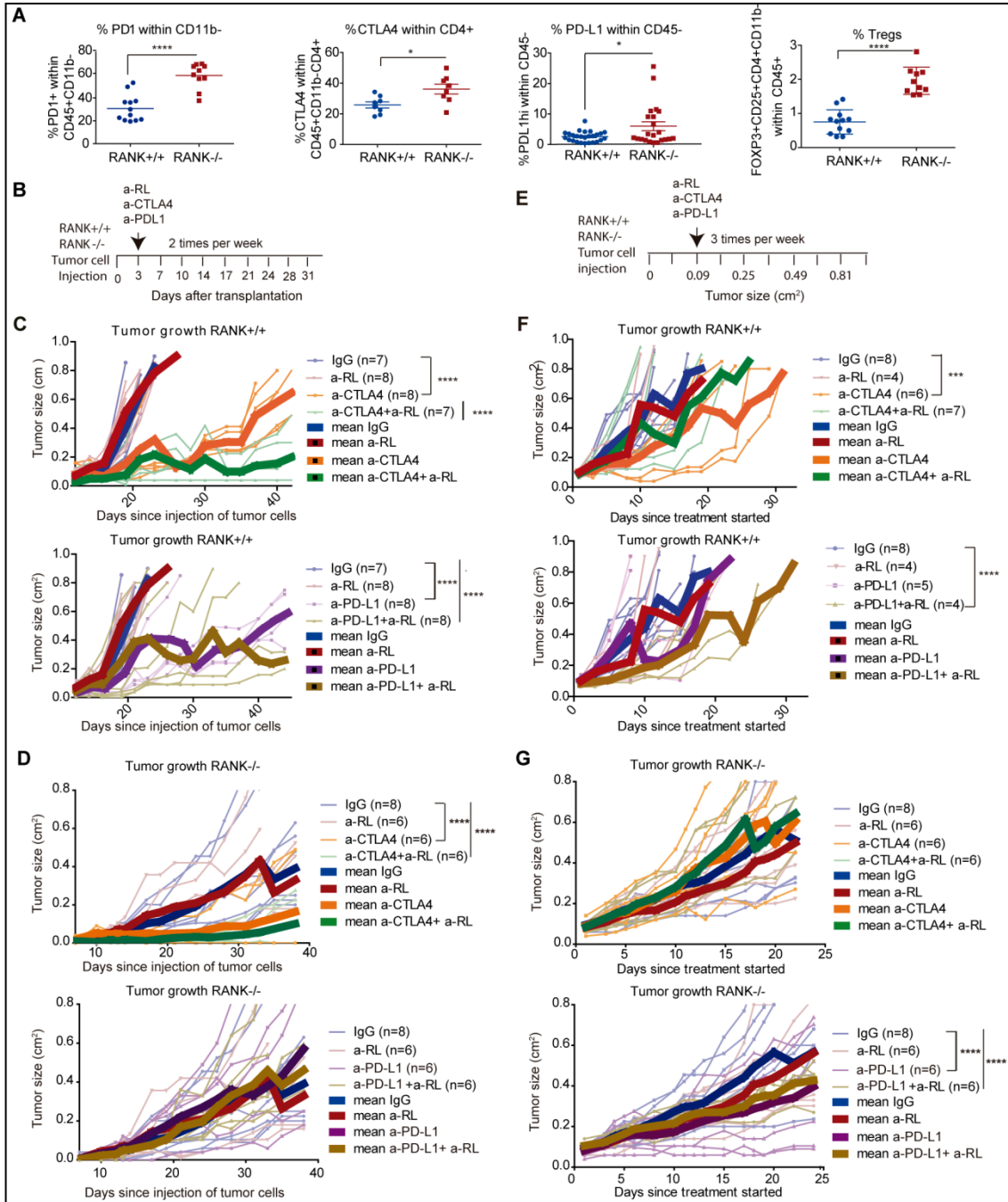
<sup>#</sup>: each dot represents one tumor. Mean, SEM and t test two-tailed p-values are shown. (\*, p < 0.05; \*\*, p < 0.01; \*\*\*, p < 0.001; \*\*\*\*, p < 0.0001). Tumors of similar size were analyzed at endpoint (> 0.2 cm<sup>2</sup>). For panels d-e: each dot represents a technical replicate from healthy donors. Representative dot blots are shown below.

Altogether, these results suggest that RANK activation in tumor cells induces an immunosuppressive microenvironment that favors neutrophil survival restricting T cell immunity.

### 1.5 RL inhibition in tumor cells increases responsiveness to immunotherapy

Despite the stronger anti-tumor immune response, RANK<sup>-/-</sup> tumors eventually evade the immune response and grow. Increased expression of checkpoint regulators such as PD-1 in lymphoid cells and CTLA4 in CD4<sup>+</sup> T cells was found in RANK<sup>-/-</sup> relative to RANK<sup>+/+</sup> tumors (Figure 4A). The level of PD-L1 expression in RANK<sup>-/-</sup> tumor cells was also higher than in RANK<sup>+/+</sup> tumors (Figure 4A). Tregs (FoxP3<sup>+</sup> CD25<sup>+</sup> CD4<sup>+</sup> CD11b<sup>-</sup>) were more frequent in RANK<sup>-/-</sup> than in RANK<sup>+/+</sup> tumors, possibly as a result of the enhanced cytotoxic response, as reported elsewhere (Spranger et al., 2013) (Figure 4A). These results suggest that the exacerbated T cell response in RANK<sup>-/-</sup> tumors may facilitate the induction of negative immune checkpoint regulators and Tregs, evading immune surveillance and allowing tumor growth. This prompted us to investigate the effects of anti-PD-L1 and/or anti-CTLA4 checkpoints inhibitors in combination with the loss of RANK signaling. In RANK<sup>+/+</sup> tumors early treatment (72 h after tumor implantation) with anti-RL did not affect tumor growth;

however, anti-CTLA4 combined with anti-RL reduced tumor growth to a greater extent than did single anti-CTLA4 treatment (28.5% of implanted tumors did not even grow) (Figure 4B-C). No benefit of combining anti-RL and anti-PD-L1 compared to anti-PD-L1 alone was observed in RANK<sup>+/+</sup> tumors in the early setting (Figure 4B-C).



**Figure 4. RANKL pharmacological inhibition reinforces anti-CTLA4 and anti-PD-L1 anti-tumor response in RANK<sup>+/+</sup> but not in RANK<sup>-/-</sup> tumors.** A, Graphs showing the percentage of PD-1<sup>+</sup> cells within CD11b<sup>-</sup> lymphocytes (n= 12 RANK<sup>+/+</sup> tumors, n=10 RANK<sup>-/-</sup> tumors; PD-1<sup>+</sup> within CD11b<sup>-</sup> CD45<sup>+</sup>; \*\*\*\* p < 0.0001), CTLA4 within CD4<sup>+</sup> T cells (n=8; CTLA4 within CD3<sup>+</sup> CD8<sup>-</sup> CD11b<sup>-</sup> CD45<sup>+</sup>; \* p = 0.0166), PD-L1 within tumor CD45<sup>-</sup> cells (n= 26 RANK<sup>+/+</sup> tumors, n=22 RANK<sup>-/-</sup> tumors; \* p =



0.017), and Tregs (n= 12 RANK<sup>+/+</sup> tumors, n=10 RANK<sup>-/-</sup> tumors; FoxP3<sup>+</sup> CD25<sup>+</sup> CD4<sup>+</sup> CD11b<sup>-</sup> within CD45<sup>+</sup>; \*\*\*\* p < 0.0001) in RANK<sup>+/+</sup> and RANK<sup>-/-</sup> transplants in syngeneic C57BL/6 mice. Each dot represents an individual tumor transplant derived from 2-5 different primary tumors. Mean, SEM and t-test two-tailed p-values are shown. (\*, p < 0.05; \*\*\*\*, p < 0.0001). B, Experimental scheme for early treatments with anti-RANKL (a-RL), anti-CTLA4, anti-PD-L1 or their respective isotype controls (rat IgG2A and mouse IgG2b). All treatments were administered i.p, two times/week and started 3 days after injection of RANK<sup>+/+</sup> and RANK<sup>-/-</sup> tumor cells into the mammary gland of syngeneic C57BL/6 mice. C-D. Tumor growth curves for early treatments (scheduled as in Fig. 4b) of RANK<sup>+/+</sup> (C) and RANK<sup>-/-</sup> (D) tumor cells injected in syngeneic C57BL/6. Each thin curve represents one single tumor. Each thick curve represents the mean of all the tumors that received the specific treatment. Linear regression analysis was performed and a two-tailed p-value was calculated to compare the tumor growth slopes after the specified treatments (\*\*\*\*, p<0.0001). E, Experimental scheme for late treatments with anti-RL, anti-CTLA4, anti-PD-L1, or their respective isotype controls (rat IgG2A and mouse IgG2b). All treatments were administered i.p., three times/week and started when transplanted tumors reached a size of 0.09 cm<sup>2</sup>. F-G, Tumor growth curves for late treatments (scheduled as in Fig 4E) of RANK<sup>+/+</sup> (F) and RANK<sup>-/-</sup> (G) tumor cells injected in syngeneic C57BL/6. Each thin curve represents one single tumor. Each thick curve represents the mean of all the tumors that received the specific treatment. Linear regression analysis was performed and a two-tailed p-value was calculated to compare the tumor growth slopes after the specified treatments \*\*\*, p = 0.0002; \*\*\*\*, p < 0.0001).

Early treatment with anti-CTLA4, but not with anti-PD-L1 or anti-RL, significantly attenuated RANK<sup>-/-</sup> tumor growth (66.7% of implanted tumors did not grow) compared with the isotype-treated control (Figure 4d). Addition of anti-RL did not improve the response to anti-CTLA4 (or anti-PD-L1) in RANK<sup>-/-</sup> tumors as did in RANK<sup>+/+</sup> tumors, suggesting that the augmented benefit of the anti-RL/anti-CTLA4 combination was driven by inhibition of RANK signaling in tumor cells (Figure 4D). Next, we tested the effect of checkpoint inhibitors on the growth of already palpable, actively growing tumors (Figure 4E). None of the RANK<sup>+/+</sup> tumors responded to anti-PD-L1 or anti-RL as single agents but their combination significantly reduced tumor growth in 50% of the tumors (Figure 4F). Anti-RL did not improve the response to anti-CTLA4 (Figure 4F). In tumors lacking RANK, anti-PD-L1 treatment was more efficient than anti-CTLA4, but no improvement was observed after the addition of anti-RL (Figure 4g), in contrast with the observations on RANK<sup>+/+</sup> tumors.

Collectively, these results demonstrate that in this luminal-like BC, RL inhibition improves the anti-tumor response to anti-CTLA4 (in the early setting) and anti-PD-L1 (for established tumors) through inhibition of RANK signaling in the tumor cells.

## **1.6 A short course of denosumab treatment in early-stage BC increased TILs**

To confirm the immunomodulatory role of RANK pathway inhibition in the clinical setting, we analyzed denosumab-treated BC clinical samples from the D-BEYOND study (NCT01864798): a prospective, preoperative window-of-opportunity, single-arm, multicenter trial assessing the effect of denosumab in premenopausal women with early-stage BC. Twenty-seven patients were included in this study and received two doses of denosumab

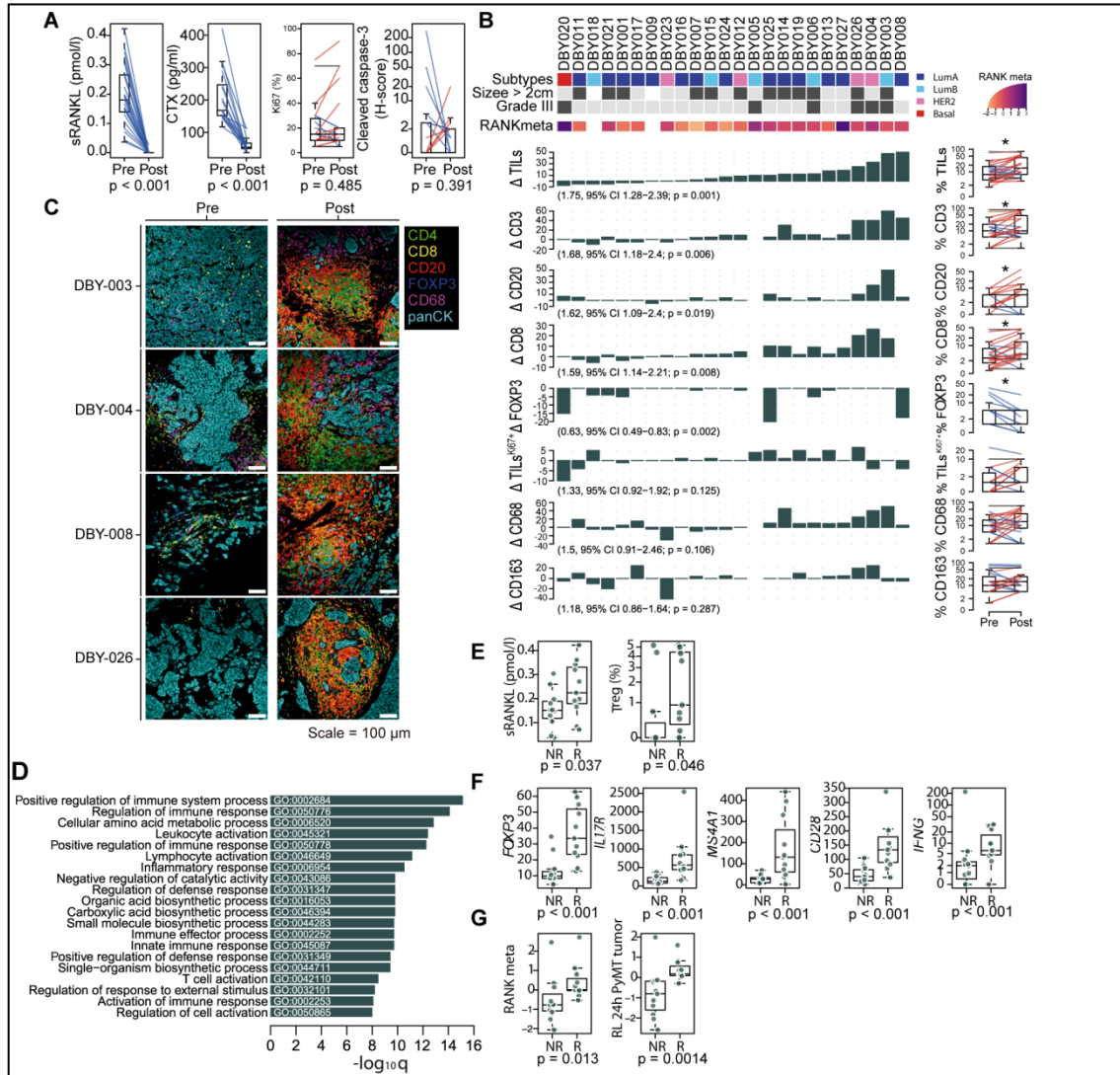
120 mg subcutaneously one week apart, followed by surgery. The median time interval between the first administration of denosumab and surgery was 13 days. No serious adverse events (AEs) were reported. All non-serious AEs are summarized in Supplementary Data 6, the most frequent being arthralgia (4/27 patients, 14.8%). Table 1 summarizes the clinicopathological features of the 24 patients subsequently analyzed. In brief, the median age at diagnosis was 45 years (range, 35-51 years); tumors of 19 patients were hormone receptor-positive (79.2%), four were HER2<sup>+</sup> (16.7%) and one was triple-negative (4.2%). After treatment, serum levels of sRL (unbound to denosumab) and CTX, a surrogate marker for denosumab activity, decreased in all patients evaluated ( $P < 0.001$ , Fig. 5a), confirming the target inhibition. Given its correlation with clinical response in luminal BC (Ellis et al., 2011; Horimoto et al., 2014; Yoshioka et al., 2015), the primary study endpoint was a geometric mean (GM) decrease in the percentage of Ki-67-positive cells. Secondary endpoints included tumor cell survival assessed by cleaved caspase-3, as well as tumor immune infiltration. There was no significant reduction in the percentage of Ki-67-positive cells (GM change from baseline; 1.07, 95% CI 0.87–1.33;  $P = 0.485$ , Figure 5a) and no absolute Ki-67 or cleaved caspase-3 responders were identified (Figure 5A, Supplementary Figure 5A).

Collectively, these data confirm that a short course of denosumab was associated with effective systemic RL inhibition, but not with a reduction in tumor proliferation or survival.

Next, we assessed the effect of denosumab on tumor immune infiltration in 24 available paired samples. Of note, similar to our preclinical model, we observed a significant increase in stromal and intratumoral lymphocyte levels after short exposure to denosumab (GM change from baseline: 1.75, 95% CI 1.28–2.39;  $P = 0.006$  and 1.59, 95% CI 1.14–2.21,  $P = 0.008$ , respectively, Figure 5B-C and Supplementary Figure 5A). In particular, 11/24 patients (45.8%), including 6/14 luminal A, 3/5 luminal B and 2/4 HER2<sup>+</sup> cases, showed an immunomodulatory response defined as a  $\geq 10$  percent increase in stromal TILs (sTILs) in tumor samples. Analyses of the percentage of Ki-67<sup>+</sup> TILs suggested a trend to increase after denosumab treatment, particularly in responders (7/11) (Figure 5B).

The composition of the immune infiltrate associated with denosumab treatment was analyzed by IHC in 23 available pairs of pre- and post-denosumab treatment tumor tissues (Figure 5b and Supplementary Figure 5A-B). These analyses revealed a significant increase in the percentage of T (CD3<sup>+</sup>) and B (CD20<sup>+</sup>) cells after denosumab treatment (GM change from baseline: 1.68, 95% CI 1.18–2.40;  $P = 0.006$  and 1.62, 95% CI 1.09–2.40;  $P = 0.019$ , respectively) and increased levels of CD8<sup>+</sup> T cells, validating our preclinical observations

(GM change from baseline: 1.59, 95% CI 1.14–2.21; P = 0.008). Moreover, there was a significant decrease in FOXP3<sup>+</sup>/CD4<sup>+</sup> T regs cell frequency (GM change from baseline: 0.63, 95% CI



**Figure 5. The immunomodulatory role of anti-RANKL in BC.** A, Change from baseline in serum levels of free-sRANKL (n = 23, p = 2.384e-07) and CTX (n = 17, p = 1.526e-05), (significance assessed by the two tailed sign test), the percentage of Ki-67-positive cells (p = 0.485) and the staining of activated caspase-3 (p = 0.391) (H-score) (n = 24) (significance assessed by two tailed paired t-tests)<sup>#</sup>. Boxplots display median line, IQR boxes, 1.5\*IQR whiskers and data points. B, Each bar-plot shows the change from baseline ( $\Delta$ ; post- minus pre-treatment values) of the immune parameters assessed using HE (TILs) and IHC (CD3, CD20, CD8, FOXP3, proliferative TILs (TILs<sup>Ki67+</sup>), CD68 and CD163). Each bar represents one patient, which are ranked by their increase in stromal TIL levels. Geometric mean changes, 95% CIs and p-values are shown below each bar-plot. For each measured parameter, the corresponding boxplot is displayed on the right-hand side. Boxplots display median line, IQR boxes, 1.5\*IQR whiskers and data points. Tumor characteristics and tumor RANK metagene expression at baseline are shown above. p; p-values derived from two tailed paired t-tests (\*, p<0.05)<sup>#</sup>. C, Representative micrographs of multiplex IHC of pre- and post-treatment tumor sections from the four patients with the highest immunomodulatory response. White scale bar, 100  $\mu$ m. D, Top 20 significantly enriched pathways after denosumab treatment, identified

by GAGE. E, Comparison of baseline serum levels of sRANKL between non-responders (NR; n = 13) vs. responders (R; n = 11) and comparison of baseline percentage of regulatory T cells (Tregs) as inferred from CIBERSORT. Boxplots display median line, IQR boxes, 1.5\*IQR whiskers and data points. Significance determined by the two tailed Mann–Whitney U test. F, Comparison of baseline mRNA expression levels of indicated genes (normalized counts) between non-responder (NR; n = 11) and responder (R; patients with  $\geq 10\%$  increase in TILs after denosumab treatment. n = 11) groups. Boxplots display median line, IQR boxes, 1.5\*IQR whiskers and data points. Significance determined by the two tailed Mann–Whitney U test p values: *FOXP3* ( $p = 1.61e-05$ ), *IL7R* ( $p = 1.53e-07$ ), *MS4A1* ( $p = 1.00E-06$ ), *CD28* ( $p = 5.63e-06$ ), *IFNG* ( $p = 4.15e-05$ ). G, Comparison of baseline RANK metagene and RANKL-treated PyMT tumor acini derived gene signature between non-responder (n = 11) and responder (n = 11) patients. Significance determined by the two tailed Mann–Whitney U test.

For panels a-b: each colored line represents one patient and indicates increase (red), decrease (blue) or no change (black) relative to baseline. Note that all variables were analyzed for all patients, but values for some lines overlap or the indicated population was not detected. Boxplots display median line, IQR boxes, 1.5\*IQR whiskers and data points.

#Responder patients are those with  $\geq 10\%$  increase in TIL infiltration after denosumab treatment. Significance determined by the two-tailed Mann–Whitney U test.

0.49–0.83;  $P = 0.002$ , Figure 5B), even in patients with no increase in TILs. No significant differences in macrophage infiltration ( $CD68^+$  or  $CD163^+$ ) were observed (Figure 5B and Supplementary Figure 5A). Intratumoral immune population abundance was also quantified, and an increase of TILs and  $CD3^+$  T cells was observed (Supplementary Figure 5A). These findings were illustrated using multiplex IHC of the top four tumors associated with the highest TIL increase (Figure 5C).

To investigate the biological effect of denosumab in early BC further, we performed RNA sequencing on 22 available pre- and post-treatment tumor samples and identified 379 genes that were differentially expressed (Supplementary Data 7). Pathway analysis using GO and GAGE revealed the enrichment of several genes related to immune activation, immune cell migration and cytokine-mediated signaling pathways (Figure 5D, Supplementary Data 9-10). In line with these findings, the expression levels of several chemokines were increased after treatment, including that of the well-known  $CD8^+$  T cell chemoattractants CCL4 and CXCL10 (Dufour et al., 2002; Honey, 2006) (Supplementary Figure 5C). Additionally, we performed RNA sequencing on 11 available pre- and post-treatment normal samples using RNA extracted from normal tissues. Sufficient normal RNA quantity from both pre- and post-treatment was obtained from eleven patients. Only ten genes were differentially expressed between pre- and post-treatment normal samples (Supplementary Data 8) and all of them were also differentially expressed in tumor tissue (Supplementary Data 7). No significant changes in RANK/RL at the protein (IHC) (Supplementary Figure 5D-E) or at the gene expression levels (RNAseq) (Supplementary Data 7 and 8) were found. Of note, no differences in genes related to immature mammary epithelial cell populations (*ALDH1*) or

related to estrogen receptor pathway (*ESR1*, *PR*, *BCL2*) both in tumor and normal samples were observed (D-BEYOND secondary endpoints) (Supplementary Data 7 and 8).

To further explore the impact of denosumab treatment on the immune cell landscape of BC we used CIBERSORT (Newman et al., 2015b), a deconvolution method for inferring immune cell content from gene expression data. Consistent with the IHC results, this analysis confirmed the increase in the relative frequencies of CD8<sup>+</sup> T cells, B cells and CD4<sup>+</sup> T cells, and the decrease in the frequencies of Tregs after denosumab treatment (Supplementary Figure 6A). Despite the overall increase in immune infiltration the relative frequency of macrophage infiltration was reduced after denosumab, particularly in responders (8/11) (Supplementary Figure 6A). No significant changes in NK cells, dendritic cells, mast cells, neutrophils and eosinophils were noted, because these populations may be too scarce to be captured properly by this method (Supplementary Figure 6A). Of note, after denosumab treatment, neutrophils correlated negatively with sTILs (Supplementary Figure 6B), and the neutrophil chemotaxis and migration pathways were modulated after denosumab treatment (Supplementary Data 9), supporting the preclinical findings.

To ensure that these changes are specific to denosumab treatment and not a consequence of the presurgical biopsy procedure, we interrogated the publicly available gene expression data of patients from the control-arm (untreated) of the POETIC study, a large BC window-of-opportunity study evaluating the role of perioperative aromatase inhibitor for which gene expression data were obtained from presurgical biopsies and surgical specimens. Similar to the D-BEYOND study, biopsies were taken at diagnosis and 2 weeks later at the time of surgery. The comparison of surgery and biopsy samples from the POETIC study did not reveal any enrichment of immune cells assessed by CIBESORT or an immune pathway, as assessed by GAGE analyses (Supplementary Figure 6C and Supplementary Data 11). Together, our results indicate that a short course of denosumab enhances immune infiltration as determined by the increased levels of TILs, B and T lymphocytes, CD4<sup>+</sup> and CD8<sup>+</sup> T cells in luminal and HER2<sup>+</sup> breast tumors, validating the clinical relevance of the findings in the preclinical models.

Finally, we investigated the baseline features associated with the immunomodulatory effect of denosumab. We identified 11 responder (R) cases, defined by a  $\geq 10\%$  increase in TIL infiltration after denosumab treatment and 13 non-responder (NR) cases. No associations were found between any baseline clinicopathological features and the immune modulation induced by denosumab (Supplementary Data 12). Of the characteristics compared between R and NR patients, high sRL serum levels, a high percentage of Tregs measured by

CIBERSORT, and the presence of intratumoral FOXP3+ cells measured by IHC, were significantly associated with increased TIL infiltration after denosumab treatment (Figure 5E, Supplementary Data 12). CD20 IHC staining at baseline was also associated with response, but this finding was not corroborated by CIBERSORT (Supplementary Data 12). A differential gene expression analysis using RNA-seq data from biopsy samples evidenced 42 genes expressed at higher levels in R than in NR, including *FOXP3*, *IL7R*, *MS4A1* (CD20), *CD28* and *IFNG* (Figure 5f, Supplementary Data 13) and the enrichment of genes involved in lymphocyte activation and immunoglobulin production in R patients (Supplementary Data 14 which may be indicative of an enhanced immune response).

RANK and RL IHC was performed on tumor and normal tissue samples. We did not find any difference between pre and post treatment samples (Supplementary Figure 5D-E) and neither was predictive of the immunomodulatory effects of denosumab (Supplementary Figure 7A). However, since it has been reported that RANK IHC is an unreliable tool to detect RANK protein on breast tumor samples (Infante et al., 2019; Taylor et al., 2017), we computed RANK and RL metagenes to increase the potency and reliability of RANK and RL detection. These metagenes included the expression levels of the top 100 genes that are co-expressed at baseline with *RANK* and *RL* mRNA, respectively (see methods, Supplementary Data 15). Importantly, high expression level of RANK metagene in the tumors at baseline (Figure 5G), but neither RL metagene nor individual gene expression of *RANK* or *RL*, is predictive of denosumab-induced immune response (Supplementary Figure 7B).

GO analyses showed that the RANK metagene includes genes associated with NF- $\kappa$ B pathway activation as well as with immune response (Supplementary Figure 7C). Indeed, the RANK metagene strongly correlated with several public signatures of the RANK and NF- $\kappa$ B pathways, as well as with RL-induced genes in mouse mammary epithelial cells (MECs) (WT and Rank overexpressing) and PyMT tumor cells (Supplementary Figure 8A). These results demonstrate that RANK metagene captures RANK pathway activation and support the relevance of the PyMT model. Accordingly, tumors responding to denosumab presented at baseline higher scores for these RL-driven genes in mouse MECs and PyMT tumor cells (Figure 5G; Supplementary Figure 8B) and RANK and NF- $\kappa$ B pathway gene signatures (Supplementary Figure 8C). Thus, tumors with increased RANK pathway activation at baseline are more likely to show increased TILs after RL inhibition, corroborating the preclinical findings: inhibition of RANK signaling in tumor cells contributes to the immunomodulatory effect of denosumab in BC.

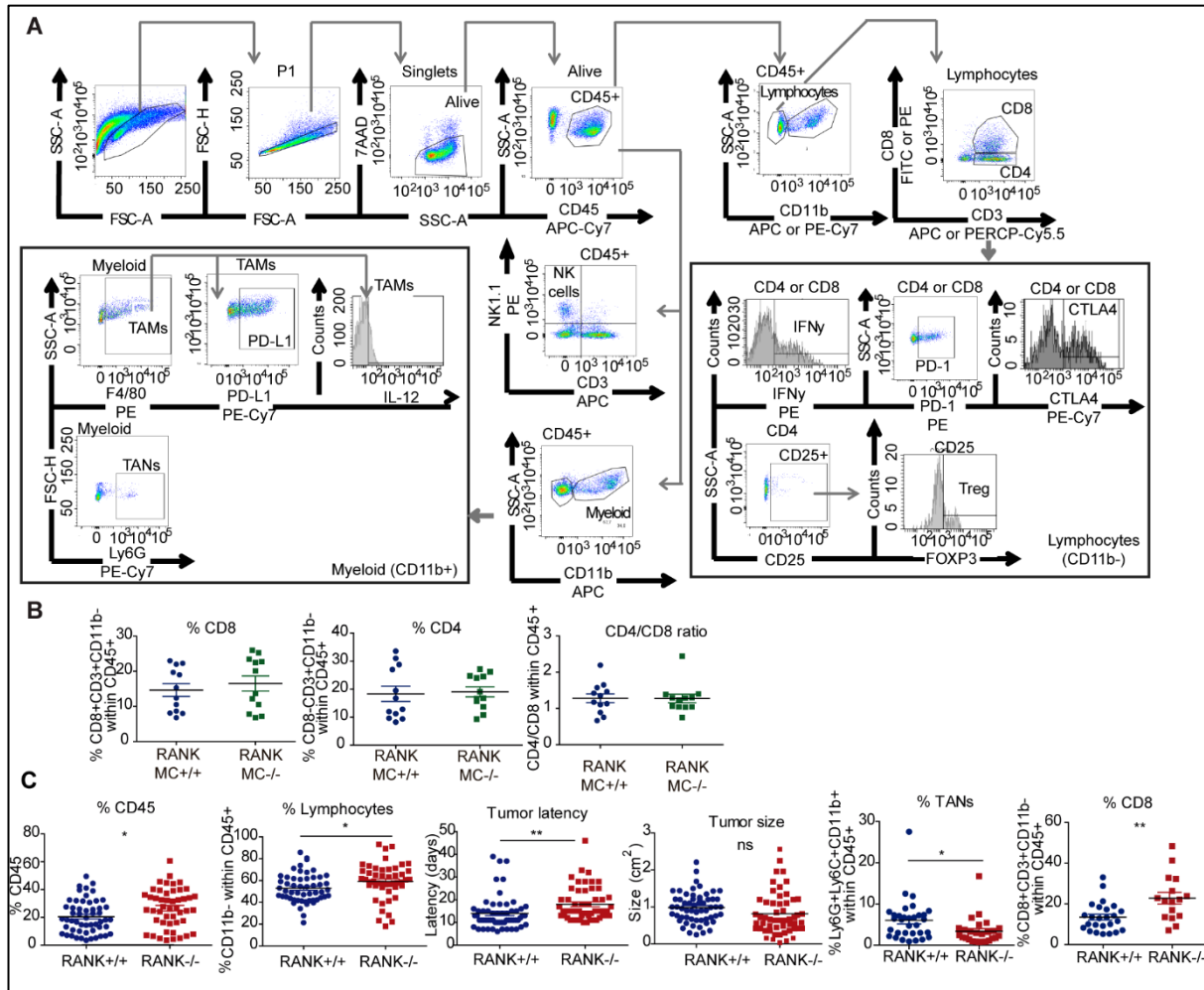
Together, these results indicate that higher RANK pathway activation, soluble RL and the presence of Tregs at baseline, are predictive biomarkers of the immunomodulatory response induced by denosumab in BC patients.





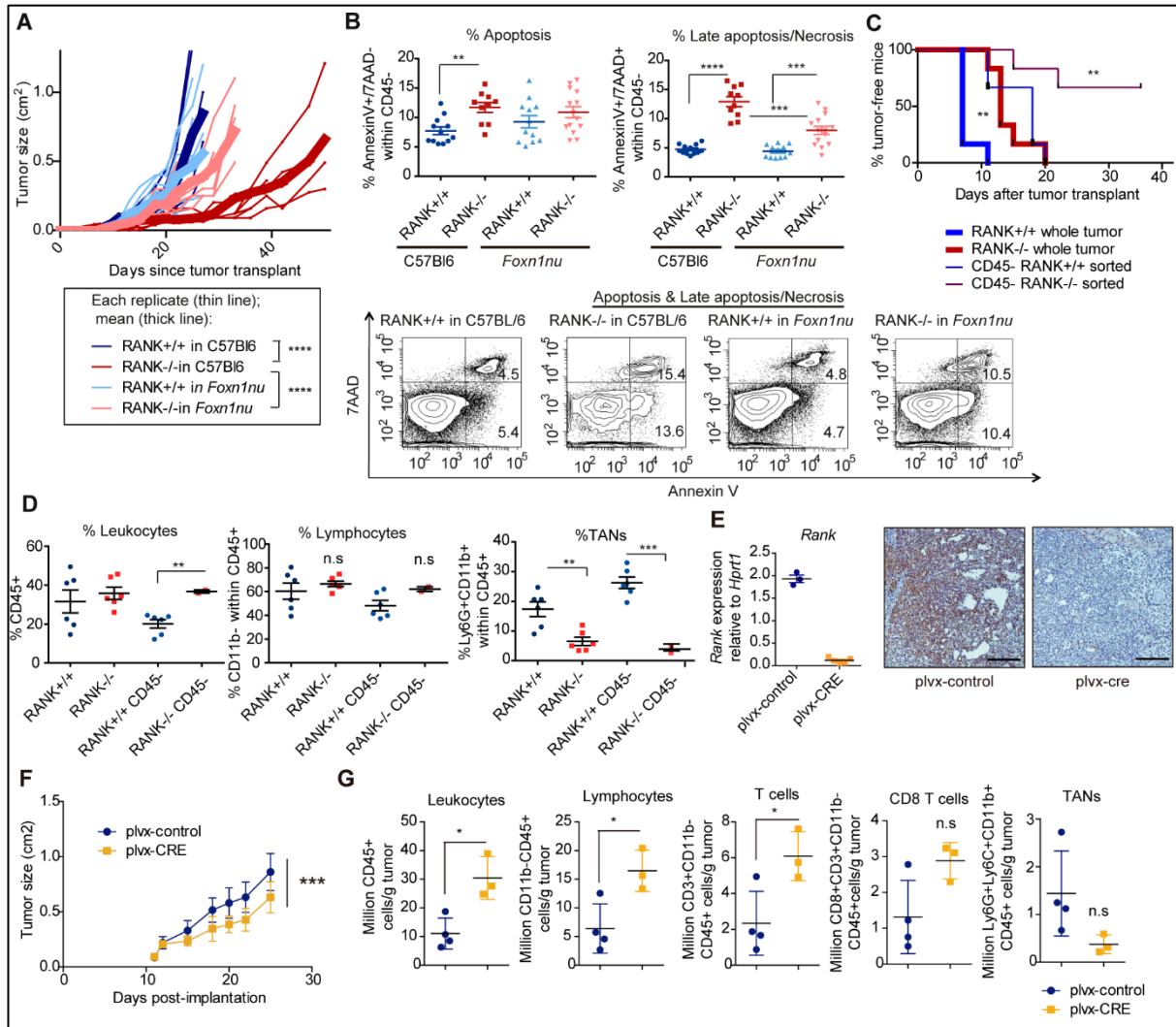
## **Supplementary Figures**





**Supplementary Figure 1. Flow Cytometry gating strategy and data from the different immune populations infiltrating mouse tumor transplants.** A. Gating strategy for tumor immune populations. Debris is excluded with FSC-SSC; and single, live, CD45<sup>+</sup> cells are selected. CD11b<sup>-</sup> cells are gated to enrich in lymphocytes and T cells are gated using CD3. CD8<sup>+</sup> T cells are differentiated from CD4<sup>+</sup> T cells based on CD8 expression. INF $\gamma$ , CTLA4 and PD-1 are gated within CD4<sup>+</sup> and CD8<sup>+</sup> T cells. Tregs are identified by gating CD25<sup>+</sup> and FOXP3<sup>+</sup> cells within CD4<sup>+</sup> T cells. Myeloid cells are enriched by gating the CD11b<sup>+</sup> population. TAMs are identified by F4/80<sup>+</sup> staining and TANs by Ly6G<sup>+</sup> staining. PDL1<sup>+</sup> and IL12<sup>+</sup> populations are gated within TAMs. NK cells are gated in the CD45<sup>+</sup> population as NK1.1<sup>+</sup>CD3<sup>-</sup> cells. B. Graphs showing the percentages of tumor-infiltrating CD8<sup>+</sup> T cells (CD8<sup>+</sup> CD3<sup>+</sup> CD11b<sup>-</sup> within CD45<sup>+</sup>), CD4<sup>+</sup> T cells (CD8<sup>-</sup> CD3<sup>+</sup> CD11b<sup>-</sup> within CD45<sup>+</sup>), and CD4/CD8 ratio in RANK<sup>+/+</sup> tumor transplants in RANK MC<sup>-/-</sup> and RANK MC<sup>+/+</sup> mice. Each dot represents one tumor transplant (n=12). Mean  $\pm$  SEM is shown. C. Graphs showing the percentage of leukocytes CD45<sup>+</sup> (n= 54 RANK<sup>+/+</sup> tumors, n=48 RANK<sup>-/-</sup> tumors; \* p = 0.019), lymphocytes (n= 54 RANK<sup>+/+</sup> tumors, n=48 RANK<sup>-/-</sup> tumors, CD11b<sup>-</sup> within CD45<sup>+</sup>; \* p = 0.0367), TANs (n= 32 RANK<sup>+/+</sup> tumors, n=26 RANK<sup>-/-</sup> tumors; Ly6G<sup>+</sup>Ly6G<sup>+</sup>CD11b<sup>+</sup> within CD45<sup>+</sup>, \* p = 0.0224) and CD8<sup>+</sup> T cells (n= 25 RANK<sup>+/+</sup> tumors, n=16 RANK<sup>-/-</sup> tumors CD8<sup>+</sup>CD3<sup>+</sup>CD11b<sup>-</sup> within CD45<sup>+</sup>, \*\* p = 0.0024) in whole-tumor transplants of RANK<sup>+/+</sup> and RANK<sup>-/-</sup> in syngeneic C57BL/6 mice. Tumor size at the time of analyses (p = 0.076) and tumor latency (\* p = 0.018) is shown (n= 54 RANK<sup>+/+</sup> tumors, n=48 RANK<sup>-/-</sup> tumors). Each dot represents one tumor transplant derived from 12-13 different primary tumors. Means, SEMs and t test two-tailed p values are shown.



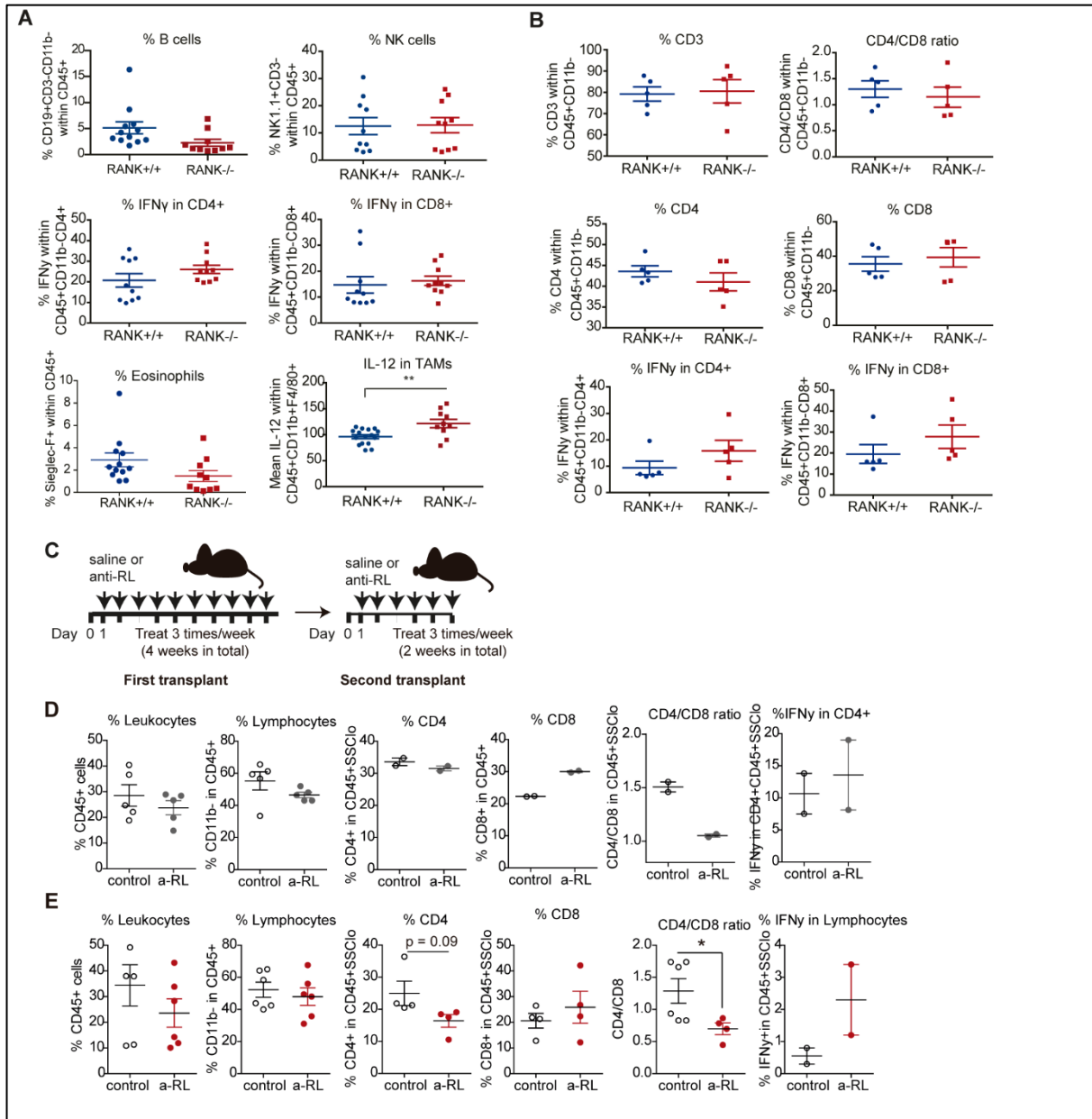


**Supplementary Figure 2. Differences in tumor growth and immune infiltration are confirmed upon transplantation of FACS-sorted RANK<sup>+/+</sup> and RANK<sup>-/-</sup> cells and upon RANK deletion in an alternative PyMT RANK floxed mouse model.** A. Tumor growth curves after tumor transplantation of RANK<sup>+/+</sup> and RANK<sup>-/-</sup> whole tumor cells in syngeneic C57BL/6 (n=6) and *Foxn1*<sup>nu</sup> (n=8) mice. Thin curves represent each tumor, thick curves represent the mean of all the tumors in each arm.###. B. Graphs showing the percentages of apoptotic (AnnexinV<sup>+</sup>7AAD<sup>-</sup>; \*\* p = 0.0011) and necrotic (AnnexinV<sup>+</sup>7AAD<sup>+</sup>; \*\*\*\* p < 0.0001, \*\* p = 0.002) tumor cells in RANK<sup>+/+</sup> (n = 12) or RANK<sup>-/-</sup> tumor transplants (n=10 in C57BL/6 or n=14 in *Foxn1*<sup>nu</sup> hosts) in syngeneic C57BL/6 and *Foxn1*<sup>nu</sup> mice (n = 10-14 tumors analyzed at endpoint (>0.2 cm<sup>2</sup>)). Two different primary tumors were used. Representative dot plots are shown below#. C. Kinetics of palpable tumor onset after tumor transplantation of RANK<sup>+/+</sup> and RANK<sup>-/-</sup> whole tumor cells (1,000,000 cells injected) or CD45<sup>-</sup> sorted cells (300,000 cells injected) in syngeneic C57BL/6 mice (n = 6). Note that only 2/6 RANK<sup>-/-</sup> tumor -sorted cells were able to give rise to transplants. Means and SEMs are shown. Log-rank test with two-tailed p value (whole tumor \*\*, p = 0.013; sorted cells \*\* p = 0.085). D. Graphs showing the percentage of CD45<sup>+</sup> (p = 0.006), lymphocytes (CD11b<sup>-</sup> within CD45<sup>+</sup>) and TANs (Ly6G<sup>+</sup>CD11b<sup>+</sup> within CD45<sup>+</sup>; \*\*\* p = 0.0009, \*\* p = 0.003) in tumors described in panel c (n = 6 except for RANK<sup>-/-</sup> tumor -sorted cells: n=2, see S2c)#. E. *Rank* mRNA levels determined by RT-PCR and IHC on PyMT; RANK<sup>fl/fl</sup> tumors infected with either control or pLVX-cre lentivirus. Scale = 100 μm. (n=3 control and n=4 pLVX-cre-infected tumors). Mean +/- SEM is shown. F. Growth curves from orthotopically transplanted PyMT; RANK<sup>fl/fl</sup> tumors infected with control or pLVX-cre lentivirus (n = 6). Mean and SEM are shown (\*\*\*, p = 0.0002)###. G. Graphs showing the total number per gram of tumor of

leukocytes (CD45<sup>+</sup>, \* p = 0.01), lymphocytes (CD11b<sup>-</sup> within CD45<sup>+</sup>, \* p = 0.022), T cells (CD3<sup>+</sup> CD11b<sup>-</sup> within CD45<sup>+</sup>, \* p = 0.03), CD8<sup>+</sup> T cells (CD8<sup>+</sup> CD3<sup>+</sup> CD11b<sup>-</sup> within CD45<sup>+</sup>, p = 0.061) and TANs (Ly6G<sup>+</sup>Ly6C<sup>-</sup>CD11b<sup>+</sup> within CD45<sup>+</sup>, p = 0.103) in tumors described in panel f (n=4 control tumors; n=3 pLVX-cre tumors)#.

#Each dot represents one tumor. Mean, SEM and t test two-tailed p values are shown. (\*, p < 0.05; \*\*, p < 0.01; \*\*\*, p < 0.001; \*\*\*\*, p < 0.0001).

##Linear regression analysis was performed and a two-tailed p-value was calculated to compare the tumor growth slopes after the specified treatments (\*\*\*, p<0.001; \*\*\*\*, p < 0.0001).

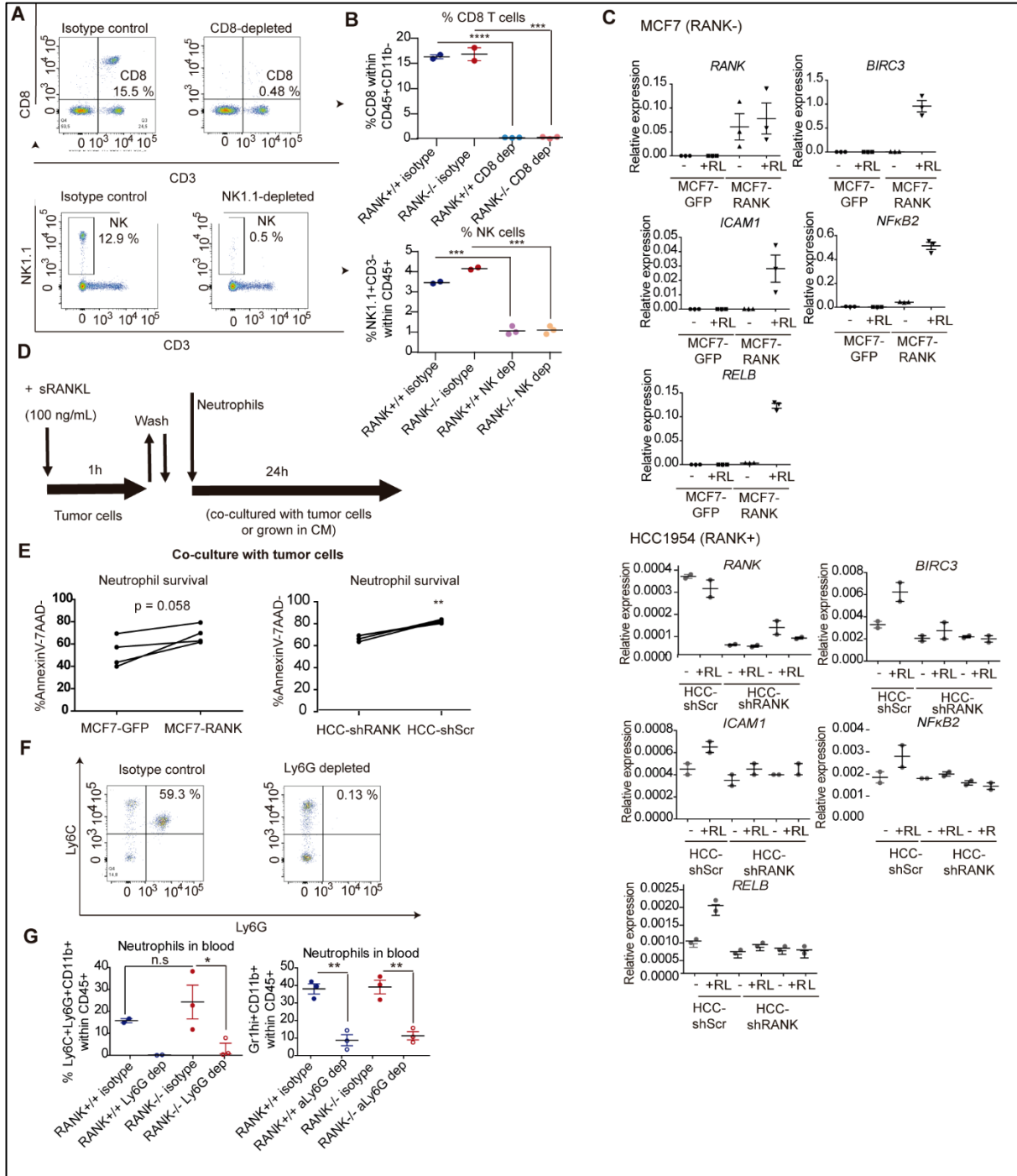


### Supplementary Figure 3. RL inhibition and immune cell population depletion experiments

A. Graphs showing the percentage of B cells (CD19<sup>+</sup> CD3<sup>-</sup> CD11b<sup>-</sup> within CD45<sup>+</sup>), NK cells (NK1.1<sup>+</sup> CD3<sup>-</sup> within CD45<sup>+</sup>), IFN $\gamma$  within CD4<sup>+</sup> (CD4<sup>+</sup> CD11b<sup>-</sup> CD45<sup>+</sup>) and CD8<sup>+</sup> (CD8<sup>+</sup> CD11b<sup>-</sup> CD45<sup>+</sup>), eosinophils (SiglecF<sup>+</sup> F4/80<sup>+</sup> CD11b<sup>+</sup> within CD45<sup>+</sup>) and IL-12 within TAMs (IL-12 within F4/80<sup>+</sup> CD11b<sup>+</sup> CD45<sup>+</sup>) in whole-tumor transplants of RANK<sup>+/+</sup> (n = 12) or RANK<sup>-/-</sup> (n = 10) injected into syngeneic C57BL/6 mice. Each dot represents one tumor. Means and SEMs and t-test two-tailed p values are shown (\*\*, p = 0.0036). Tumor transplants were derived from two representative primary tumors. B. Graphs showing the percentage of CD3<sup>+</sup>, CD4<sup>+</sup>, CD8<sup>+</sup>, within CD45<sup>+</sup> cells, CD4/CD8 ratio and IFN $\gamma$  expression levels in CD4<sup>+</sup> and CD8<sup>+</sup> cells in the draining lymph nodes of syngeneic C57BL/6 mice transplanted with RANK<sup>+/+</sup> and RANK<sup>-/-</sup> tumor cells (n=5). Each dot represents a pool of two draining lymph nodes from the same mouse. Means and SEMs are indicated. Tumor transplants derived from two representative tumors are considered. C. Schematic overview of RANK pathway inhibition anti-RL (RANK-Fc) treatments in orthotopic PyMT FvB/NJ tumors. One million cells isolated from a pool of two PyMT carcinomas were orthotopically injected into syngeneic FvB/N mice, which were randomized 1:1 for RANK-Fc (10 mg/kg, three times per week, for 4 weeks) or mock treatment

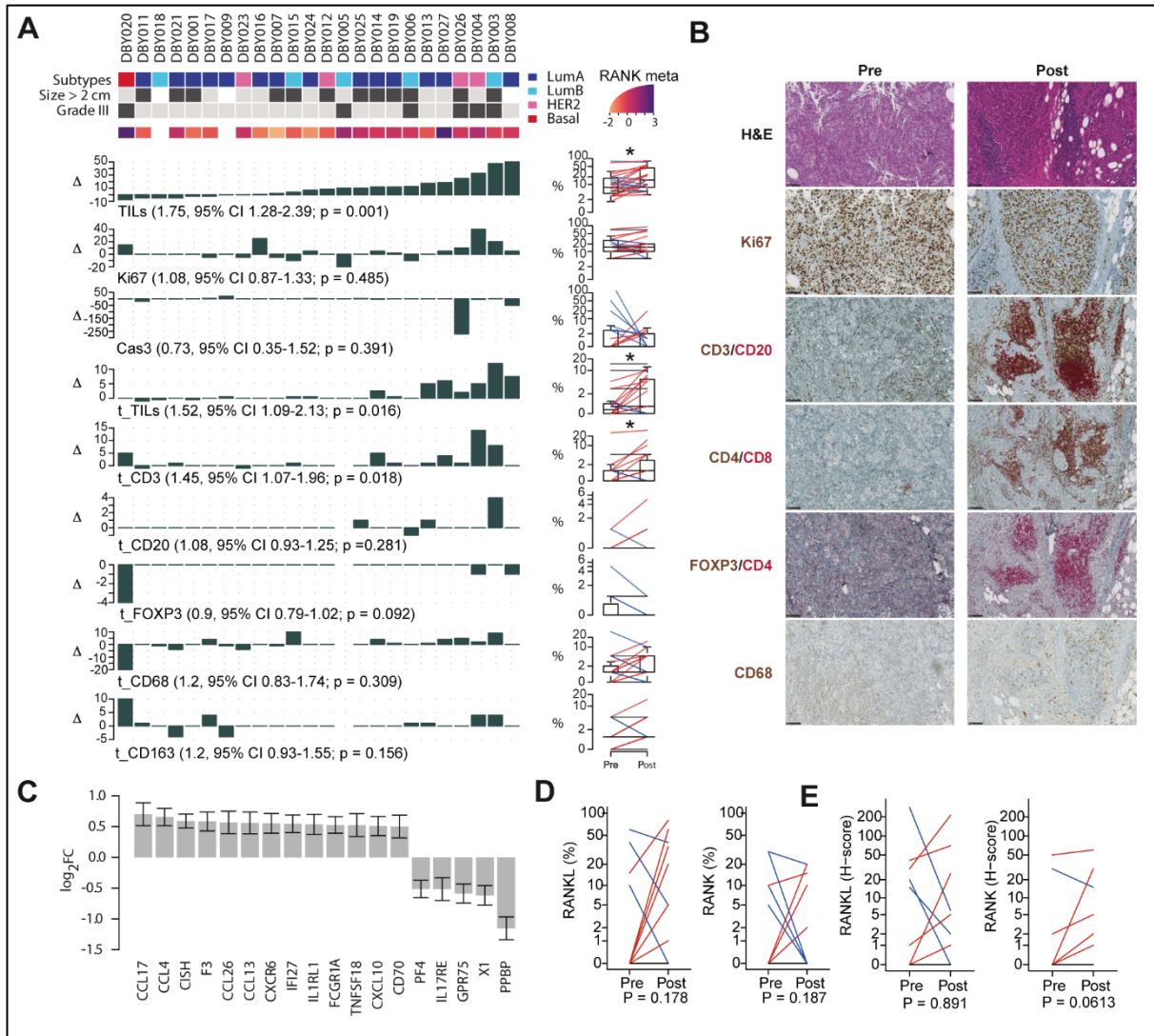
starting 24 h later (first transplant). Tumors were excised 24 h after last treatment analyzed by flow cytometry and cells isolated from each treatment arm were pooled and orthotopically injected into syngeneic FvB/NJ mice (second serial transplant) and treated for 2 weeks with RANK-Fc or mock treatment starting 24 h later. See (Yoldi et al., 2016). D-E. Graphs showing the percentage of leukocytes CD45<sup>+</sup> cells (d, n = 5; e, n = 6), lymphocytes (CD11b<sup>-</sup> within CD45<sup>+</sup>; d, n = 5; e, n = 6), CD4<sup>+</sup> (CD8<sup>-</sup> CD4<sup>+</sup> CD11b<sup>-</sup> within CD45<sup>+</sup>; d, n = 2; e, n = 4), CD8<sup>+</sup> (CD4<sup>-</sup> CD8<sup>+</sup> CD11b<sup>-</sup> within CD45<sup>+</sup>; d, n = 2; e, n = 4), CD4/CD8 ratio (d, n = 2; e, n = 4), and IFN $\gamma$  within CD4<sup>+</sup> (IFN $\gamma$  within CD45<sup>+</sup> CD11b<sup>-</sup> CD4<sup>+</sup> CD8<sup>-</sup>, n = 2) from first (D) or second (E) transplant tumors treated with RANK-Fc or control (n=4) (d) or . Mean, SEM and t test two-tailed p values are shown. (\*, p = 0.045).





**Supplementary Figure 4. RANK pathway activation in breast tumor cells increases survival of immunosuppressive neutrophils.** A-B. Representative dot blots (A) and quantifications (B) showing the percentage of CD8<sup>+</sup> (CD3<sup>+</sup> CD8<sup>+</sup> CD11b<sup>-</sup> CD45<sup>+</sup>; \*\*\*\*,  $p < 0.0001$ , \*\*\*  $p = 0.0005$ ) or NKs (NK1.1<sup>+</sup> CD3<sup>+</sup>; \*\*\*  $p = 0.0007$  for RANK<sup>+/+</sup> samples and  $p = 0.0003$  for RANK<sup>-/-</sup> samples) in CD8 depleted ( $n=3$ ), NK depleted ( $n=3$ ) and isotype controls ( $n=3$ ) blood samples from both RANK<sup>+/+</sup> and RANK<sup>-/-</sup> tumor transplants 10 days after first treatment with depletion antibodies. Means and SEMs and two-tailed t-test  $p$  values are shown. C. mRNA expression levels of the indicated genes after RL stimulation for 24 h in MCF7-GFP and MCF7-RANK (above,  $n=3$ ); and HCC1954-shScr and HCC1954-shRANK (below,  $n=2$ ). Mean  $\pm$  SEM is shown. D. Experimental scheme: human neutrophils isolated from blood of healthy donors are either co-cultured or cultured 1:1 in conditioned

medium (CM) from MCF7 (GFP or RANK) or HCC1954 (shScr and shRANK) pre-stimulated with RL for 24 h. E. Percentage of Annexin-V<sup>-</sup> 7AAD<sup>-</sup> neutrophils (n=4, 2 healthy donors) co-cultured (1:1) for 24 h with the indicated RL-treated tumor cells (MCF7, p = 0.058; HCC-1954, \*\* p = 0.0047). Each dot represents neutrophils from technical replicates. F. Representative dot blots showing the percentage of neutrophils (Ly6G<sup>+</sup> Ly6C<sup>+</sup> CD11b<sup>+</sup> within CD45<sup>+</sup>) in Ly6G-depleted (n=3) and isotype control (n=3) mouse blood samples. G. Quantification of neutrophils in blood extracted from mice with RANK<sup>+/+</sup> and RANK<sup>-/-</sup> tumor transplants 15 days after first treatment with depletion antibody. Left panel shows Ly6G<sup>+</sup> Ly6C<sup>+</sup> CD11b<sup>+</sup> (\* p = 0.05) and right panel shows Gr1<sup>hi</sup> CD11b<sup>+</sup> within CD45<sup>+</sup> (\*\* p = 0.0024 for RANK<sup>+/+</sup> samples and p = 0.0036 for RANK<sup>-/-</sup> samples) Means and SEMs and t-test two-tailed p values are shown.

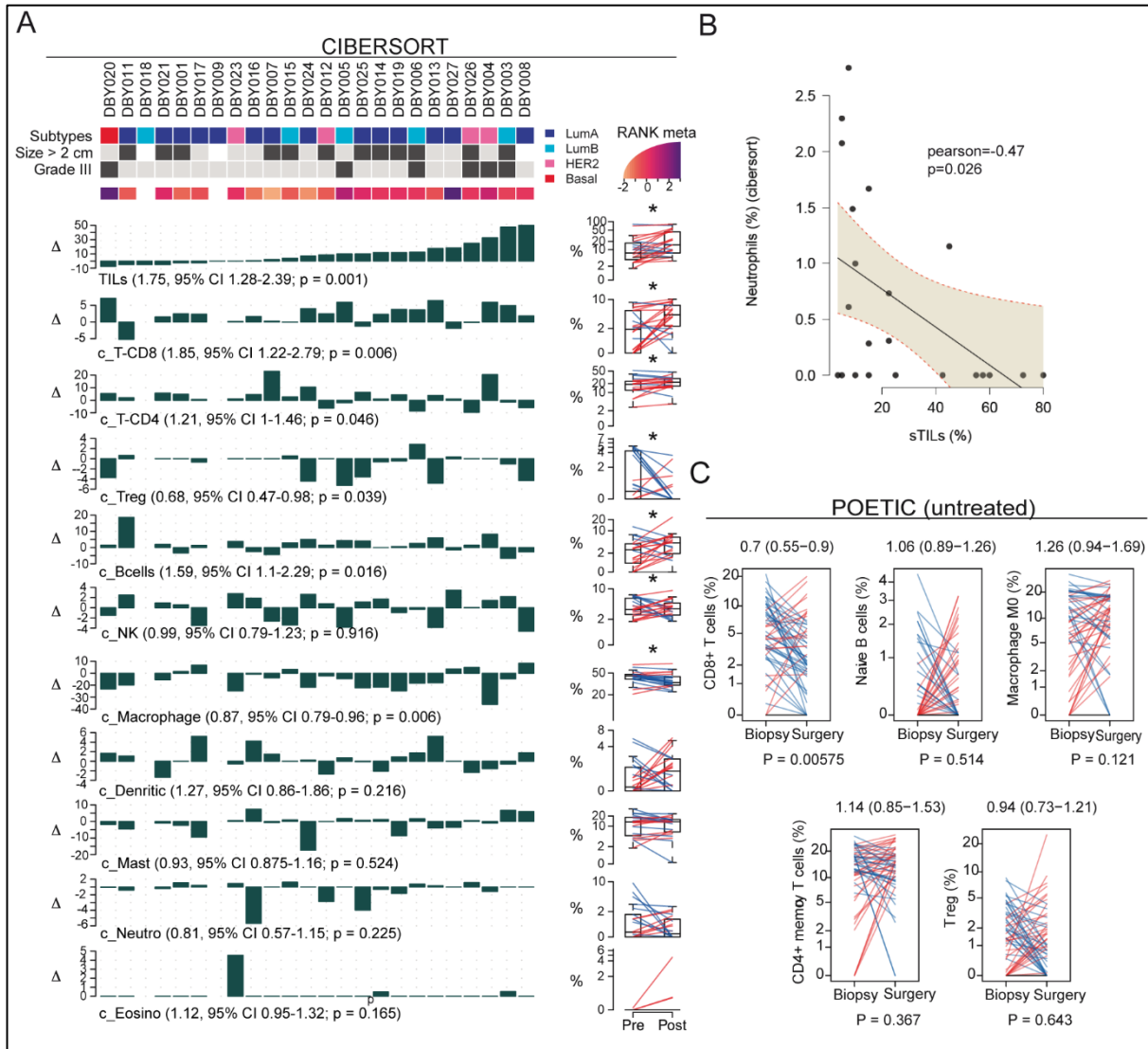


**Supplementary Figure 5. Changes in D-BEYOND patient samples after denosumab treatment.**

A. Each bar-plot shows the change from baseline ( $\Delta$ ; post- minus pre-treatment values  $n=24$ ) of each parameter measured using H&E (TILs), IHC (Ki-67 and cleaved caspase-3 tumor cells) and immune intra-tumoral compartment ( $t\_TILs$ ,  $t\_CD3$ ,  $t\_CD20$ ,  $t\_FOXP3$ ,  $t\_CD68$ ,  $t\_CD163$ ) #, ##. For each measured parameter, the corresponding boxplot is displayed on the right-hand side. Boxplots display median line, IQR boxes, 1.5\*IQR whiskers and data points. Significance assessed by two-tailed paired t-tests. B. H&E and IHC stainings of pre- and post-treatment tumor sections. One representative patient (DBY003) out of 24 is shown. Scale = 100  $\mu$ m. C. Genes differentially expressed between pre- and post-treatment samples ( $n=24$  patients) identified using RNAseq analysis. Boxplots illustrating the  $\log_2$  fold change of the differentially expressed genes involved in the GO:0019221 cytokine-mediated signaling pathway. Error bars are plus or minus two times the standard error. D-E. Change from baseline in protein levels of RL and RANK (H-score,  $n = 24$ , significance assessed by the sign test) in normal mammary gland adjacent to tumor tissue (D) or in tumor tissue (E). Colored lines indicate increase (red), decrease (blue) or no change (black) relative to baseline. Significance assessed by two-tailed paired t-tests.

#Geometric mean changes, 95% CIs and p-values are shown below each bar-plot. Colored lines indicate increase (red), decrease (blue) or no change (black) relative to baseline for each patient. All variables were analyzed for all patients, but values for some lines overlap or the indicated population

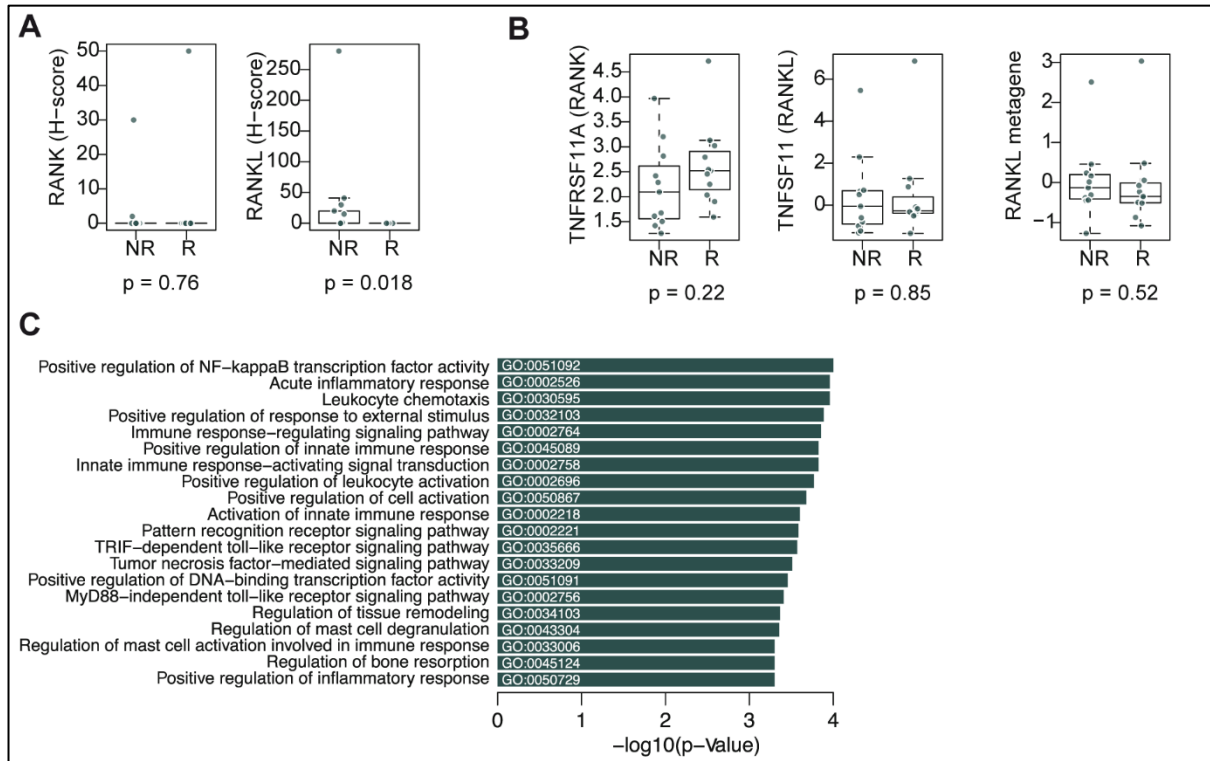
was not detected. Group differences were examined by a two tailed paired t-test (\*,  $p < 0.05$ ). ##Each bar represents one patient, ordered by increase in stromal TIL levels. For each measured parameter, the corresponding ladder-plot is displayed on the right-hand side. Tumor characteristics and tumor RANK metagene expression at baseline are shown above.



**Supplementary Figure 5. Changes in D-BEYOND and POETIC patient samples by RNAseq after denosumab treatment.** A. Each bar-plot shows the change from baseline ( $\Delta$ ; post- minus pre-treatment values) of each nine immune parameters measured using CIBERSORT in 24 patients. Significance assessed by two-tailed paired t-tests. #. ##. B. Association between the percentage of neutrophils, as inferred by CIBERSORT, and stromal TIL infiltrations assessed by IHC in surgery samples from D-BEYOND patients. Pearson; P-value derived from the Spearman's correlation,  $\rho$ ; Spearman's rho. The grey area indicates the 95% confidence interval. C. Comparison of immune cell fractions as inferred by CIBERSORT, between presurgical biopsies (B) and surgical (S) specimens ( $n = 57$ ) from the control arm (untreated) of the POETIC study<sup>#</sup>.

<sup>#</sup>Geometric mean changes, 95% CIs and p-values are shown below each bar-plot. Colored lines indicate increase (red), decrease (blue) or no change (black) relative to baseline for each patient. All variables were analyzed for all patients, but values for some lines overlap or the indicated population was not detected. Group differences were examined by a two-tailed paired t-test (\*,  $p < 0.05$ ). <sup>##</sup>Each bar represents one patient, ordered by increase in stromal TIL levels. For each measured parameter, the corresponding ladder-plot is displayed on the right-hand side. Tumor characteristics and tumor RANK metagene expression at baseline are shown above.

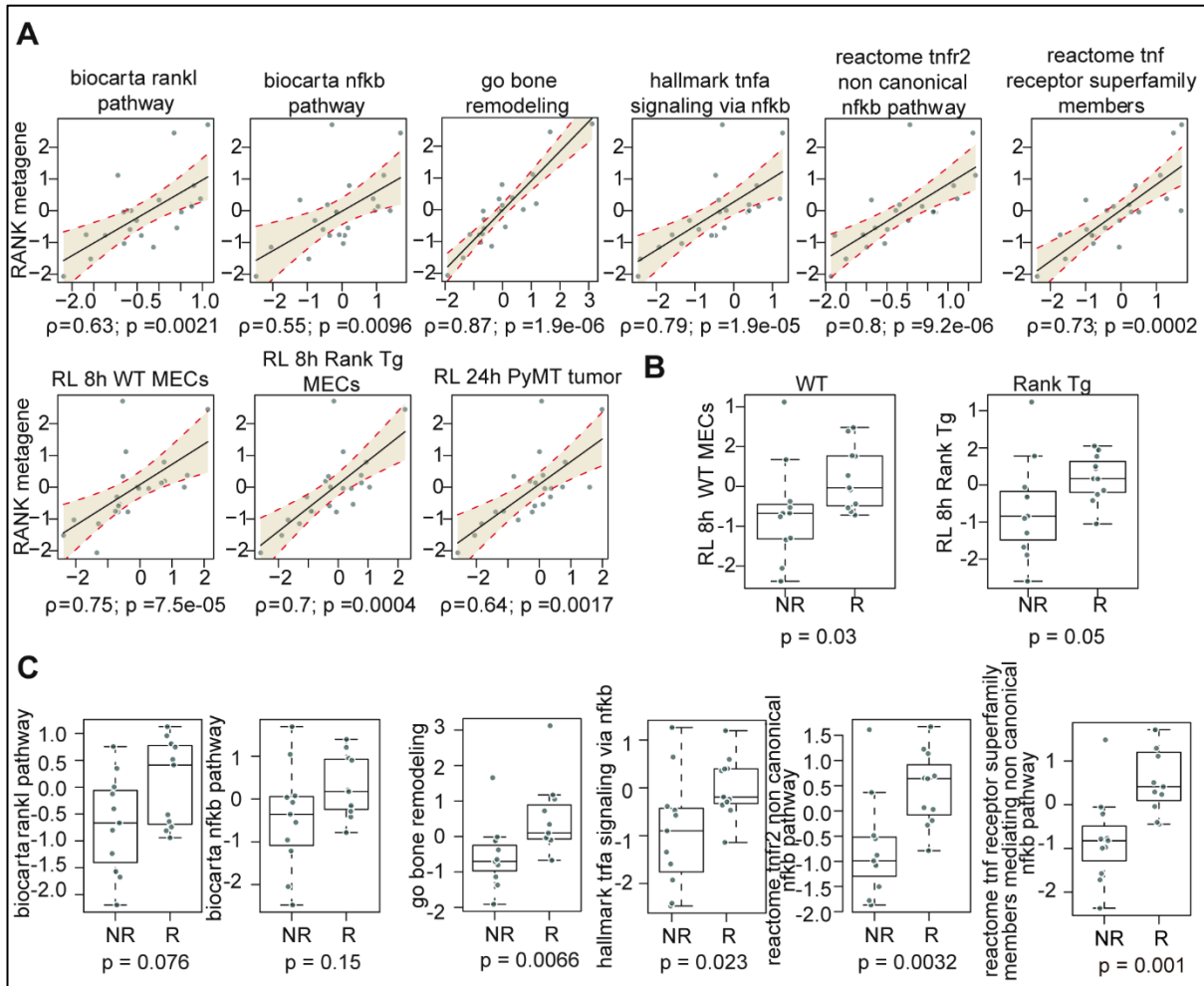




**Supplementary Figure 6. RANK expression on responder and non-responder patients.** A. Comparison of RANK and RL IHC score in baseline tumor samples between responders (R, n=11) and non-responders (NR, n=11). p, p-values assessed with two tailed Wilcoxon tests. Boxplots display median line, IQR boxes, 1.5\*IQR whiskers and data points. B. Comparison of *TNFRSF11A* (RANK) and *TNFSF11* (RL) mRNA expression and RL metagene levels in tumor samples between responders (R, n=11) and non-responders (NR, n=11). Boxplots display median line, IQR boxes, 1.5\*IQR whiskers and data points. p, p-values assessed with two tailed Mann-Whitney U test. C. Top 20 most significantly enriched gene ontology (GO) pathways associated with genes included in the RANK metagene. P-values were derived from the two tailed Fisher's exact test.







**Supplementary Figure 7. RANK metagene as a surrogate marker of RANK activation in biopsy samples and as predictive tool of denosumab-induced immunomodulation.** A. Correlation between RANK metagene and six public signatures related to RANK pathway/NF $\kappa$ B activation from MSigDB (upper) and two signatures derived from the top upregulated genes in WT (left) and RANK-overexpressing (RANK-Tg) 3D cultures of mouse mammary epithelial cells treated with RL for 8 h, and RL-treated (24 h) PyMT tumor acini-derived gene signature (lower panel).  $\rho$ ; p-values assessed with the Spearman's correlation coefficient. The grey area indicates the 95% confidence interval. B. Comparison of two signatures derived from the top upregulated genes in WT (left) and RANK-overexpressing (RANK-Tg) 3D cultures of mouse mammary epithelial cells treated with RL for 8 h between responders (R, n=11) and non-responders (NR, n=11).  $p$ , p-values assessed with the two tailed Mann–Whitney U test. Boxplots display median line, IQR boxes, 1.5\*IQR whiskers and data points. C. Comparison of six public signatures related to RANK pathway/NF $\kappa$ B activation from MSigDB between responders (R, n=11) and non-responders (NR, n=11).  $p$ , p-values assessed with the two tailed Mann–Whitney U test. Boxplots display median line, IQR boxes, 1.5\*IQR whiskers and data points.



## **Supplementary Data**



**Supplementary Data 1: Differentially expressed genes between between RANK+/+ and RANK-/- tumor cells (CD45-) implanted in**

GeneSymbol	GO	TIGRID	FC	logFC	logFC.CI.L	logFC.CI.R	AveExpr	t	P.Value	adj.P.Val
Tchh	GO:0005737	TC1707494	24.69493	4.626143	4.249473	5.002813	7.273212	28.71501	7.13E-09	0.000139
Krt28	GO:0005198	TC1584658	8.676048	3.117038	2.645145	3.588931	6.356815	15.44365	6.60E-07	0.00084
Glycam1	GO:0005576	TC1615593	8.043494	3.007822	1.897769	4.117875	6.135775	6.335192	3.08E-04	0.019418
Clca3	GO:0005254	TC1577725	7.838218	2.970526	1.714989	4.226063	8.122477	5.531654	7.19E-04	0.032152
Bex4	GO:0003674	TC1576728	6.714429	2.747265	1.821703	3.672826	9.112328	6.939792	1.71E-04	0.013827
Krt27	GO:0005198	TC1582100	6.239034	2.641323	2.43422	2.848425	6.831079	29.81859	5.40E-09	0.000139
Galnt14	GO:0003674	TC1584750	5.806805	2.537745	2.29342	2.782069	6.467184	24.28463	2.44E-08	0.000357
Aqp3	GO:0002684	TC1595433	5.775169	2.529863	1.791914	3.267812	6.726343	8.258677	1.20E-04	0.011004
Tacstd2	GO:0003674	TC1578728	5.372766	2.425665	1.774763	3.076567	8.185098	8.712974	3.74E-05	0.005802
Cyp26a1	GO:0001972	TC1585212	5.154784	2.365912	2.10569	2.626134	6.938349	21.25719	6.47E-08	0.000478
S100a9	GO:0002523	TC1578387	4.798769	2.262664	1.921606	2.603723	7.281492	15.5111	6.39E-07	0.00084
Krt6b	GO:0002009	TC1600985	4.738999	2.244582	1.873226	2.615939	6.106568	14.13174	1.25E-06	0.001143
Csn2	GO:0005215	NP748821	4.543066	2.183666	1.948772	2.41856	5.823405	21.7353	5.50E-08	0.000478
Klk10	GO:0003674	TC1581497	4.518489	2.17584	1.521492	2.830189	6.966313	7.774444	8.07E-05	0.008786
Krt16	GO:0005198	TC1583688	4.502052	2.170583	1.597998	2.743168	9.894225	8.86314	3.33E-05	0.005601
Wif1	GO:0005576	TC1595629	4.415085	2.142441	1.848171	2.436712	11.72745	18.29153	4.46E-06	0.002026
Nfe2l3	GO:0003677	TC1580069	4.410038	2.140791	1.862095	2.419487	6.743214	17.95954	2.21E-07	0.000577
Padi3	GO:0004668	TC1585715	4.377091	2.129972	1.813052	2.446893	6.462037	15.71357	5.82E-07	0.000831
Rspo	GO:0001658	TC1588960	4.33725	2.116781	1.853038	2.380524	6.859815	18.76489	1.61E-07	0.000537
Krt19	GO:0005198	TC1572673	4.31137	2.108146	1.098939	3.117354	13.22867	4.883952	1.51E-03	0.048544
4732456N10	GO:0003674	TC1594299	4.302299	2.105108	1.822885	2.38733	5.412121	17.4395	2.74E-07	0.000616
Gin1	GO:0003676	TC1585099	4.292455	2.101803	1.848292	2.355314	7.726803	19.38411	1.27E-07	0.000516
Krt28	GO:0005198	TC1584658	4.189616	2.066818	1.602671	2.530965	5.289486	10.41113	1.09E-05	0.003256
Sostdc1	GO:0005515	TC1579772	4.161781	2.057201	1.762871	2.351531	7.341859	16.34154	4.39E-07	0.000755
Calm4	GO:0005509	TC1579290	4.142418	2.050473	1.60893	2.492017	5.885456	10.85755	8.13E-06	0.002866
Raet1e	GO:0001913	TC1590096	4.094406	2.033654	1.427315	2.639993	8.935342	7.841743	7.62E-05	0.008585
Dynap	GO:0003674	TC1591109	4.076473	2.027321	1.65028	2.404363	5.461749	12.57142	2.88E-06	0.001706
Gpr87	GO:0004871		4.059977	2.021471	1.606588	2.436355	6.248832	11.39182	5.80E-06	0.002375
S100a8	GO:0002523	TC1580152	4.05774	2.020677	1.803961	2.237392	11.33094	21.80009	5.38E-08	0.000478
Klk8	GO:0003824	TC1586091	4.002953	2.001065	1.578465	2.423664	6.26081	11.07091	7.09E-06	0.0026
Col17a1	GO:0005515	TC1582740	3.99556	1.998398	1.372405	2.62439	8.488859	7.46387	1.06E-04	0.010303
Muc4	GO:0001953	TC1609504	3.981495	1.99331	1.744057	2.242563	8.282767	18.69759	1.65E-07	0.000537
Stra6	GO:0001568	TC1581999	3.879766	1.95597	1.498414	2.413526	7.242503	9.994685	1.45E-05	0.0037
Cers3	GO:0003677	TC1682009	3.809792	1.929712	1.717213	2.142211	8.133084	21.23178	6.53E-08	0.000478
Ptprz1	GO:0004721	TC1650287	3.702479	1.888492	1.40358	2.373403	8.772849	9.105508	2.76E-05	0.005072
Klk11	GO:0003824	TC1586339	3.675148	1.877802	1.451685	2.303919	5.62729	10.3032	1.17E-05	0.003337
Raet1c	GO:0005515		3.660444	1.872018	1.11439	2.629647	6.948186	5.777038	5.51E-04	0.027364
2410076I21R	GO:0005515	TC1586526	3.654134	1.869529	1.388709	2.35035	6.258768	9.090768	2.79E-05	0.005077
Adh6a	GO:0005575		3.633518	1.861367	1.451812	2.270922	5.956765	10.62603	9.46E-06	0.003027
Gjb6	GO:0005515	TC1596634	3.553542	1.829258	1.563247	2.095269	6.842105	16.07779	4.93E-07	0.000781
Zfp711	GO:0005634	TC1599821	3.552883	1.82899	1.253979	2.404002	6.135225	7.436799	1.09E-04	0.010484
Krt5	GO:0005198	TC1774657	3.536572	1.822352	1.208748	2.435955	7.403049	6.94377	1.70E-04	0.013801
S100a3	GO:0005509	TC1581703	3.489509	1.803024	1.567169	2.038879	7.355362	17.87339	2.29E-07	0.000577
Krt6b	GO:0002009	NP967698	3.47106	1.795376	1.106726	2.484027	6.254231	6.095482	3.94E-04	0.022572
2410076I21R	GO:0005515	TC1586526	3.451067	1.787042	1.471548	2.102537	6.250039	13.6453	5.60E-06	0.002357
As3mt	GO:0005737	NP744933	3.448857	1.786118	1.441594	2.130642	7.507952	12.1211	3.74E-06	0.001883
Btn1a1	GO:0005515	TC1591871	3.448774	1.786084	1.16088	2.411288	5.913893	6.679308	2.19E-04	0.016293
Foxq1	GO:0000122	TC1585447	3.443481	1.783868	1.359084	2.208651	6.330768	11.23951	2.05E-04	0.0157
Gja1	GO:0001649	TC1573904	3.42536	1.776256	1.277922	2.27459	9.438774	9.539753	4.13E-04	0.023074
Gm13043	GO:0003674	TC1587477	3.379835	1.756953	1.496908	2.016998	5.109083	15.79658	5.60E-07	0.00082

**Supplementary Data 1. First 50 genes differentially expressed between RANK+/+ and RANK-/- tumor cells.**

Supplementary Data 2: Gene ontology enrichment analyses between RANK+/+ and RANK-/- tumor cells (CD45-) implanted in syngeneic hosts

GO.ID	Term	Annotated	Significant	Expected	classicFisher
GO:0042771	intrinsic apoptotic signaling pathway in...	40	10	2.42	0.0001
GO:0000187	activation of MAPK activity	101	17	6.12	0.00011
GO:0001657	ureteric bud development	101	17	6.12	0.00011
GO:0072163	mesonephric epithelium development	101	17	6.12	0.00011
GO:0072164	mesonephric tubule development	101	17	6.12	0.00011
GO:0002504	antigen processing and presentation of p...	20	7	1.21	0.00011
GO:0007254	JNK cascade	173	24	10.47	0.00012
GO:0045620	negative regulation of lymphocyte differ...	41	10	2.48	0.00013
GO:0042060	wound healing	321	37	19.44	0.00013
GO:0048709	oligodendrocyte differentiation	84	15	5.09	0.00014
GO:0001501	skeletal system development	457	48	27.67	0.00014
GO:0072006	nephron development	133	20	8.05	0.00015
GO:0045860	positive regulation of protein kinase ac...	359	40	21.74	0.00015
GO:0001819	positive regulation of cytokine producti...	347	39	21.01	0.00015
GO:0002483	antigen processing and presentation of e...	15	6	0.91	0.00015
GO:0001525	angiogenesis	409	44	24.76	0.00016
GO:0033561	regulation of water loss via skin	21	7	1.27	0.00016
GO:0001823	mesonephros development	104	17	6.3	0.00016
GO:0006469	negative regulation of protein kinase ac...	198	26	11.99	0.00016
GO:0042692	muscle cell differentiation	373	41	22.58	0.00016
GO:0070167	regulation of biomineral tissue developm...	76	14	4.6	0.00017
GO:0031214	biomineral tissue development	124	19	7.51	0.00017
GO:0022612	gland morphogenesis	145	21	8.78	0.00017
GO:0003179	heart valve morphogenesis	35	9	2.12	0.00018
GO:0070228	regulation of lymphocyte apoptotic proce...	59	12	3.57	0.00018
GO:1905209	positive regulation of cardiocyte differ...	28	8	1.7	0.00018
GO:0030500	regulation of bone mineralization	68	13	4.12	0.00019
GO:0031343	positive regulation of cell killing	51	11	3.09	0.00019
GO:0035137	hindlimb morphogenesis	43	10	2.6	0.00019
GO:0045807	positive regulation of endocytosis	126	19	7.63	0.00021
GO:0051272	positive regulation of cellular componen...	427	45	25.85	0.00021
GO:0033674	positive regulation of kinase activity	390	42	23.61	0.00022
GO:0007389	pattern specification process	465	48	28.15	0.00022
GO:0002697	regulation of immune effector process	378	41	22.89	0.00022
GO:0048663	neuron fate commitment	78	14	4.72	0.00022
GO:1901888	regulation of cell junction assembly	69	13	4.18	0.00022
GO:0030335	positive regulation of cell migration	403	43	24.4	0.00022
GO:0002577	regulation of antigen processing and pre...	22	7	1.33	0.00022
GO:0045444	fat cell differentiation	213	27	12.9	0.00022
GO:0016202	regulation of striated muscle tissue dev...	127	19	7.69	0.00023
GO:0060485	mesenchyme development	236	29	14.29	0.00023
GO:0002827	positive regulation of T-helper 1 type i...	16	6	0.97	0.00023
GO:0040037	negative regulation of fibroblast growth...	16	6	0.97	0.00023
GO:1905314	semi-lunar valve development	16	6	0.97	0.00023
GO:2000147	positive regulation of cell motility	416	44	25.19	0.00023
GO:0001912	positive regulation of leukocyte mediate...	44	10	2.66	0.00024
GO:0033081	regulation of T cell differentiation in ...	29	8	1.76	0.00024
GO:0040036	regulation of fibroblast growth factor r...	29	8	1.76	0.00024
GO:2000398	regulation of thymocyte aggregation	29	8	1.76	0.00024
GO:0032872	regulation of stress-activated MAPK casc...	192	25	11.62	0.00025

Supplementary Data 2. First 50 Gene Ontology pathways differentially expressed between RANK+/+ and RANK-/- tumor cells.

**Supplementary Data 3: Pathway analysis using the generally applicable gene-set enrichment (GAGE) method to identify significantly upregulated pathways in RANK-/- compared to RANK+/+ tumor transplants**

GO_BP_ID	p.geomean	stat.mean	p.val	q.val	set.size	exp1
GO:0048002 antigen processing and presentation of peptide antigen	7.73E-05	-4.056049725	7.73E-05	0.322202885	36	7.73E-05
GO:0019882 antigen processing and presentation	0.000217761	-3.64881617	0.000217761	0.322202885	58	0.000217761
GO:0071230 cellular response to amino acid stimulus	0.000228351	-3.690638488	0.000228351	0.322202885	34	0.000228351
GO:0030198 extracellular matrix organization	0.000306587	-3.464057654	0.000306587	0.32444614	157	0.000306587
GO:0043062 extracellular structure organization	0.000383435	-3.400678451	0.000383435	0.32461606	158	0.000383435
GO:0019884 antigen processing and presentation of exogenous antigen	0.000925387	-3.359402426	0.000925387	0.652860634	25	0.000925387
GO:0030199 collagen fibril organization	0.001170185	-3.170284204	0.001170185	0.684867046	35	0.001170185
GO:0043200 response to amino acid stimulus	0.001294339	-3.104170647	0.001294339	0.684867046	44	0.001294339
GO:0002478 antigen processing and presentation of exogenous peptide antigen	0.001463796	-3.246312228	0.001463796	0.688472035	21	0.001463796
GO:0034341 response to interferon-gamma	0.00182137	-2.988574657	0.00182137	0.705439926	54	0.00182137
GO:0045087 innate immune response	0.001973032	-2.894579231	0.001973032	0.705439926	303	0.001973032
GO:0034097 response to cytokine stimulus	0.002115375	-2.870209897	0.002115375	0.705439926	355	0.002115375
GO:0071229 cellular response to acid	0.002229432	-2.928883234	0.002229432	0.705439926	40	0.002229432
GO:0001916 positive regulation of T cell mediated cytotoxicity	0.002485026	-3.016241131	0.002485026	0.705439926	19	0.002485026
GO:0006956 complement activation	0.002499787	-2.887598294	0.002499787	0.705439926	41	0.002499787
GO:0002474 antigen processing and presentation of peptide antigen via MHC class II	0.002729649	-2.962721074	0.002729649	0.722162644	19	0.002729649
GO:0001501 skeletal system development	0.003096886	-2.746459608	0.003096886	0.771124577	353	0.003096886
GO:0010934 macrophage cytokine production	0.003569356	-3.024691559	0.003569356	0.795554966	11	0.003569356
GO:0048588 developmental cell growth	0.003570882	-2.722078489	0.003570882	0.795554966	89	0.003570882
GO:0042832 defense response to protozoan	0.003926859	-2.782458894	0.003926859	0.831119641	24	0.003926859
GO:0048193 Golgi vesicle transport	0.004502196	-2.636967176	0.004502196	0.852781321	113	0.004502196
GO:0048706 embryonic skeletal system development	0.00452862	-2.632220159	0.00452862	0.852781321	118	0.00452862
GO:0048704 embryonic skeletal system morphogenesis	0.004633586	-2.631020348	0.004633586	0.852781321	90	0.004633586
GO:0001101 response to acid	0.00523303	-2.60679487	0.00523303	0.859218929	59	0.00523303
GO:0006958 complement activation, classical pathway	0.005859143	-2.621439371	0.005859143	0.859218929	26	0.005859143
GO:0010935 regulation of macrophage cytokine production	0.005932773	-2.834439277	0.005932773	0.859218929	10	0.005932773
GO:0001562 response to protozoan	0.006095122	-2.604010048	0.006095122	0.859218929	27	0.006095122
GO:0051893 regulation of focal adhesion assembly	0.007055427	-2.569605974	0.007055427	0.859218929	21	0.007055427
GO:0090109 regulation of cell-substrate junction assembly	0.007055427	-2.569605974	0.007055427	0.859218929	21	0.007055427
GO:0060271 cilium morphogenesis	0.007819936	-2.438427156	0.007819936	0.859218929	107	0.007819936
GO:0030308 negative regulation of cell growth	0.007913494	-2.427888805	0.007913494	0.859218929	139	0.007913494
GO:0018108 peptidyl-tyrosine phosphorylation	0.008000329	-2.419255904	0.008000329	0.859218929	212	0.008000329
GO:0072376 protein activation cascade	0.008056793	-2.4537572	0.008056793	0.859218929	45	0.008056793
GO:0030534 adult behavior	0.008162337	-2.417833048	0.008162337	0.859218929	127	0.008162337
GO:0018212 peptidyl-tyrosine modification	0.008369475	-2.402441959	0.008369475	0.859218929	214	0.008369475
GO:0002711 positive regulation of T cell mediated immunity	0.008765419	-2.448373665	0.008765419	0.859218929	31	0.008765419
GO:0008354 germ cell migration	0.009300507	-2.565609809	0.009300507	0.859218929	12	0.009300507
GO:0051825 adhesion to other organism involved in symbiotic interaction	0.009919724	-2.539744948	0.009919724	0.859218929	11	0.009919724
GO:0010243 response to organic nitrogen	0.010058025	-2.329486092	0.010058025	0.859218929	364	0.010058025
GO:0002495 antigen processing and presentation of peptide antigen via MHC class II	0.010250189	-2.495717967	0.010250189	0.859218929	17	0.010250189
GO:0055013 cardiac muscle cell development	0.010338627	-2.365619541	0.010338627	0.859218929	38	0.010338627
GO:0071345 cellular response to cytokine stimulus	0.010525587	-2.314161727	0.010525587	0.859218929	277	0.010525587
GO:0002252 immune effector process	0.010659602	-2.306781043	0.010659602	0.859218929	415	0.010659602
GO:0019886 antigen processing and presentation of exogenous peptide antigen	0.011106485	-2.508785715	0.011106485	0.859218929	14	0.011106485
GO:0071417 cellular response to organic nitrogen	0.011366075	-2.287161116	0.011366075	0.859218929	204	0.011366075
GO:0016559 peroxisome fission	0.012253657	-2.49442285	0.012253657	0.859218929	10	0.012253657
GO:0045859 regulation of protein kinase activity	0.012313553	-2.250998575	0.012313553	0.859218929	470	0.012313553
GO:0050730 regulation of peptidyl-tyrosine phosphorylation	0.012672732	-2.246956223	0.012672732	0.859218929	167	0.012672732
GO:0002460 adaptive immune response based on somatic recombination of immunoglobulin genes	0.013421082	-2.224371055	0.013421082	0.859218929	173	0.013421082
GO:0007623 circadian rhythm	0.014100653	-2.216359774	0.014100653	0.859218929	76	0.014100653

**Supplementary Data 3. First 50 gene pathways upregulated in RANK+/+ tumor cells, compared to RANK-/- tumor cells, as analyzed using the GAGE method.**

**Supplementary Data 4: Pathway analysis using the generally applicable gene-set enrichment (GAGE) method to identify significantly downregulated pathways in RANK-/- compared to RANK+/+ tumor transplants**

GO_BP_ID	p.geomean	stat.mean	p.val	q.val	set.size	exp1
GO:0008544 epidermis development	7.74E-06	4.382555043	7.74E-06	0.032749893	216	7.74E-06
GO:0006364 rRNA processing	5.78E-05	3.948614072	5.78E-05	0.056285037	104	5.78E-05
GO:0042254 ribosome biogenesis	7.54E-05	3.846449018	7.54E-05	0.056285037	153	7.54E-05
GO:0016072 rRNA metabolic process	9.65E-05	3.8077817	9.65E-05	0.056285037	108	9.65E-05
GO:0034470 ncRNA processing	0.000108558	3.739186101	0.000108558	0.056285037	200	0.000108558
GO:0030216 keratinocyte differentiation	0.000108781	3.800819494	0.000108781	0.056285037	81	0.000108781
GO:0000280 nuclear division	0.000118614	3.69768158	0.000118614	0.056285037	307	0.000118614
GO:0007067 mitosis	0.000118614	3.69768158	0.000118614	0.056285037	307	0.000118614
GO:0022613 ribonucleoprotein complex biogenesis	0.000119671	3.710448481	0.000119671	0.056285037	205	0.000119671
GO:0009913 epidermal cell differentiation	0.000159157	3.67780344	0.000159157	0.064728529	100	0.000159157
GO:0000087 M phase of mitotic cell cycle	0.000168205	3.605499781	0.000168205	0.064728529	315	0.000168205
GO:0042475 odontogenesis of dentin-containing tissue	0.000225853	3.627630276	0.000225853	0.076736994	66	0.000225853
GO:0042476 odontogenesis	0.000235668	3.584985671	0.000235668	0.076736994	87	0.000235668
GO:0034660 ncRNA metabolic process	0.000344767	3.417846615	0.000344767	0.104242828	260	0.000344767
GO:0031424 keratinization	0.000553272	3.473284662	0.000553272	0.156133301	30	0.000553272
GO:0000279 M phase	0.000624835	3.237391821	0.000624835	0.165307924	459	0.000624835
GO:0006412 translation	0.000689344	3.210645413	0.000689344	0.171646687	397	0.000689344
GO:0042303 molting cycle	0.000951969	3.165767619	0.000951969	0.204662566	89	0.000951969
GO:0042633 hair cycle	0.000951969	3.165767619	0.000951969	0.204662566	89	0.000951969
GO:0045103 intermediate filament-based process	0.000966986	3.336266139	0.000966986	0.204662566	32	0.000966986
GO:0045104 intermediate filament cytoskeleton organization	0.001105418	3.296950503	0.001105418	0.222820694	31	0.001105418
GO:0048285 organelle fission	0.001645817	2.949875161	0.001645817	0.31667007	331	0.001645817
GO:0042274 ribosomal small subunit biogenesis	0.001825387	3.130788055	0.001825387	0.335950606	22	0.001825387
GO:0006397 mRNA processing	0.001942209	2.899004666	0.001942209	0.342557054	315	0.001942209
GO:0001942 hair follicle development	0.002771409	2.822331883	0.002771409	0.434495417	82	0.002771409
GO:0022404 molting cycle process	0.002771409	2.822331883	0.002771409	0.434495417	82	0.002771409
GO:0022405 hair cycle process	0.002771409	2.822331883	0.002771409	0.434495417	82	0.002771409
GO:0030855 epithelial cell differentiation	0.002957876	2.765307509	0.002957876	0.447167411	265	0.002957876
GO:0045109 intermediate filament organization	0.003469372	2.977634297	0.003469372	0.506408626	20	0.003469372
GO:0006261 DNA-dependent DNA replication	0.004013365	2.692282409	0.004013365	0.566285771	69	0.004013365
GO:0006403 RNA localization	0.004498797	2.645266854	0.004498797	0.614303439	91	0.004498797
GO:0042487 regulation of odontogenesis of dentin-containing tissue	0.005053542	3.005605908	0.005053542	0.668488864	10	0.005053542
GO:0050657 nucleic acid transport	0.005624289	2.569722924	0.005624289	0.676114785	85	0.005624289
GO:0050658 RNA transport	0.005624289	2.569722924	0.005624289	0.676114785	85	0.005624289
GO:0051236 establishment of RNA localization	0.005624289	2.569722924	0.005624289	0.676114785	85	0.005624289
GO:0002710 negative regulation of T cell mediated immunity	0.00575009	2.880592459	0.00575009	0.676114785	10	0.00575009
GO:0002820 negative regulation of adaptive immunity	0.006053567	2.672238715	0.006053567	0.692560734	18	0.006053567
GO:0016071 mRNA metabolic process	0.00668498	2.480302509	0.00668498	0.744671587	366	0.00668498
GO:0019370 leukotriene biosynthetic process	0.008768091	2.512847585	0.008768091	0.932604986	18	0.008768091
GO:0051983 regulation of chromosome segregation	0.00881271	2.462808436	0.00881271	0.932604986	25	0.00881271
GO:0002823 negative regulation of adaptive immunity	0.009278534	2.5157751	0.009278534	0.954087957	16	0.009278534
GO:0007059 chromosome segregation	0.0094665	2.361058749	0.0094665	0.954087957	139	0.0094665
GO:0008380 RNA splicing	0.009812399	2.341894876	0.009812399	0.95527528	248	0.009812399
GO:0031069 hair follicle morphogenesis	0.010118456	2.43702487	0.010118456	0.95527528	27	0.010118456
GO:0010564 regulation of cell cycle process	0.01019185	2.324713214	0.01019185	0.95527528	339	0.01019185
GO:0007159 leukocyte cell-cell adhesion	0.010380974	2.377489133	0.010380974	0.95527528	37	0.010380974
GO:0042481 regulation of odontogenesis	0.011069428	2.421023211	0.011069428	0.984544793	22	0.011069428
GO:0070486 leukocyte aggregation	0.011386	2.578706437	0.011386	0.984544793	11	0.011386
GO:0051301 cell division	0.01139681	2.280817349	0.01139681	0.984544793	449	0.01139681
GO:0006270 DNA replication initiation	0.012229885	2.392435254	0.012229885	0.989123505	16	0.012229885

**Supplementary Data 4. First 50 gene pathways downregulated in RANK+/+ tumor cells, compared to RANK-/- tumor cells, as analyzed using the GAGE method.**



**Supplementary Data 5: Cytokine profiles in the supernatants of cultured RANK+/+ and RANK-/- tumor acini during 72h, calculated as the fold change between RANK+/+ and RANK-/-.**

Cytokine	RANK+/+ SN expression	RANK-/- SN expression	RANK+/+ v.s RANK -/- Fold Change	Cytokine	RANK+/+ SN expression	RANK-/- SN expression	RANK+/+ v.s RANK -/- Fold Change
SDF-1 alpha	555128.88	200605.39	2.767	OPN	6962954.1	6794951.3	1.025
MIP-1 alpha	5066396.12	1988648.2	2.548	GITR	495309.96	487410.91	1.016
IL-1 alpha	2180359.74	1054217.4	2.068	PF-4	4592271.4	4560073.8	1.007
SCF	506878.975	260353.25	1.947	LIX	8189412.9	8371088.3	-1.022494888
TPO	2447167.18	1276558.5	1.917	Dtk	391801.25	402959.94	-1.028806584
TECK	746579.125	404907.39	1.844	CD30L	333213.42	348072.84	-1.044932079
TCA-3	2815773.63	1567674.6	1.796	CXCL16	5430431.4	5674632.6	-1.044932079
IL-3 Rb	682831.675	395084.94	1.728	GCSF	7081815.5	7473280.1	-1.054852321
L selectin	757550.19	445726.02	1.7	IGFBP-2	5790524.3	6212626	-1.072961373
TNF alfa	707692.29	438289.97	1.615	MCP-5	1655786	1780398.5	-1.075268817
IGFBP3	2686585.32	1678393	1.601	CD26	408585.34	448105.81	-1.096491228
IL-13	1130657.09	710580.94	1.591	MIP-1 gamma	7647864.7	8418091.4	-1.100110011
M-CSF	3160460.13	2070428.7	1.526	CRG-2	435307.06	479373.71	-1.101321586
TIMP-1	5543897.2	3651404.8	1.518	MMP-2	2582911.3	2862643.6	-1.10864745
CTACK	1381395.6	910587.81	1.517	MCP 1	9197627.5	10227986	-1.112347052
Leptin	777440.425	513162.66	1.515	MIP-2	8830053.2	9859358.5	-1.116071429
IL-12 p70	1727710.86	1170907.6	1.476	IGF-2	791604.1	891469.95	-1.126126126
Fas Ligand	755235.185	513978.77	1.469	Flt-3 LIGAND	278716.56	314008.28	-1.126126126
IL-10	474307.955	326861.64	1.451	IL-7	508848.36	579632.82	-1.138952164
MIG	710727.195	491153.76	1.447	Eotaxin 2	1388131.9	1582873.1	-1.140250855
IL-4	1425707.78	989543.4	1.441	KC	8901799.8	10209315	-1.146788991
IL-2	628139	443129.73	1.418	IL-6	10281790	11795510	-1.146788991
CXCL1	897027.275	638006.95	1.406	IL-17B R	611086.555	705418.52	-1.154734411
IL-17	665470.925	480927.93	1.384	Axl	416038.16	481701.2	-1.157407407
P selectin	2028675.76	1499635.4	1.353	TIMP-2	647892.555	766516.35	-1.183431953
Ltn/XCL1	1963717.98	1455115.9	1.35	VEGF R1	349775.95	415870.13	-1.189060642
Leptin R	1110496.67	824251.06	1.347	TCK-1	6000759.79	7154184.2	-1.191895113
TARC	933524.975	704201.34	1.326	MDC	4405995.72	5255817.9	-1.193317422
MIP-3 beta	1540120.55	1172256.6	1.314	VEGF D	228011.55	276051.18	-1.210653753
IL-1 beta	430393.965	328293.69	1.311	E selectin	424034.255	515947.15	-1.216545012
IGFBP5	2509107.67	1923861.1	1.304	I-TAC	470106.875	574801.13	-1.222493888
VCAM-1	1012833.83	783648.68	1.292	IL-15	355646.535	435019.67	-1.222493888
MIP-3 alpha	6209643.84	4840545.7	1.283	GM-CSF	8897904.18	10983213	-1.234567901
IGF-1	1892363.16	1520586.6	1.244	ICAM-1	1922453.58	2400460.2	-1.248439451
VEGF	2564854.82	2108557.6	1.216	RANTES	5441416.42	6856369.2	-1.259445844
TSLP	4393405.1	3612072.2	1.216	IL-3	599963.04	758970.52	-1.265822785
IFN gamma	596654.01	515632.42	1.157	Resistin	788867.51	1001655.3	-1.269035533
MMP-3	9772556.9	8528363.4	1.146	Lungkine	1118363.5	1458127.6	-1.303780965
CD30	364680.29	322626.1	1.13	IL-5	694451.94	908442.09	-1.308900524
Pro MMP-9	5537238.9	4973379.8	1.113	HGF R	533134.43	720316.26	-1.351351351
VEGF R2	319832.98	291395.19	1.098	Shh-N	420096.79	578084.91	-1.375515818
sTNFR2	3694609.9	3369811.6	1.096	TRANCE	491648.47	683384.3	-1.390820584
sTNFR1	7930174.2	7324966.4	1.083	TROY	611665.84	915374.93	-1.497005988
OPG	4718723.9	4366398.8	1.081	BLC	548300.28	820679.32	-1.497005988
IL-9	789527.74	736041.74	1.073	Fc gamma R2B	497533.77	780556.49	-1.569858713
bFGF	755318.77	717434.38	1.053	IL12 p40/p70	1147215.9	2045315.4	-1.782531194
VEGF R3	225254.98	214124.31	1.052	CD40	201318.74	361924.3	-1.798561151
IGFBP 6	1513476.9	1455841.3	1.04	Eotaxin 1	387163.33	756142.92	-1.953125

**Supplementary Data 5. Cytokine fold change secreted by RANK+/+ and RANK-/- tumor cell acini for 72 hours.**

<b>MedDRA SOC</b> <i>MedDRA PT</i>	<b>Number of subjects affected</b>	<b>All AE occurrences</b>	<b>AE occurrences causally related to IMP</b>
<b>Gastrointestinal disorders</b>			
<i>Nausea</i>	1	1	1
<i>Vomiting</i>	1	1	1
<b>General disorders and administration</b>			
<i>Injection site pain</i>	1	2	2
<i>Localised oedema</i>	1	1	
<i>Oedema peripheral</i>	1	1	
<i>Pain</i>	1	1	
<b>Infections and infestations</b>			
<i>Hordeolum</i>	1	1	
<i>Skin infection</i>	2	2	
<i>Upper respiratory tract infection</i>	1	1	
<i>Wound infection</i>	1	1	
<b>Injury, poisoning and procedural</b>			
<i>Eschar</i>	1	1	
<i>Incision site hypoaesthesia</i>	1	1	
<i>Procedural pain</i>	4	4	
<i>Seroma</i>	1	1	
<i>Wound complication</i>	1	1	
<i>Wound dehiscence</i>	1	1	
<b>Metabolism and nutrition disorders</b>			
<i>Hyperkalaemia</i>	1	1	
<b>Musculoskeletal and connective tissue</b>			
<i>Arthralgia</i>	4	4	4
<i>Back pain</i>	1	1	1
<i>Bone pain</i>	1	1	
<i>Musculoskeletal pain</i>	1	1	
<i>Myalgia</i>	1	2	2
<b>Neoplasms benign, malignant and</b>			
<i>Tumour pain</i>	1	1	
<b>Nervous system disorders</b>			
<i>Headache</i>	1	1	1
<i>Presyncope</i>	1	1	
<b>Psychiatric disorders</b>			
<i>Stress</i>	1	1	
<b>Reproductive system and breast</b>			
<i>Breast haematoma</i>	3	3	
<i>Breast inflammation</i>	1	1	
<i>Breast pain</i>	1	1	
<b>Vascular disorders</b>			
<i>Deep vein thrombosis</i>	1	1	
<i>Haematoma</i>	1	1	
<i>Lymphoedema</i>	1	1	

**Supplementary Data 6: All non-serious adverse events reported for D-BEYOND clinical trial sorted by MedDRA SOC and MedDRA PT.**

Genes	baseMean	log2FoldChange	lfcSE	stat	pvalue	padj	is differentially expressed
NR4A1	232.2774241	1.247002073	0.160200352	7.784015817	7.03E-15	5.80E-11	TRUE
LOC613037	126.0106677	-0.787249351	0.101231677	-7.77670959	7.44E-15	5.80E-11	TRUE
LINC01000	633.0429928	-0.623177408	0.085659512	-7.27505202	3.46E-13	1.80E-09	TRUE
MGC27345	146.9557912	-0.584618578	0.085546816	-6.83390228	8.26E-12	3.22E-08	TRUE
SETD1B	304.0712358	-0.557459079	0.082360512	-6.76852375	1.30E-11	4.06E-08	TRUE
NPIP5	163.900017	-0.74215298	0.110752136	-6.70102632	2.07E-11	5.38E-08	TRUE
SMG1P1	1013.56739	-0.555161236	0.084370722	-6.58002237	4.70E-11	9.17E-08	TRUE
ANP32A-IT1	30.66202866	-0.85986296	0.13284397	-6.47272856	9.62E-11	1.67E-07	TRUE
ARHGAP8	68.39112979	-0.665854749	0.105642584	-6.30290099	2.92E-10	3.61E-07	TRUE
PPBP	26.71589043	-1.153053749	0.185297104	-6.22272947	4.89E-10	4.76E-07	TRUE
TBC1D3	79.72880974	-0.699886383	0.113983323	-6.14025248	8.24E-10	7.14E-07	TRUE
HPGDS	64.72151474	0.765971724	0.125845911	6.086584117	1.15E-09	8.99E-07	TRUE
ANXA2	7375.010291	0.562838325	0.092762746	6.067503931	1.30E-09	9.64E-07	TRUE
LOC729603	27.51473947	-0.837204066	0.1403622	-5.96459777	2.45E-09	1.66E-06	TRUE
TAS2R4	10.65542498	-1.005516575	0.173999505	-5.77884733	7.52E-09	4.19E-06	TRUE
BCL9L	384.0243389	-0.604261662	0.106371165	-5.68069044	1.34E-08	6.53E-06	TRUE
TBC1D3H	61.29019882	-0.681083897	0.120088705	-5.6715067	1.42E-08	6.69E-06	TRUE
TTL3	115.6491923	-0.631862361	0.113346628	-5.57460219	2.48E-08	1.10E-05	TRUE
WNK2	100.3387956	-0.801045645	0.145232561	-5.51560641	3.48E-08	1.50E-05	TRUE
SND1-IT1	26.41115105	-0.811563135	0.148189932	-5.47650656	4.34E-08	1.73E-05	TRUE
NPIP3	81.04039032	-0.739655272	0.135357067	-5.46447472	4.64E-08	1.81E-05	TRUE
GUSBP11	310.303934	-0.589510132	0.108218216	-5.44742053	5.11E-08	1.88E-05	TRUE
CCDC17	25.38520494	-0.813597002	0.149499933	-5.44212287	5.26E-08	1.88E-05	TRUE
FABP5	226.5897335	0.731599889	0.135381276	5.403996114	6.52E-08	2.12E-05	TRUE
PRRT2	73.41718364	-0.634412996	0.117830475	-5.38411644	7.28E-08	2.18E-05	TRUE
HIST1H1E	3371.940134	0.616882963	0.114765676	5.375152084	7.65E-08	2.21E-05	TRUE
KCNQ1OT1	1012.894141	-0.767049939	0.143019119	-5.3632685	8.17E-08	2.27E-05	TRUE
SLC4A1	10.09789654	-0.91757877	0.173561175	-5.28677436	1.24E-07	3.15E-05	TRUE
MIR600HG	74.99793585	-0.720837839	0.136372617	-5.28579605	1.25E-07	3.15E-05	TRUE
TNK2	407.6273518	-0.603739866	0.11449737	-5.27295839	1.34E-07	3.27E-05	TRUE
SRRM2	2683.61365	-0.506891058	0.09659484	-5.24759977	1.54E-07	3.41E-05	TRUE
DUSP7	68.60544563	-0.585992335	0.11166885	-5.24758996	1.54E-07	3.41E-05	TRUE
LINC00167	9.894225163	-0.934160956	0.178106497	-5.24495721	1.56E-07	3.41E-05	TRUE
ZNF252P-AS1	19.49583324	-0.760012042	0.144979542	-5.24220199	1.59E-07	3.41E-05	TRUE
CISH	233.921374	0.58977672	0.112743163	5.231152876	1.68E-07	3.50E-05	TRUE
TAGLN	3569.052207	0.555676212	0.106226921	5.231030028	1.69E-07	3.50E-05	TRUE
SEC31B	110.3184853	-0.532766021	0.101959275	-5.22528258	1.74E-07	3.57E-05	TRUE
AVIL	89.16301445	-0.540798173	0.104048695	-5.19754884	2.02E-07	3.78E-05	TRUE
BMS1P6	68.39411547	-0.693912809	0.134137326	-5.17315224	2.30E-07	4.22E-05	TRUE
ACTG1P20	28.03860528	-0.66332733	0.128516055	-5.16143549	2.45E-07	4.32E-05	TRUE
CRTC1	131.6030063	-0.527363391	0.10224089	-5.15804775	2.50E-07	4.32E-05	TRUE
FBRS	296.9943468	-0.524071403	0.102267003	-5.12454053	2.98E-07	5.00E-05	TRUE
PCDHGA12	39.30854519	-0.599456758	0.119804257	-5.00363487	5.63E-07	8.43E-05	TRUE
ATN1	371.7181222	-0.525521983	0.105772146	-4.96843455	6.75E-07	9.56E-05	TRUE
GLRX	462.0494382	0.510308249	0.103270341	4.941479252	7.75E-07	0.000105219	TRUE
ZBTB39	138.3605064	-0.504756292	0.10215161	-4.94124658	7.76E-07	0.000105219	TRUE
MAATS1	65.64682487	-0.575466094	0.116864814	-4.92420324	8.47E-07	0.000111052	TRUE

**Supplementary Data 7: First 50 genes differentially expressed between pre- and post-treatment tumor samples from the D-BEYOND clinical trial.**

Genes	baseMean	log2FoldChan	lfcSE	stat	pvalue	padj	is differentially expressed
NR4A1	235.5372569	3.541408264	0.351112781	10.0862414	6.36E-24	7.50E-20	TRUE
CCL4	19.32957818	2.089466021	0.43088829	4.849205857	1.24E-06	0.007309109	TRUE
IGSF10	267.6091231	-0.838115163	0.185842399	-4.509816746	6.49E-06	0.019129322	TRUE
MT1X	376.5616039	0.99534327	0.220079827	4.522646549	6.11E-06	0.019129322	TRUE
TERF2	77.72035188	0.767314408	0.174640003	4.393692136	1.11E-05	0.019536794	TRUE
ZBTB16	175.2797874	1.287437112	0.293597646	4.385038949	1.16E-05	0.019536794	TRUE
PER1	242.0273768	1.312710628	0.299082982	4.389118435	1.14E-05	0.019536794	TRUE
SEC11A	371.5032825	0.673017582	0.156027114	4.313465554	1.61E-05	0.023691428	TRUE
SLC19A2	111.1033237	0.730652686	0.176825662	4.132051194	3.60E-05	0.045267193	TRUE
KLHL8	154.7288358	0.80018288	0.194361008	4.116992845	3.84E-05	0.045267193	TRUE

**Supplementary Data 7: First 50 genes differentially expressed between pre- and post-treatment adjacent normal tissue samples from the D-BEYOND clinical trial.**

GO.ID	Term	Annotated	Significant	Expected	classicFisher
GO:0070734	histone H3-K27 methylation	16	4	0.27	0.00013
GO:0002548	monocyte chemotaxis	49	6	0.84	0.00018
GO:0032103	positive regulation of response to exter...	234	13	4	0.0002
GO:0050729	positive regulation of inflammatory resp...	100	8	1.71	0.00031
GO:0097529	myeloid leukocyte migration	136	9	2.33	0.00055
GO:0050909	sensory perception of taste	61	6	1.04	0.0006
GO:0071674	mononuclear cell migration	63	6	1.08	0.00071
GO:0071621	granulocyte chemotaxis	87	7	1.49	0.00072
GO:0015672	monovalent inorganic cation transport	454	18	7.77	0.00084
GO:0060425	lung morphogenesis	45	5	0.77	0.00098
GO:0060326	cell chemotaxis	213	11	3.64	0.00112
GO:0019221	cytokine-mediated signaling pathway	468	18	8.01	0.00118
GO:0097530	granulocyte migration	95	7	1.63	0.00121
GO:0080182	histone H3-K4 trimethylation	13	3	0.22	0.00125
GO:2000651	positive regulation of sodium ion transm...	13	3	0.22	0.00125
GO:0048247	lymphocyte chemotaxis	48	5	0.82	0.00132
GO:0002690	positive regulation of leukocyte chemota...	71	6	1.21	0.00134
GO:0072676	lymphocyte migration	72	6	1.23	0.00144
GO:0030593	neutrophil chemotaxis	73	6	1.25	0.00154
GO:0006935	chemotaxis	481	18	8.23	0.0016
GO:0042330	taxis	481	18	8.23	0.0016
GO:0030595	leukocyte chemotaxis	163	9	2.79	0.00198
GO:1990266	neutrophil migration	78	6	1.33	0.00217
GO:0002685	regulation of leukocyte migration	135	8	2.31	0.00225
GO:0006123	mitochondrial electron transport, cytoch...	16	3	0.27	0.00235
GO:0050921	positive regulation of chemotaxis	108	7	1.85	0.00254
GO:0031338	regulation of vesicle fusion	58	5	0.99	0.00308
GO:0001938	positive regulation of endothelial cell ...	59	5	1.01	0.00332
GO:1902307	positive regulation of sodium ion transm...	18	3	0.31	0.00334
GO:0002688	regulation of leukocyte chemotaxis	86	6	1.47	0.00355
GO:0034968	histone lysine methylation	89	6	1.52	0.0042
GO:0050900	leukocyte migration	330	13	5.65	0.00457
GO:0002687	positive regulation of leukocyte migrati...	96	6	1.64	0.00608
GO:0018022	peptidyl-lysine methylation	96	6	1.64	0.00608
GO:0042775	mitochondrial ATP synthesis coupled elec...	69	5	1.18	0.0065
GO:0050848	regulation of calcium-mediated signaling	69	5	1.18	0.0065
GO:0042773	ATP synthesis coupled electron transport	70	5	1.2	0.00691
GO:0046330	positive regulation of JNK cascade	99	6	1.69	0.00704
GO:0051568	histone H3-K4 methylation	46	4	0.79	0.00777
GO:0030816	positive regulation of cAMP metabolic pr...	73	5	1.25	0.00823
GO:0060441	epithelial tube branching involved in lu...	25	3	0.43	0.00862
GO:0006906	vesicle fusion	138	7	2.36	0.00961
GO:0019932	second-messenger-mediated signaling	209	9	3.58	0.00996

**Supplementary Data 9: Gene ontology enrichment analysis of differentially expressed genes between pre- and post-treatment with denosumab.**

GO.ID	p.geomean	stat.mean	p.val	q.val	set.size
GO:0002684 positive regulation of immune system process	6.80E-06	1.94631596	1.72E-19	7.28E-16	471
GO:0050776 regulation of immune response	1.37E-05	1.869251553	3.69E-18	7.79E-15	468
GO:0006520 cellular amino acid metabolic process	0.010954743	1.758805961	1.03E-16	1.45E-13	435
GO:0045321 leukocyte activation	2.98E-05	1.74825057	3.81E-16	4.03E-13	489
GO:0050778 positive regulation of immune response	0.0001373	1.738038176	6.52E-16	5.51E-13	310
GO:0046649 lymphocyte activation	4.38E-05	1.66339115	1.01E-14	7.11E-12	416
GO:0006954 inflammatory response	0.000395461	1.606508824	4.78E-14	2.88E-11	441
GO:0043086 negative regulation of catalytic activity	0.021563262	1.53828551	3.15E-13	1.58E-10	464
GO:0031347 regulation of defense response	0.000883432	1.547376903	3.73E-13	1.58E-10	375
GO:0016053 organic acid biosynthetic process	0.027468419	1.532607123	4.10E-13	1.58E-10	268
GO:0046394 carboxylic acid biosynthetic process	0.027468419	1.532607123	4.10E-13	1.58E-10	268
GO:0044283 small molecule biosynthetic process	0.016050703	1.52173122	5.78E-13	1.86E-10	412
GO:0002252 immune effector process	0.00024595	1.540617857	6.02E-13	1.86E-10	393
GO:0045087 innate immune response	0.000341166	1.532607075	6.17E-13	1.86E-10	452
GO:0031349 positive regulation of defense response	0.005244485	1.511720005	1.31E-12	3.70E-10	200
GO:0044711 single-organism biosynthetic process	0.017999085	1.494588747	1.42E-12	3.74E-10	424
GO:0042110 T cell activation	0.000188176	1.450538196	1.33E-11	3.30E-09	307
GO:0032101 regulation of response to external stimulus	0.003655642	1.415397366	2.62E-11	6.15E-09	338
GO:0002253 activation of immune response	0.000482241	1.421593808	3.62E-11	8.06E-09	248
GO:0050865 regulation of cell activation	0.000412347	1.408243237	4.60E-11	9.72E-09	313
GO:0051270 regulation of cellular component movement	0.002294171	1.390354714	5.34E-11	1.07E-08	422
GO:0002697 regulation of immune effector process	0.003532011	1.380921163	9.89E-11	1.90E-08	196
GO:0044282 small molecule catabolic process	0.025903999	1.354063652	1.36E-10	2.40E-08	238
GO:0044712 single-organism catabolic process	0.025903999	1.354063652	1.36E-10	2.40E-08	238
GO:0002694 regulation of leukocyte activation	0.000581089	1.37102306	1.42E-10	2.40E-08	294
GO:0043068 positive regulation of programmed cell death	0.007343113	1.344900365	2.03E-10	3.30E-08	376
GO:0032103 positive regulation of response to external stimulus	0.012037206	1.342115336	3.02E-10	4.72E-08	136
GO:0043065 positive regulation of apoptotic process	0.008145243	1.328199653	3.31E-10	4.76E-08	372
GO:0032787 monocarboxylic acid metabolic process	0.021855508	1.322183575	3.33E-10	4.76E-08	386
GO:0019882 antigen processing and presentation	0.021175212	1.329175465	3.38E-10	4.76E-08	180
GO:0001944 vasculature development	0.002442369	1.324449163	3.68E-10	4.98E-08	467
GO:0030001 metal ion transport	0.05708202	1.314360337	3.77E-10	4.98E-08	469
GO:0010942 positive regulation of cell death	0.008601635	1.316764279	4.54E-10	5.82E-08	389
GO:0006091 generation of precursor metabolites and energy	0.02223826	1.296632373	7.15E-10	8.49E-08	406
GO:0002764 immune response-regulating signaling pathway	0.001087523	1.319215886	7.19E-10	8.49E-08	213
GO:2000145 regulation of cell motility	0.002515498	1.304264213	7.23E-10	8.49E-08	375
GO:0001568 blood vessel development	0.003125172	1.287042165	1.08E-09	1.19E-07	444
GO:0007610 behavior	0.052624343	1.278131804	1.10E-09	1.19E-07	466
GO:0040008 regulation of growth	0.037578556	1.278904137	1.10E-09	1.19E-07	469
GO:0002250 adaptive immune response	0.003288505	1.299663748	1.34E-09	1.42E-07	166
GO:0030334 regulation of cell migration	0.002801498	1.282275615	1.38E-09	1.42E-07	354
GO:0052547 regulation of peptidase activity	0.04914933	1.262025345	1.88E-09	1.90E-07	234
GO:0001816 cytokine production	0.000855184	1.269224121	2.18E-09	2.14E-07	383
GO:0016054 organic acid catabolic process	0.034131066	1.256053625	2.46E-09	2.31E-07	185
GO:0046395 carboxylic acid catabolic process	0.034131066	1.256053625	2.46E-09	2.31E-07	185
GO:0051240 positive regulation of multicellular organismal process	0.016271153	1.24173518	3.41E-09	3.14E-07	476
GO:0034097 response to cytokine stimulus	0.003723888	1.241500373	3.91E-09	3.51E-07	441
GO:0002757 immune response-activating signal transduction	0.001474005	1.256482968	4.33E-09	3.81E-07	203
GO:0002443 leukocyte mediated immunity	0.004986611	1.249879719	4.91E-09	4.23E-07	170
GO:0048534 hematopoietic or lymphoid organ development	0.00355757	1.224209886	6.31E-09	5.32E-07	478

**Supplementary Data 10: First 50 gene pathways enriched between pre- and post-treatment with denosumab in the D-BEYOND study, as analyzed by the GAGE method.**

GO.ID	p.geomean	stat.mean	p.val	q.val	set.size
GO:0051591 response to cAMP	0.087515088	1.053161386	4.02E-15	1.76E-11	60
GO:0046683 response to organophosphorus	0.09375373	1.028912004	1.21E-14	2.64E-11	85
GO:0014074 response to purine-containing compound	0.093015878	1.001673253	5.32E-14	7.75E-11	98
GO:0051592 response to calcium ion	0.101312079	0.991399655	9.77E-14	1.07E-10	86
GO:0051248 negative regulation of protein metabolic process	0.051639188	0.950129058	6.72E-13	5.87E-10	480
GO:0071277 cellular response to calcium ion	0.120353545	0.941325187	3.40E-12	2.48E-09	30
GO:0032269 negative regulation of cellular protein metabolic process	0.079390549	0.901283024	8.58E-12	4.76E-09	418
GO:0031400 negative regulation of protein modification process	0.091862037	0.901408364	8.71E-12	4.76E-09	319
GO:0001933 negative regulation of protein phosphorylation	0.074354614	0.854337933	1.05E-10	5.12E-08	199
GO:0097305 response to alcohol	0.099300473	0.844271697	1.58E-10	6.92E-08	218
GO:0048545 response to steroid hormone stimulus	0.085717704	0.832304508	2.80E-10	1.11E-07	256
GO:0009612 response to mechanical stimulus	0.083878402	0.827750726	3.96E-10	1.21E-07	133
GO:0070848 response to growth factor stimulus	0.039960111	0.824295391	3.97E-10	1.21E-07	447
GO:0043065 positive regulation of apoptotic process	0.056850295	0.823463778	4.09E-10	1.21E-07	422
GO:0042326 negative regulation of phosphorylation	0.077181991	0.823985324	4.33E-10	1.21E-07	214
GO:0043068 positive regulation of programmed cell death	0.055777334	0.82185669	4.41E-10	1.21E-07	427
GO:0071363 cellular response to growth factor stimulus	0.042341103	0.815916142	5.89E-10	1.52E-07	434
GO:0002237 response to molecule of bacterial origin	0.038719672	0.81665145	6.96E-10	1.69E-07	212
GO:0043408 regulation of MAPK cascade	0.03417352	0.810871547	7.53E-10	1.73E-07	461
GO:0010563 negative regulation of phosphorus metabolic process	0.067323798	0.803779251	1.10E-09	2.22E-07	256
GO:0045936 negative regulation of phosphate metabolic process	0.067323798	0.803779251	1.10E-09	2.22E-07	256
GO:0031329 regulation of cellular catabolic process	0.074310948	0.800877438	1.12E-09	2.22E-07	447
GO:0010038 response to metal ion	0.094800144	0.794050342	1.70E-09	3.20E-07	217
GO:0033673 negative regulation of kinase activity	0.109739532	0.793468843	1.80E-09	3.20E-07	160
GO:0032496 response to lipopolysaccharide	0.042377739	0.795842629	1.83E-09	3.20E-07	201
GO:0006954 inflammatory response	0.005315662	0.785585678	2.94E-09	4.95E-07	492
GO:0007178 transmembrane receptor protein serine/threonine kinase signaling pathway	0.058892681	0.774671935	3.99E-09	6.45E-07	272
GO:0009314 response to radiation	0.146394175	0.770684062	4.31E-09	6.72E-07	312
GO:0031347 regulation of defense response	0.021516108	0.764667579	6.64E-09	9.91E-07	430
GO:0006469 negative regulation of protein kinase activity	0.111804437	0.763923699	6.80E-09	9.91E-07	149
GO:0071248 cellular response to metal ion	0.112875242	0.764853775	8.13E-09	1.15E-06	79
GO:0007179 transforming growth factor beta receptor signaling pathway	0.093124326	0.757775393	8.71E-09	1.19E-06	171
GO:0010741 negative regulation of intracellular protein kinase cascade	0.096307696	0.752160038	1.17E-08	1.55E-06	145
GO:0071241 cellular response to inorganic substance	0.114879745	0.751402517	1.41E-08	1.81E-06	83
GO:0009416 response to light stimulus	0.179322272	0.741840221	1.52E-08	1.90E-06	211
GO:0071559 response to transforming growth factor beta stimulus	0.081361472	0.739181749	1.89E-08	2.30E-06	199
GO:0071560 cellular response to transforming growth factor beta stimulus	0.087587267	0.734276306	2.31E-08	2.73E-06	198
GO:0001706 endoderm formation	0.18593816	0.741458789	2.54E-08	2.93E-06	28
GO:0000289 nuclear-transcribed mRNA poly(A) tail shortening	0.167784587	0.73847816	3.00E-08	3.37E-06	26
GO:0042493 response to drug	0.088983293	0.722436448	3.53E-08	3.86E-06	335
GO:0051348 negative regulation of transferase activity	0.118669165	0.72332274	3.71E-08	3.96E-06	171
GO:1901654 response to ketone	0.180962229	0.719660475	4.58E-08	4.77E-06	72
GO:1901216 positive regulation of neuron death	0.197806285	0.720728407	4.73E-08	4.81E-06	41
GO:0051385 response to mineralocorticoid stimulus	0.193598105	0.730658961	4.87E-08	4.84E-06	21
GO:0060395 SMAD protein signal transduction	0.198270837	0.731011562	5.36E-08	5.21E-06	17
GO:0009617 response to bacterium	0.030383205	0.711142442	6.38E-08	6.07E-06	339
GO:0043409 negative regulation of MAPK cascade	0.104970338	0.696223052	1.27E-07	1.18E-05	103
GO:0007611 learning or memory	0.168593512	0.688781061	1.38E-07	1.26E-05	154
GO:0002757 immune response-activating signal transduction	0.028299681	0.693744813	1.46E-07	1.31E-05	234
GO:1901652 response to peptide	0.121202528	0.685601278	1.54E-07	1.34E-05	361

**Supplementary Data 11: First 50 gene pathways enriched between biopsy and surgery in POETIC clinical trial, as analysed by the GAGE method.**

**Clinicopathological features at baseline**

		Non-responder	Responder	P
<b>N</b>		13	11	
<b>Age (years, range)</b>		44 (38-51)	45 (35-50)	0.907a
<b>Tumor size</b>	≤ 2cm	5 (55.6%)	4 (44.4%)	1
	> 2cm	6 (50%)	6 (50%)	
<b>Nodal status</b>	Negative	11 (52.4%)	10 (47.6%)	1
	Positive	2 (66.7%)	1 (33.3%)	
<b>Grade</b>	I-II	12 (66.7%)	6 (33.3%)	0.061
	III	1 (16.7%)	5 (83.3%)	
<b>Ki-67</b>	≤ 20%	10 (58.8%)	7 (41.2%)	0.66
	> 20%	3 (42.9%)	4 (57.1%)	
<b>Molecular subtypes</b>	LumA	8 (57.1%)	6 (42.9%)	0.92
	LumB	2 (40%)	3 (60%)	
	HER2	2 (50%)	2 (50%)	
	TNBC	1 (100%)	0 (0%)	

P, p-value derived from  $\chi^2$  test or the Fisher exact test when appropriate (a, except continuous variable derived from Mann-Whitney U test)

**Immune markers at baseline**

		Non-responder	Responder	P
<b>N</b>		13	11	
<b>sTILs &gt; 10%</b>	FALSE	9 (56.2%)	7 (43.8%)	1
	TRUE	4 (50%)	4 (50%)	
<b>tTILs &gt; 0%</b>	FALSE	8 (66.7%)	4 (33.3%)	0.41
	TRUE	5 (41.7%)	7 (58.3%)	
<b>CD3 &gt; 10%</b>	FALSE	9 (64.3%)	5 (35.7%)	0.42
	TRUE	4 (44.4%)	5 (55.6%)	
<b>tCD3 &gt; 0%</b>	FALSE	9 (69.2%)	4 (30.8%)	0.22
	TRUE	4 (40%)	6 (60%)	
<b>CD20 &gt; 10%</b>	FALSE	11 (73.3%)	4 (26.7%)	0.039
	TRUE	2 (25%)	6 (75%)	
<b>tCD20 &gt; 0%</b>	FALSE	13 (56.5%)	10 (43.5%)	0.53
	TRUE	0 (0%)	0 (0%)	
<b>FOXP3 &gt; 1%</b>	FALSE	8 (66.7%)	4 (33.3%)	0.41
	TRUE	5 (45.5%)	6 (54.5%)	
<b>tFOXP3 &gt; 0%</b>	FALSE	12 (70.6%)	5 (29.4%)	0.052
	TRUE	1 (16.7%)	5 (83.3%)	
<b>CD68 &gt; 10%</b>	FALSE	9 (56.2%)	7 (43.8%)	1
	TRUE	4 (57.1%)	3 (42.9%)	
<b>CD68 &gt; 0%</b>	FALSE	2 (40%)	3 (60%)	0.62
	TRUE	11 (61.1%)	7 (38.9%)	
<b>RANK &gt; 1 (H-score)</b>	FALSE	7 (43.8%)	9 (56.2%)	0.21
	TRUE	6 (75%)	2 (25%)	
<b>RANKL &gt; 1 (H-score)</b>	FALSE	8 (50%)	8 (50%)	0.68
	TRUE	5 (62.5%)	3 (37.5%)	

P, p-value derived from  $\chi^2$  test or the Fisher exact test when appropriate

**Immune cell fractions, as inferred by CIBERSORT**

		Non-responder	Responder	P
<b>N</b>		11	11	
<b>T.cells.CD8</b>	Absence	3 (50%)	3 (50%)	1
	Presence	8 (50%)	8 (50%)	
<b>T.cells.CD4</b>	Absence	0 (0%)	0 (0%)	1
	Presence	11 (50%)	11 (50%)	
<b>T.cells.regulatory.Tregs</b>	Absence	8 (80%)	2 (20%)	0.032
	Presence	3 (25%)	9 (75%)	
<b>B.cells</b>	Absence	2 (50%)	2 (50%)	1
	Presence	9 (50%)	9 (50%)	
<b>NK.cells.activated</b>	Absence	0 (0%)	0 (0%)	1
	Presence	11 (50%)	11 (50%)	
<b>Macrophages</b>	Absence	0 (0%)	0 (0%)	1
	Presence	11 (50%)	11 (50%)	
<b>Dendritic.cells</b>	Absence	8 (61.5%)	5 (38.5%)	0.39
	Presence	3 (33.3%)	6 (66.7%)	
<b>Mast.cells.resting</b>	Absence	0 (0%)	0 (0%)	1
	Presence	11 (50%)	11 (50%)	
<b>Neutrophils</b>	Absence	2 (22.2%)	7 (77.8%)	0.08
	Presence	9 (69.2%)	4 (30.8%)	
<b>Eosinophil</b>	Absence	10 (47.6%)	11 (52.4%)	1
	Presence	1 (100%)	0 (0%)	

P, p-value derived from  $\chi^2$  test or the Fisher exact test when appropriate

**Supplementary Data 12: Parameters at baseline and their association with an immunomodulatory response induced by denosumab.**



Genes	baseMean	log2FoldChan	lfcSE	stat	pvalue	padj	
IL7R	436.446438	1.732719647	0.33014702	5.248327392	1.53E-07	0.002812484	TRUE
MS4A1	94.50012932	1.824752987	0.373060476	4.891306115	1.00E-06	0.009177487	TRUE
PI15	668.240279	-1.84265192	0.397533211	-4.63521503	3.57E-06	0.014108594	TRUE
SEPT6	322.5652358	1.013013971	0.222855391	4.545611233	5.48E-06	0.014108594	TRUE
CD28	91.5813806	1.35094251	0.297582619	4.539722497	5.63E-06	0.014108594	TRUE
GLYATL2	170.1115399	-1.80083333	0.397856822	-4.52633517	6.00E-06	0.014108594	TRUE
TDRD1	78.98235489	-1.79965015	0.397823413	-4.52374117	6.08E-06	0.014108594	TRUE
EFHD2	270.0716741	0.781280792	0.174855423	4.468153043	7.89E-06	0.014108594	TRUE
TMEM156	139.381602	1.7576819	0.394489017	4.455591474	8.37E-06	0.014108594	TRUE
SPOCK2	211.5448987	1.530041705	0.344098864	4.446517752	8.73E-06	0.014108594	TRUE
BLK	15.99722301	1.720790346	0.387335982	4.442629721	8.89E-06	0.014108594	TRUE
SLC28A3	69.54284007	-1.74029414	0.392466574	-4.43424806	9.24E-06	0.014108594	TRUE
BANK1	45.85428514	1.497380951	0.343583805	4.358124357	1.31E-05	0.017303022	TRUE
STAT4	111.2696293	1.242273597	0.285158467	4.356432447	1.32E-05	0.017303022	TRUE
FOXP3	23.70991712	1.296679372	0.300652884	4.312878541	1.61E-05	0.018547658	TRUE
GNMT	44.37137577	-1.68325908	0.390507301	-4.31044202	1.63E-05	0.018547658	TRUE
ALDH3B2	482.536248	-1.7035179	0.396829723	-4.2928183	1.76E-05	0.018547658	TRUE
C11orf21	20.17444515	1.490784389	0.347854054	4.285660526	1.82E-05	0.018547658	TRUE
BEX1	45.49517965	-1.68133488	0.396660058	-4.23872998	2.25E-05	0.021679012	TRUE
CD79A	52.59247054	1.612542527	0.383401344	4.205886471	2.60E-05	0.023826767	TRUE
PTPRQ	18.45330436	-1.65374062	0.394983137	-4.18686386	2.83E-05	0.024679405	TRUE
GVINP1	214.3212803	1.350166023	0.327661068	4.120617786	3.78E-05	0.030556928	TRUE
RAC2	183.5412262	1.225972409	0.298241034	4.110676495	3.95E-05	0.030556928	TRUE
IFNG	6.398681753	1.589530372	0.387808551	4.098750193	4.15E-05	0.030556928	TRUE
TIFAB	10.88864826	1.566853002	0.382354192	4.097909827	4.17E-05	0.030556928	TRUE
GNG4	34.29366375	1.551147405	0.380007045	4.081891179	4.47E-05	0.030847512	TRUE
LIMD2	209.4925637	1.222853246	0.299876594	4.077854925	4.55E-05	0.030847512	TRUE
SH2D2A	32.44431292	1.347402915	0.331361195	4.066266469	4.78E-05	0.031063213	TRUE
CCR4	49.70723081	1.417762198	0.349238771	4.059578477	4.92E-05	0.031063213	TRUE
FCRLA	14.04268303	1.550712133	0.38472693	4.030682581	5.56E-05	0.033969708	TRUE
DGKA	240.2827623	0.876660492	0.218927802	4.004336059	6.22E-05	0.03562451	TRUE
IL10RA	452.767784	1.175937336	0.293671775	4.00425726	6.22E-05	0.03562451	TRUE
CXCR5	12.30654738	1.577638007	0.395776747	3.986181656	6.71E-05	0.037152127	TRUE
PLEKHO1	455.4330627	0.75734537	0.190411283	3.97741856	6.97E-05	0.037152127	TRUE
LINC00861	48.08055096	1.347248307	0.339098106	3.973034002	7.10E-05	0.037152127	TRUE
RHOF	105.8797233	1.154445489	0.294040154	3.926149108	8.63E-05	0.042838311	TRUE
CD177	24.68061032	1.557707755	0.396941027	3.924280058	8.70E-05	0.042838311	TRUE
GPR132	53.73877428	1.219716569	0.311397749	3.916908747	8.97E-05	0.042838311	TRUE
ZNF831	64.6461118	1.411039671	0.360607585	3.912950614	9.12E-05	0.042838311	TRUE
FAM78A	110.523722	1.072739711	0.275341465	3.896034014	9.78E-05	0.044615472	TRUE
MFHAS1	165.138534	0.746707255	0.191905697	3.891011406	9.98E-05	0.044615472	TRUE
MIR2052HG	13.43725811	-1.52746662	0.39345697	-3.88216944	0.000103529	0.045168091	TRUE

**Supplementary Data 13: All differentially expressed genes between non-responders and responders at baseline.**

GO.ID	Term	Annotated	Significant	Expected	classicFisher	Annotated.GeneSymbol
GO:0051249	regulation of lymphocyte activation	357	6	0.77	1.00E-04	IFNG, IL7R, FOXP3, BANK1, RAC2, CD28
GO:0016447	somatic recombination of immunoglobulin ...	43	3	0.09	0.00011	IFNG, FOXP3, CD28
GO:0002381	immunoglobulin production involved in im...	44	3	0.09	0.00011	IFNG, FOXP3, CD28
GO:0002819	regulation of adaptive immune response	118	4	0.25	0.00012	IFNG, IL7R, FOXP3, CD28
GO:0002637	regulation of immunoglobulin production	46	3	0.1	0.00013	IFNG, FOXP3, CD28
GO:0016445	somatic diversification of immunoglobuli...	50	3	0.11	0.00017	IFNG, FOXP3, CD28
GO:0046635	positive regulation of alpha-beta T cell...	50	3	0.11	0.00017	IFNG, FOXP3, CD28
GO:0042129	regulation of T cell proliferation	133	4	0.29	0.00018	IFNG, FOXP3, RAC2, CD28
GO:0045619	regulation of lymphocyte differentiation	134	4	0.29	0.00019	IFNG, IL7R, FOXP3, CD28
GO:0002562	somatic diversification of immune recept...	53	3	0.11	2.00E-04	IFNG, FOXP3, CD28
GO:0016444	somatic cell DNA recombination	53	3	0.11	2.00E-04	IFNG, FOXP3, CD28
GO:0002694	regulation of leukocyte activation	409	6	0.88	0.00021	IFNG, IL7R, FOXP3, BANK1, RAC2, CD28
GO:0002443	leukocyte mediated immunity	261	5	0.56	0.00023	IFNG, IL7R, FOXP3, RAC2, CD28
GO:0032700	negative regulation of interleukin-17 pr...	11	2	0.02	0.00025	IFNG, FOXP3
GO:0033089	positive regulation of T cell differenti...	11	2	0.02	0.00025	IL7R, FOXP3
GO:2000400	positive regulation of thymocyte aggrega...	11	2	0.02	0.00025	IL7R, FOXP3
GO:0002699	positive regulation of immune effector p...	145	4	0.31	0.00026	IFNG, FOXP3, RAC2, CD28
GO:0050863	regulation of T cell activation	271	5	0.58	0.00027	IFNG, IL7R, FOXP3, RAC2, CD28
GO:0002440	production of molecular mediator of immu...	149	4	0.32	0.00029	IFNG, IL7R, FOXP3, CD28
GO:0002200	somatic diversification of immune recept...	61	3	0.13	3.00E-04	IFNG, FOXP3, CD28
GO:0002312	B cell activation involved in immune res...	61	3	0.13	3.00E-04	IFNG, FOXP3, CD28
GO:0050865	regulation of cell activation	442	6	0.95	0.00033	IFNG, IL7R, FOXP3, BANK1, RAC2, CD28
GO:0002429	immune response-activating cell surface ...	284	5	0.61	0.00033	IFNG, FOXP3, BLK, CD28, CD79A
GO:1903037	regulation of leukocyte cell-cell adhesi...	284	5	0.61	0.00033	IFNG, IL7R, FOXP3, RAC2, CD28
GO:0042098	T cell proliferation	158	4	0.34	0.00036	IFNG, FOXP3, RAC2, CD28
GO:0045582	positive regulation of T cell differenti...	66	3	0.14	0.00038	IFNG, IL7R, FOXP3
GO:0002697	regulation of immune effector process	294	5	0.63	0.00039	IFNG, IL7R, FOXP3, RAC2, CD28
GO:0002708	positive regulation of lymphocyte mediat...	67	3	0.14	4.00E-04	IFNG, FOXP3, CD28
GO:0046634	regulation of alpha-beta T cell activati...	67	3	0.14	4.00E-04	IFNG, FOXP3, CD28
GO:0048535	lymph node development	14	2	0.03	4.00E-04	IL7R, CXCR5
GO:0030098	lymphocyte differentiation	297	5	0.64	0.00041	IFNG, IL7R, FOXP3, CD28, CD79A
GO:0002824	positive regulation of adaptive immune r...	68	3	0.15	0.00042	IFNG, FOXP3, CD28
GO:0033077	T cell differentiation in thymus	68	3	0.15	0.00042	IL7R, FOXP3, CD28
GO:0071594	thymocyte aggregation	68	3	0.15	0.00042	IL7R, FOXP3, CD28
GO:0002710	negative regulation of T cell mediated i...	15	2	0.03	0.00047	IL7R, FOXP3
GO:0002821	positive regulation of adaptive immune r...	72	3	0.16	0.00049	IFNG, FOXP3, CD28
GO:0002250	adaptive immune response	315	5	0.68	0.00053	IFNG, IL7R, FOXP3, CD28, CD79A
GO:0002768	immune response-regulating cell surface ...	315	5	0.68	0.00053	IFNG, FOXP3, BLK, CD28, CD79A
GO:0050670	regulation of lymphocyte proliferation	177	4	0.38	0.00055	IFNG, FOXP3, RAC2, CD28
GO:0032944	regulation of mononuclear cell prolifera...	178	4	0.38	0.00056	IFNG, FOXP3, RAC2, CD28
GO:0045621	positive regulation of lymphocyte differ...	78	3	0.17	0.00063	IFNG, IL7R, FOXP3
GO:0070663	regulation of leukocyte proliferation	185	4	0.4	0.00065	IFNG, FOXP3, RAC2, CD28
GO:0042100	B cell proliferation	79	3	0.17	0.00065	IL7R, MS4A1, CD79A
GO:0050870	positive regulation of T cell activation	186	4	0.4	0.00066	IFNG, IL7R, FOXP3, CD28
GO:0045830	positive regulation of isotype switching	18	2	0.04	0.00068	IFNG, CD28
GO:0002705	positive regulation of leukocyte mediate...	81	3	0.17	7.00E-04	IFNG, FOXP3, CD28
GO:0045076	regulation of interleukin-2 biosynthetic...	19	2	0.04	0.00076	FOXP3, CD28
GO:0045911	positive regulation of DNA recombination	19	2	0.04	0.00076	IFNG, CD28
GO:1903039	positive regulation of leukocyte cell-ce...	193	4	0.42	0.00076	IFNG, IL7R, FOXP3, CD28
GO:0002449	lymphocyte mediated immunity	194	4	0.42	0.00077	IFNG, IL7R, FOXP3, CD28

**Supplementary Data 14: First 50 gene pathways enriched in responders, as analysed by Gene ontology enrichment analysis of differentially expressed genes between non-responders and responders at baseline.**

RANK metagene			
Gene	Weight	Gene	Weight
<i>TNFRSF11A</i>	1	<i>MRPS15</i>	0.68204831
<i>HKDC1</i>	0.82571939	<i>SEMA7A</i>	0.68201196
<i>CSF1</i>	0.7933109	<i>UPP1</i>	0.68075093
<i>EIF4E2</i>	0.79108886	<i>TM4SF19</i>	0.68026699
<i>MCTP2</i>	0.78628008	<i>VNN1</i>	0.67996669
<i>CCNYL1</i>	0.77889865	<i>MYLK3</i>	0.67941685
<i>WDR49</i>	0.76679088	<i>CEACAM21</i>	0.67789757
<i>LOC10013047</i>	0.76500483	<i>HMSD</i>	0.67562533
<i>AMPD3</i>	0.76323696	<i>MATK</i>	0.67446888
<i>CD58</i>	0.75847346	<i>STK11IP</i>	0.67390288
<i>CD84</i>	0.7539867	<i>SH3BP2</i>	0.67382806
<i>LOC10050715</i>	0.74846983	<i>APOL1</i>	0.67145128
<i>TRPV2</i>	0.74465089	<i>SLC16A10</i>	0.67111045
<i>ST3GAL6</i>	0.7404945	<i>ESYT3</i>	0.66974076
<i>CXCL5</i>	0.7394194	<i>ISL1</i>	0.66950278
<i>RIN3</i>	0.73850166	<i>CHST2</i>	0.66927236
<i>KLRC1</i>	0.73824426	<i>NFKB2</i>	0.6682327
<i>KLRD1</i>	0.73791969	<i>FCHO1</i>	0.66744531
<i>IRAK3</i>	0.73771574	<i>F5</i>	0.66704732
<i>TMIGD2</i>	0.73583181	<i>LILRB4</i>	0.66691077
<i>NFE2L3</i>	0.73550545	<i>NXPE2</i>	0.66651071
<i>RELB</i>	0.73342638	<i>LINC01539</i>	0.66377184
<i>IL7</i>	0.73326004	<i>NFAM1</i>	0.65844731
<i>IKBKE</i>	0.73248895	<i>RUNX3</i>	0.65844524
<i>ST18</i>	0.73151151	<i>TTC24</i>	0.65775022
<i>SCARF1</i>	0.72905478	<i>BCL2A1</i>	0.65683228
<i>SUCNR1</i>	0.72707554	<i>NIPAL4</i>	0.65627099
<i>IL15</i>	0.72574293	<i>TMEM38B</i>	0.65575359
<i>IL31RA</i>	0.72210044	<i>ABI3</i>	0.65525771
<i>PTPN22</i>	0.72170401	<i>SERTM1</i>	0.65468096
<i>LIMS3-LOC44</i>	0.72014134	<i>GRIK1-AS2</i>	0.65418604
<i>TANK</i>	0.71491984	<i>MYD88</i>	0.65375664
<i>TMC1</i>	0.7122579	<i>LINC00636</i>	0.65349844
<i>TNFRSF9</i>	0.70837532	<i>PTPN7</i>	0.65249869
<i>ARSB</i>	0.70807206	<i>RGPD1</i>	0.65153996
<i>UBASH3B</i>	0.70425552	<i>GMIP</i>	0.650618
<i>SLC45A4</i>	0.70401534	<i>SLC39A12</i>	0.65031595
<i>CXCL3</i>	0.70297494	<i>UNC13D</i>	0.64918692
<i>TRG-AS1</i>	0.70122301	<i>SLC43A3</i>	0.64906023
<i>ARNTL2</i>	0.70014141	<i>XPNPEP2</i>	0.64852689
<i>RGS10</i>	0.69820937	<i>POPDC3</i>	0.64759253
<i>FUOM</i>	0.69745919	<i>CHODL</i>	0.64741898
<i>CD4</i>	0.69624687	<i>TNFRSF11B</i>	0.64717437
<i>SULT1B1</i>	0.69407316	<i>RRAS2</i>	0.64711458
<i>TRAF3</i>	0.6909277	<i>TMC6</i>	0.64652289
<i>ACTN2</i>	0.68588165	<i>AMBRA1</i>	0.64589902
<i>SPATS1</i>	0.68506794	<i>YWHAEP1</i>	0.64550458
<i>RNF19B</i>	0.68450746	<i>HAVCR1</i>	0.64460705
<i>ICAM1</i>	0.68355154	<i>LINC00598</i>	0.64412183
<i>HK3</i>	0.68266413	<i>DAZL</i>	0.64385161

RANKL metagene			
Gene	Weight	Gene	Weight
<i>TNFSF11</i>	1	<i>EIF2B3</i>	0.6364743
<i>PPP1R36</i>	0.7735635	<i>TRAPPC3</i>	0.6362604
<i>ZNF596</i>	0.7680214	<i>RGS1</i>	0.6349142
<i>SNX25</i>	0.7536862	<i>RGS2</i>	0.6338303
<i>FHOD1</i>	0.7497591	<i>ZNF582-AS1</i>	0.6317195
<i>MTHFR</i>	0.7423526	<i>NLRP13</i>	0.6306304
<i>CXCL13</i>	0.7354165	<i>PLA2G4D</i>	0.6303404
<i>PCBP3</i>	0.7345966	<i>RARS</i>	0.6288644
<i>TPH1</i>	0.731475	<i>SLC35B3</i>	0.628536
<i>JDP2</i>	0.7173	<i>BNIP1</i>	0.6264815
<i>LINC00959</i>	0.7172234	<i>ERRF1</i>	0.6264101
<i>ZBTB8A</i>	0.7079394	<i>PTRHD1</i>	0.6260318
<i>EXTL1</i>	0.7031998	<i>RAG1</i>	0.6239348
<i>SUPT3H</i>	0.7015091	<i>GPATCH3</i>	0.6235912
<i>ANKFN1</i>	0.696222	<i>ST7L</i>	0.6204885
<i>FOCAD</i>	0.6946434	<i>SLC9B2</i>	0.6198557
<i>ACYP2</i>	0.6939061	<i>SENP8</i>	0.6187792
<i>ZNF280D</i>	0.691644	<i>SPATA7</i>	0.6175691
<i>RABGEF1</i>	0.6867897	<i>TFPT</i>	0.6175248
<i>DENND1A</i>	0.6860203	<i>PCAT19</i>	0.6151975
<i>FSTL5</i>	0.685434	<i>MRPS15</i>	0.6149709
<i>MRRF</i>	0.6847717	<i>GMDS-AS1</i>	0.6140896
<i>ARPC1A</i>	0.6727761	<i>SUCLG1</i>	0.6137151
<i>SEL1L2</i>	0.672668	<i>ZNF8</i>	0.6134918
<i>NLRP8</i>	0.6720287	<i>NEFH</i>	0.6129876
<i>ZNF865</i>	0.67103	<i>NYAP2</i>	0.6126778
<i>ATP5O</i>	0.6704749	<i>ASL</i>	0.6122174
<i>DAGLB</i>	0.6679742	<i>FNDC5</i>	0.6106057
<i>FAM109A</i>	0.6668637	<i>MRPL35</i>	0.6105154
<i>DENND2A</i>	0.6667998	<i>SWT1</i>	0.607525
<i>TAS1R1</i>	0.6659313	<i>NFATC1</i>	0.6056097
<i>MRPS33</i>	0.6642192	<i>DHDDS</i>	0.6054681
<i>CCDC107</i>	0.6636276	<i>ANKAR</i>	0.6053279
<i>NMNAT1</i>	0.6635114	<i>SETD3</i>	0.6030397
<i>NDRG4</i>	0.6632966	<i>WDR78</i>	0.6018466
<i>GRHPR</i>	0.6615084	<i>SLC13A3</i>	0.6017783
<i>TG</i>	0.6602645	<i>ATP5J</i>	0.6011681
<i>MMP9</i>	0.654549	<i>LAMTOR4</i>	0.6010901
<i>ATP5J2</i>	0.6543919	<i>FAM229B</i>	0.6001875
<i>SMIM12</i>	0.6470009	<i>ZP1</i>	0.5999491
<i>SULT1B1</i>	0.6458719	<i>BANP</i>	0.5983288
<i>GABRB3</i>	0.6448511	<i>KRIT1</i>	0.5981262
<i>L1CAM</i>	0.6445776	<i>FAM20C</i>	0.5974409
<i>GNPTAB</i>	0.6429871	<i>NECTIN3</i>	0.5974021
<i>CREG2</i>	0.642158	<i>PRPF31</i>	0.5970603
<i>CLCN1</i>	0.6419846	<i>GYPA</i>	0.5951258
<i>ZNF784</i>	0.6418378	<i>GHRHR</i>	0.5950997
<i>HSPBP1</i>	0.6397248	<i>IAH1</i>	0.5948577
<i>OLFM3</i>	0.6380186	<i>CARTPT</i>	0.5948539
<i>HYAL1</i>	0.6366223	<i>SNX5</i>	0.5946754

**Supplementary Data 15: Gene name and weight of the RANK and RL metagene signature.**

MMTV_PyMT tumors + 24h RL UP_24h_Acini	
C3	IL1B
UBD	PARP14
PLXND1	TRAF3
NFKBIE	IL18R1
NFKBIA	MAPK11
C1QTNF1	PLXNB1
SPNS3	LTBP2
TRAF1	ECSCR
ADAMTS8	HLA-C
BACE2	LTB
RELB	HDAC9
CHADL	TJP3
NFKB2	BCL9
ARMCX4	CTNNAL1
FOXA2	HNRNPA3
EPN2	RND1
BCL2L15	RAB20
ZMYND15	HAS2
TRIM47	ADAMTS9
PLEKHS1	SLC5A8
PDE2A	TNIP1
LBH	KIFC1
C3orf80	CC2D2A
TNFAIP2	FLRT3
CXCL10	DCLK1
GALNT18	EFEMP1
TRAF2	ST8SIA4
MT1M	RNF19B
ICAM1	CXCR4
IL23A	CCDC141
BIRC3	TNFAIP3
CFB	PAPSS2
MUC15	SLCO3A1
MX1	TRAM2
CD47	CSMD1
CXCL16	KIAA1328
UPP1	BEND4
EXOC3L4	TUBB2B
SLC39A4	SLC5A9
FAS	BEND5
PTPRG	C1orf115
TNF	BPIFB1
DRAM1	IGFALS
LMNB1	MAPK1
NRP2	HP
SCIN	EPGN
IFNGR1	ANO6
PSMB9	GSDMD
TAP2	IFNGR2
TRIM5	ZMYND19

MG + 8h RL UP_8h_WT	
NFKBIE	ARC
NFKBIA	MAFG
ICAM1	PDE4B
CCL20	SLC31A2
NCOA7	SLC15A2
BIRC3	RNF125
RELB	SLC2A4
UBD	NUDT7
SAA2	
SOAT1	
HP	
C3	
TNFAIP3	
TLR2	
ADM	
CDKN1A	
NOXO1	
TNFAIP2	
IRF1	
BCL3	
RSPO1	
PDGFB	
VCAM1	
TNF	
EGR2	
NFKB2	
WNT4	
CX3CL1	
BIRC2	
PLSCR1	
RAB20	
FAS	
BCL6	
CXCL16	
CD47	
EPN2	
ARHGEF3	
IFNGR1	
RGS11	
CFB	
ZFP36L1	
ZMYND15	
IFNGR2	
IGFBP3	
ARRDC4	
ZC3H12A	
SEMA4C	
FUS	
SF3B3	
RGS16	

MG with RANK overexpression + 8h RL UP_8h_Tg	
CCL20	MYO1B
VCAM1	PARP8
CCL2	NUDT7
ICAM1	SCIN
BCL2A1	PARP14
CALCB	INHBA
TRAF1	BCL3
NFKBIA	IL1RN
UBD	TRIM47
NFKBIE	NUAK1
CXCL10	FUT4
EXTL1	ARHGEF3
FOXA2	ARRDC4
TNFAIP2	SLPI
RELB	ITGAV
PDGFB	CCND1
PPP1R12B	IRF1
ZBTB7C	GDPD5
C3	KRT16
CD47	ST3GAL3
GAD1	SLCO3A1
CX3CL1	STX11
PGLYRP2	WNT11
PTHLH	PGLYRP1
TNFAIP3	HS6ST1
NFKB2	PIK3R5
IL18R1	IFNGR2
BIRC3	ITGB6
EDN1	PAPPA
RSPO1	SPIB
SYT13	TLR2
PLSCR1	IKBKE
ADAMTS9	DTX4
TNF	HP
RND1	ZFP36L1
CFB	HMGA1
CBX7	SERPINA3
CXCL16	SLC25A25
IFNGR1	IL23A
TNIP1	MFHAS1
NCOA7	GADD45A
RAB20	RGS16
LTB	PMAIP1
SOAT1	NOXO1
JAG1	CSF2
BIRC2	FBNP1
ADAMTS8	SEMA4C
GLIPR2	PARD6B
CSF1	ABTB2
PFKFB3	GRPEL2

**Supplementary Data 16: Top 100 human converted genes up-regulated after RL exposure in mouse mammary gland and tumor *in vitro* cultures.**

Primary endpoint		
	Description	Observations
0	Assess whether denosumab induces geometric mean change in tumor Ki67 expression as assessed by immunohistochemistry (IHC)	Endpoint not met. No significant changes in Ki67 geometric mean change were observed.
Secondary endpoints		
	Description	Observations
1	Identify absolute Ki67 responders (defined as below 2.7% Ki67 IHC staining in the post treatment tumor biopsy)	No absolute Ki67 responder patients were identified.
2	Observe a decrease in serum C-terminal telepeptide (CTX) levels as marker of RANKL inhibition	Significant decrease was observed.
3	Determine whether Denosumab alters RANK/RANKL expression as assessed by IHC and RNAseq	No changes were observed in RANK/RANKL expression.
4	Determine whether there are changes in tumor proliferation rates using gene expression (single genes and gene modules, i.e. AURKA, Ki-67) and proliferation-related gene modules, i.e.GGI) in the tumor from baseline to prior to surgery	No significant changes were observed.
5	Determine changes in tumor apoptosis rates as measured using TUNEL and caspase-3 IHC from baseline to prior to surgery	No changes in caspase-3 IHC were observed. TUNEL assay was not performed.
6	Determine changes in expression levels from genes corresponding to immature mammary epithelial cell populations (MaSCs and luminal progenitors developed by Lim et al; Nature 2009), and in IHC expression of ALDH1, a stem cell marker in the tumor.	No significant changes in gene expression were observed. ALDH1 IHC was not performed.
7	Determine changes in expression levels from single genes related to the estrogen pathways (i.e. ESR1, PgR, BCL2 using both gene expression and IHC) and estrogen-related gene expression modules (i.e. ESR module) in the tumor	No significant changes in gene expression were observed. IHC analyses for BCL2 were not performed.
8	Change in expression levels from single genes related to immune pathways using both gene expression and IHC, and in immune-related gene expression modules, to explore the hypothesis that RANKL can modulate T regulatory cells in the tumor	The abundance of certain immune populations was altered by denosumab treatment. Treg abundance was significantly decreased.
9	Change in the quantity of tumor infiltrating lymphocytes as measured by percentage infiltration of surrounding tumor stroma and intra-tumoral on the H&E slide pre and post treatment	Denosumab significantly increased TILs.
10	Determine the safety and tolerability of a short course of denosumab	Denosumab was well tolerated
11	Determine changes in parameters from points 1-10 in in surrounding serial normal tissue biopsies	RNAseq data from pre- and post- denosumab treatment in available normal tissue samples was performed. Epithelial content in these biopsies was too low for most patients making data inconclusive.
Exploratory endpoints		
	Description	Observations
12	Determine changes according to subgroups defined on PgR status (positive vs. negative)	Only one patient negative for PgR was included. The statistical power was too low to conclude any effect.
13	Determine these changes according to subgroups defined as RANKL high and low in tumor and normal tissue.	RANKL was not detected on most of the biopsy samples, impeding a proper analysis.
14	Determine RANK status in normal and tumor tissue by IHC	Expression was often undetectable, probably due to lack of sensitivity of RANK IHC.
15	Determine these relative changes described above according to the phase of the menstrual cycle.	Among the 24 patients, 16 were in follicular phase, 5 were in luteal phase, one was in ovulatory phase and for two patients the menstrual phase was not available at baseline. No significant changes regarding the primary and secondary endpoints were observed according to the menstrual cycle.

**Supplementary Data 17: Clinical outcomes from the D-BEYOND clinical trial.**



**Appendix: RNAseq data analysis from  
RANK<sup>+/+</sup> and RANK<sup>-/-</sup> tumor transplants**

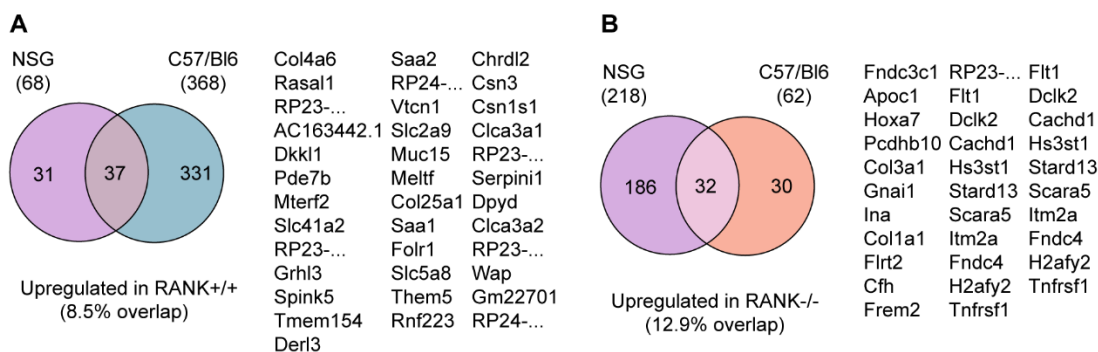




## The potential effects of immunoediting in gene expression changes between RANK+/+ and RANK-/- tumors

Given the observations that RANK+/+ tumors present an immunosuppressive microenvironment while loss of RANK results in recruitment of anti-tumorigenic immune cells, it is possible that analyzing tumor transplants at endpoint will hinder the discovery of targets due to a different immunoediting process. To explore this possibility, the same RANK+/+ or RANK-/- primary tumor was transplanted into syngeneic C57/BI6 and immunodeficient NSG hosts. Three different primary tumor transplants were FACs-sorted to perform RNAseq analysis on CD24+CD45-CD31- tumor cells.

When analyzing the upregulated genes in RANK+/+ vs. RANK-/- transplants on an immunocompetent or immunodeficient mouse (see Tables 1-2 below), the number of genes overlapping between tumors transplanted in NSG vs C57/BI6 (syngeneic) hosts was comparable regardless of RANK status: 8.5% and 12.9% overlap in RANK+/+ and RANK-/- tumors respectively (Appendix Figure A1). This suggest that, although immunoediting will likely affect gene expression, it does so in a comparable manner between RANK+/+ and RANK-/- tumors.



**Figure A1. Gene expression change overlap between tumors transplanted in immunodeficient and syngeneic hosts.** A, Gene expression change overlap between RANK+/+ tumors transplanted in immunodeficient and syngeneic hosts. List of overlapping gene ID is shown. B, Gene expression change overlap between RANK-/- tumors transplanted in immunodeficient and syngeneic hosts. List of overlapping gene ID is shown.

Analysis directly comparing the expression between tumors implanted in C57/BI6 vs NSG mice indeed show that the host plays a major effect on tumor gene expression (Tables 3-4 below). Intriguingly, RANK+/+ tumors show more upregulated genes when transplanted on immunodeficient hosts (Table 5), while RANK-/- tumors show more upregulated genes when transplanted in syngeneic hosts (Table 6). This might be due to technical reasons, but it

could also suggest that there might be general transcriptional changes depending on the interactions between RANK+ tumor cells and the immune microenvironment.

Upregulated					Downregulated				
Geneid	FC	logFC	P.Value	adj.P.Val.	Geneid	FC	logFC	P.Value	adj.P.Val.
RP24-378G4.3	29.99927884	4.906856	0.004147	0.999952	Fndc3c1	-44.63	-5.48	0.00762	0.99995
Gm22701	11.10512118	3.473153	0.005254	0.999952	Hoxa2	-29.35	-4.88	0.00060	0.99995
Pcdhga3	8.045855664	3.008246	0.024706	0.999952	Apoc1	-25.29	-4.66	0.00001	0.14585
Wap	7.967916704	2.994203	0.001269	0.999952	Hoxa7	-19.84	-4.31	0.00359	0.99995
RP23-285J17.1	6.557919572	2.713238	0.001841	0.999952	Raly1	-17.52	-4.13	0.04747	0.99995
Clca3a2	5.975756083	2.579121	0.006219	0.999952	RP23-333L19.2	-13.95	-3.80	0.03697	0.99995
Dpyd	5.974105959	2.578723	0.016204	0.999952	C1qc	-13.70	-3.78	0.00980	0.99995
Serpini1	5.883752573	2.556737	0.000384	0.999952	Hoxa5	-11.02	-3.46	0.00901	0.99995
Pinc	5.549987308	2.472484	0.042241	0.999952	Plek	-10.29	-3.36	0.02978	0.99995
RP23-393G10.1	5.458292961	2.44845	0.024069	0.999952	C1qa	-9.76	-3.29	0.01922	0.99995
Clca3a1	5.308560117	2.408321	0.006077	0.999952	Lyz2	-9.75	-3.29	0.01565	0.99995
Csn1s1	5.228609412	2.386427	0.00443	0.999952	Fcgr3	-9.35	-3.22	0.01407	0.99995
Csn3	4.759503097	2.250811	0.019395	0.999952	Tyrobp	-9.33	-3.22	0.02792	0.99995
Chrdl2	4.509244598	2.172886	0.042113	0.999952	Cybb	-8.68	-3.12	0.04048	0.99995
Rnf223	4.278636134	2.097151	0.032932	0.999952	C1qb	-8.66	-3.11	0.01571	0.99995
Them5	4.191726917	2.067545	0.004687	0.999952	Ahsg	-8.33	-3.06	0.00965	0.99995
Plin5	4.175726503	2.062027	0.036234	0.999952	Lilrb4a	-7.97	-2.99	0.04974	0.99995
Slc5a8	4.174199665	2.0615	0.001541	0.999952	Dpt	-7.64	-2.93	0.00058	0.99995
Folr1	4.150601666	2.05332	0.021607	0.999952	RP23-103L13.9	-7.63	-2.93	0.03010	0.99995
Saa1	3.97731692	1.991796	0.001058	0.999952	Sema3d	-7.61	-2.93	0.03199	0.99995
Col25a1	3.966699005	1.987939	0.008209	0.999952	Pcdhb10	-7.54	-2.92	0.02605	0.99995
Meltf	3.964189618	1.987026	0.013559	0.999952	Spi1	-7.41	-2.89	0.02137	0.99995
Afap11	3.84305888	1.942255	0.024886	0.999952	RP24-386G2.2	-7.26	-2.86	0.04491	0.99995
Muc15	3.697954341	1.886727	0.00199	0.999952	Clec3b	-6.93	-2.79	0.00528	0.99995
Slc28a3	3.66947967	1.875576	0.033384	0.999952	Rbp4	-6.77	-2.76	0.03258	0.99995
Slc2a9	3.327828765	1.734581	0.038329	0.999952	Zfp677	-6.67	-2.74	0.03680	0.99995
Vtcn1	3.282545237	1.714815	0.044238	0.999952	Abca8a	-6.52	-2.70	0.04486	0.99995
RP24-143K11.2	3.228677561	1.690943	0.009987	0.999952	Col3a1	-6.47	-2.69	0.00023	0.99995
Rec114	3.198878811	1.677566	0.04196	0.999952	Gnai1	-6.44	-2.69	0.00104	0.99995
Saa2	3.130537833	1.646411	0.011244	0.999952	Rarres2	-6.43	-2.69	0.01464	0.99995
Trpm6	3.016480077	1.592866	0.03932	0.999952	Golga7b	-6.43	-2.69	0.03840	0.99995
Derl3	2.919447921	1.545696	0.002777	0.999952	Ina	-6.39	-2.68	0.00558	0.99995
Crispld2	2.908132459	1.540093	0.014389	0.999952	Cpxm1	-6.36	-2.67	0.00052	0.99995
Tmem154	2.889077452	1.530609	0.006315	0.999952	Chrdl1	-6.36	-2.67	0.04332	0.99995
Aqp9	2.886654672	1.529399	0.035789	0.999952	RP24-62C22.1	-6.34	-2.66	0.04862	0.99995
Spink5	2.805467159	1.488241	0.030618	0.999952	Col1a1	-6.27	-2.65	0.00298	0.99995
Acta1	2.778858887	1.474493	0.027284	0.999952	Hoxa3	-6.26	-2.65	0.03265	0.99995
Grhl3	2.742301831	1.455387	0.016756	0.999952	Pcdh7	-6.26	-2.65	0.01825	0.99995
Rpl3-ps2	2.643769768	1.402597	0.033534	0.999952	Mfap4	-5.90	-2.56	0.00299	0.99995
RP23-136I22.1	2.586304747	1.370892	0.040891	0.999952	RP23-182A11.1	-5.89	-2.56	0.00384	0.99995
Tmed10-ps	2.584415775	1.369838	0.030344	0.999952	Col14a1	-5.83	-2.54	0.01539	0.99995
Calr-ps	2.580329853	1.367556	0.035638	0.999952	Col1a2	-5.82	-2.54	0.00029	0.99995
Prrg4	2.534776848	1.341859	0.041232	0.999952	Penk	-5.64	-2.50	0.00669	0.99995
RP23-386K20.4	2.528825934	1.338468	0.049022	0.999952	Mfap5	-5.47	-2.45	0.00457	0.99995
Slc41a2	2.477968306	1.309158	0.014176	0.999952	Pi16	-5.45	-2.45	0.00095	0.99995
Mir5099	2.45739832	1.297132	0.021753	0.999952	Ccl11	-5.42	-2.44	0.00661	0.99995
Psap1	2.313653912	1.210173	0.002055	0.999952	Serping1	-5.33	-2.41	0.00511	0.99995
Ndufs5	2.306458353	1.205679	0.027737	0.999952	Mfap2	-5.32	-2.41	0.01053	0.99995
Ttll7	2.254485702	1.172798	0.004926	0.999952	Lsp1	-5.29	-2.40	0.00372	0.99995
Gm10643	2.22359734	1.152896	0.034823	0.999952	Cd34	-5.28	-2.40	0.01202	0.99995

**Table 1. First 50 up- or downregulated genes between RANK+/+ and RANK-/- tumors transplanted in immunodeficient hosts.**

Upregulated					Downregulated				
Geneid	FC	logFC	P.Value	adj.P.Val.	Geneid	FC	logFC	P.Value	adj.P.Val.
RP24-378G4.3	67.98146601	6.08707	0.001463	0.955544	Fndc3c1	-28.25	-4.82	0.01942	0.95554
RP23-115O21.7	9.407639622	3.233833	0.007559	0.955544	Pcdha10	-17.07	-4.09	0.00400	0.95554
Wap	9.398649544	3.232453	0.00054	0.955544	Apoc1	-15.37	-3.94	0.00003	0.34999
RP23-363J15.2	9.228015897	3.20602	0.010101	0.955544	Glycam1	-7.64	-2.93	0.02723	0.95554
Wfdc5	8.870995013	3.149096	0.017971	0.955544	Pcdhb10	-6.79	-2.76	0.04104	0.95554
Dpyd	8.695293299	3.120235	0.007381	0.955544	Gata6	-5.20	-2.38	0.03084	0.95554
Amtn	8.418366989	3.07354	0.016544	0.955544	Hoxa7	-4.89	-2.29	0.02964	0.95554
RP23-393G10.1	8.26557154	3.047115	0.018732	0.955544	Prrx2	-4.23	-2.08	0.00921	0.95554
Sox15	8.107639476	3.019282	0.009472	0.955544	Cxcl5	-4.22	-2.08	0.00790	0.95554
RP24-225H21.4	7.866659167	2.975751	0.019952	0.955544	Bmp6	-4.15	-2.05	0.03477	0.95554
Dlx5	7.422041814	2.891816	0.006178	0.955544	RP23-242K3.2	-4.14	-2.05	0.01209	0.95554
Rims2	7.235407231	2.855074	0.007499	0.955544	Frem2	-4.10	-2.03	0.01208	0.95554
Serpini1	7.092811798	2.826358	0.000356	0.955544	Ina	-3.91	-1.97	0.01385	0.95554
Saa1	6.899638012	2.786521	3.81E-05	0.349992	Kcne1l	-3.81	-1.93	0.00937	0.95554
RP23-63O14.2	6.821158637	2.770017	0.026157	0.955544	Flrt2	-3.77	-1.91	0.01689	0.95554
RP23-277J20.1	6.5705171	2.716007	0.006368	0.955544	Gnai1	-3.77	-1.91	0.01806	0.95554
Clca3a1	6.386254812	2.67497	0.001895	0.955544	Prrg3	-3.69	-1.89	0.02960	0.95554
Slc2a12	6.368841128	2.671031	0.04433	0.955544	Col1a1	-3.68	-1.88	0.02572	0.95554
Gpa33	6.347498669	2.666188	0.014969	0.955544	Tlx3	-3.57	-1.83	0.04320	0.95554
Saa2	6.270030398	2.648472	0.000266	0.955544	Pcdhb11	-3.45	-1.79	0.04006	0.95554
Rab38	6.262549589	2.64675	0.028512	0.955544	Cxcl1	-3.41	-1.77	0.03219	0.95554
RP24-98O21.4	6.132387834	2.616449	0.046262	0.955544	Trim55	-3.32	-1.73	0.03625	0.95554
Sec14l4	6.088733114	2.606142	0.013679	0.955544	Fstl1	-3.11	-1.64	0.01432	0.95554
Tfap2b	6.069518104	2.601582	0.029545	0.955544	Mmp2	-3.05	-1.61	0.01758	0.95554
Prol1	6.063374415	2.600121	0.01885	0.955544	Flt1	-3.01	-1.59	0.00091	0.95554
RP24-372P19.2	6.012032804	2.587853	0.032371	0.955544	Cfh	-2.95	-1.56	0.02027	0.95554
Sgpp2	5.847857338	2.547908	0.027584	0.955544	Col3a1	-2.88	-1.53	0.01978	0.95554
RP23-285J17.1	5.812690627	2.539206	0.005619	0.955544	Ramp2	-2.80	-1.49	0.02921	0.95554
Tll1	5.732183924	2.519085	0.021175	0.955544	Gm23639	-2.75	-1.46	0.03398	0.95554
Il18r1	5.712681908	2.514168	0.018925	0.955544	Serpib8	-2.73	-1.45	0.03953	0.95554
RP24-345B5.3	5.70761787	2.512889	0.037776	0.955544	Heph	-2.71	-1.44	0.04869	0.95554
Clca3a2	5.699487944	2.510832	0.006077	0.955544	Kcnb1	-2.71	-1.44	0.00953	0.95554
Ptprn	5.614494072	2.489156	0.01935	0.955544	Plekhd1	-2.59	-1.37	0.04434	0.95554
Gpr152	5.546403185	2.471552	0.042318	0.955544	RP23-375N21.2	-2.58	-1.37	0.00517	0.95554
Naip2	5.474079071	2.452616	0.032708	0.955544	Fabp5	-2.54	-1.35	0.00977	0.95554
RP24-95O4.9	5.370817972	2.425142	0.013279	0.955544	Tril	-2.48	-1.31	0.01786	0.95554
Tcf24	5.295214072	2.404689	0.036102	0.955544	Hs3st1	-2.43	-1.28	0.00120	0.95554
Muc16	5.238013287	2.38902	0.03311	0.955544	Tnfrsf19	-2.41	-1.27	0.00322	0.95554
Chrne	5.227121672	2.386017	0.028897	0.955544	Itm2a	-2.41	-1.27	0.02945	0.95554
Slc2a9	5.203084288	2.379367	0.006195	0.955544	Adamts4	-2.39	-1.26	0.03771	0.95554
Rasgrf1	5.192889127	2.376537	0.015082	0.955544	Rnase4	-2.37	-1.25	0.00854	0.95554
Chrdl2	5.140778189	2.361987	0.0325	0.955544	Prodh	-2.37	-1.24	0.02282	0.95554
Smpd3	5.116134633	2.355054	0.040875	0.955544	Dclk2	-2.31	-1.21	0.01351	0.95554
Tnni2	5.055078749	2.337734	0.030668	0.955544	Gulp1	-2.30	-1.20	0.00355	0.95554
Vtcn1	4.959185209	2.310103	0.009639	0.955544	Glipr1	-2.30	-1.20	0.03788	0.95554
AC161108.3	4.905169471	2.294303	0.021971	0.955544	Jam2	-2.29	-1.20	0.00610	0.95554
RP24-571B18.2	4.904697579	2.294164	0.013516	0.955544	Sdr39u1	-2.23	-1.16	0.00549	0.95554
Il12a	4.867590044	2.283208	0.037252	0.955544	Fndc4	-2.22	-1.15	0.02806	0.95554
RP23-156O5.4	4.811983039	2.266632	0.04529	0.955544	Gas7	-2.22	-1.15	0.01588	0.95554
Csn1s1	4.795830188	2.261781	0.003449	0.955544	Pcsk6	-2.22	-1.15	0.00359	0.95554

**Table 2. First 50 up- or downregulated genes between RANK+/+ and RANK-/- tumors transplanted in syngenic hosts.**

Upregulated					Downregulated				
Geneid	FC	logFC	P.Value	adj.P.Val.	Geneid	FC	logFC	P.Value	adj.P.Val.
Gm23287	5.067424	2.341253	0.012136	0.914296	Ighg2c	-19.1276	-4.25758	0.003718	0.914296
RP24-568B16.1	4.858021	2.280369	0.032753	0.914296	Mmrn1	-16.0839	-4.00754	0.001425	0.914296
Pbp2	4.327208	2.113436	0.026517	0.914296	Tgtp1	-15.7213	-3.97465	0.039313	0.914296
Snai3	4.273416	2.09539	0.003187	0.914296	Gm4841	-14.8048	-3.88799	0.011711	0.914296
RP23-432O2.2	4.061759	2.022104	0.037529	0.914296	Aoc1	-14.3504	-3.84302	0.003227	0.914296
Krt84	3.64729	1.866825	0.046075	0.914296	Tph1	-13.9173	-3.7988	0.000191	0.914296
Acta1	3.260455	1.705073	0.002673	0.914296	Agtr1a	-12.6441	-3.66039	0.040264	0.914296
Itih3	3.219637	1.686898	0.007928	0.914296	Ido1	-12.5976	-3.65507	0.019641	0.914296
Tlx3	2.691113	1.428203	0.040116	0.914296	Olfm4	-11.4195	-3.51343	0.016818	0.914296
Foxd2	2.36128	1.239569	0.026119	0.914296	Nphp4	-11.0849	-3.47052	0.005715	0.914296
RP23-172P1.1	2.326504	1.218164	0.048648	0.914296	Stse	-11.0469	-3.46558	0.015878	0.914296
RP23-20E10.5	2.21222	1.145495	0.032866	0.914296	Stk32a	-9.74367	-3.28446	0.021593	0.914296
					Adra1a	-9.6267	-3.26704	0.036559	0.914296
					Gbp5	-9.26109	-3.21118	0.038893	0.914296
					RP24-499A8.3	-8.70304	-3.12152	0.029104	0.914296
					Muc13	-8.69423	-3.12006	0.03568	0.914296
					Ccdc170	-8.54059	-3.09434	0.044039	0.914296
					Dcaf12l1	-8.17411	-3.03106	0.018902	0.914296
					Ndst4	-8.07809	-3.01401	0.029858	0.914296
					Gbp8	-7.81709	-2.96663	0.023908	0.914296
					Capn8	-7.70789	-2.94634	0.022558	0.914296
					Crmp1	-7.35251	-2.87824	0.031672	0.914296
					9930111J21Rik1	-7.24219	-2.85643	0.007306	0.914296
					Batf2	-7.1738	-2.84274	0.020223	0.914296
					Gbp4	-7.08971	-2.82573	0.004588	0.914296
					Slc14a1	-6.84456	-2.77496	0.005431	0.914296
					RP24-93F20.9	-6.48649	-2.69744	0.010279	0.914296
					RP23-14F5.8	-6.47358	-2.69456	0.008838	0.914296
					RP23-160G19.4	-6.29616	-2.65447	0.044282	0.914296
					RP23-14F5.7	-6.2403	-2.64161	0.020783	0.914296
					Adarb2	-6.14192	-2.61869	0.047452	0.914296
					Col6a4	-6.04181	-2.59498	0.007793	0.914296
					RP24-358M18.2	-5.84125	-2.54628	0.026984	0.914296
					Acsbg1	-5.82292	-2.54174	0.018312	0.914296
					Csn2	-5.81712	-2.5403	0.041925	0.914296
					AC157555.1	-5.799	-2.5358	0.037263	0.914296
					Gbp10	-5.73918	-2.52085	0.006289	0.914296
					Aldh1a2	-5.71742	-2.51536	0.043102	0.914296
					Chgb	-5.70497	-2.51222	0.025379	0.914296
					Spef2	-5.7001	-2.51099	0.023011	0.914296
					RP23-74K24.1	-5.64892	-2.49798	0.034198	0.914296
					RP23-332G12.1	-5.62113	-2.49086	0.041408	0.914296
					Il18r1	-5.5532	-2.47332	0.003541	0.914296
					Cntn4	-5.55238	-2.47311	0.044049	0.914296
					RP23-42H18.4	-5.48041	-2.45428	0.025073	0.914296
					Serpina3g	-5.45185	-2.44675	0.036168	0.914296
					Zbtb16	-5.45096	-2.44651	0.001124	0.914296
					Dscam	-5.37431	-2.42608	0.047032	0.914296
					RP23-52N2.1	-5.35825	-2.42176	0.023397	0.914296
					Slc44a5	-5.33548	-2.41562	0.003952	0.914296

**Table 3. First 50 up- or downregulated genes between RANK+/+ tumors transplanted in NSG vs C57/Bl6 hosts.**

## Upregulated

RP23-390G1.4	22.10087	4.466031	0.000413	0.962314
RP23-282N17.7	12.52389	3.646611	0.018174	0.962314
RP23-115O21.7	10.71431	3.421468	0.000856	0.962314
Lilrb4a	9.398979	3.232504	0.021704	0.962314
Serpina3h	9.104616	3.186598	0.031024	0.962314
RP24-321J24.3	8.57937	3.100872	0.00533	0.962314
Rarres2	8.086317	3.015483	0.003535	0.962314
Ccl8	6.307145	2.656987	0.002841	0.962314
C1qa	6.005364	2.586252	0.008981	0.962314
Dpt	5.814002	2.539532	0.000134	0.962314
Clec3b	5.78527	2.532384	0.001709	0.962314
Nptx2	5.767228	2.527878	0.047441	0.962314
RP23-103E11.8	5.715278	2.514824	0.010341	0.962314
Lilr4b	5.635913	2.494649	0.043476	0.962314
Pianp	5.591436	2.483219	0.009046	0.962314
Prg4	5.532329	2.467887	0.000746	0.962314
RP23-468A19.2	5.436278	2.442619	0.041225	0.962314
Fgl2	5.384503	2.428813	0.000564	0.962314
RP23-63O14.2	5.349871	2.419504	0.01626	0.962314
RP23-392C8.4	5.219536	2.383922	0.004384	0.962314
C1qc	5.052051	2.336869	0.006215	0.962314
Kcng1	5.014596	2.326133	0.019864	0.962314
Msr1	4.984996	2.317592	0.015078	0.962314
RP23-428G22.6	4.969408	2.313074	0.013275	0.962314
Gatm	4.922753	2.299465	0.002941	0.962314
Mir98	4.879306	2.286676	0.010233	0.962314
Penk	4.834284	2.273302	0.001917	0.962314
RP23-156A3.1	4.772772	2.254827	0.037697	0.962314
Gm24596	4.756144	2.249793	0.009635	0.962314
Chd3os	4.5627	2.189888	0.024076	0.962314
En2	4.558018	2.188407	0.014294	0.962314
Tgfb1	4.530234	2.179586	0.016714	0.962314
Tyrobp	4.490254	2.166797	0.022873	0.962314
Col3a1	4.46756	2.159487	8.43E-05	0.962314
RP23-180A14.5	4.455334	2.155534	0.009337	0.962314
Plek	4.440513	2.150726	0.023372	0.962314
Pi16	4.379022	2.130609	0.000228	0.962314
Tcf24	4.358644	2.12388	0.020912	0.962314
Efemp1	4.324555	2.112552	0.006422	0.962314
Spi1	4.298342	2.10378	0.014769	0.962314
Il1b	4.230528	2.080838	0.037079	0.962314
RP24-191C23.2	4.223478	2.078432	0.04131	0.962314
RP23-403H2.5	4.156592	2.055401	0.005857	0.962314
Rpl30-ps3	4.094751	2.033776	0.002024	0.962314
RP24-191C15.3	4.041856	2.015018	0.038053	0.962314
Mmp3	3.958034	1.984784	0.001531	0.962314
Trem2	3.933962	1.975983	0.02589	0.962314
Mfap2	3.928712	1.974056	0.00449	0.962314
Lyz2	3.91482	1.968946	0.016768	0.962314
Lum	3.866159	1.950901	0.00122	0.962314

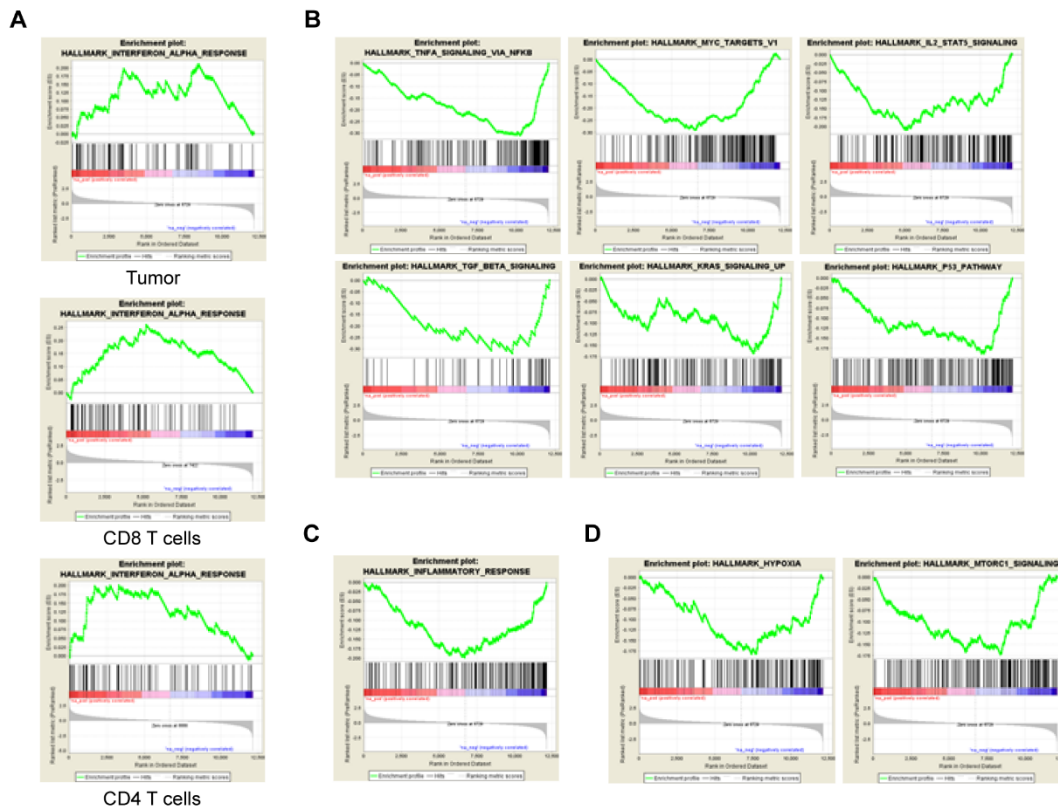
## Downregulated

RP23-178F20.2	-3.43973	-1.78229	0.00759	0.962314
Aoc1	-3.26215	-1.70582	0.0414	0.962314
Glycam1	-2.82594	-1.49873	0.040483	0.962314
Rpl22-ps1	-2.57275	-1.36331	0.014481	0.962314
Rpl3-ps2	-2.47015	-1.3046	0.012599	0.962314
RP23-383I7.4	-2.46481	-1.30148	0.039926	0.962314
Kif27	-2.45387	-1.29506	0.028459	0.962314
Tpt1-ps3	-2.24072	-1.16396	0.024639	0.962314
P4ha3	-2.12834	-1.08973	0.041687	0.962314
Zfp934	-2.07645	-1.05412	0.025939	0.962314

**Table 4. First 50 up- or downregulated genes between RANK<sup>-/-</sup> tumors transplanted in NSG vs C57/Bl6 hosts.**

## Effects of RANK depletion in tumor cells, CD8 and CD4 T cells.

In order to explore changes within different populations in the tissue microenvironment, a RNAseq was performed with sorted tumor cells (CD45-CD31-), CD8 (CD45+CD11b-CD3+CD8+) and CD4 T cells (CD45+CD11b-CD3+CD8-) from RANK+/+ and RANK-/- tumor transplants. GSEA was performed to identify protein pathways which could be altered by the lack of RANK signaling in the tumor microenvironment, comparing each population within RANK+/+ tumors vs. RANK-/- tumors (Tables 5-7). The most consistent observation is in the RANK+/+ tumors and their microenvironment, where both tumor cells and T cell populations associate with an enrichment in response to interferon alpha genes (Figure A2.A). RANK-/- tumors are found enriched for several alternative pathways, including TNF- $\alpha$ -NF $\kappa$ B, MYC, IL2-STAT5, P53, TGFB and KRAS, maybe as compensatory mechanisms after RANK loss (Figure A2.B). Inflammatory response is higher in RANK-/-, in accordance with their higher immune infiltration (Figure A2.C). And metabolic pathways are also altered, with an enrichment for hypoxia-response genes and mTOR pathway activation (Figure A2.D).



**Figure A2. GSEA enrichment analysis in RANK+/+ and RANK-/- tumor cells.** A, GSEA IFN $\alpha$  pathway enrichment in tumor cells, CD4 and CD8 T cells. B, Alternative pathways enriched in RANK-/- tumor cells. C, Inflammatory response pathway in RANK-/- tumors. D, Metabolic pathways altered in tumor cells.

Upregulated						
NAME	SIZE	ES	NES	NOM p-val	FDR q-val	FWER p-val
HALLMARK_INTERFERON_ALPHA_RESPONSE	83	0.211	2.25	0.002	0.008706	0.027
HALLMARK_MITOTIC_SPINDLE	191	0.097	1.53	0.06118143	0.239845	0.77
HALLMARK_FATTY_ACID_METABOLISM	130	0.113	1.47	0.07201646	0.210119	0.867
HALLMARK_BILE_ACID_METABOLISM	80	0.117	1.22	0.21174005	0.423052	0.996
HALLMARK_SPERMATOGENESIS	77	0.098	1.01	0.44117647	0.679531	1
HALLMARK_PROTEIN_SECRETION	91	0.079	0.88	0.6359918	0.797798	1
HALLMARK_INTERFERON_GAMMA_RESPONSE	179	0.055	0.87	0.59411764	0.696567	1
HALLMARK_PEROXISOME	83	0.081	0.87	0.6294821	0.611916	1
Downregulated						
NAME	SIZE	ES	NES	NOM p-val	FDR q-val	FWER p-val
HALLMARK_TNFA_SIGNALING_VIA_NFKB	188	-0.31	-4.98	0	0	0
HALLMARK_MYC_TARGETS_V1	190	-0.29	-4.68	0	0	0
HALLMARK_IL2_STAT5_SIGNALING	191	-0.21	-3.3	0	0	0
HALLMARK_INFLAMMATORY_RESPONSE	166	-0.2	-2.99	0	0	0
HALLMARK_P53_PATHWAY	188	-0.19	-2.96	0	0	0
HALLMARK_EPITHELIAL_MESENCHYMAL_TRANSITION	172	-0.19	-2.95	0	0	0
HALLMARK_ALLOGRAFT_REJECTION	179	-0.18	-2.83	0	0.000261	0.001
HALLMARK_MTORC1_SIGNALING	196	-0.17	-2.82	0	0.000228	0.001
HALLMARK_HYPOXIA	174	-0.18	-2.8	0	0.000203	0.001
HALLMARK_TGF_BETA_SIGNALING	50	-0.32	-2.66	0	0.000314	0.002
HALLMARK_KRAS_SIGNALING_UP	164	-0.17	-2.51	0	0.000606	0.004
HALLMARK_DNA_REPAIR	137	-0.17	-2.27	0	0.002842	0.021
HALLMARK_XENOBIOTIC_METABOLISM	150	-0.16	-2.22	0	0.003018	0.024
HALLMARK_MYC_TARGETS_V2	57	-0.24	-2.16	0	0.00472	0.04
HALLMARK_APICAL_JUNCTION	156	-0.14	-2.02	0.0040404	0.011321	0.097
HALLMARK_CHOLESTEROL_HOMEOSTASIS	70	-0.2	-1.92	0.00970874	0.019388	0.168
HALLMARK_MYOGENESIS	152	-0.13	-1.91	0.0039604	0.019512	0.179
HALLMARK_COAGULATION	101	-0.16	-1.9	0.01004016	0.020263	0.198
HALLMARK_WNT_BETA_CATENIN_SIGNALING	36	-0.26	-1.86	0.002	0.023236	0.238
HALLMARK_APOPTOSIS	152	-0.12	-1.78	0.02191235	0.037068	0.359
HALLMARK_UV_RESPONSE_UP	131	-0.13	-1.74	0.03205128	0.044143	0.424
HALLMARK_ESTROGEN_RESPONSE_EARLY	177	-0.11	-1.7	0.0362173	0.049879	0.476
HALLMARK_ANGIOGENESIS	31	-0.25	-1.65	0.02574257	0.062065	0.576
HALLMARK_OXIDATIVE_PHOSPHORYLATION	173	-0.1	-1.59	0.04216867	0.07859	0.677
HALLMARK_UNFOLDED_PROTEIN_RESPONSE	104	-0.13	-1.58	0.05128205	0.079631	0.703
HALLMARK_IL6_JAK_STAT3_SIGNALING	77	-0.15	-1.57	0.05436893	0.079079	0.712
HALLMARK_KRAS_SIGNALING_DN	102	-0.12	-1.39	0.0916497	0.170032	0.946
HALLMARK_ESTROGEN_RESPONSE_LATE	168	-0.09	-1.39	0.10912699	0.164731	0.946
HALLMARK_COMPLEMENT	158	-0.09	-1.35	0.13894325	0.187074	0.97
HALLMARK_HEDGEHOG_SIGNALING	28	-0.2	-1.24	0.18712273	0.281064	1
HALLMARK_ANDROGEN_RESPONSE	91	-0.11	-1.2	0.21073559	0.307691	1
HALLMARK_NOTCH_SIGNALING	29	-0.19	-1.2	0.20824742	0.301352	1
HALLMARK_GLYCOLYSIS	178	-0.07	-1.1	0.34567901	0.41069	1
HALLMARK_ADIPOGENESIS	177	-0.07	-1.06	0.37475345	0.447414	1
HALLMARK_UV_RESPONSE_DN	133	-0.08	-1.05	0.368	0.455647	1
HALLMARK_G2M_CHECKPOINT	184	-0.06	-0.98	0.44402984	0.544549	1
HALLMARK_PANCREAS_BETA_CELLS	16	-0.2	-0.96	0.4759036	0.555785	1
HALLMARK_REACTIVE_OXIGEN_SPECIES_PATHWAY	45	-0.12	-0.96	0.5217391	0.543703	1
HALLMARK_E2F_TARGETS	193	-0.06	-0.95	0.4831683	0.536003	1
HALLMARK_PI3K_AKT_MTOR_SIGNALING	96	-0.08	-0.94	0.50784314	0.540991	1
HALLMARK_APICAL_SURFACE	37	-0.12	-0.88	0.5968689	0.619672	1
HALLMARK_HEME_METABOLISM	161	-0.05	-0.78	0.7412731	0.749808	1

**Table 5. GSEA between RANK+/+ and RANK-/- tumor cells (CD45-CD31-) implanted in syngeneic hosts**



Upregulated						
NAME	SIZE	ES	NES	NOM p-val	FDR q-val	FWER p-val
HALLMARK_E2F_TARGETS	193	0.193	3.2	0	0	0
HALLMARK_G2M_CHECKPOINT	184	0.178	2.84	0	0	0
HALLMARK_MITOTIC_SPINDLE	191	0.155	2.47	0	7.50E-04	0.003
HALLMARK_INTERFERON_ALPHA_RESPONSE	83	0.201	2.19	0	0.007353	0.035
HALLMARK_EPITHELIAL_MESENCHYMAL_TRANSITION	172	0.115	1.8	0.01581028	0.065321	0.34
HALLMARK_INTERFERON_GAMMA_RESPONSE	179	0.108	1.66	0.03853565	0.110138	0.574
HALLMARK_APICAL_JUNCTION	156	0.106	1.57	0.05220884	0.146167	0.741
HALLMARK_MYOGENESIS	152	0.106	1.5	0.07188161	0.17549	0.839
HALLMARK_UV_RESPONSE_DN	133	0.105	1.41	0.10891089	0.227792	0.942
HALLMARK_BILE_ACID_METABOLISM	80	0.131	1.38	0.10392157	0.235136	0.957
HALLMARK_COAGULATION	101	0.103	1.21	0.23684211	0.416914	0.998
HALLMARK_NOTCH_SIGNALING	29	0.179	1.14	0.264	0.481152	0.998
HALLMARK_INFLAMMATORY_RESPONSE	166	0.064	0.95	0.48971194	0.770009	1
HALLMARK_KRAS_SIGNALING_DN	102	0.079	0.95	0.50503016	0.716221	1
HALLMARK_ESTROGEN_RESPONSE_EARLY	177	0.051	0.8	0.70841485	0.955376	1
HALLMARK_DNA_REPAIR	137	0.059	0.8	0.73558646	0.899989	1
HALLMARK_ANGIOGENESIS	31	0.113	0.76	0.78630704	0.904527	1
HALLMARK_SPERMATOGENESIS	77	0.07	0.74	0.81504065	0.885672	1
HALLMARK_APICAL_SURFACE	37	0.084	0.61	0.94011974	0.989593	1
HALLMARK_WNT_BETA_CATENIN_SIGNALING	36	0.084	0.59	0.9585062	0.947825	1
Downregulated						
NAME	SIZE	ES	NES	NOM p-val	FDR q-val	FWER p-val
HALLMARK_IL2_STATS5_SIGNALING	191	-0.22	-3.5	0	0	0
HALLMARK_OXIDATIVE_PHOSPHORYLATION	173	-0.16	-2.46	0	0.006968	0.011
HALLMARK_MTORC1_SIGNALING	196	-0.15	-2.39	0	0.00691	0.017
HALLMARK_PROTEIN_SECRETION	91	-0.19	-2.15	0.00389105	0.018859	0.062
HALLMARK_UNFOLDED_PROTEIN_RESPONSE	104	-0.18	-2.14	0.0038835	0.015525	0.064
HALLMARK_CHOLESTEROL_HOMEOSTASIS	70	-0.19	-1.83	0.0212766	0.070101	0.301
HALLMARK_PEROXISOME	83	-0.17	-1.82	0.0101833	0.062456	0.31
HALLMARK_HEME_METABOLISM	161	-0.12	-1.76	0.01405623	0.080209	0.422
HALLMARK_COMPLEMENT	158	-0.11	-1.62	0.04225352	0.137532	0.637
HALLMARK_ADIPOGENESIS	177	-0.1	-1.47	0.07983194	0.236216	0.865
HALLMARK_HYPOXIA	174	-0.09	-1.38	0.11507937	0.310634	0.946
HALLMARK_TNFA_SIGNALING_VIA_NFKB	188	-0.08	-1.34	0.14137214	0.338388	0.969
HALLMARK_P53_PATHWAY	188	-0.08	-1.31	0.15157895	0.348504	0.98
HALLMARK_PI3K_AKT_MTOR_SIGNALING	96	-0.11	-1.29	0.17623763	0.354969	0.989
HALLMARK_GLYCOLYSIS	178	-0.08	-1.27	0.17436975	0.350186	0.991
HALLMARK_XENOBIOTIC_METABOLISM	150	-0.09	-1.26	0.17131475	0.34732	0.994
HALLMARK_ESTROGEN_RESPONSE_LATE	168	-0.08	-1.19	0.23091976	0.412743	0.998
HALLMARK_MYC_TARGETS_V1	190	-0.07	-1.15	0.30897704	0.45924	0.999
HALLMARK_UV_RESPONSE_UP	131	-0.09	-1.14	0.28601694	0.444842	0.999
HALLMARK_KRAS_SIGNALING_UP	164	-0.08	-1.11	0.32459676	0.465845	0.999
HALLMARK_MYC_TARGETS_V2	57	-0.12	-1.11	0.29637095	0.445752	0.999
HALLMARK_REACTIVE_OXYGEN_SPECIES_PATHWAY	45	-0.13	-1.02	0.4092664	0.563112	1
HALLMARK_PANCREAS_BETA_CELLS	16	-0.21	-1.01	0.43541667	0.55715	1
HALLMARK_ALLOGRAFT_REJECTION	179	-0.06	-0.98	0.46745563	0.570279	1
HALLMARK_TGF_BETA_SIGNALING	50	-0.12	-0.96	0.49105367	0.585003	1
HALLMARK_IL6_JAK_STAT3_SIGNALING	77	-0.09	-0.93	0.51731604	0.604356	1
HALLMARK_ANDROGEN_RESPONSE	91	-0.08	-0.89	0.58551306	0.647324	1
HALLMARK_HEDGEHOG_SIGNALING	28	-0.12	-0.73	0.80991733	0.866833	1
HALLMARK_FATTY_ACID_METABOLISM	130	-0.05	-0.65	0.9107505	0.932565	1
HALLMARK_APOPTOSIS	152	-0.04	-0.59	0.951782	0.95322	1

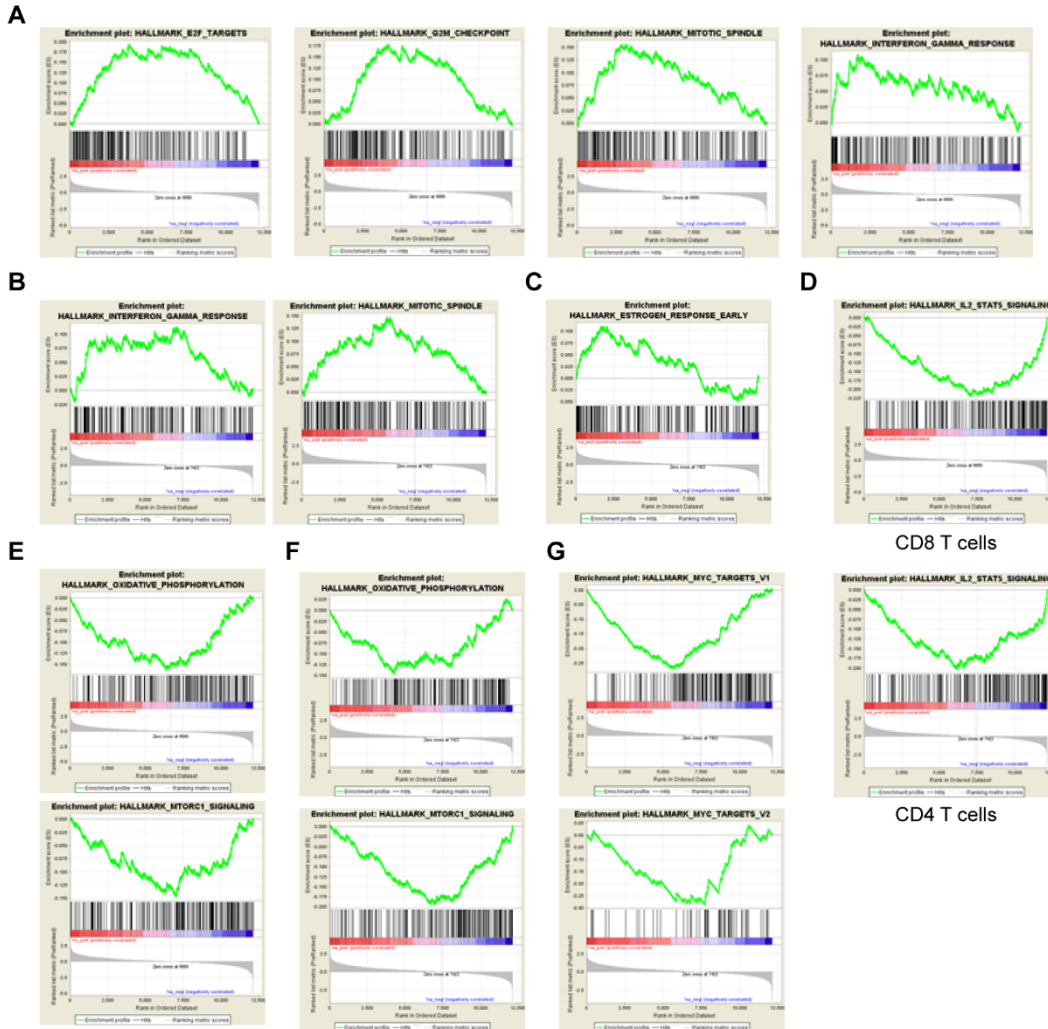
**Table 6. GSEA between RANK+/+ and RANK-/- CD8 T cells (CD45+CD3+CD8-) implanted in syngeneic hosts**



Upregulated						
NAME	SIZE	ES	NES	NOM p-val	FDR q-val	FWER p-val
HALLMARK_INTERFERON_ALPHA_RESPONSE	83	0.261	2.795	0.000	0.000	0.000
HALLMARK_MITOTIC_SPINDLE	191	0.147	2.353	0.002	0.005	0.015
HALLMARK_INTERFERON_GAMMA_RESPONSE	179	0.112	1.761	0.008	0.102	0.395
HALLMARK_APICAL_JUNCTION	156	0.119	1.734	0.019	0.088	0.441
HALLMARK_BILE_ACID_METABOLISM	80	0.164	1.714	0.030	0.077	0.470
HALLMARK_ESTROGEN_RESPONSE_EARLY	177	0.111	1.694	0.025	0.072	0.506
HALLMARK_HEDGEHOG_SIGNALING	28	0.255	1.616	0.058	0.093	0.647
HALLMARK_ADIPOGENESIS	177	0.105	1.599	0.037	0.088	0.668
HALLMARK_MYOGENESIS	152	0.110	1.573	0.055	0.087	0.708
HALLMARK_UV_RESPONSE_DN	133	0.091	1.225	0.215	0.342	0.996
HALLMARK_EPITHELIAL_MESENCHYMAL_TRANSITION	172	0.078	1.195	0.243	0.344	0.998
HALLMARK_APICAL_SURFACE	37	0.153	1.090	0.331	0.447	1.000
HALLMARK_ESTROGEN_RESPONSE_LATE	168	0.072	1.074	0.359	0.433	1.000
HALLMARK_WNT_BETA_CATENIN_SIGNALING	36	0.150	1.058	0.370	0.422	1.000
HALLMARK_NOTCH_SIGNALING	29	0.163	1.045	0.402	0.409	1.000
HALLMARK_KRAS_SIGNALING_DN	102	0.063	0.727	0.810	0.812	1.000
Downregulated						
NAME	SIZE	ES	NES	NOM p-val	FDR q-val	FWER p-val
HALLMARK_MYC_TARGETS_V1	190	-0.27	-4.28	0	0	0
HALLMARK_UNFOLDED_PROTEIN_RESPONSE	104	-0.29	-3.46	0	0	0
HALLMARK_IL2_STAT5_SIGNALING	191	-0.2	-3.18	0	0	0
HALLMARK_MTORC1_SIGNALING	196	-0.19	-3.15	0	0	0
HALLMARK_MYC_TARGETS_V2	57	-0.29	-2.55	0	0.002121	0.007
HALLMARK_OXIDATIVE_PHOSPHORYLATION	173	-0.15	-2.21	0.00192678	0.008665	0.037
HALLMARK_DNA_REPAIR	137	-0.14	-1.89	0.00607287	0.045181	0.206
HALLMARK_GLYCOLYSIS	178	-0.12	-1.86	0.01244813	0.04728	0.241
HALLMARK_PI3K_AKT_MTOR_SIGNALING	96	-0.13	-1.54	0.05415861	0.221413	0.765
HALLMARK_COAGULATION	101	-0.13	-1.51	0.05882353	0.221999	0.802
HALLMARK_UV_RESPONSE_UP	131	-0.11	-1.47	0.0734127	0.2478	0.864
HALLMARK_E2F_TARGETS	193	-0.09	-1.47	0.07905138	0.229731	0.868
HALLMARK_TNFA_SIGNALING_VIA_NFKB	188	-0.08	-1.27	0.17382413	0.468256	0.987
HALLMARK_PROTEIN_SECRETION	91	-0.12	-1.27	0.20618556	0.437659	0.988
HALLMARK_REACTIVE_OXIGEN_SPECIES_PATHWAY	45	-0.16	-1.26	0.19144602	0.428538	0.991
HALLMARK_ANGIOGENESIS	31	-0.18	-1.19	0.24796748	0.502637	0.997
HALLMARK_TGF_BETA_SIGNALING	50	-0.14	-1.19	0.24324325	0.483619	0.997
HALLMARK_XENOBIOTIC_METABOLISM	150	-0.08	-1.11	0.30859375	0.599368	1
HALLMARK_PEROXISOME	83	-0.1	-1.09	0.34960938	0.606961	1
HALLMARK_FATTY_ACID_METABOLISM	130	-0.08	-1.07	0.35984096	0.60396	1
HALLMARK_HYPOXIA	174	-0.07	-1.04	0.39183673	0.638932	1
HALLMARK_G2M_CHECKPOINT	184	-0.06	-1.02	0.39034206	0.633142	1
HALLMARK_IL6_JAK_STAT3_SIGNALING	77	-0.1	-1	0.45061728	0.643522	1
HALLMARK_CHOLESTEROL_HOMEOSTASIS	70	-0.1	-0.98	0.444	0.651611	1
HALLMARK_ALLOGRAFT_REJECTION	179	-0.06	-0.95	0.47692308	0.678599	1
HALLMARK_PANCREAS_BETA_CELLS	16	-0.19	-0.94	0.51937985	0.670375	1
HALLMARK_HEME_METABOLISM	161	-0.06	-0.94	0.5177165	0.652422	1
HALLMARK_P53_PATHWAY	188	-0.05	-0.88	0.61676645	0.724464	1
HALLMARK_COMPLEMENT	158	-0.06	-0.82	0.6910569	0.805851	1
HALLMARK_KRAS_SIGNALING_UP	164	-0.06	-0.81	0.7034068	0.792731	1
HALLMARK_ANDROGEN_RESPONSE	91	-0.07	-0.78	0.7425743	0.817897	1
HALLMARK_APOPTOSIS	152	-0.05	-0.69	0.8545082	0.91088	1
HALLMARK_INFLAMMATORY_RESPONSE	166	-0.04	-0.58	0.9675456	0.984683	1
HALLMARK_SPERMATOGENESIS	77	-0.05	-0.56	0.96940726	0.967586	1

**Table 7. GSEA between RANK+/+ and RANK-/- CD4 T cells (CD45+CD3+CD8-) implanted in syngeneic hosts**

In the RANK+/+ tumor microenvironment, CD8 T cells are enriched in pathways involving T cell proliferation/activity, such as those associated with mitotic spindle, E2F and G2M targets, and the IFN $\gamma$  response pathway (Figure A3.A).



**Figure A3. GSEA in T cell populations from RANK+/+ and RANK-/- tumors.** A, GSEA for pathways enriched in CD8 T cells from RANK+/+ tumors. B, GSEA for pathways enriched in CD4 T cells from RANK+/+ tumors. C, Estrogen response pathway GSEA for CD4 T cells. D, IL2-STAT5 pathway GSEA for CD8 and CD4 T cells. E, CD8 T cells GSEA for metabolic pathways. F, CD4 T cells GSEA for metabolic pathways. G, MYC pathway GSEA in CD4 T cells.

CD4 T cells in RANK+/+ tumors also have an enrichment in IFN $\gamma$  response and mitotic spindle genes (Figure A3.B) and CD4 T cells in RANK+/+ tumors present higher early estrogen-response gene enrichment (Figure A3C). The Estrogen pathway has been described to be necessary to downmodulate CD4 T cell responses and prevent autoimmunity(Kim et al., 2019).

In RANK<sup>-/-</sup> tumors, both CD8 and CD4 T cells present an enrichment in IL2-STAT5 pathway (Figure A3D), as did tumor cells. In a T cell population, this pathway might reflect a higher T cell activity, as suggested by the rest of the data in the tumor transplants.

CD8 T cells in RANK<sup>+/+</sup> tumors present changes in metabolism, with higher mTOR and oxidative phosphorylation (Figure A3E), which are also found in CD4 T cells (Figure A3F). Additionally, CD4 T cells present a stronger MYC pathway activation (Figure A3G).



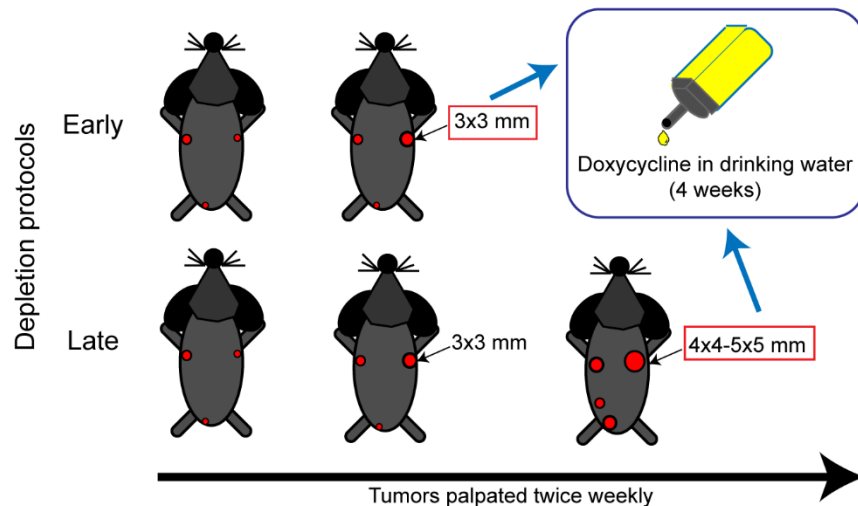
## CHAPTER 2

### **Characterization of an inducible, tissue-specific RANK depletion model of mammary gland tumorigenesis**



## 2.1 The K8-PyMT model allows RANK depletion in luminal MG epithelium at different stages during tumorigenesis.

The RANK<sup>ΔK8</sup> model is the result of crossing 5 different transgenic mouse strains: K8-rtTA (Watson et al., 2015), TetOCre (Perl et al., 2002), ROSA26-mTmG, RANK<sup>flox/flox</sup>, and MMTV-PyMT (see methods section). This murine model of mammary gland tumorigenesis develops multifocal mammary gland tumors driven by the expression of the PyMT oncogene. The K8-rtTA, TetOCre and RANK<sup>flox/flox</sup> constructs allow depletion of RANK exons 2-3 in K8+ tissues upon doxycycline administration, resulting in the loss of RANK protein. The ROSA26-mTmG reporter construct facilitates the identification of cells where RANK has been depleted, which turn from expressing Tomato fluorescent protein to being GFP+. Thus, this model allows the depletion of RANK at different timepoints of tumorigenesis. MMTV-PyMT tumors are mainly composed of K8+ tumor cells (Fluck and Schaffhausen, 2009). Doxycycline would then induce RANK depletion exclusively on tumor cells and luminal MG epithelium within the tumor microenvironment. However, it should be noted that K8 is also expressed in other epithelial compartments (intestine, thymus, uterus, kidney, etc) (Zhang et al., 2012).

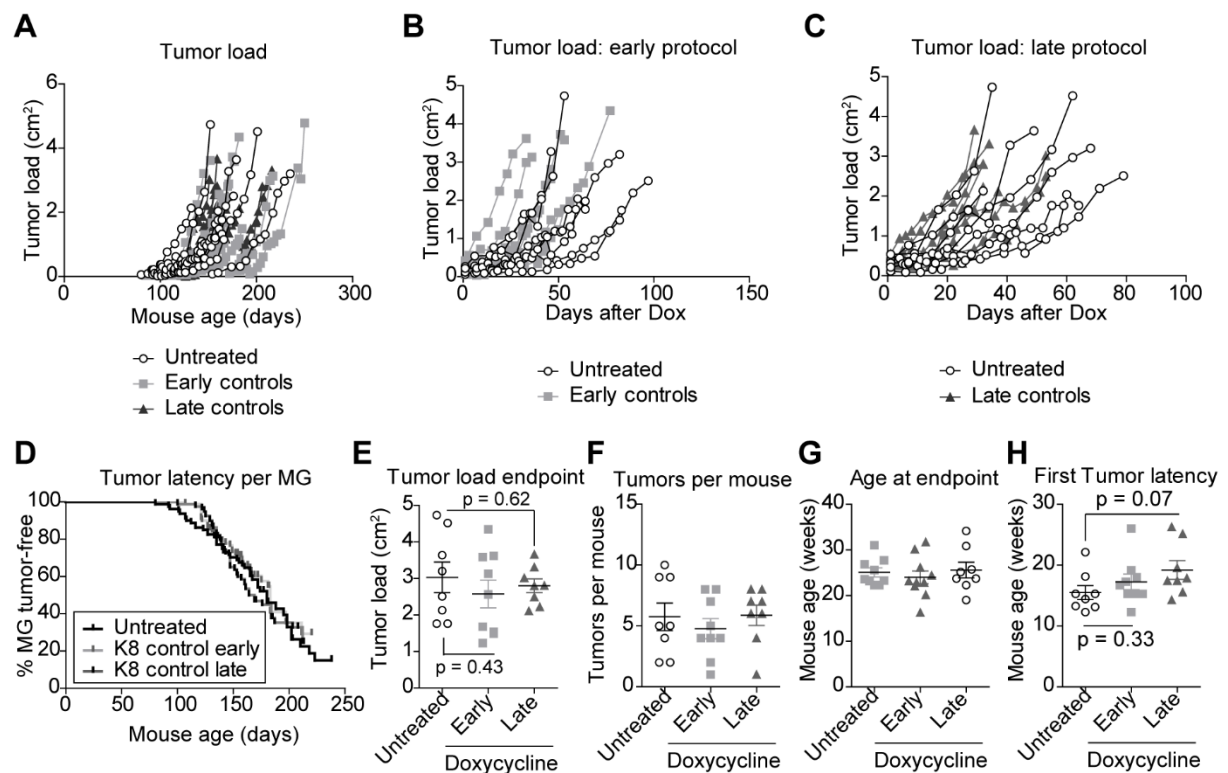


**Figure 2.1 RANK depletion protocols in the RANK<sup>ΔK8</sup> model.** RANK<sup>ΔK8</sup> female mice are monitored twice weekly for tumor growth. For depletion early during tumorigenesis, doxycycline is administered when the first 3x3 mm tumor is detected. For depletion late during tumorigenesis, doxycycline is administered when the first 4x5-5x5 mm tumor is detected. Mice are euthanized once a tumor surpasses a 10x10 mm size.

The tumor-initiating role of RANK in preneoplastic MG has been extensively studied, but in order to explore its potential as therapeutic target, we planned to deplete RANK in the tumor stage. To discern the impact of RANK pathway during early vs later stages of tumorigenesis, two depletion protocols were explored. For “early” RANK depletion, doxycycline was given

when the first tumor was palpated ( $0.09 \text{ cm}^2$ ), for “late” depletion, the first growing tumor was allowed to reach  $0.2\text{-}0.25 \text{ cm}^2$  before inducing RANK depletion (Figure 2.1).

Doxycycline had no effects on tumor growth as shown by comparing untreated mice with control mice under the early or late depletion protocols (Figure 2.2A-C). Tumor latency was also not significantly altered by doxycycline or with the treatment schedule (Figure 2.2D). Other parameters analyzed such as tumor load and number of tumors at endpoint; the age of the mice upon first tumor palpation and at experimental endpoint, remained unchanged by doxycycline (Figure 2.2E-H). Overall, these parameters manifest the variability of tumor onset and growth of this tumor model.



**Figure 2.2. Doxycycline treatment does not alter tumor latency or growth on the  $\text{RANK}^{\text{AK8}}$  tumor model.**

A, Tumor burden per mice represented from mouse birth until experimental endpoint ( $n = 8\text{-}9$ ). B, Tumor burden of the control group under the early depletion protocol. Mice untreated with doxycycline are represented since the first tumor with a  $0.09 \text{ cm}^2$  size was palpated ( $n = 8\text{-}9$ ). C, Tumor burden of the control group under the late depletion protocol. Mice untreated with doxycycline are represented since the first tumor with a  $0.2\text{-}0.25 \text{ cm}^2$  size was palpated ( $n = 8$ ). D, Tumor latency per mammary gland (MG), represented as the percentage of tumor-free MG since mouse birth. Log-rank (Mantel-Cox) Test was performed, and p values between the different groups revealed no significant differences (No dox vs Early control,  $p = 0.42$ ; No dox vs Late control,  $p = 0.76$ ; Early control vs Late control,  $p = 0.27$ ) ( $n = 8\text{-}9$ ). E-H, Representation of the parameters indicated. Each dot represents one mouse ( $n = 8\text{-}9$ ). Mean and SEM are shown, and t-tests were performed to calculate statistical significance.

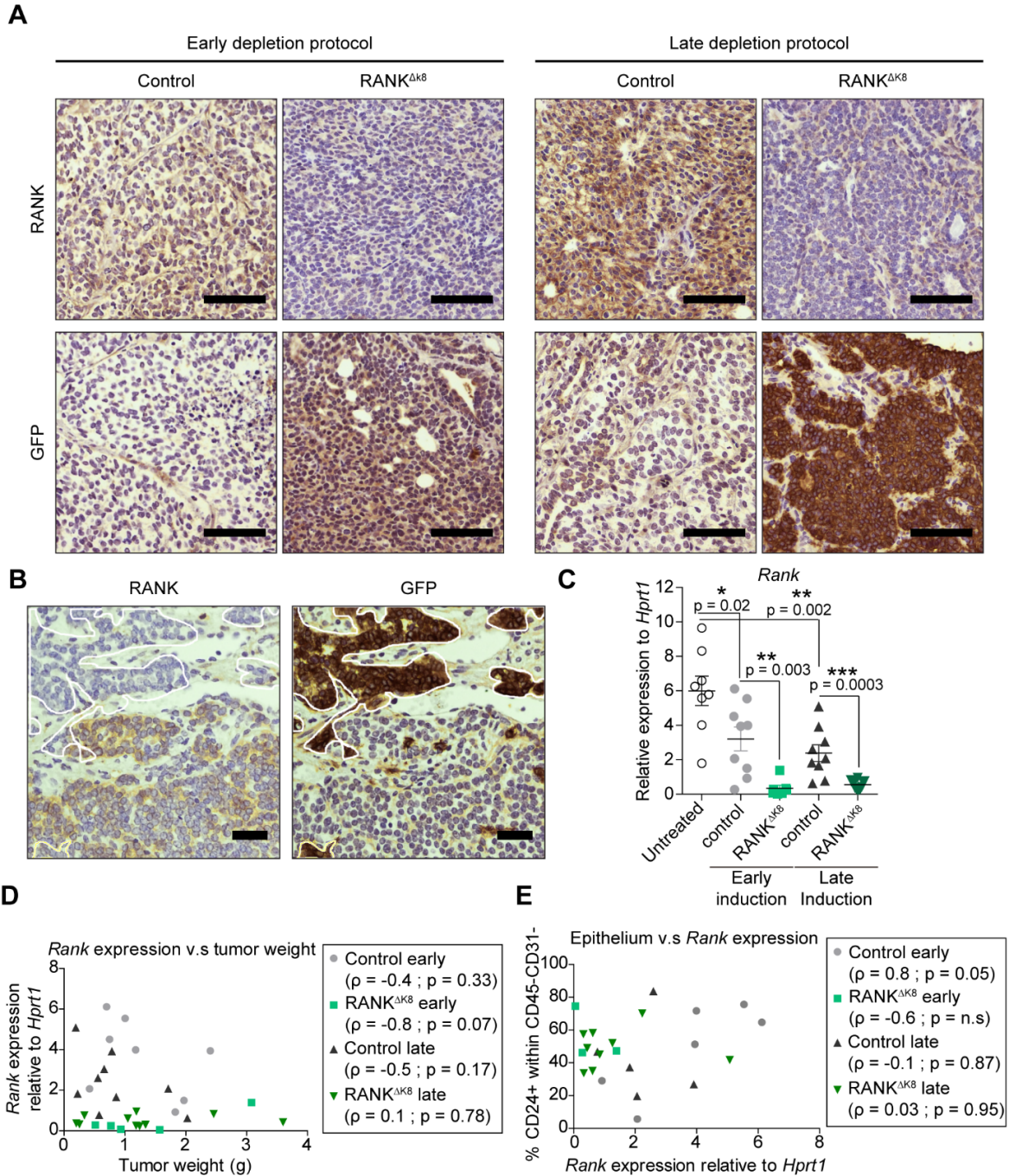


To validate RANK depletion, IHC was performed in tumors from control and RANK<sup>ΔK8</sup> mice (Figure 2.3A). However, some tumors presented areas of RANK+ cells, which remained GFP- (Figure 2.3B). This observation confirms the correlation between loss of RANK and GFP but indicates that a full RANK depletion on tumor cells might not be always achieved in this model.

*Rank* gene expression analysis in tumor pieces showed variability on the mRNA levels in tumors from control mice (Figure 2.3C). As expected, *Rank* expression in dox-treated RANK<sup>ΔK8</sup> tumors was significantly decreased (Figure 2.3C). However, it is worth noting that some *Rank* mRNA is detected in some of these samples. These observations might be influenced by the fact that the samples used consist of a mixed cell population and by the partial depletion within the tumor compartment observed by IHC in some tumor samples (Figure 2.3B). Interestingly, doxycycline treatment alone downregulates *Rank* expression on control tumors (Figure 2.3C).

Modulation of RANK expression has been previously described to occur during MMTV-PyMT tumor development (Yoldi et al., 2016). To corroborate whether this might explain the differences in RANK mRNA levels in the controls, RT-PCR data was plotted against tumor weight, as surrogate of tumor stage. However, no significant correlation between these two parameters was observed (Figure 2.3D). To account for the mixed cell populations present in primary tumor samples, *Rank* mRNA levels were compared to the abundance of CD24+CD45-CD31- tumor cells present in the same tumor piece from which RNA was purified. *Rank* levels in early control tumors positively correlated with the abundance of tumor cells in the sample, but this association was not observed for RANK-depleted tumors or in the late control group (Figure 2.3E).

The different levels of expression observed in tumor controls are thus probably due to the intrinsic variability of the tumors developed by the MMTV-PyMT model. The small amount of *Rank* mRNA detected in RANK<sup>ΔK8</sup> samples can be partially attributed to stromal sources, but IHC data reveals that there is also partial recombination in the tumor epithelia from some samples.



**Figure 2.3 RANK<sup>ΔK8</sup> tumors present variable RANK depletion efficacy.** A, RANK and GFP IHC performed on control and RANK<sup>ΔK8</sup> tumor samples. Representative images from each mouse group are shown. Scale = 50  $\mu$ m. B, Detail of RANK and GFP IHC performed on serial cuts from the same RANK<sup>ΔK8</sup> tumor showing patchy recombination. White areas are drawn to indicate GFP+ sections. Scale = 25  $\mu$ m. C, *Rank* expression relative to *Hprt1* analyzed by RT-PCR on control and RANK<sup>ΔK8</sup> tumor samples treated or not with doxycycline. Mean and SEM is shown, t-test is used to calculate statistical significance. Each dot represents one tumor. D-E, *Rank* expression relative to *Hprt1* plotted against tumor weight at experimental endpoint (D) and against % of CD24+ cells as analyzed by flow cytometry in single-cell suspensions from the same tumor samples (E). Correlation analysis is performed. Pearson  $r$  and  $p$  value are indicated. Each dot represents one tumor.

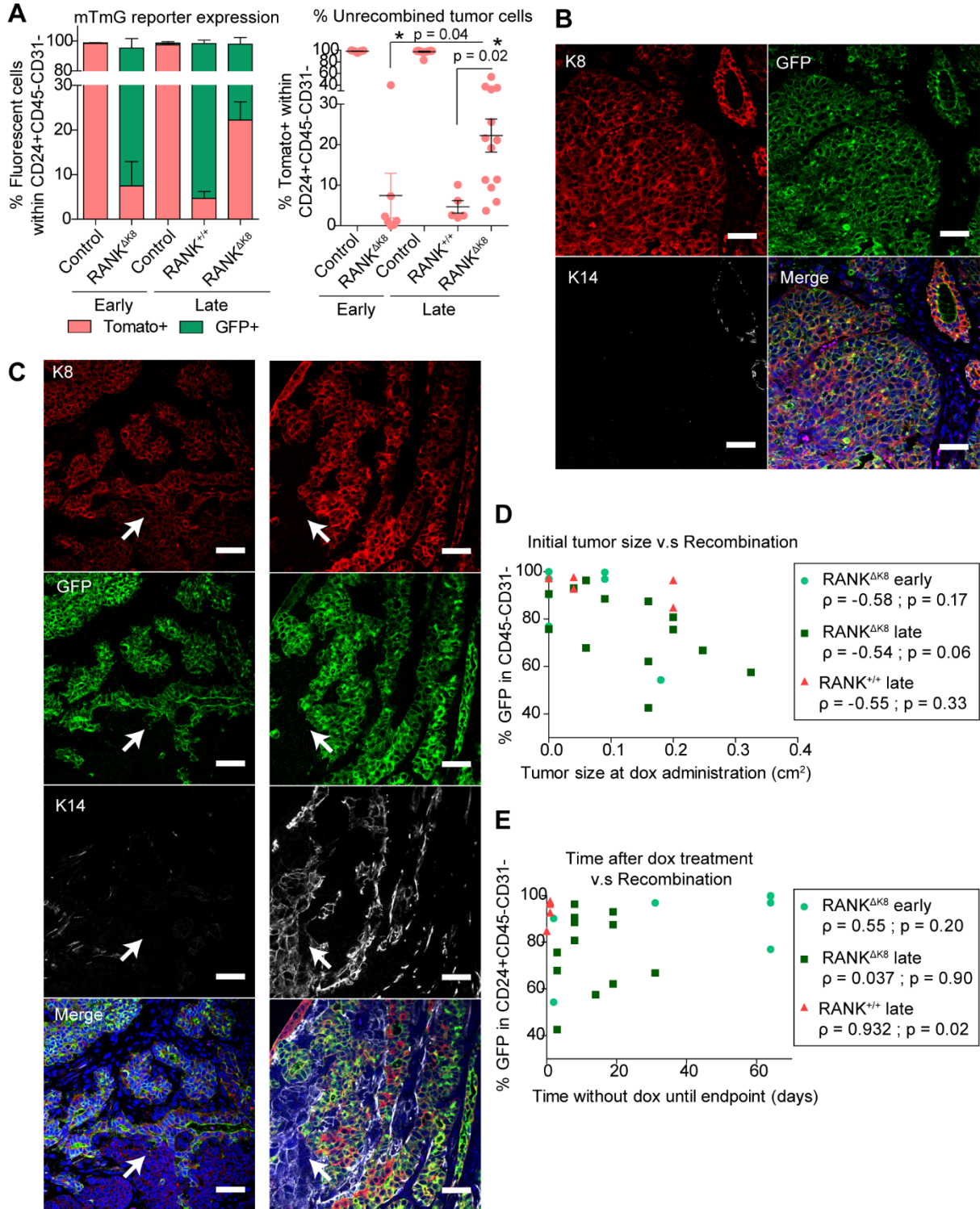
## 2.2 RANK depletion is achieved in luminal-like tumor cell populations but is avoided in undifferentiated or basal-like areas.

Flow cytometry analysis of reporter expression in single-cell suspensions from tumor samples confirmed that GFP expression within the CD24+ tumor epithelium population is not complete in some of the tumors analyzed (Figure 2.4A). The unrecombined population is more abundant in the RANK<sup>ΔK8</sup> tumors under the late depletion protocol compared to those tumors following the early-depletion protocol (Figure 2.4A). In order to verify whether the changes observed for the recombination were due to RANK depletion, K8-rtTA;TetoCre;RANK<sup>+/+</sup>;mTmG<sup>+/-</sup> mice were administered doxycycline under the late depletion protocol. Tumors developed by these mice will present reporter recombination without resulting in RANK depletion. Recombination in these tumors was significantly more efficient than for RANK<sup>ΔK8</sup> tumors (Figure 2.4A), suggesting that the more abundant Tomato+ populations are suggesting the loss of RANK+ positive cells during tumorigenesis. RANK-depleted tumor cells could have survival/proliferation disadvantages which could promote a niche for the growth of remaining RANK+ tumor cell populations.

To further characterize the reason why some tumors presented incomplete recombination, luminal-like and basal-like tumor populations were stained by IF together with GFP. Tumor areas with high K8 expression were mostly positive for GFP, while the stroma remained GFP-negative (Figure 2.4B). Areas presenting lower K8 expression were often not recombined and the less abundant K14+K8- tumor areas were also found to be GFP- (Figure 2.4C). Therefore, the different cell populations within the tumor would determine the effectiveness of RANK depletion in the epithelial compartment.

If these K8-low and K14+ tumor areas were present upon doxycycline administration, the incomplete depletion would be an intrinsic characteristic of the model. By contrast, these populations might become selected due to a growth advantage compared to the populations bearing a RANK depletion. Analyzing tumor samples at endpoint limits the ability to discern between these two possibilities but these analyses could guide the design of future experiments to validate these hypotheses.

In untransformed mammary gland epithelium, recombination with the K8-rtTA; TetoCre system in luminal mammary gland epithelium is 95-100% (data not shown, A. Semiao, *et al.*, publication pending). Therefore, it is possible that the downregulation of the K8 promoter activity in tumor cells compared to normal mammary gland epithelium could explain the



**Figure 2.4 Recombination in  $RANK^{\Delta K8}$  tumors is most efficient in luminal-like tumor subpopulations.** A, Flow cytometry analysis of Tomato and GFP expression on epithelial cells ( $CD24+CD45-CD31-$ ) from digested  $RANK^{\Delta K8}$  tumors and controls ( $n= 7-18$  tumors), or  $K8-rtTA;TetoCre;RANK^{+/+}mTmG^{+/-}$  (reporter recombination without  $RANK$  depletion,  $n= 5$  tumors). On the right, individual tumor values for Tomato+ cells are shown. Mean and SEM are shown, t-test was performed. B, Representative tumor with complete recombination. Scale = 100  $\mu m$ . C, Representative



areas from tumors with incomplete recombination (white arrows). On the left, images showing GFP-negative, K8-low areas. On the right, images showing GFP-negative K14+K8- areas. Scale = 100  $\mu$ m. D-E, Graphs showing the correlation between the % of GFP expression on tumor epithelial cells (CD24+CD45-CD31-) at experimental endpoint and the size of the same tumor when dox was first administered (E) and the days past between dox was administered and experimental endpoint (D) (n= 7-13 tumors). Correlation analysis is performed. Pearson r and p value are indicated.

incomplete recombination. When plotting the percentage of GFP+ epithelial cells within RANK-depleted tumors versus the size of the tumor at the time of doxycycline administration, there is a non-significant trend for an inverse correlation for each condition (Figure 2.4D). When all conditions are pooled together, the trend becomes statistically significant ( $\rho = -0,55$ ,  $p = 0,004$ , \*\*). This might indicate that more advanced tumors have certain characteristics (such as lower K8 expression, due to a process of de-differentiation; or a worse vascularization which lowers the amount of dox reaching tumor cells), which influence the recombination efficiency.

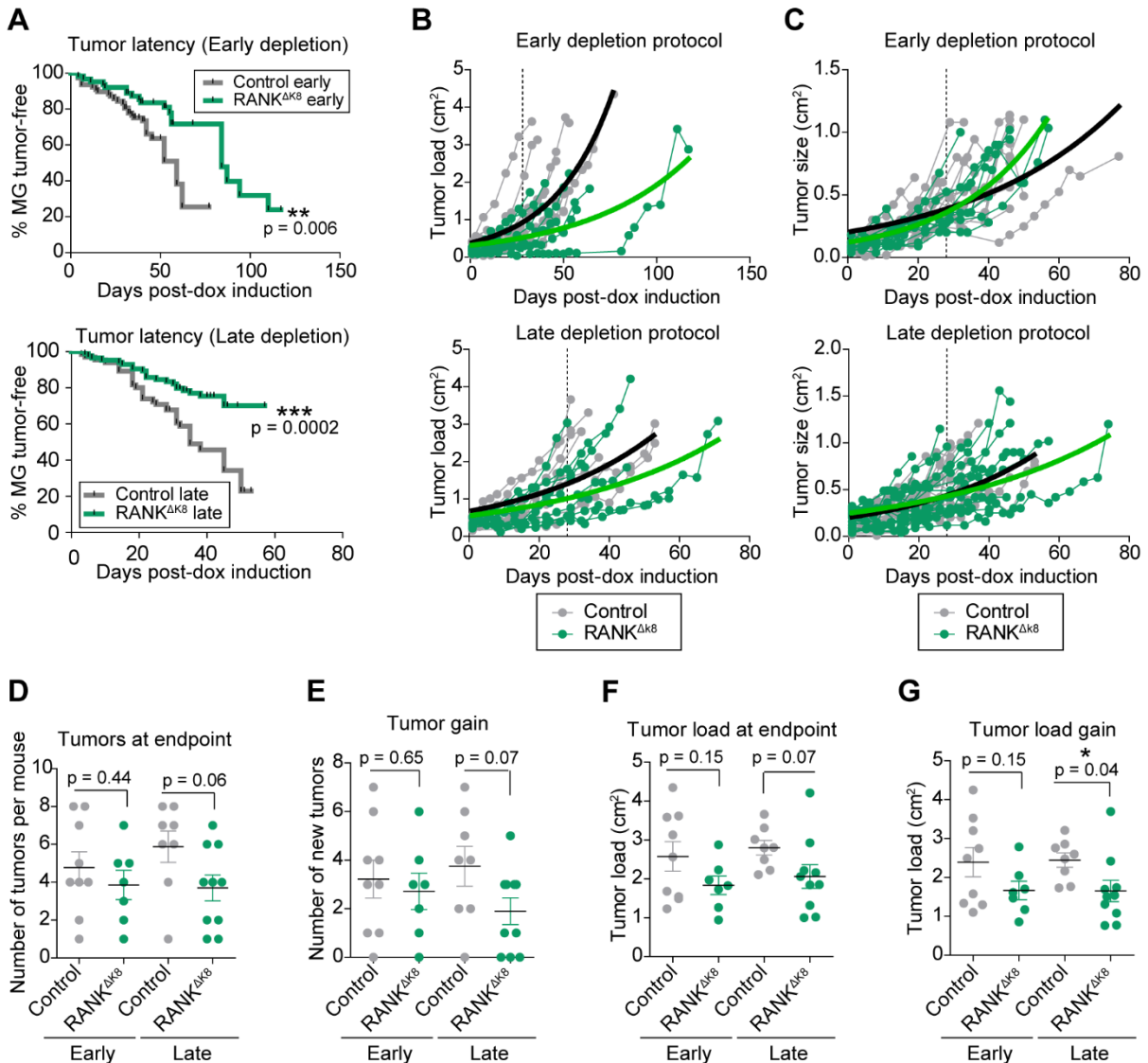
On the other hand, to test whether unrecombined, RANK+Tomato+ cell populations have an evolutionary advantage compared to RANK-GFP+ cell populations, the time from the removal of dox treatment until experimental endpoint was compared to the amount of unrecombined epithelium. No clear correlation between these two parameters was observed. In fact, tumors which were without doxycycline for only 2-3 days already show variable recombination efficiency (Figure 2.4E). However, data from K8-rtTA;TetoCre;RANK<sup>+/+</sup>;mTmG<sup>+/-</sup> controls (Figure 2.4A) suggests that these populations become enriched due to a survival/proliferation disadvantage on RANK- tumor cells, and not due to technical issues of the transgenic model.

Taken together, these data indicate that the K8-PyMT tumors will show partial RANK depletion in undifferentiated or basal-like areas, and that these populations could be enriched after late RANK depletion, due to a stronger evolutionary fitness compared to RANK-negative tumor cells.

### **2.3 RANK depletion during late tumorigenesis affects tumor initiation.**

Despite the incomplete recombination observed in some of the tumors analyzed, RANK depletion influenced certain steps of tumorigenesis (Figure 2.5A-E). When individual mammary glands are considered for tumor initiation, both early and late RANK depletion greatly affected the appearance of new tumors (Figure 2.5A). Tumor growth, considered as total tumor load since the start of doxycycline administration, revealed that RANK depletion

attenuated tumor growth, although the high variability of the model hinders reaching robust conclusions (Figure 2.5B). Since the differences observed in tumor initiation may affect the results of tumor growth when considering all mammary glands, the growth of independent tumors palpable at the beginning of doxycycline administration was also plotted. Both RANK depletion protocols show no effect on tumor growth on those tumors present upon doxycycline administration (Figure 2.5C).

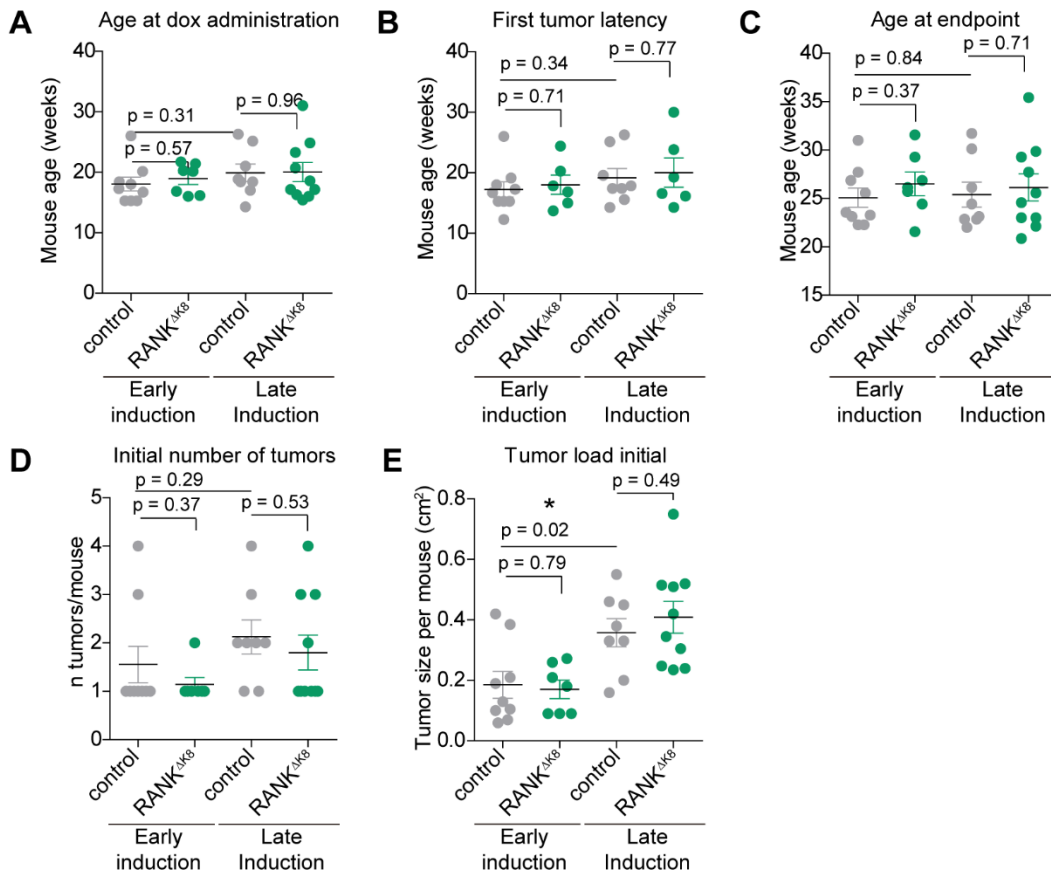


**Figure 2.5 RANK depletion late during tumorigenesis affects tumor initiation.** A, Tumor latency per mammary gland (MG), represented as the percentage of MG without tumors since doxycycline was administered. Log-rank (Mantel-Cox) Test was performed, and p values between the different groups are shown (n = 7-10 mice). B, Tumor growth from RANK<sup>Δk8</sup> tumors represented since start of doxycycline administration. The size from all tumors from each mouse is represented. The dotted line indicates the end of doxycycline treatment. Exponential growth equation is applied and represented for each group (black for controls, green for RANK depletion) (n = 7-10). C, Tumor growth from

individual tumors in RANK<sup>AK8</sup> mice palpable before doxycycline administration. Dotted line indicates the end of doxycycline treatment. Exponential growth equation is applied and represented for each group (black for controls, green for RANK depletion) (n = 7-10 mice). D-G, Representation of the parameters indicated. Each dot represents one mouse (n = 7-10). Mean and SEM are represented, and t-tests were performed to calculate statistical significance.

Additional parameters indicative of alterations of tumorigenesis were also analyzed. Mice where RANK was depleted late during tumorigenesis present a trend to have less tumors at experimental endpoint, while early RANK depletion has no effect on tumor numbers as compared to controls (Figure 2.5D). When correcting for the number of tumors already palpable before RANK depletion, a similar trend is observed for late RANK depletion. Early RANK depletion again shows no effect in appearance of new tumors as compared to controls (Figure 2.5E). Regarding total tumor burden at experimental endpoint, both depletion protocols show a reduction of tumor load, but none reached statistical significance (Figure 2.5F). When correcting for the tumor load measured upon doxycycline administration, mice with late RANK depletion present a significantly lower gain of tumor mass when compared to controls, while early RANK depletion again has no significant effect (Figure 2.5G).

In order to verify that the mouse experimental groups were comparable and to discard protocol bias, several parameters of tumorigenesis were analyzed. There were no significant differences regarding mouse age at doxycycline administration, age at experimental endpoint or the time to first tumor palpation (Figure 2.6A-C). Both tumor load and number of tumors upon dox administration were different between the groups of early and late RANK depletion, as expected, but no differences between each pair of control and depleted groups were observed (Figure 2.6D-E).



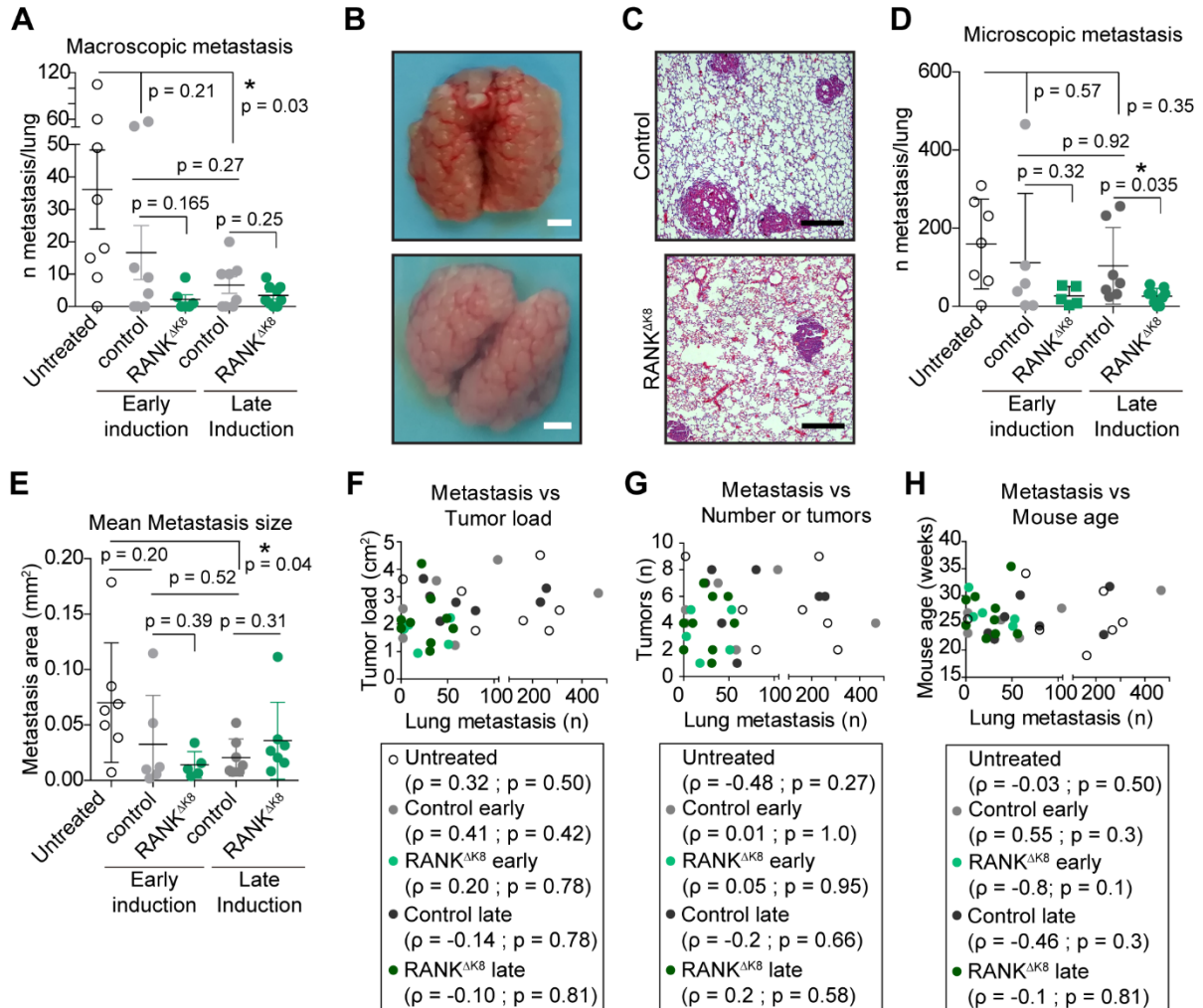
**Figure 2.6 Control and RANK-depleted mouse groups are comparable.** A, Mouse age at the time dox was first administered<sup>#</sup>. B, Mouse age at the palpation of the first tumor with a 0.09 cm<sup>2</sup> size which showed growth at the next measurement. Two RANK-depleted tumors under the late depletion protocol were eliminated because tumors were palpated already when the size was over 0.09 cm<sup>2</sup><sup>#</sup>. C, Mouse age at experimental endpoint (when a tumor surpasses 10x10 mm)<sup>#</sup>. D, Number of tumors when dox was first administered<sup>#</sup>. E, Sum of tumor mass size per mouse when dox was first administered<sup>#</sup>. <sup>#</sup>Each dot represents one mouse (n = 7-10). Mean and SEM are represented, and t-test was performed to calculate statistical significance.

## 2.4 Late RANK depletion reduces the number of microscopic metastatic lung nodules

The MMTV\_PyMT tumor model has been described to develop lung metastasis (Fluck and Schaffhausen, 2009; Guy et al., 1992). At experimental endpoint, macroscopic metastases in the lung were quantified in both control and RANK-depleted mice (Figure 2.7A). Again, the variability of the model is evident in the broad differences in metastatic burden even between control groups. In fact, three tumors (one from an early-treated control, other two from early and late-RANK-depletion groups respectively) were excluded from the analysis because the whole lung was covered with metastatic nodules (Figure 2.7B). No significant differences were observed upon early or late RANK depletion (Figure 2.7A). Doxycycline



treatment alone is shown to have an effect in reducing lung metastasis, reaching only statistical significance when comparing untreated mice with those from the late control group (Figure 2.7A).



**Figure 2.7 Lung metastasis analyses in RANK<sup>ΔK8</sup> models.** A, Macroscopic metastasis quantification in RANK<sup>ΔK8</sup> lungs during mouse necropsy<sup>#</sup>. B, Examples of lungs which were excluded from the analyses due to the extremely high metastatic load. Scale = 0.3 cm. C, Representative images from H&E-stained lung samples from control and RANK<sup>ΔK8</sup> mice treated with doxycycline. Scale = 100 μm. D, Quantification of metastasis in 8 H&E-stained cuts from lungs in A. Cuts were separated each by a 75 μm depth (n = 5-7) <sup>#</sup>. E, Mean of lung metastasis areas quantified in D, analyzed using ImageJ software (n = 5-7) <sup>#</sup>. F-H, Graphs showing the correlation between the metastasis quantified as in D and tumor load (F), number of tumors (G) or mouse age (H) at experimental endpoint. n= 5-7 tumors. Correlation analysis is performed. Spearman rho and p value are indicated. <sup>#</sup> Mean and SEM are shown and t-test was performed to calculate statistical significance.

To quantify both macroscopic and microscopic metastatic nodules, 8 lung histology sections per lung, separated by 75 μm, were prepared and stained with H&E (Figure 2.7C). The

number of metastasis quantified using this technique also reflects the high variability observed between the mice analyzed. Late-RANK depletion results in significantly less metastatic nodules in the lung, while early RANK-depletion does not show the same results (Figure 2.7D). The mean size of these metastases was not significantly altered by RANK depletion under none of the treatment schedules (Figure 2.7E). Again, for both the number and size of the metastasis, doxycycline treatment alone was observed to have an effect in reducing lung metastatic burden (Figure 2.7D-E).

Several parameters which could affect the final number of lung metastasis observed were evaluated for the controls and RANK<sup>ΔK8</sup> mice. However, no association between the number of metastasis and tumor load, number of tumors or mouse age at endpoint was observed (Figure 2.7F-H).

These data indicate that late RANK depletion on K8+ compartments reduced the number of lung metastatic nodules and that this reduction is not a direct effect of the lower primary tumor burden observed in this experimental group.

## **2.5 RANK depletion alters immune infiltration in MMTV\_PyMT primary tumors**

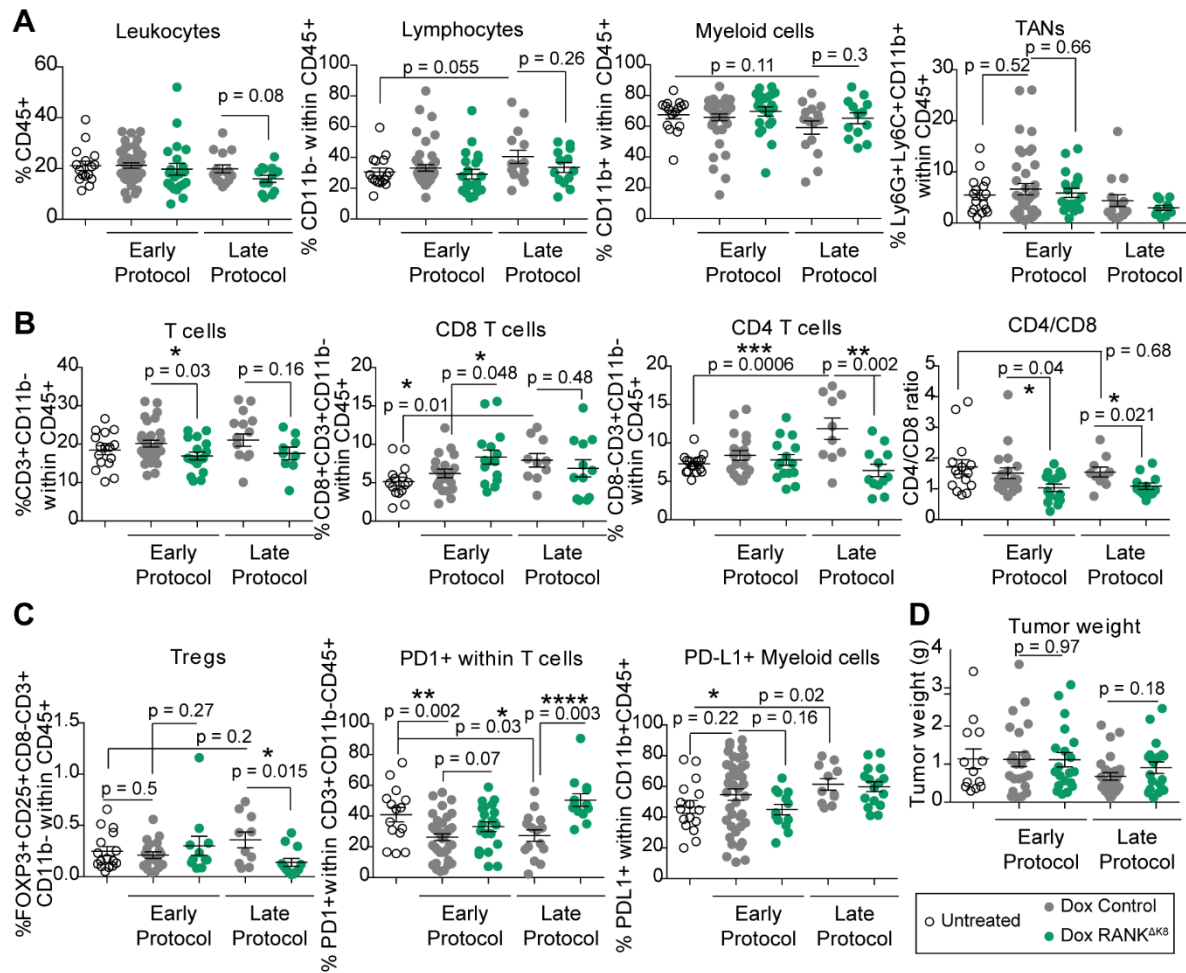
The previous chapter described that RANK KO tumor transplants had several differences in immune infiltration when compared with controls. However, the effects of RANK loss on the immune infiltration of primary mammary gland tumors has not been addressed, due to the defects on several immune populations reported for the full-body RANK KO. The RANK<sup>ΔK8</sup> model thus presents an opportunity to analyze immune infiltration upon RANK loss in a more physiological setting than tumor transplants. This model also opens the possibility to study immune infiltration changes due to RANK loss in luminal tumor cells among different stages of tumorigenesis.

Due to the mTmG reporter, the markers which can be analyzed by flow cytometry are limited, but the main immune populations were analyzed in digested tumors from RANK<sup>ΔK8</sup> mice untreated with dox, and under the early or late depletion protocol (Figure 2.8).

Immune cell abundance did not vary regardless of the mouse group examined. Doxycycline showed a tendency to increase the percentage of lymphocytes on the controls under the late RANK depleted protocol. However, RANK-depletion under either of the depletion

protocols did not alter myeloid/lymphoid cell percentages. TAN infiltration was also not changed by RANK loss in luminal tumor cells (Figure 2.8A).

Regarding T cell infiltration, both depletion protocols resulted in a reduction of T cell abundance in the tumors, reaching only statistical significance for the early-depletion tumor group. CD4/CD8 ratio was reduced upon RANK depletion in tumors under both depletion protocols. This observation results from an increase of CD8 T cells when RANK is depleted early during tumorigenesis, while it is due to a reduction in CD4 T cells when tumors deplete RANK later during tumorigenesis (Figure 2.8B).



**Figure 2.8. RANK depletion alters immune infiltration in RANK<sup>ΔK8</sup> primary tumors.** A-C, Flow cytometry data of the indicated immune cell populations in digested tumors extracted from mice untreated with doxycycline or treated with doxycycline following the early or late depletion protocols (see methods and Figure 2.1).# D, Weight (in grams) of the tumors analyzed by flow cytometry.# Each dot represents one tumor (n = 5-10 mice). Mean and SEM are shown and t-test was performed to calculate statistical significance.

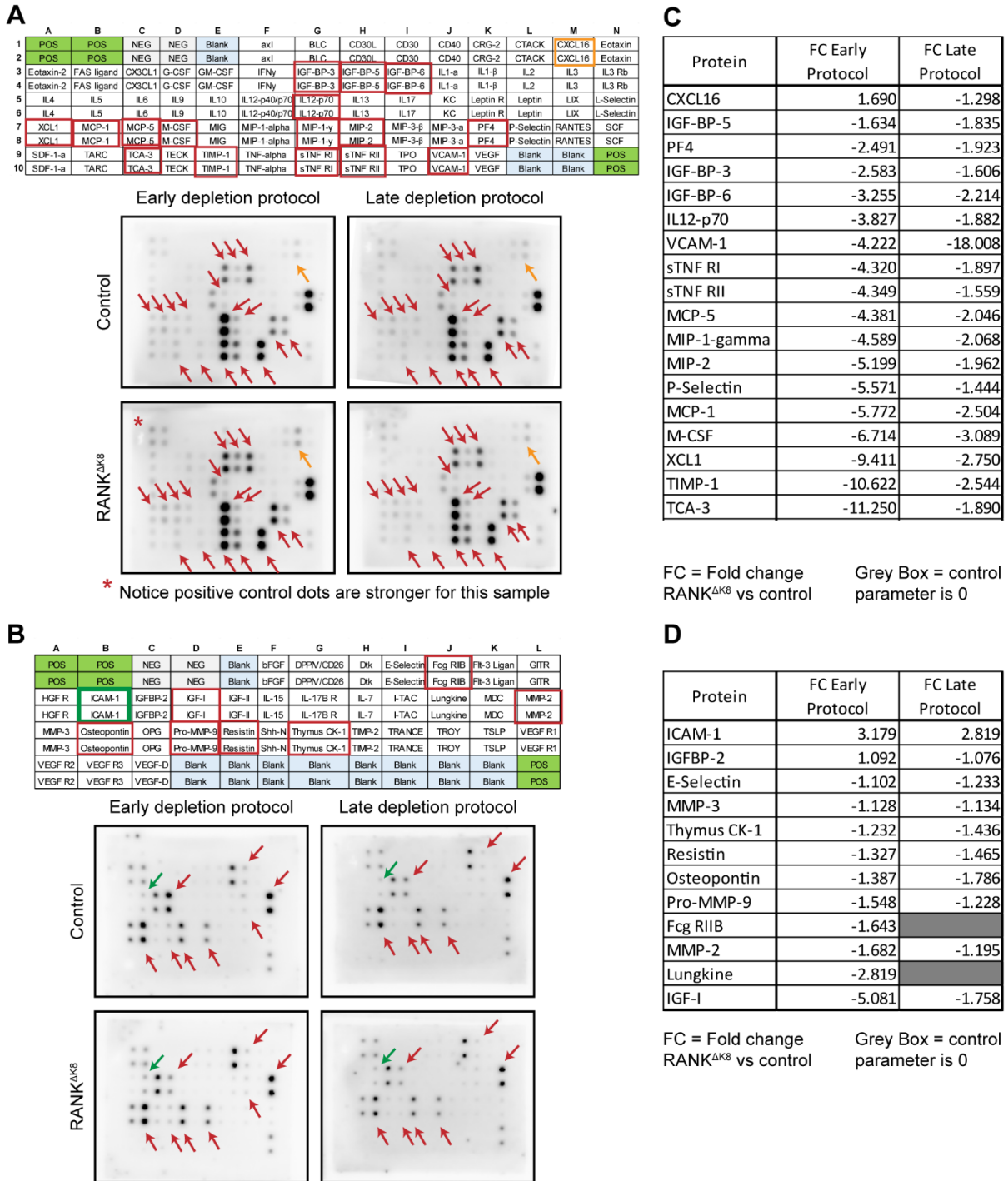
When RANK is depleted late during tumorigenesis, Treg levels are significantly reduced. PD1, a marker of T cell activation (and activation-mediated T cell exhaustion) is less abundant in the control tumors treated with doxycycline compared to untreated controls. Interestingly, RANK depletion induces an increase in the percentage of PD1+ T cells infiltrating the tumors, although only reaching statistical significance under the late-depletion protocol. The ligand of PD1, PD-L1, is barely expressed in tumor cells (data not shown) but is found at variable levels within the myeloid cell compartment. No differences were found upon RANK loss under any of the depletion protocols, but doxycycline administered late during tumorigenesis significantly increased the amount of PD-L1+ myeloid cells infiltrating the tumor (Figure 2.8C). There were no significant differences between the weight of the tumors analyzed by flow cytometry for control and RANK-depleted groups (Figure 2.8D), confirming that the differences observed in immune populations were not due to differences in tumor size.

Thus, doxycycline treatment itself alters immune populations and it can affect differently depending on the administration timing. RANK depletion influences the composition of immune populations, promoting a lower CD4/CD8 ratio and an enrichment of PD1+ T cells.

## **2.6 RANK depletion affects several proteins found in mice serum**

In order to explore putative protein and pathways which could be systemically mediating the effects observed in the RANK<sup>ΔK8</sup> models, a cytokine array of serum proteins was performed (Figure 2.9). Serum from three different mice was pooled together for each condition and two different membranes were blotted for each pooled sample to detect the levels of 96 different cytokines (Figure 2.9A-B). Pixel intensity was calculated for each protein. Background level was subtracted using the values from negative and blank controls from each membrane. Values were normalized using the positive controls present on each membrane and fold change (FC) was calculated between RANK<sup>ΔK8</sup> and control mice under the same depletion protocol (Figure 2.9C-D).

As an extra control, the serum protein levels from RANK<sup>ΔK8</sup> and control mice were compared between the early and late RANK-depletion protocol (Figure 2.10). This analysis would help identify those targets which could be more variable or affected by the stage of tumorigenesis when doxycycline was administered (i.e- treatment-specific changes) and targets which could pinpoint mechanisms involved in the differences between the early and late depletion protocols.



**Figure 2.9. Early and Late RANK depletion alters serum proteins in RANK $\Delta K8$  mice.** A-B, Cytokine array map (above) and corresponding dot-blot membrane images for each of the experimental conditions (below). Serum from three mice from each experimental condition were pooled together and incubated with the indicated membrane: C3 (A) or C4 (B). Membranes show HRP-signal for each of the dots/proteins. Red arrows/boxes indicate protein reduction in RANK $\Delta K8$  serum, green arrows/boxes indicate protein increase and orange arrow/box indicates opposite effects for early and late RANK depletion when compared to controls. C-D, Fold change observed between control and RANK $\Delta K8$  serum protein levels. Values associated to a protein without a visible dot are excluded from the analysis.

Several members of the Insulin-like growth factor (IGF) pathway were found at lower levels in the RANK<sup>ΔK8</sup> serum as compared with controls. In fact, IGF-I is the clearest target when analyzing the dot-blots without pixel quantification (Figure 2.9B). The transporter proteins, IGF-binding proteins (BP)-3, 5 and 6, are also downregulated upon RANK depletion (Figure 2.9C-D). IGFBPs are usually coupled to IGF-I, and both stabilize and regulate IGF-I availability, thus regulating the activation of IGF1-receptor (IGF1R), which classically triggers cell proliferation and the activation of anti-apoptotic pathways (Baxter, 2014; Ding and Wu, 2018), a role also described for IGF pathway in mammary gland epithelium and breast cancer (Laban et al., 2003). Interestingly, higher IGF-I serum levels were found to correlate with increased breast cancer risk (Murphy et al., 2020). IGF-I levels were comparable between the RANK<sup>ΔK8</sup> mice under the early and late depletion protocols but varied for the early and late control serums (Figure 2.10). Interestingly, Resistin, a hormone which inhibits insulin-dependent glucose uptake into adipose cells which has been associated with obesity and diabetes (Hartman et al., 2002; Steppan et al., 2001), was found downregulated in serum after RANK depletion under both protocols as compared to controls (Figure 2.9D). Resistin levels were not affected by the depletion protocol in neither controls or RANK<sup>ΔK8</sup> mice (Figure 2.10).

ICAM-I levels were found to be higher in the serum from RANK<sup>ΔK8</sup> mice (Figure 2.9B, 2.9D). ICAM-I is a target upregulated upon RANK pathway activation (Gómez-Aleza et al., 2020; Palafox et al., 2012a), but previous members of our group identified higher levels of ICAM-I expression upon RANK depletion in PyMT tumors, in accordance with its described expression on differentiated luminal mammary gland epithelia (Yoldi, 2018). ICAM-I levels were found to be affected by the depletion protocol regimen, with early doxycycline treatment inducing higher serum ICAM-I levels than in samples from mice receiving doxycycline treatment later during tumorigenesis (Figure 2.10).

Other solubilized cell-adhesion proteins (VCAM-I and P-Selectin) normally found in endothelial cells exposed to inflammatory signals were downregulated in RANK<sup>ΔK8</sup> sera compared to the corresponding controls. VCAM-I followed a trend similar to ICAM-I in the early vs late doxycycline administration comparison (Figure 2.10), while P-Selectin followed that same trend in the control comparison while showing remarkably higher expression in serum from RANK<sup>ΔK8</sup> mice under the late depletion protocol compared with RANK<sup>ΔK8</sup> mice under the early depletion protocol (Figure 2.10).



CXCL16 quantification identifies it as the single target presenting opposite patterns when comparing fold changes in early vs late RANK depletion (Figure 2.9C). CXCL16 levels increase upon RANK depletion early during tumorigenesis, while showing a mild decrease upon a later RANK depletion (Figure 2.9C). The role of CXCL16 is probably highly context dependent, as it has been described to both trigger recruitment of anti-tumor CD8 T cells after radiation (Matsumura et al., 2008) and also to attract pro-tumorigenic myeloid cells and fibroblast to the tumor microenvironment (Allaoui et al., 2016).

PF4 (CXCL4) and IL12 are both downregulated for in both RANK<sup>ΔK8</sup> sera (Figure 2.9C). PF4 is released during coagulation and has been described to inhibit angiogenesis and attract neutrophils and monocytes (Mueller et al., 2008; Reilly et al., 2001), while IL12 is known to activate the response of members of the adaptive immune system such as T cells and NK cells (Tait Wojno et al., 2019). Osteopontin is also downregulated in both RANK<sup>ΔK8</sup> sera (Figure 2.9D) and is associated with the initiation of type I immunity, by enhancing the secretion of IFN $\gamma$  and IL-12, while reducing IL-10 production (Ashkar et al., 2000).

Monocyte chemoattractant proteins (MCP-1 and MCP-5) are also downregulated in RANK<sup>ΔK8</sup> sera as compared with controls (Figure 2.9C). MCP-1 high serum levels have been described to correlate with a worse prognosis for solid tumors (Wang et al., 2014) and both MCP-1 and MCP-5 have been associated with pro-metastatic mechanisms (Marazioti et al., 2013). Other immune cell chemoattractants, TCA3 (CCL1), Treg chemoattractant (Kuehnemuth et al., 2018; Vila-Caballer et al., 2019), MIP-1 $\gamma$  (CCL9), leukocyte chemoattractant and neutrophil activator (Kitamura et al., 2010; Li et al., 2019) and MIP-2 (CXCL2), leukocyte chemoattractant (De Filippo et al., 2008; Tsutsui et al., 2018; Wuyts et al., 1996), were also found at lower levels in RANK<sup>ΔK8</sup> mice (Figure 2.9C). Less M-CSF, a crucial protein for myeloid cell population development and bone homeostasis, was also found in RANK<sup>ΔK8</sup> mouse serum when compared with the corresponding controls (Figure 2.9C).

XCL1, a lymphocyte-specific chemoattractant important for the establishment of thymic central tolerance (<https://www.uniprot.org/uniprot/P47993>), showed lower levels in RANK<sup>ΔK8</sup> mouse serum compared to controls (Figure 2.9C).

All these proteins (MCP-1, MCP-5, TCA-3, MIP-2, MIP-1 $\gamma$ , M-CSF and XCL1) show the same pattern for the controls comparing the early vs late depletion protocols: higher levels

in control mice receiving early doxycycline treatment and an opposite fold change upon RANK depletion (Figure 2.10).

Protein	FC Controls (Late/early)	FC Depleted (Late/early)	Protein	FC Controls (Late/early)	FC Depleted (Late/early)
IGFBP-2	1.025883932	-1.14589586	CXCL16	1.984017116	-1.105731347
Thymus CK-1	1.018788661	-1.14385352	IGF-BP-5	1.093746662	-1.026640108
Lungkine		-1.69412786	PF4	1.075639327	1.393060247
Osteopontin	-1.04658278	-1.34696197	IGF-BP-6	1.043891449	1.53508235
Resistin	-1.0564061	-1.16572423	IGF-BP-3	-1.204921053	1.335066163
MMP-3	-1.09472403	-1.1001057	VCAM-1	-1.318444105	-5.6238308
E-Selectin	-1.2995761	-1.4548337	IL12-p70	-1.355077042	1.5009179
MMP-2	-1.43184594	-1.01722671	Lymphotactin	-1.38030981	2.479337362
ICAM-1	-1.5861485	-1.78878765	M-CSF	-1.395551571	1.557519101
Pro-MMP-9	-1.77027433	-1.40500664	MIP-1-gamma	-1.455627952	1.524425837
IGF-I	-2.8751082	1.0051856	MCP-1	-1.478274369	1.558992375
			sTNF RI	-1.539830842	1.478494088
			MCP-5	-1.549913112	1.381285561
			P-Selectin	-1.554103009	2.482211868
			MIP-2	-1.584124087	1.672651471
			sTNF RII	-1.604421311	1.738587534
			TIMP-1	-2.227148581	1.874302082
			TCA-3	-2.38586795	2.495074705

FC = Fold change

■ = "early" parameter is 0

■ = > 30% change

**Figure 2.10. Early and Late RANK depletion alters serum proteins in RANK<sup>ΔK8</sup> mice.** Fold change observed between the early and late depletion protocol samples for either control or RANK<sup>ΔK8</sup> sera. Proteins selected for Figure 2.9 are shown.

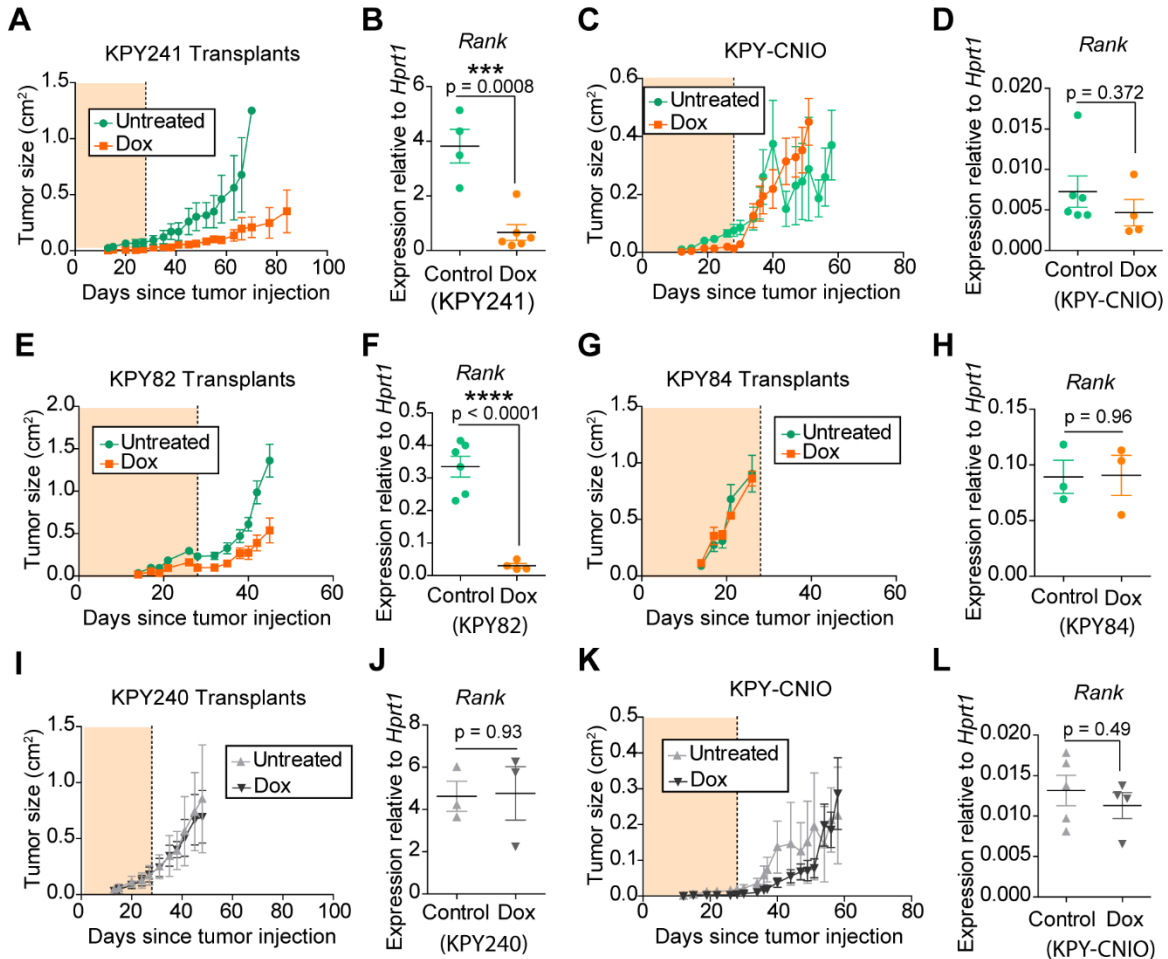
Finally, the metalloproteinase inhibitor TIMP-I was downregulated in RANK<sup>ΔK8</sup> mouse serum (Figure 2.9C), together with pro-MMP-9 and MMP-2 metalloproteinases (Figure 2.9D). All these proteins are higher in the serum from controls treated with doxycycline earlier during tumorigenesis as compared to later during tumorigenesis (Figure 2.10). In the RANK<sup>ΔK8</sup> mouse serum, MMP-2 showed no significant changes depending on doxycycline administration timing, while pro-MMP9 was detected at higher levels in mice under the early depletion protocol and TIMP-I showing lower signal for that same condition as compared to RANK depletion later during tumorigenesis (Figure 2.10).

Overall, these changes suggest that RANK depletion could cause major systemic effects through changes in serum protein levels. Metabolic targets from the insulin and insulin-like growth factor pathway are probably worth exploring. However, further validation of the identified targets would be necessary before reaching any robust conclusions.



## 2.7 RANK depletion delays growth of tumor transplants from certain primary tumors in immunodeficient mice

Since the crosstalk between the RANK pathway with the immune system may introduce additional layers of complexity, and in order to identify whether there is a tumor-intrinsic role of RANK in this model, RANK<sup>ΔK8</sup> tumors without dox treatment were transplanted into immunodeficient mice.



**Figure 2.11 RANK depletion induces delay in latency and growth in some of the tumors implanted in immunodeficient hosts.** A, Tumor growth from a RANK<sup>ΔK8</sup> tumor (KPY241) implanted in NSG<sup>TM</sup> mice<sup>#</sup>. B, RT-PCR data of *Rank* expression in tumor transplants from A<sup>##</sup>. C, Tumor growth from a RANK<sup>ΔK8</sup> tumor (KPY356) implanted in NSG<sup>TM</sup> mice<sup>#</sup>. D, RT-PCR data of *Rank* expression in tumor transplants from C<sup>##</sup>. E, Tumor growth from a RANK<sup>ΔK8</sup> tumor (KPY82) implanted in NodScid mice<sup>#</sup>. F, RT-PCR data of *Rank* expression in tumor transplants from E<sup>##</sup>. G, Tumor growth from a RANK<sup>ΔK8</sup> tumor (KPY84) implanted in NodScid mice<sup>#</sup>. H, RT-PCR data of *Rank* expression in tumor transplants from G<sup>##</sup>. I, Tumor growth from a control tumor (KPY240) implanted in NSG<sup>TM</sup> mice<sup>#</sup>. J, RT-PCR data of *Rank* expression in tumor transplants from I<sup>##</sup>. K, Tumor growth from a control tumor (KPY352) implanted in NSG<sup>TM</sup> mice<sup>#</sup>. L, RT-PCR data of *Rank* expression in tumor transplants from K<sup>##</sup>.

# Orange background indicates the duration of doxycycline administration in the indicated group. Mean and SEM from n = 6 tumors is represented.

## Each dot represents one tumor. Mean, SEM and t-test analyses are represented.

Mice were then randomized to receive dox or normal water, thus being able to compare the same tumor with or without RANK in an environment which would not be altered by immunoediting (Gross et al., 2017). Growth in tumors which are unresponsive to dox-induced RANK depletion was analyzed as control for doxycycline-mediated effects.

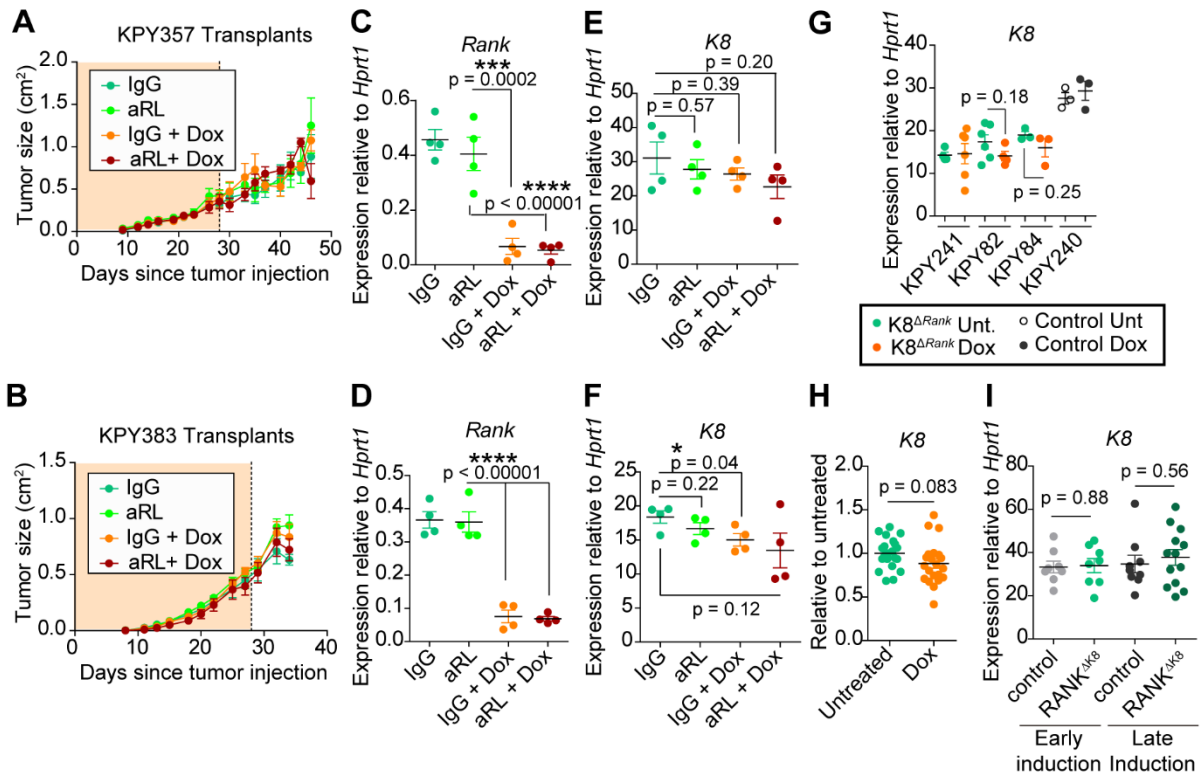
RANK depletion significantly delayed tumor growth in tumors transplanted in NSG (Figure 2.11A-B) and NodScid (Figure 2.11E-F) immunodeficient mice. In some primary tumors tested, doxycycline treatment did not delay tumor growth or latency (Figure 2.11C, 2.11G), but when *Rank* expression was analyzed by RT-qPCR in these tumors, *Rank* levels were identified to be very low in the untreated tumors and not further decreased by doxycycline treatment (Figure 2.11D and Figure 2.11H). In order to verify that doxycycline had no effect on the growth of tumor transplants, control K8-PyMT tumors were injected in NSG mice and their growth was monitored. As expected, dox had no effect on tumor growth and latency from control tumors (Figure 2.11 I and K) and RANK levels were not altered (Figure 2.11J and L). Therefore, these experiments suggest that the delay observed in RANK<sup>ΔK8</sup>tumor growth upon dox treatment would be directly due to loss of RANK in these tumor transplants.

## 2.8 The primary tumor of origin could influence the impact of RANK depletion on tumor transplants in immunodeficient hosts.

New experiments with tumor transplants in immunodeficient hosts, to compare the effects of genetic depletion of RANK with systemic pharmacological RL inhibition with aRL treatments had unexpected results. Two new primary tumors from uninduced RANK<sup>ΔK8</sup> were implanted in NSG mice, which were then treated with doxycycline, aRL, or a combination of both. Neither of these tumor transplants presented any differences in tumor latency or growth upon RANK depletion or RL inhibition (Figure 2.12A-B), despite showing an effective RANK depletion by RT-PCR (Figure 2.12C-D).

K8 expression levels showed a tendency to decrease with doxycycline treatment (Figure 2.12E-F), although only reaching significance for doxycycline-treated tumors from KPY383 (Figure 2.12F). Tumors from tumor transplants shown in 2.11A, 2.11E, 2.11G and 2.11I were also analyzed for changes in *K8* expression and a tendency to lower levels of *K8* were again observed in some of the RANK<sup>ΔK8</sup> tumors treated with doxycycline (Figure 2.12G). When *K8* expression data from all five tumor transplant experiments is represented together relative

to control tumor transplant expression, there is again a non-significant tendency to lower *K8* expression on the doxycycline-treated group (Figure 2.12H). This might imply that the *K8*+/*high* tumor populations might have a survival or growth disadvantage upon RANK depletion. However, this tendency to lower *K8* expression is not observed on the primary tumors extracted from control and RANK<sup>ΔK8</sup> treated with doxycycline under the early or late depletion protocols (Figure 2.12I), maybe due to the more direct comparison of RANK depletion vs. control, which is performed in the same original tumor on the transplant experiments.

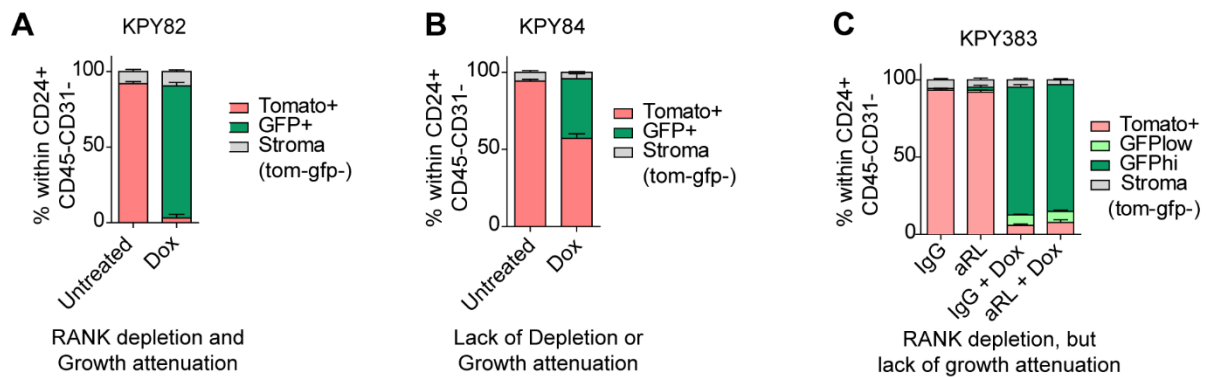


**Figure 2.12 RANK depletion or RL inhibition can show no effect on tumor growth for certain primary tumor transplants.** A-B, Tumor growth from RANK<sup>ΔK8</sup> tumor KPY357 (A) or KPY383 (B) implanted in NSG<sup>TM</sup> mice<sup>#</sup>. C-D, RT-PCR data of *Rank* expression in tumor transplants from A (C) or B (D)<sup>###</sup>. E-F, RT-PCR data of *K8* expression in tumor transplants from A (E) or B (F)<sup>###</sup>. G, RT-PCR data of *K8* expression in tumor transplants from KPY241, KPY82, KPY84 or KPY240 RANK<sup>ΔK8</sup> primary tumors (see Figure 2.11)<sup>###</sup>. H, *K8* expression as shown in panels F and G, relativized to untreated controls for each experiment<sup>###</sup>. I, RT-PCR data of *K8* expression in primary tumors from control or RANK<sup>ΔK8</sup> mice treated with dox under the early or late depletion protocols<sup>###</sup>.

<sup>#</sup> Orange background indicates the duration of doxycycline administration in the indicated group. Mean and SEM from n = 6 tumors is represented. <sup>###</sup> Mean, SEM and t-test analyses are represented.

Additionally, three of the primary tumors transplanted also had an mTmG reporter, allowing for analysis of the recombined populations at endpoint. FACS analysis revealed that a

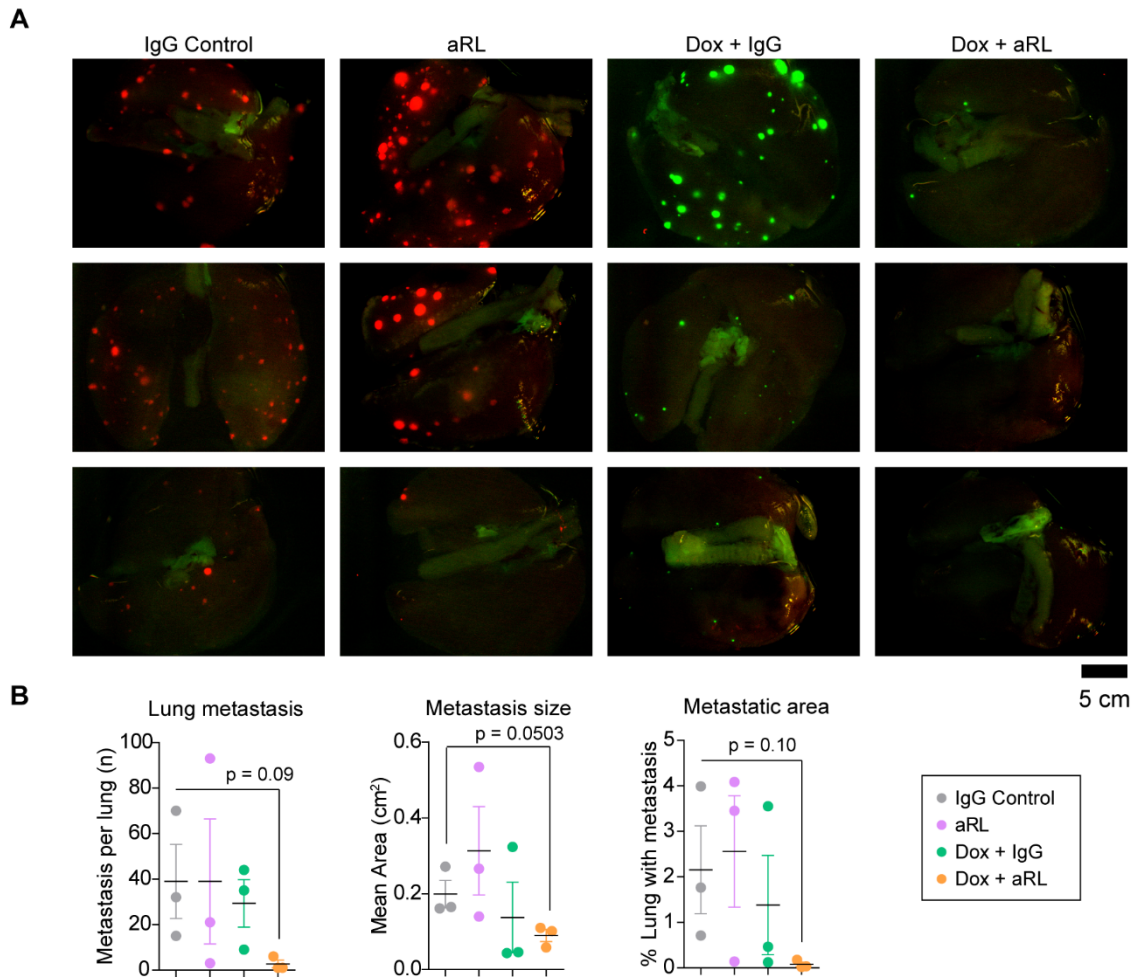
neglectable Tomato+ population remains on tumor transplants exposed to doxycycline from the KPY82 RANK<sup>ΔK8</sup> primary tumor (Figure 2.13A). These tumors had shown reduced tumor growth upon RANK depletion (Figure 2.11E-F). KPY84 tumor transplants, which did not show RANK depletion by RT-PCR (Figure 2.11H) or differences in tumor growth (Figure 2.11G), present an incomplete recombination by FACS, with only 50% of the cells being GFP+ (Figure 2.13B). The rapid growth of these tumor transplants might explain the low efficiency of recombination. However, in KPY383 transplants, where RANK was effectively depleted upon doxycycline treatment (Figure 2.12D) and no differences in tumor growth were observed (Figure 2.12B), less than 8% of tumor cells remained Tomato+ (Figure 2.13C), suggesting that the lack of differences in tumor growth may not be explained by a RANK+, unrecombined tumor population turnover.



**Figure 2.13 Unrecombined populations do not explain the lack of tumor growth differences upon doxycycline treatment in RANK<sup>ΔK8</sup> tumor transplants.** A-C Percentage of fluorescent cells detected by FACS at endpoint on RANK<sup>ΔK8</sup> tumors transplanted in NSG mice and exposed to the specified treatment(s) (n = 4-6 tumors). Mean and SEM are shown. On the bottom, specification of experimental results regarding RANK expression and effects of doxycycline on tumor growth.

## 2.9 Combined RANK depletion and aRL treatment could have a beneficial impact on lung metastasis reduction.

The lungs from NSG<sup>TM</sup> mice implanted with KPY383-derived primary RANK<sup>ΔK8</sup> tumors and treated with doxycycline, aRL or a combination of both were analyzed under the fluorescent magnifier. The expression of mTmG reporter in the transplanted tumor cells allows for detection of lung metastasis. All lung metastasis from doxycycline-treated mice were GFP+ (Figure 2.14A), according to the almost complete recombination on the primary tumor (Figure 2.13C).



**Figure 2.14. Lung metastasis from mTmG+ RANK<sup>ΔK8</sup> tumor transplants quantified under the fluorescent magnifier.** A, Images from merged fluorescent channels detecting tomato+ and GFP+ cells in whole lungs from NSG<sup>TM</sup> mice implanted with KPY383-derived primary RANK<sup>ΔK8</sup> tumors. B, Quantification of number, size and area of metastatic nodules in the lungs shown in A. Mean and SEM are shown and t-test p values calculated for statistical significance.

These tumor transplant models also present high biological variability regarding metastasis number and size, despite originating from the same primary tumor (Figure 2.14A-B). However, there is a tendency to reduce metastasis size upon RANK deletion, as well as a reduction in metastatic nodule abundance when RANK depletion is combined with RL pharmacological inhibition (Figure 2.14B). The observation with the combined genetic deletion and RL inhibition is specially surprising given the lack of metastatic burden reduction when systemically inhibiting RANK pathway with aRL treatment (Figure 2.1B).

These observations will be validated on the available material from other experiments, as well as in new tumor transplant experiments with the model. An additional control where sucrose is administered to control mice will be included in these future experiments, since

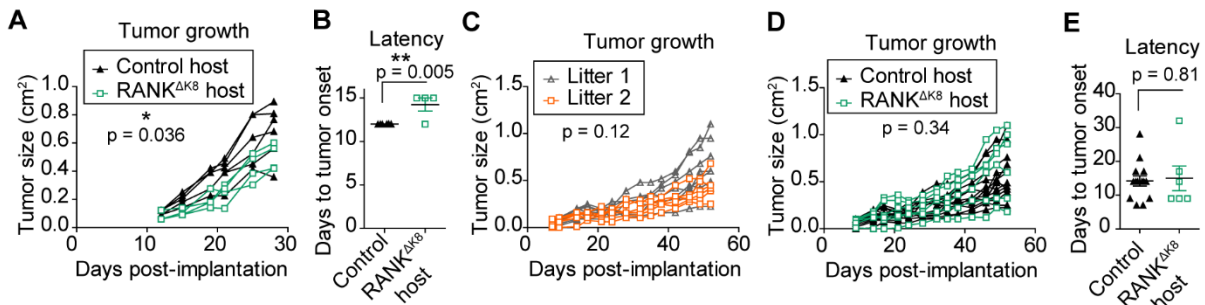


doxycycline needs to be diluted in sucrose water to compensate its sour taste and the proper sucrose-drinking controls were not included in these transplant experiments.

## 2.10 Exploring RANK depletion in K8+ organs from host mice in tumor transplant models.

Depletion of RANK in K8+ cells led to an overall delay in tumor initiation (Figure 2.5A), as well to a reduction in lung metastasis when the depletion is initiated later during tumorigenesis (Figure 2.7D). This depletion also resulted in differences in immune infiltrates, such as a reduction in the CD4/CD8 ratio (Figure 2.8B).

These observations might be directly due to tumor-intrinsic effects of RANK depletion, as indicated for some of the RANK<sup>ΔK8</sup> tumors transplanted in immunodeficient hosts. However, in order to discard potential effects of RANK depletion in other organs, such as the thymus, PyMT tumors were transplanted in K8-rtTA;TetoCre;RANK<sup>fllox/fllox</sup> hosts which were backcrossed for at least 8 generations into the C57/Bl6 background (from now on, RANK<sup>ΔK8</sup>;C57/Bl6). After tumor transplantation, mice received doxycycline in drinking water for 4 weeks. Littermates without one of the transgenes necessary for the depletion were also treated with doxycycline and were used as controls.

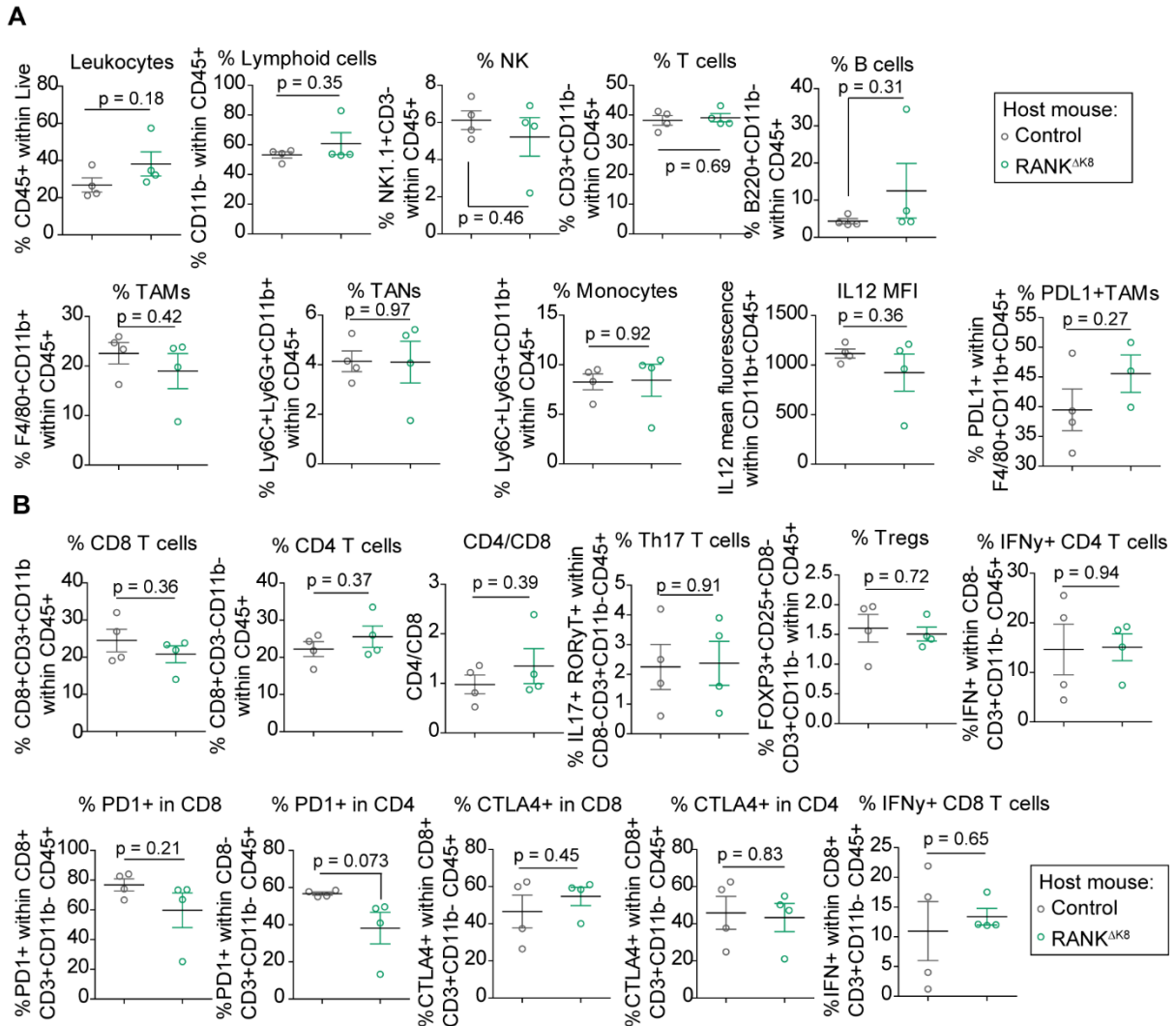


**Figure 2.15 RANK depletion on tumor transplant hosts with the RANK<sup>ΔK8</sup> model.** A, Tumor growth from an MMTV-PyMT tumor implanted in RANK<sup>ΔK8</sup>;C57/Bl6 or control littermates which thereafter received doxycycline in drinking water for 4 weeks (n = 2-3 mice, n = 4-6 tumors)<sup>#</sup>. B, Latency to tumor onset in tumors from A<sup>##</sup>. C, Tumor growth from an MMTV-PyMT tumor implanted in control mice from two different litters from the RANK<sup>ΔK8</sup>;C57/Bl6 colony. All mice received doxycycline in drinking water for 4 weeks (n = 3-4 mice, n = 6-8 tumors)<sup>#</sup>. D, Tumor growth from an MMTV-PyMT tumor implanted in RANK<sup>ΔK8</sup>;C57/Bl6 or control littermates which thereafter received doxycycline in drinking water for 4 weeks (n = 3-7 mice, n = 6-14 tumors)<sup>#</sup>. E, Latency to tumor onset in tumors from D<sup>##</sup>.

<sup>#</sup> ANOVA test was performed to assess statistical significance. <sup>##</sup> Mean and SEM are shown, t-test p-value calculated to assess statistical significance.

Three different litters of mice were implanted with a MMTV-PyMT tumor and tumor growth was monitored until the first tumor reached a size of 10 mm in any direction. One of the

tumors transplanted presented a significantly reduced tumor latency and growth when implanted in RANK<sup>ΔK8</sup>;C57/BI6 hosts compared to controls (Figure 2.15A-B). However, another primary tumor implanted into two litters of RANK<sup>ΔK8</sup>;C57/BI6 mice and their littermate controls did not show the same results. The tumors grew similarly on the controls of both litters (Figure 2.15C), so the growth results from both litters are pooled together. No differences in tumor growth or tumor latency were observed for this primary tumor upon RANK depletion in K8+ organs from the host mice (Figure 2.15D-E).



**Figure 2.16. RANK depletion in K8+ organs from host mice does not affect immune infiltration in RANK+ tumor transplants.** A-B, Flow cytometry data of the indicated immune cell populations in transplanted tumors implanted in either RANK<sup>ΔK8</sup>; C57/BI6 and control littermate mice treated with doxycycline for 4 weeks, starting 24 hours after tumor implantation. Each dot represents one tumor (n = 2 mice, 4 tumors). Mean and SEM are shown, and t-test was performed to calculate statistical significance.

Analysis of the tumor immune infiltrates revealed no major changes due to RANK depletion in K8+ organs from the host mice (Figure 2.16A-B). The only immune marker which could be highlighted is the percentage of PD1+ CD4 T cells, which is decreased in tumors from RANK<sup>ΔK8</sup>;C57/Bl6 mice as compared to controls (Figure 2.16B). PD1+ CD8 T cells also show a trend but could be mainly due to one tumor sample which also corresponds to other outliers seen through the other immune populations (Figure 2.16B). Higher n should confirm these observations in the future. This result contrasts with the more abundant PD1+ T cells found upon RANK depletion in the primary tumor setting (Figure 2.8C), which could be due to a tumor-RANK depletion or to the differences between the immune response towards a primary tumor versus a tumor transplant.

Overall, it is unlikely that RANK depletion on K8+ populations other than tumor cells has a major effect on tumor growth, at least in the transplant tumor system.



## CHAPTER 3

# Rank Pathway in Intestinal Epithelium



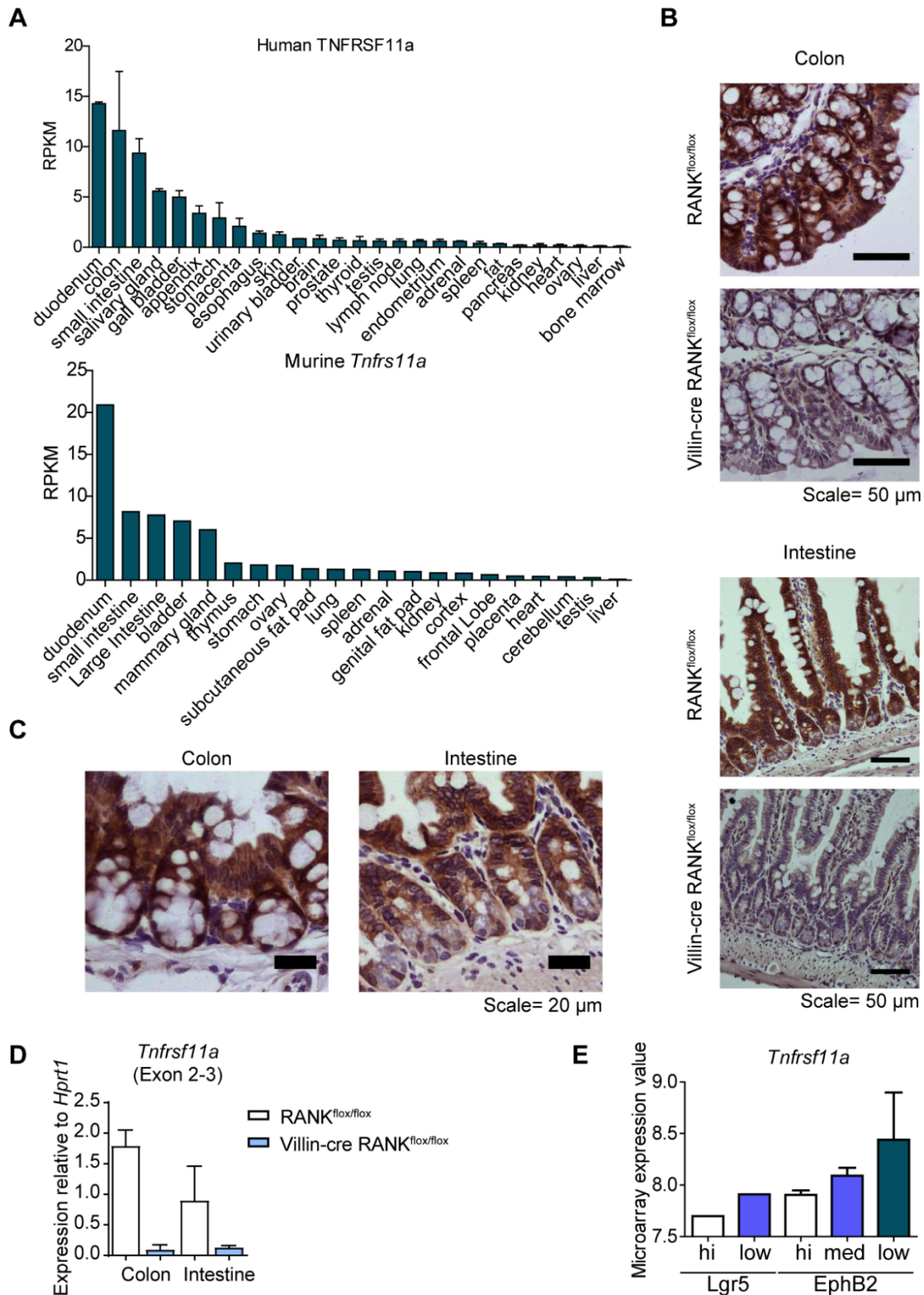
### 3.1 RANK expression is higher on differentiated intestinal epithelium

The intestine and colon show the highest RANK expression when compared to other organs both in humans and in mice, as shown by gene expression data from BioProjects PRJEB4337 and PRJNA66167, publicly available at the NCBI webpage (Figure 3.1A). As stated in the introduction, the only described role for RANK pathway in the intestinal epithelium is to commit epithelial cells into the M cell lineage (Kimura et al., 2015a, 2020; Knoop et al., 2009). However, the high expression of the protein in this organ, together with its described role in maintaining the balance between proliferation and differentiation in the mammary gland epithelium (Beleut et al., 2010; Fata et al., 2000a; Gonzalez-Suarez et al., 2007; Joshi et al., 2010, 2015b; Srivastava et al., 2003), raise the question of whether RANK could also be also involved in intestinal epithelium functions other than M cell differentiation.

With this aim, mice bearing RANK deletion specifically in intestinal and colonic epithelium were generated: Villin-Cre; Rank<sup>flox/flox</sup> (see methods). RANK depletion was confirmed by both IHC and qPCR in intestinal and colon samples from adult mice (Figure 3.1B, D). Interestingly, a previously undescribed gradient of RANK protein expression was observed in intestinal epithelium, with lower levels found in the bottom of the crypts (Figure 3.1C). This gradient was less dramatic in colon samples (Figure 3.1C). However, when using publicly available gene expression data from sorted colon cell populations based on their expression of stem cell markers (Lgr5 and EphB)(Merlos-Suárez et al., 2011), RANK expression gradient is again observed (Figure 3.1E). Thus, RANK expression levels correlate with an increasing differentiation status of intestinal and colon epithelial cells.

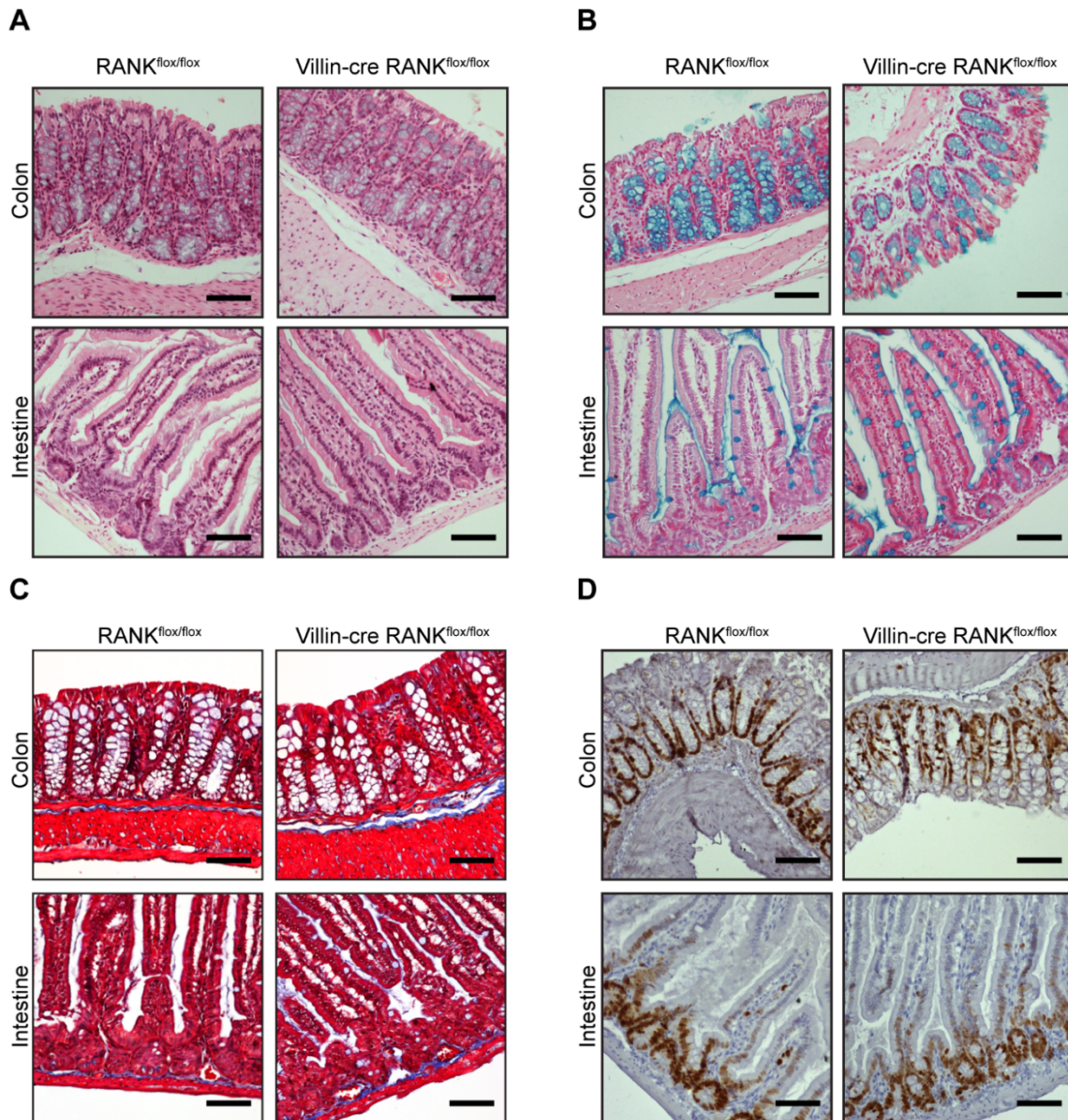
### 3.2 RANK loss has no evident effect on intestinal epithelium homeostasis *in vivo* and *in vitro*.

Observation of intestine and colon histological cuts stained with H&E did not reveal any major differences between Rank<sup>flox/flox</sup> (control) and Villin-Cre; Rank<sup>flox/flox</sup> mice (Figure 3.2A). Detection of Goblet cells using Alcian blue stain or of collagen fibers using Masson's trichrome stain did not show any remarkable changes in RANK-depleted samples (Figure 3.2B-C). Proliferation (as assessed by ki67 staining) was also comparable between Villin-Cre; Rank<sup>flox/flox</sup> and control littermates in terms of qualitative assessment of proliferative cell localization along the crypt-villi axis (Figure 3.2D).



**Figure 3.1. Differentiated intestinal epithelial cells express high RANK levels.** A, RANK mRNA levels in human and murine organs. Data obtained from NCBI BioProjects PRJEB4337 and PRJNA66167 respectively. B, Representative RANK IHC images of colon and intestine from Villin-Cre;  $Rank^{flox/flox}$  and control littermates at 20x magnification. C, Details from RANK IHC on control  $Rank^{flox/flox}$  and control littermates at 20x magnification. D, Quantification of RANK mRNA levels in colon and intestine. E, Quantification of RANK mRNA levels in Lgr5 and EphB2 genotypes.

mice. D, RT-PCR from colon and intestinal samples from Villin-Cre; Rank<sup>flox/flox</sup> and control littermates (n=2). E, Rank expression in colon epithelial cells sorted based on their expression levels of stem cell markers (Lgr5 or EphB2). Data obtained from GSE27605, published in Merlos-Suárez A. *et al*, Cell Stem Cell 2011(Merlos-Suárez et al., 2011).



**Figure 3.2. Basic characterization of Villin-Cre; Rank<sup>flox/flox</sup> intestinal and colon epithelium.** A, Hematoxylin-Eosin staining of Villin-Cre; Rank<sup>flox/flox</sup> and control littermates. Representative images from n=3 mice. Scale = 50 μm. B, Alcian-blue stained intestine (n=2) and colon (n=1), Goblet cells present blue color. Scale = 50 μm. C, Masson's trichrome stained intestine (n=2) and colon (n=1). Collagen fibers from the stroma are marked in blue. Scale = 50 μm. D, ki67 IHC, marking proliferative cells. Representative images from n=3 mice. Scale = 50 μm.

When plated *in vitro*, intestinal organoids from Villin-Cre; Rank<sup>flox/flox</sup> mice developed resembling those from controls, starting to present branching from day 4-5 (Figure 3.3).



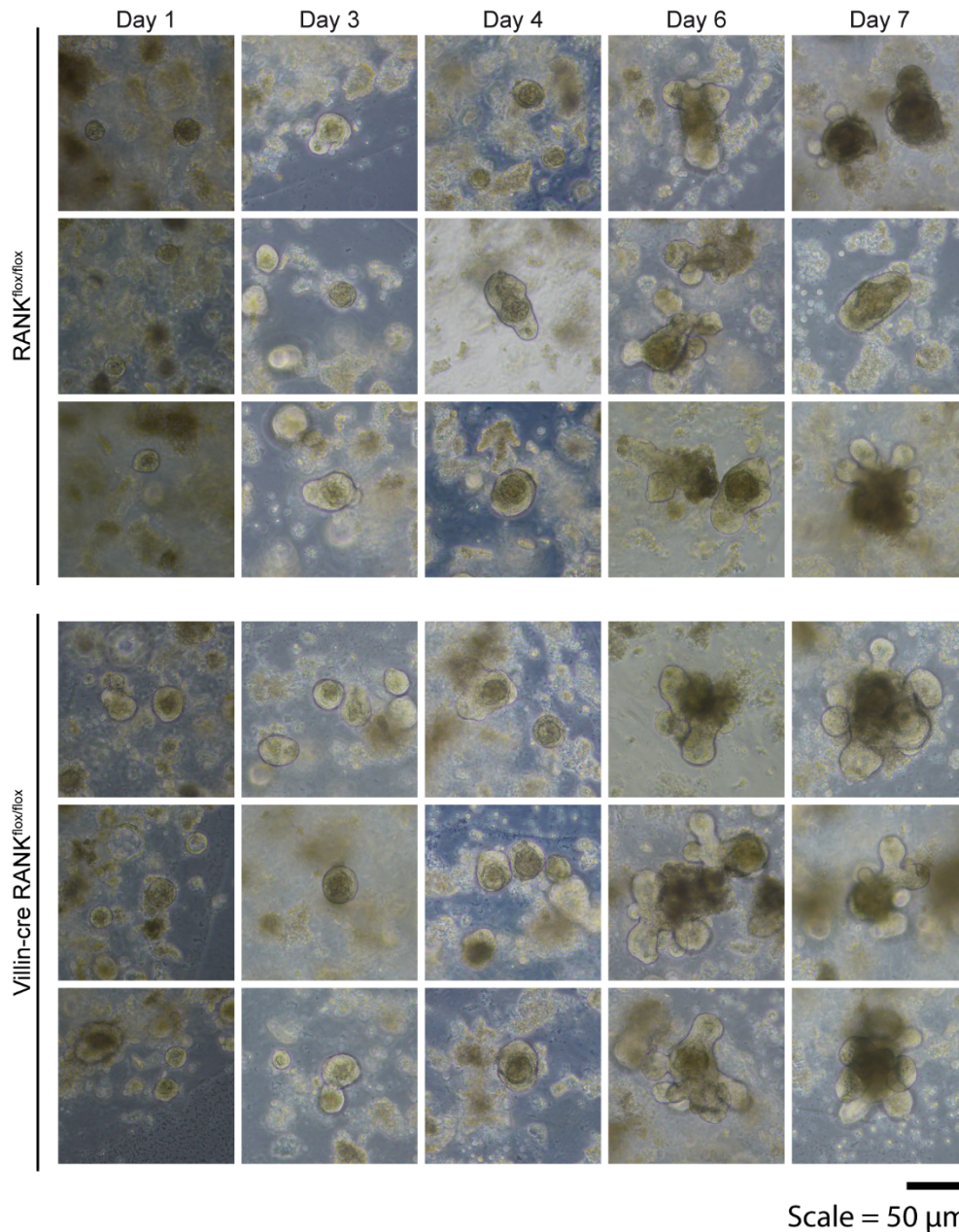
These organoids are viable and keep growing through at least 3 passages in culture, maintaining their proliferation and branching, indicative of their differentiation ability (data not shown).

### 3.3 RANKL induces M cell differentiation *in vitro* but high doses disrupt intestinal organoid maintenance.

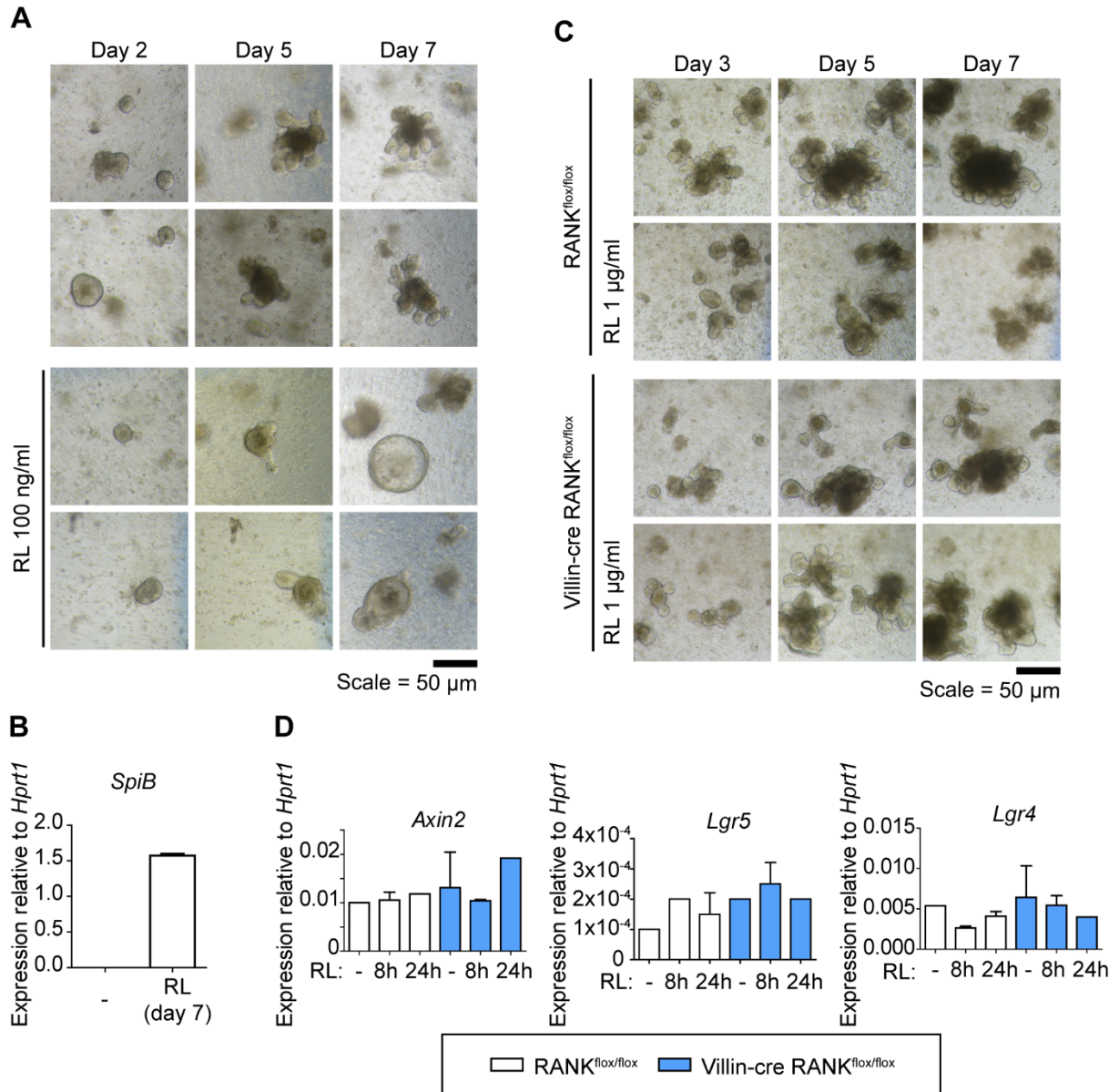
Adding RANKL to intestinal organoids *in vitro* at a 100 ng/ml concentration resulted in a reduced branching observed in the organoids (day 5-7) and the upregulation of the M cell marker SpiB (day 7); with the morphology mimicking luminal differentiation in the mammary epithelia. (Figure 3.4A-B), as previously described (de Lau et al., 2012). Strikingly, higher doses of RANKL (1000 ng/ml), used in other experimental setups (Yoldi et al., 2016), resulted in the disassembly of organoids by day 7 of culture, which is often a sign of cell death. Villin-Cre; Rank<sup>flox/flox</sup> organoids remained unaffected by these high doses of RANKL (Figure 3.4C).

At day 5 of culture in presence of high doses of RL, organoid morphology corresponded to an M cell differentiation phenotype, without showing signs of disassembly (Figure 3.4C). To verify whether RANK pathway activation was directly affecting Wnt pathway and thus organoid survival, RANKL at high doses was added and samples collected at different timepoints to analyze the expression of target genes by qPCR. Neither *Axin2*, *Lgr5* or *Lgr4* expression was affected by RANK signaling (Figure 3.4D). RANKL and *Rspo1* mRNA levels were also analyzed but intestinal epithelium cells express neither (data not shown).

Additionally, *Rank* expression was not altered by Wnt3a treatment, although it upregulated *Trail* and *Opg* expression (Figure 3.5A). Interestingly, RANKL treatment also increases the expression of *Rank* (Figure 3.5B), suggesting the possibility of feedback loops occurring to modulate RANKL response. *Trail* and *Opg* also seem to get upregulated by RANKL but their low expression levels and variability might reflect that only a minor subpopulation of cells might be upregulating them after RANKL treatment (Figure 3.5B). The upregulation must be specific of RANK signaling and not due to inter-well variability, since Villin-Cre; Rank<sup>flox/flox</sup> organoids remain unresponsive (Figure 3.5B). Indeed, other known Rank/NFκB targets (*Icam1* and *Nos2*) were also confirmed to be upregulated by RANKL treatment in control intestinal organoids, while their expression was not altered in Villin-Cre-Rank<sup>flox/flox</sup> organoids (Figure 3.5C).

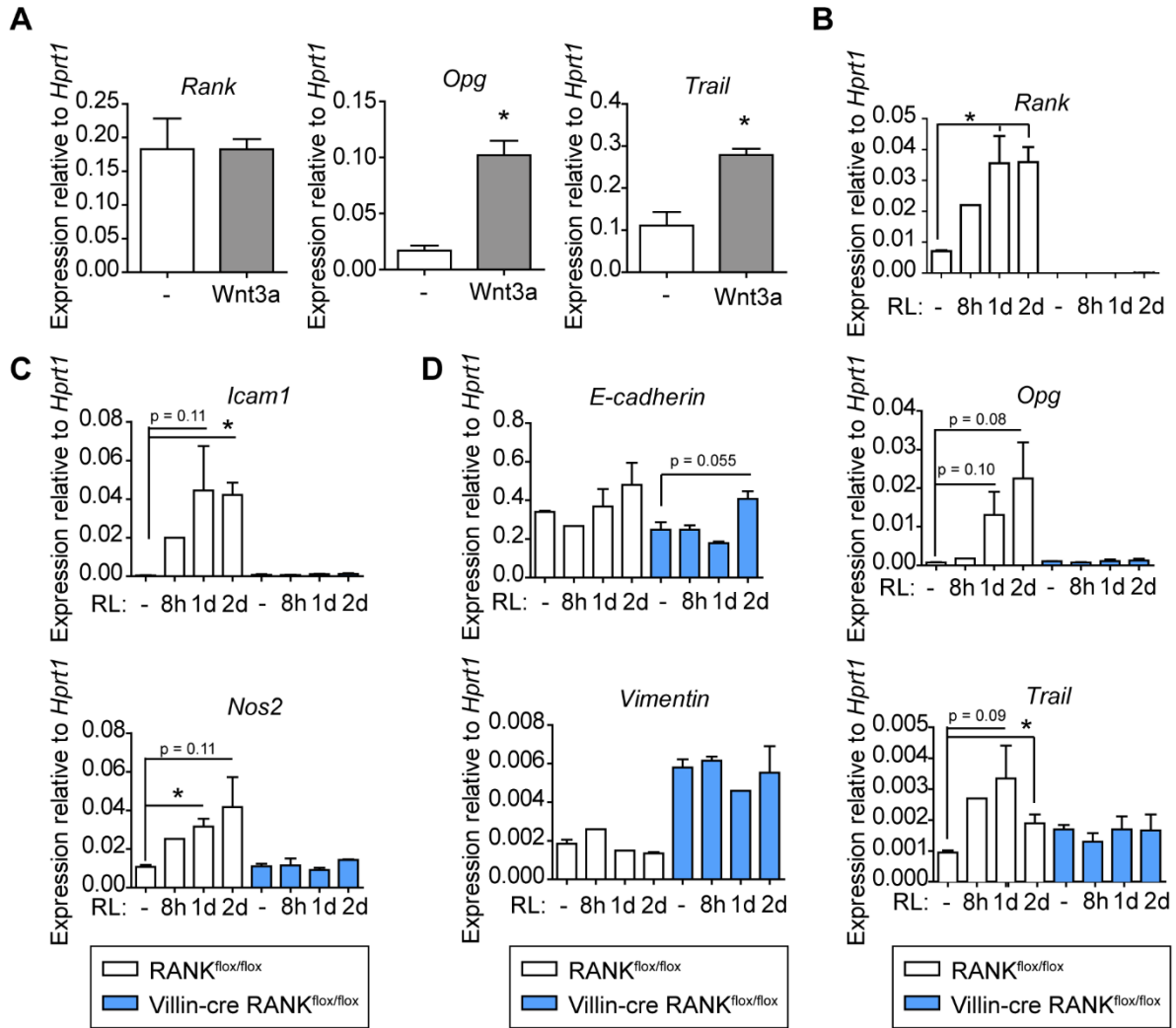


**Figure 3.3. Villin-Cre; Rank<sup>flox/flox</sup> intestinal organoids present similar morphology and growth as those from Rank<sup>flox/flox</sup> controls.** Intestinal organoids were freshly isolated from proximal intestines from Villin-Cre; Rank<sup>flox/flox</sup> and control littermates. Medium was refreshed every 2-3 days and pictures were taken at random. Panels show representative images from n=6 mice. Scale= 50  $\mu$ m.



**Figure 3.4. Sustained RANKL at high concentration results in organoid disassembly.** A, Pictures from intestinal organoids from control Rank<sup>flox/flox</sup> mice cultured with or without RANKL (100 ng/ml) for one week (n=2). B, RT-PCR from organoids in A showing *SpiB* expression levels at day 7 of culture. C, Pictures from intestinal organoids from control and Villin-Cre Rank<sup>flox/flox</sup> mice treated (or not) with RANKL (1  $\mu$ g/ml). The same position within the well is shown in different days. Pictures representative from n=4 mice, two different experiments. D, RT-PCR from organoids from control and Villin-Cre Rank<sup>flox/flox</sup> mice treated for 8 or 24 hours with RL(1  $\mu$ g/ml). Representative data from two experiments performed with n=2 mice each.





**Figure 3.5. Effects of Wnt pathway on RANK family members and RANKL-RANK downstream targets in intestinal organoids.** A, RT-PCR of the indicated genes in  $\text{Rank}^{\text{flox/flox}}$  intestinal organoids cultured with or without Wnt3a (100 ng/ml) for one week ( $n=2$ ). B, RT-PCR of the indicated genes in organoids from control and Villin-Cre  $\text{Rank}^{\text{flox/flox}}$  mice treated for 8 hours, 1 or 2 days with RANKL (1  $\mu\text{g/ml}$ ). Representative data from two experiments performed with  $n=2$  mice each. C, RT-PCR of the indicated genes in organoids from control and Villin-Cre  $\text{Rank}^{\text{flox/flox}}$  mice treated for 8 hours, 1 or 2 days with RANKL (1  $\mu\text{g/ml}$ ) ( $n=2$ ). D, RT-PCR of the indicated genes in organoids from control and Villin-Cre  $\text{Rank}^{\text{flox/flox}}$  mice treated for 8 hours, 1 or 2 days with RANKL (1  $\mu\text{g/ml}$ ). Representative data from two experiments performed with  $n=2$  mice each.

EMT genes were also tested to discard effects of RANK pathway activation described for mammary gland cell lines (Palafox et al., 2012a) on RANKL-mediated organoid disassembly, but no differences on *E-cadherin* or *Vimentin* expression was found upon RANK stimulation (Figure 3.5D). The differences between basal levels of gene expression for some of the targets (i.e., *Vimentin*) found between control and Villin-Cre- $\text{Rank}^{\text{flox/flox}}$  organoids is due to variability, since in other experiments similar expression levels were

observed (Figure 3.6). Thus, a direct effect of RANK pathway on WNT pathway or the EMT program is not likely to be responsible for organoid disassembly/cell death.

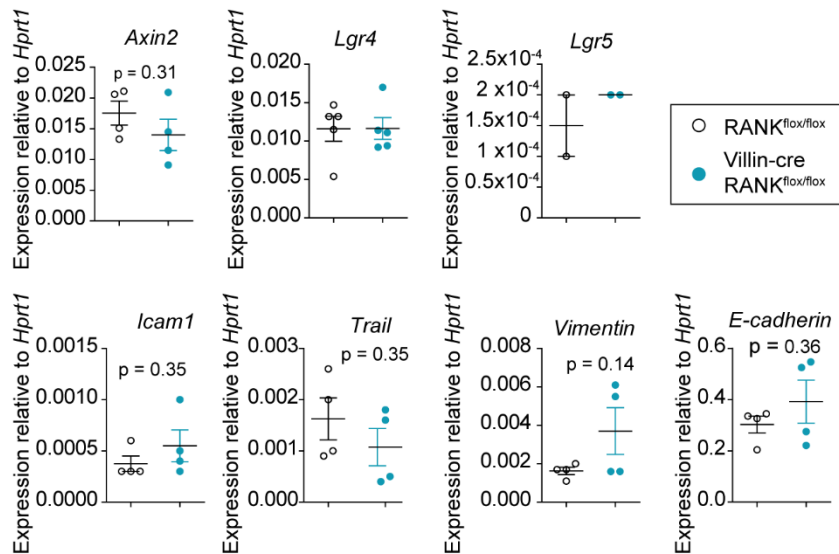


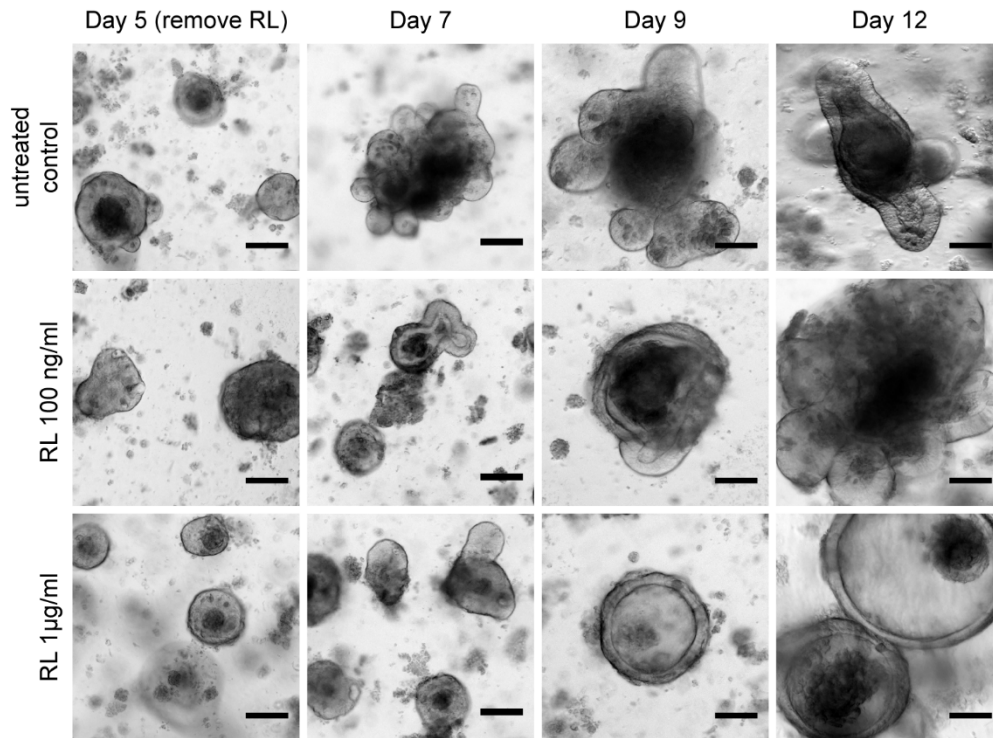
Figure 3.6. **None of the explored targets are differentially expressed between control and Villin-cre RANK<sup>flox/flox</sup> intestinal organoids.** RT-PCR of the indicated genes in organoids from control and Villin-Cre Rank<sup>flox/flox</sup> mice at 48h of culture. Each dot represents organoids from one mouse. Results from two independent experimental days are shown.

Another possible explanation for the observed effect of high RANKL doses is that the stem compartment of the organoids undergoes M cell differentiation only at elevated doses of RL. This will disrupt organoid cell self-renewal and would limit their viability *in vitro* to the lifespan of fully differentiated M cells. In order to verify this hypothesis, RANKL was transiently added to organoid cultures at either low (100 ng/ml) or high (1000 ng/ml) concentrations.

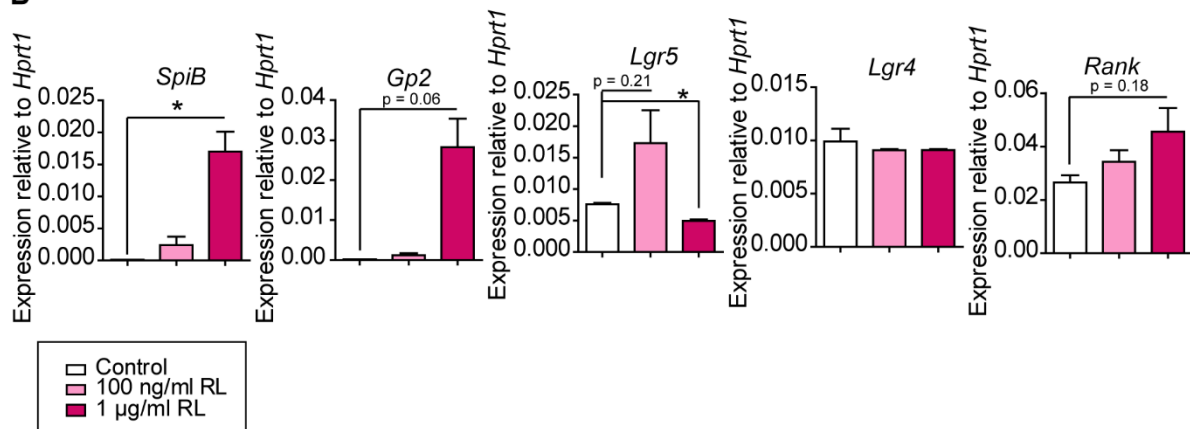
Upon RANKL removal, organoids treated with lower doses were able to recover branching ability, while those treated with higher doses had their numbers greatly reduced and presented mostly swollen, rounded structures by day 10 of culture (Figure 3.5E). RT-PCR at day 12 (7 days after RANKL removal) revealed that those organoids treated with high doses of RANKL still expressed abundant M cell markers *Spib* and *Gp2* (Kanaya et al., 2012; Kimura et al., 2015a), while those treated with low doses had much lower expression (Figure 3.7A). Interestingly, *Lgr5* was significantly higher in organoids transiently treated with low RANKL concentration as compared with controls and organoids treated with higher RANKL doses, which show similar levels between them (Figure 3.7B). This might suggest an enrichment of stem cells in the organoids after being exposed to low levels of RL, but further

characterization of this timepoint would be needed to confirm this hypothesis. *Rank* and *Lgr4* expression were similar in all conditions (Figure 3.7B).

**A**



**B**



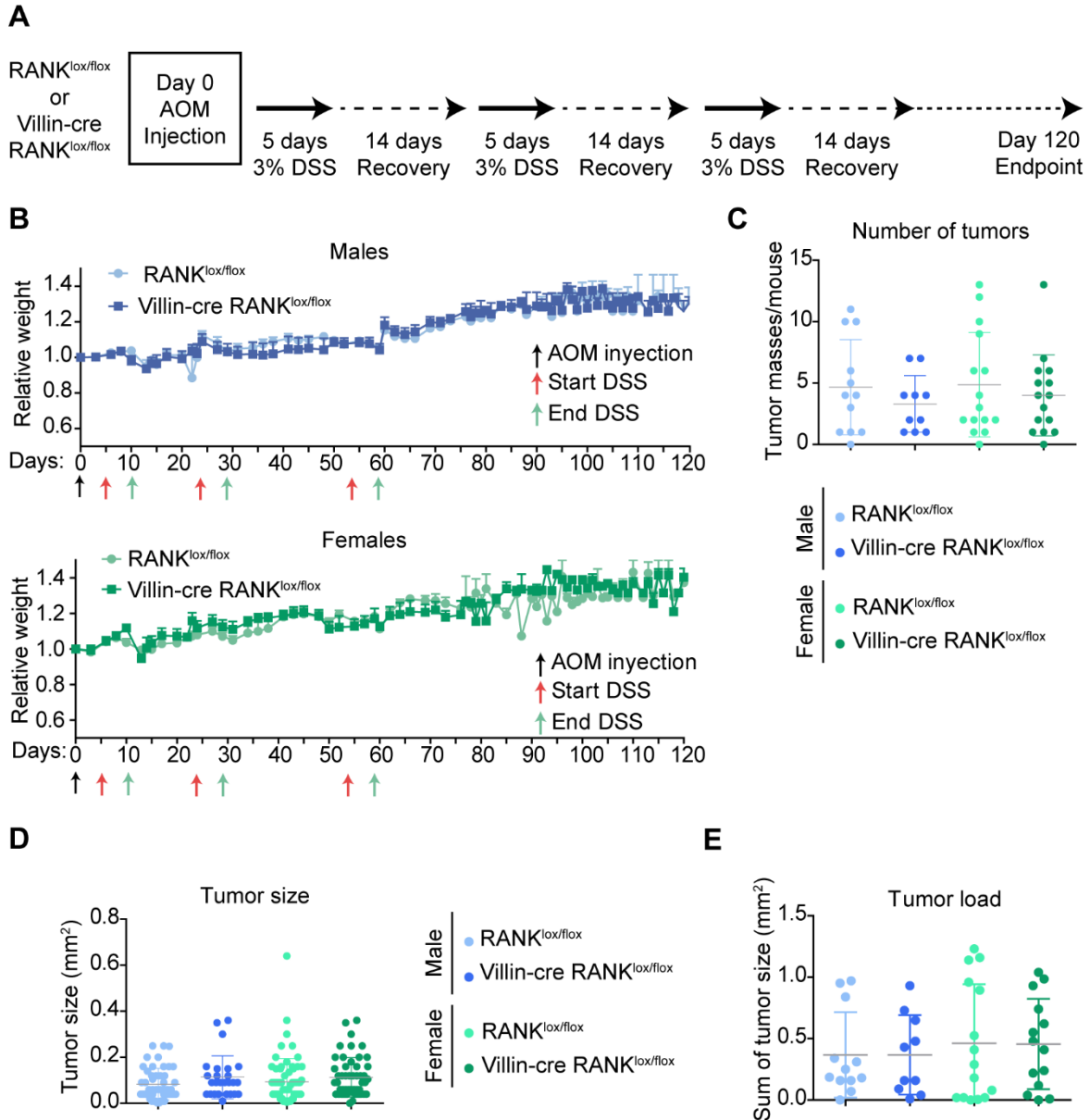
**Figure 3.7. Effects of RANKL treatment are partially reversible.** A, Pictures from intestinal organoids treated with the indicated RANKL concentration for 5 days. On day 5, RANKL was removed, and organoids were monitored for an additional week. n = 2. Scale = 100 µm. B, RT-PCR of the indicated genes in organoids from A, at day 12.

### 3.4 Loss of RANK in the intestinal epithelia or myeloid cells does not affect the development of colorectal adenomas in mice under the AOM/DSS protocol

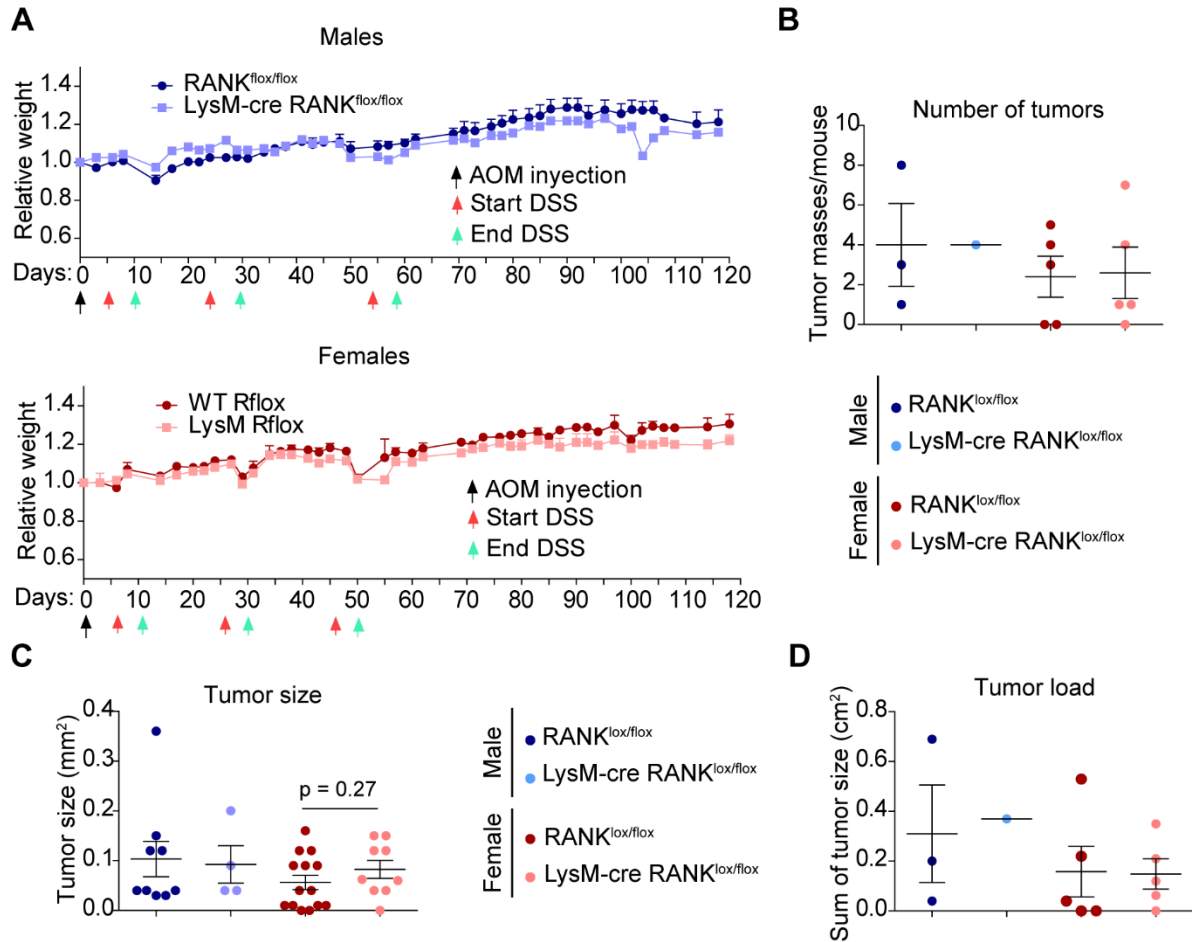
Given the described role of RANK pathway in intestinal immune response and colitis (Ashcroft et al., 2003; Dougall et al., 1999a; Kanaya et al., 2018; Kong et al., 1999; Moschen et al., 2005; Rios et al., 2016), together with its involvement in mammary gland tumorigenic processes (Gonzalez-Suarez et al., 2010; Nolan et al., 2016; Schramek et al., 2010; Sigl et al., 2016; Yoldi et al., 2016), the effect of RANK loss on models of inflammation-driven colorectal carcinogenesis was evaluated (Figure 3.8A).

Villin-Cre; Rank<sup>fllox/fllox</sup> mice and Rank<sup>fllox/fllox</sup> littermates were injected with the carcinogen AOM and received three cycles of DSS 3%, inducing intestinal inflammation (Figure 3.8A). The combined effect of increased mutations driven by the carcinogen with an inflammatory environment prompted the development of polyps and non-invasive adenomas in the colon of mice receiving the treatment (Tanaka et al., 2003). Body-weight loss was monitored during the three months following the injection of the carcinogen as a surrogate for disease severity. Since male and female mice had been previously described to respond differently to this tumor-inducing protocol (Tanaka et al., 2003), data was considered separately for each of the two groups. No significant differences were found in body-weight loss due to RANK loss in intestinal epithelium in either male or female groups (Figure 3.8B).

At experimental endpoint, intestine and colon were examined for macroscopic tumoral masses, and the size of each mass was measured using a caliper. Intestines rarely presented any masses, as expected (data not shown). The severity of adenoma development was remarkably variable in mice within the same experimental group, with the number of masses ranging from 0 to 13 (Figure 3.8C). Overall, no difference in the number of colorectal tumor numbers (Figure 3.8C) or macroscopic size (Figure 3.8D) was found between Villin-Cre; Rank<sup>fllox/fllox</sup> and control mice. When the size of all the tumoral masses per colon is added, as a surrogate of tumorigenic severity in each mouse, again no differences are observed between control and RANK-depleted groups (Figure 3.8E). These data suggest that RANK expression on intestinal epithelium does not affect colorectal tumorigenesis in this model.



**Figure 3.8. RANK loss on intestinal epithelium does not affect colorectal tumorigenesis.** A, Scheme of AOM/DSS inflammation-induced tumorigenic protocol. B, Mouse weight monitoring during the AOM/DSS protocol relativized to experimental day 0 on male (blue) and female (green) Villin-Cre; Rank<sup>lox/flox</sup> mice and Rank<sup>lox/flox</sup> littermates. Graph representative of 4 independent experiments. n = 5-9. C, Graph representing the number of colonic tumor masses as detected at experimental endpoint. Data from four independent experiments is shown. Each dot represents one mouse. D, Graph representing the size of colonic tumor masses measured at experimental endpoint. Each dot represents one tumor mass. Data from four independent experiments is shown (n = 10-15 mice). E, Graph representing the total tumoral mass found per mouse at experimental endpoint. Data from four independent experiments is shown. Each dot represents one mouse (n = 10-15).



**Figure 3.9. RANK loss on macrophages does not affect colorectal tumorigenesis.** A, Mouse weight monitoring during the AOM/DSS protocol relativized to experimental day 0 on male (above,  $n=1-3$ ) and female (below,  $n = 5$ )  $LysM\text{-}cre; Rank^{lox/lox}$  mice and  $Rank^{lox/lox}$  littermates. B, Graph representing the number of colonic tumor masses as detected at experimental endpoint. Each dot represents one mouse. C, Graph representing the size of colonic tumor masses measured at experimental endpoint. Each dot represents one tumor mass. ( $n = 1-5$  mice). D, Graph representing the total tumoral mass found per mouse at experimental endpoint. Data from four independent experiments is shown. Each dot represents one mouse ( $n = 1-5$ ).

In order to explore the effects of RANK depletion in other cellular compartments on inflammation-driven colorectal tumorigenesis, mice from the  $LySM\text{-}cre\ RANK^{lox/lox}$  model were treated under the AOM/DSS carcinogenic protocol. No differences between control and  $LySM\text{-}cre\ RANK^{lox/lox}$  weight loss were observed during the 3 months of monitoring (Figure 3.8A). Colon samples extracted at endpoint did not show any differences in terms of number of tumoral masses (Figure 3.9B), size of tumoral masses (Figure 3.9C) and total tumor mass (Figure 3.9D). The  $n$  of male mice used was too low to extract solid conclusions but, given the overall negative results obtained with both Villin-cre and female  $LysM\text{-}cre$

tissue-specific RANK depletion models, no further experiments were performed to increase the n.

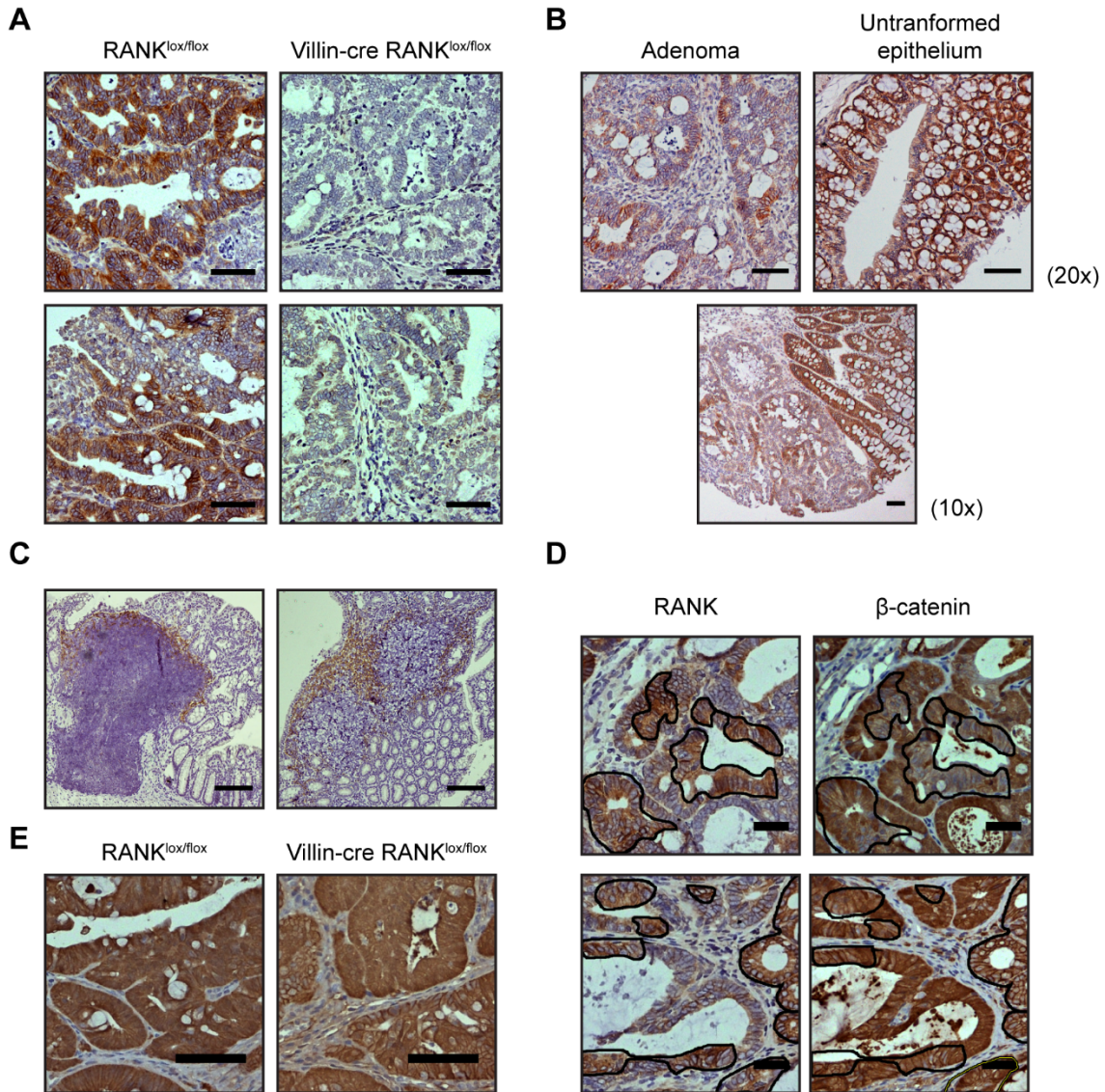
### 3.5 High RANK expression in colorectal adenomas is found on differentiated epithelium

Exploratory histological analyses were performed in AOM/DSS-treated Villin-Cre; Rank<sup>flox/flox</sup> and littermate colon samples. RANK protein presented variable expression levels on adenomas from the AOM/DSS mouse model (Figure 3.9A). As expected, the protein was absent in tumors from Villin-Cre; Rank<sup>flox/flox</sup> samples (Figure 3.9A). Interestingly, RANK expression was clearly downregulated in adenomas when compared to untransformed epithelium, and even lower in areas where colon epithelium presented a highly disorganized pattern, due to the malignization process (Figure 3.9B). RANKL remained compartmentalized in the lymphoid-associated tissue. However, these areas were increased in size and number due to the inflammation induced by the DSS treatment (Figure 3.9C).

When performing a staining for  $\beta$ -catenin and RANK in serial cuts from adenoma samples, an inverse correlation was found between RANK and nuclear  $\beta$ -catenin (Figure 3.9D).  $\beta$ -catenin nuclear localization is a marker of active canonical Wnt signaling. However, when analyzing adenomas from Villin-Cre; Rank<sup>flox/flox</sup> mice, no clear increase in nuclear  $\beta$ -catenin was observed (Figure 3.9E), ruling out a direct regulation of Wnt pathway by RANK.

These data suggest that high RANK expression correlates with untransformed or WNT-low/differentiated colon epithelial cells in colorectal adenomas. This expression gradient is reminiscent of that found in untransformed intestinal epithelium.





**Figure 3.9. RANK expression in adenomas correlates with dedifferentiation and active Wnt signaling.** A, RANK IHC on adenomas from Villin-Cre  $Rank^{lox/flox}$  and control littermates. Scale = 50  $\mu$ m. B, RANK IHC pictures showing the different expression levels in adenomas and untransformed epithelium. Scale = 50  $\mu$ m. C, RANKL IHC images showing localization in tertiary lymphoid structures within the colon epithelium. Scale = 100  $\mu$ m. D, RANK and  $\beta$ -catenin IHCs on serial histological cuts. Images from the same region of two adenomas are shown as examples, RANK-high regions are selected with black lines and the same outlines are printed on the  $\beta$ -catenin IHC image. Scale = 25  $\mu$ m. E,  $\beta$ -catenin IHC on adenomas from Villin-Cre  $Rank^{lox/flox}$  and control littermates. Scale = 50  $\mu$ m.



# **DISCUSSION**



## **Discussion Chapter 1: Inhibition of RANK signaling in breast cancer induces an anti-tumor immune response orchestrated by CD8<sup>+</sup> T cells.**

Several studies have shown the prognostic and predictive value of TILs, especially in HER2<sup>+</sup> and triple-negative BC (Salgado and Loi, 2018; Savas et al., 2016). However, TILs continue to be infrequent in most luminal breast tumors. The identification of a therapy that could convert immune “cold” tumors into “hot” ones would represent a major step towards the development of immune-related therapies. Based on our clinical and preclinical findings, denosumab appears to be just this type of promising therapeutic agent. This question is particularly relevant for luminal BC which is poorly infiltrated and insensitive to immunotherapies.

The results of the D-BEYOND clinical trial provide strong evidence of the immunomodulatory effect of denosumab in luminal early BC and identify predictive biomarkers of response. The mouse genetic studies demonstrate that inhibition of RANK signaling in the tumor cells increases TILs and CD8<sup>+</sup> T cell infiltration and attenuates tumor growth. Mechanistically we found that activation of RANK signaling in tumor cells induces a proinflammatory microenvironment that favors survival of TANs and restricts T cell anti-tumor response.

The strength of our work resides in the fact that two independent studies, a clinical trial and preclinical research on tumor-prone mouse models, equally conclude that the inhibition of RANK signaling increases the anti-tumor immune response and set the basis for additional trials combining denosumab with immunotherapy in presumably immune “cold” luminal BC. Although the clinical trial primary efficacy endpoint was not met, since tumor cell proliferation was not reduced, a short course of denosumab did induce an increase in the levels of TILs, T and B cells and CD8<sup>+</sup> T cell infiltration. In contrast with the increased levels of T cells and CD8<sup>+</sup> T cells, which were associated with enhanced TIL infiltration, the reduction of Tregs was observed equally in responders and non-responders, suggesting that it may be driven by additional systemic effects of denosumab, rather than by the loss of RANK signaling in the tumor cells, as suggested by the different results seen in RANK<sup>-/-</sup> tumors.

Importantly, preclinical genetic mouse approaches evidence that the main immunomodulatory changes induced by denosumab in D-BEYOND -increased in TILs and CD8<sup>+</sup> T cells- are replicated when RANK is lost specifically in the tumor compartment. Additionally, they add functional relevance to the changes in immune infiltration since T lymphocytes and CD8<sup>+</sup> T cells are responsible for the delayed tumor onset and reduction of tumor-initiating ability observed in RANK null tumors. In contrast, RANK loss in myeloid cells (driven by LysM) does not change the tumor immune infiltration. In the PyMT mouse model

the frequency CD8<sup>+</sup> T cells also increase after systemic anti-RL treatment and the CD4/CD8 ratio was reduced, but no differences in total leukocyte or lymphocyte infiltration were observed. Differences with the D-BEYOND results might be due to drug specific aspects, treatment schedule or tumor divergences.

RANK expression in tumor cells led to a significant increase in the levels of several cytokines and chemokines involved in macrophage and neutrophil recruitment and polarization (Griffith et al., 2014; Oliveira et al., 2008; Ramos, 2005), in line with the increased infiltration of TAMs and TANs in RANK<sup>+/+</sup> tumors. Indeed, we found that RANK-expressing human BC cells promote survival of inflammatory neutrophils. Neutrophil depletion significantly delayed tumor appearance in RANK<sup>+/+</sup>, but not in RANK<sup>-/-</sup> models, supporting a pro-tumorigenic role for neutrophils recruited by RANK<sup>+/+</sup> tumor cells. Neutrophils have different polarization states and can promote tumorigenesis and metastasis (Fridlender et al., 2009). Our mouse and human data are consistent with the previously reported negative correlation of neutrophils and CD8<sup>+</sup> T cell infiltration in NSCLC (Kargl et al., 2017). Neutrophils have a well-defined role in the suppression of the action of CD8<sup>+</sup> T cells (Michaeli et al., 2017). Our results demonstrate that RANK activation in tumor cells increases neutrophil survival and activation inducing an immunosuppressive environment which could restrict the cytotoxic T cell response. These findings support the connection between RANK activation in tumor cells, neutrophils and CD8<sup>+</sup> T cells (see Figure 6).

A critical aspect of current and future clinical trials is the selection of BC patients who may benefit from denosumab treatment, considering the limitations of the RANK immunohistochemistry. We demonstrate that the RANK metagene we generated captures RANK activation and predicts the denosumab-driven increase in TILs in BC. Higher RANK metagene, RANK/NF- $\kappa$ B activation in the tumors and soluble RANKL at baseline could be better biomarkers than the individual expression levels of RANK or RANKL for the selection of BC patients who might benefit from denosumab treatment.

The D-BEYOND trial has some limitations, such as the small sample size, the inclusion of only premenopausal patients and the limited number of triple-negative and HER2<sup>+</sup> cases. Whether the immunomodulatory response associated with RANKL inhibition could also be effective in postmenopausal patients will be addressed in the ongoing trial: D-BIOMARK (NCT03691311). It will be also worth reassessing the clinical outcome of two recent large phase III trials of adjuvant denosumab in early BC, D-CARE and ABCSG-18, according to the predictive biomarkers we defined: baseline RANK metagene, sRANKL levels, and the presence of Tregs. The D-CARE study reported no differences in disease-free survival

(DFS), whereas the ABCSG-18 trial showed DFS improvement in postmenopausal patients (Coleman et al., 2020, 2018; Gnant et al., 2019).

Results in the RANK<sup>-/-</sup> mouse tumors suggest that up-regulation of negative checkpoints and Tregs occurs as a consequence of a proinflammatory, anti-tumor IFN $\gamma$ -enriched microenvironment (Spranger et al., 2013; Taube et al., 2012) and may allow RANK<sup>-/-</sup> tumor cells to evade immune surveillance and grow. The blockade of CTLA4 and PD-1/PD-L1 has revolutionized treatment of highly immunogenic tumors such as melanoma and NSCLC (Hodi et al., 2010; Owen and Chaft, 2018), but, so far, results in BC have been restricted to basal-like tumors in combination with radiotherapy or chemotherapy (Adams et al., 2019).

CTLA4 blockade affects mainly the priming phase of the immune response, whereas PD-L1 inhibition works mostly during the effector phase to restore the immune function of previously activated T cells (Buchbinder and Desai, 2016). In both scenarios, we have shown an increased benefit after the addition of RANKL inhibitors to immune checkpoints in RANK<sup>+/+</sup> tumors, which is highly relevant in poorly immunogenic tumors such as luminal BC. Importantly, the combined treatments show no increased benefit in RANK<sup>-/-</sup> tumors, indicating that it is driven by the inhibition of RANK signaling in tumor cells. This is a novel mechanism of action, as previous preclinical studies reporting the benefit of the combination were done in melanoma and colon cancer cell lines highly responsive to immunotherapy but lacking RANK expression (Ahern et al., 2017) (Ahern et al., 2018). Although we cannot rule out that denosumab may have additional systemic effects, our findings support that a tumor cell-driven effect contributes to the immunomodulatory effect of denosumab in BC.

The benefit of the combined effect of anti-RANKL and immune checkpoint inhibitors will be investigated in the CHARLI trial (NCT03161756), a phase I/II study of the effect of denosumab in combination with nivolumab (an anti-PD-1), with or without ipilimumab (anti-CTLA4), in metastatic melanoma patients, and in the POPCORN trial (ACTRN12618001121257), which will evaluate immune changes in NSCLC patients treated with nivolumab alone or in combination with denosumab. Clinical and preclinical evidence shown in this work encourage the initiation of similar trials in BC.

In summary, compelling clinical and preclinical data reveal an unexpected immunomodulatory role for RANK pathway in luminal early-stage BC and demonstrate denosumab to be a promising agent for enhancing the immune response in luminal BC alone or in combination with immune checkpoint inhibitors.

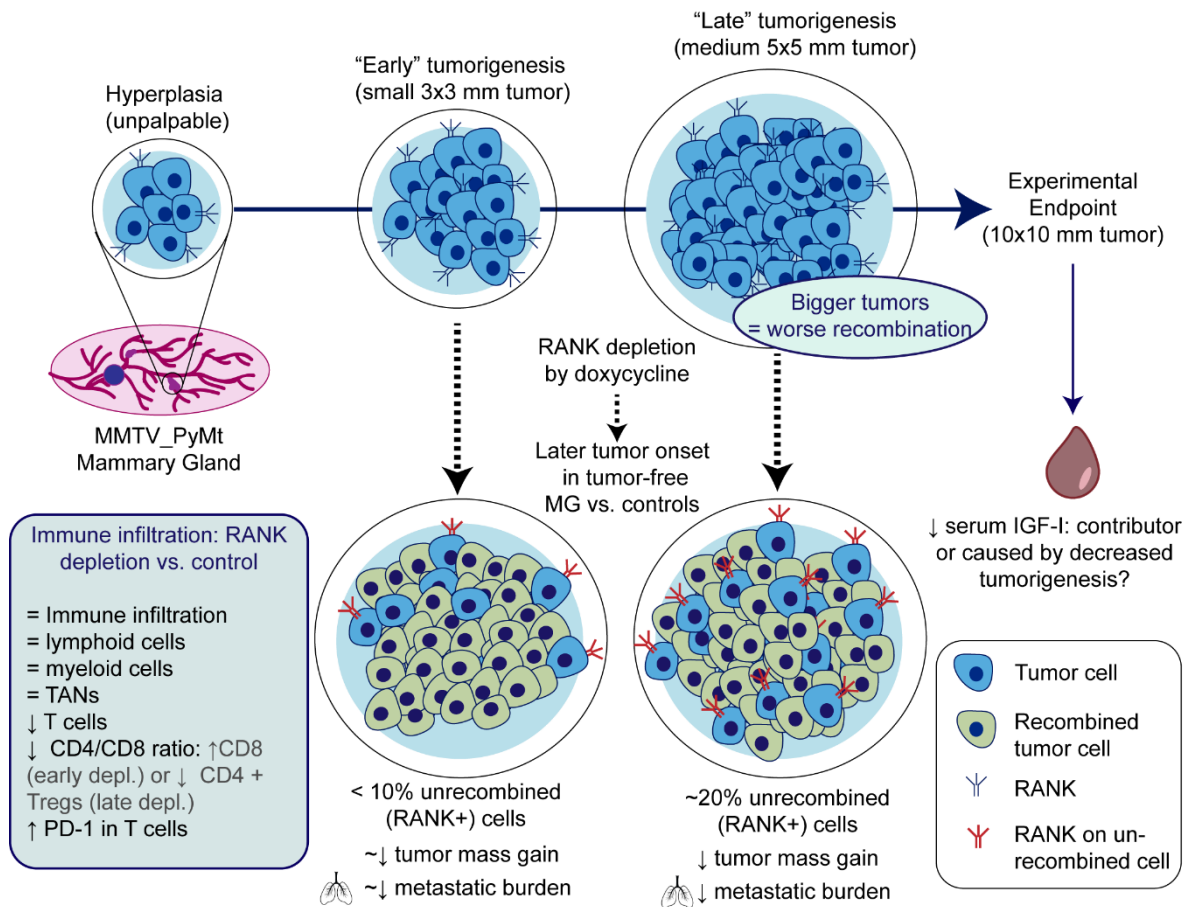


## Discussion Chapter 2: Characterization of an inducible, tissue-specific RANK depletion model of mammary gland tumorigenesis.

The RANK<sup>ΔK8</sup> model of tumorigenesis generated and characterized in this doctoral thesis presents a novel tool to study targeted RANK pathway inhibition during the different stages of mammary gland tumorigenesis. Indeed, RANK depletion or RANKL inhibition has mostly been studied in the preventive setting, with models of constitutive RANK or RANKL depletion or cre recombinase expression (Gonzalez-Suarez et al., 2010; Schramek et al., 2010; Sigl et al., 2016; Yoldi et al., 2016). Models where RANK pathway is inhibited in established tumors rely in transplant models which could be neglecting effects intrinsic to primary tumors and effects derived from the tumor developing in a RANK-null environment (Gómez-Aleza et al., 2020; Yoldi et al., 2016) (Chapter 1). However, the RANK<sup>ΔK8</sup> also presents some challenges, such as the high variability of tumor and metastasis formation, the long tumor latencies (about 4-5 months), systemic changes induced by doxycycline treatment and the logistics of maintaining a colony with 5 transgenes, 4 of which should be kept in heterozygosity. Data obtained upon RANK depletion with this model are summarized in Figure 1 below, for better follow-up and contextualization of the results discussed here.

Experiments with this model corroborated the previous observations associating RANK pathway activation in mammary gland epithelium with tumor initiation (Gonzalez-Suarez et al., 2010; Schramek et al., 2010; Sigl et al., 2016; Yoldi et al., 2016), showing that RANK loss in the K8+ luminal epithelium delays tumor appearance. Counterintuitively, this prevention seems more effective when you deplete RANK later during tumorigenesis, having more dramatic effects in the prevention of tumorigenesis and the reduction of overall tumor burden at experimental endpoint.

RANK pathway's effects on epithelium are probably highly context-dependent and subjected to several feedback loops of regulation. These findings regarding the differences between early and late RANK depletion could be highlighting one of these context-dependent roles. Given that with the early depletion protocol, RANK will also be depleted later during tumorigenesis, the fact that the results reached are not as strong as with a late RANK depletion protocol could mean that early RANK depletion allows preneoplastic mammary gland cells to adapt to RANK loss, thus selecting clones which do not rely as much on RANK signaling to establish tumor growth.



**Figure 1. Summary of findings with the RANK<sup>ΔK8</sup> primary tumor model.** RANK depletion was induced early (palpable, 3x3 mm tumors) or later during tumorigenesis (4x4-5x5 tumors), with both depletion models resulting in a delay in tumor appearance in the remaining tumor-free mammary glands (MG). A late RANK depletion resulted in worse percentage of recombined cells at endpoint, with a negative correlation observed between tumor size at the onset of depletion and the abundance of recombined cells. Late RANK depletion resulted in lower gain of tumor mass and metastatic burden in the lungs, where early RANK depletion showed tendencies in the same direction. IGF-I was decreased in the serum of RANK-depleted mice and immune infiltrates in tumors at endpoint showed a lower T cell infiltration and CD4/CD8 ratio compared with controls, with higher CD8 T cell frequency upon early RANK depletion and lower CD4 T cell and Treg infiltration after a late RANK depletion, with both depletion protocols showing higher PD-1 expression in T cell populations.

The lower recombination observed at endpoint in RANK<sup>ΔK8</sup> tumors under the late depletion protocol (as compared with the early depletion protocol and with controls with reporter recombination and lack of RANK loss), could support the hypothesis that tumor populations can adapt worse to RANK loss later during tumorigenesis. Tumors/mammary gland epithelia in a more advanced malignant stage would have RANK+ populations (K8-low or K14+), which may have become adapted to depend on RANK signaling to provide an evolutionary advantage. These populations might even support the growth of RANK- populations, for



example, setting a pro-tumorigenic immune environment (Gómez-Aleza et al., 2020) as described in the previous chapter. With an early RANK depletion, the cell populations which would give rise to tumors might still be capable of adapting to a loss of RANK. However, the analyses at experimental endpoint presented in this chapter hinder the observation of these putative population dynamics. Indeed, at endpoint there is no significant decrease of K8 expression on primary tumors where RANK was depleted. The hypothesis of whether RANK expression itself or the presence of RANK<sup>+</sup> populations give a competitive advantage for tumorigenesis could be further validated by collecting samples earlier after RANK depletion or establishing transplants co-injecting RANK<sup>+</sup> and RANK<sup>-</sup> tumor populations, and using the appropriate RANK<sup>+/+</sup> controls with the mTmG reporter.

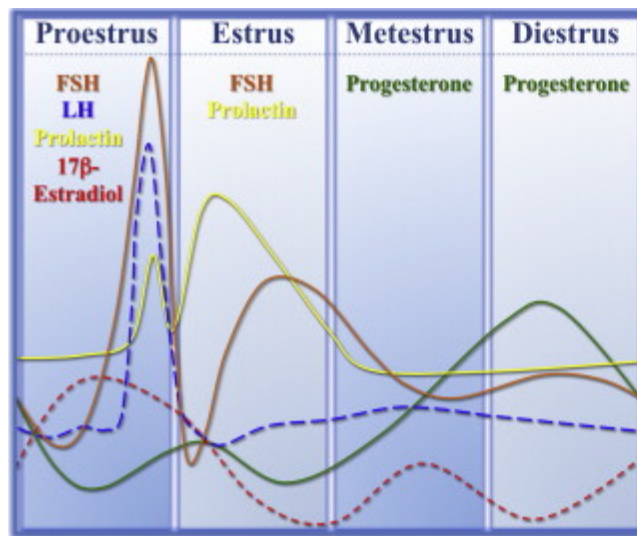
Another possibility which could explain the more exacerbated phenotype for late vs early RANK depletion is that RANK pathway in K8<sup>+</sup> cells could act as a tumor barrier during early tumorigenic stages, then switching to a pro-tumorigenic program later during tumorigenesis. In accordance with this hypothesis, recently published data from our group show that RANK MG overexpression delays tumor appearance when combined with the PyMT or NeuT. RANK overexpression is described to trigger senescence on the mammary gland epithelial cells, thus preventing tumorigenesis. However, once tumors appear, RANK overexpression promotes a faster tumor growth, arguing for its classical pro-tumorigenic role (Benítez et al., 2021). Senescent cells are not found in the advanced tumors from the RANK overexpressing mice, but yes in preneoplastic lesions, so the anti-tumorigenic role of RANK might be surpassed during the early malignant transformation of the mammary gland epithelium. However, these observations could be due to RANK pathway activation triggering feedback loops to stop epithelial proliferation which, when exacerbated or in presence of exogenous high levels of RANKL, trigger the entry into senescence (Benítez et al., 2021).

From normal mammary gland biology, it is known that progesterone during the estrous cycle induces a first wave of proliferation, followed by upregulation of RANKL triggering a second wave of proliferation in RANK<sup>+</sup> HR<sup>-</sup> cells (Beleut et al., 2010). However, these cycles need to be regulated to avoid the development of epithelial hyperplasias in the mammary gland. Indeed, an increase in apoptotic cells has been reported at the end of the estrous cycle, with a decrease in the anti-apoptotic Bcl2 expression (Andres and Strange, 1999; Fata et al., 2001). RANK pathway could be key in the coordinated hormonal cycles which modulate mammary gland homeostasis and eliminating RANK could also affect several feedback loops necessary for the return to a non-proliferative epithelium. For instance, estrogen

regulates its own signaling in a time-controlled manner during the estrous cycle by activating proteosomal degradation of ER $\alpha$ , PR, and Pax-2(Silberstein et al., 2006), thus also affecting the response of these cells to other proliferative signals.

Progesterone also has a described dual role, both promoting and preventing proliferation in mammary epithelium. As previously described, progesterone induces proliferation on PR+ cells and a subsequent second wave of proliferation due to RANKL paracrine signaling on RANK+ cells (Beleut et al., 2010); however, it has also been described to block the proliferative effects of estrogen on breast cancer cell lines (Mohammed et al., 2015; Ze-Yi et al., 2005), by binding to estrogen receptor and switching its transcriptional targets (Mohammed et al., 2015).

RANK could be also a key pathway to, not only mediate progesterone-driven proliferation, but also to activate feedback loops to coordinate the activation/deactivation of other cyclic pathways during mammary gland homeostasis (see Figure 2).



**Figure 2. Hormonal serum levels during the murine estrous cycle.** Estradiol/Estrogen levels are higher during the proestrus phase, at the end of which, Follicle Stimulating Hormone (FSH), Luteinizing Hormone (LH) and prolactin show a peak. During the Estrus, Prolactin and FSH levels rise again, decreasing during the Metestrus, when estrogen shows a small peak and Progesterone levels start to rise, reaching their peak at Diestrus. Figure from Bertolin K. and Murphy B.D., 2014(Bertolin and Murphy, 2014).

It is also important to bear in mind that the RANK $\Delta^{K8}$  model not only depletes RANK in tumor cells, but also in other K8+ populations. K8+ cells are found in the intestinal/colon epithelium, mTECs at the thymus (where RANK is crucial for antigen presentation(Hikosaka et al., 2008a; Rossi et al., 2007)), the kidney, the lung, the liver, the stomach... Therefore, the

different results that were observed in tumorigenesis upon RANK depletion could also be due to systemic effects.

There are abundant previous publications arguing for a tumor-intrinsic effect of RANK depletion in tumor latency (Gonzalez-Suarez et al., 2010; Schramek et al., 2010; Sigl et al., 2016; Yoldi et al., 2016) and, therefore, the major effects would most likely be due to mammary gland/tumor RANK loss. However, the differences between early and late RANK depletion have not been reported elsewhere, and no hypothesis to explain these differences can be fully discarded yet. Some of the transplant assays with our model in immunodeficient hosts indeed highlighted that RANK depletion in tumor cells causes significant growth delay. However, other tumors were not affected by RANK depletion, arguing that the variability of the tumors developed by PyMT models might also affect the effects and importance of RANK pathway for each tumor analyzed. Future RNAseq analyses would aim to characterize these two different types of tumors to try to discover which characteristics could make a tumor dependent on RANK pathway to grow.

Additionally, the differences in growth observed with the RANK<sup>ΔK8</sup> model transplanted into immunodeficient host argue with the previous observations with the RANK<sup>+/+</sup> and RANK<sup>-/-</sup> tumor transplant models, where transplanting into an immunodeficient environment avoided the differences in tumor latency, which were initially mediated by the establishment of an immune-suppressive microenvironment through RANK signaling. However, these observations are tumor-dependent, with some primary tumors presenting no differences in tumor latency upon RANK depletion, suggesting a more complex role for RANK regarding its role in promoting tumor growth in immunodeficient environments. The discrepancy might also be due to the different experimental setting for RANK depletion, since RANK<sup>-/-</sup> tumor transplants could have adapted to the lack of RANK signaling, while RANK<sup>ΔK8</sup> are exposed to RANK loss upon tumor implantation. However, we cannot discard that primary tumor variability could also explain the differences between the two observations.

In order to explore the possibility that RANK loss in other K8<sup>+</sup> organs could affect the observations in the primary tumors, transplant experiments of PyMT tumors into C57/Bl6-purified RANK<sup>ΔK8</sup> hosts were performed. Again, there was variability between the results obtained in two independent experiments, with RANK loss in mouse hosts leading to a delay in tumor growth or to no differences, depending on the primary tumor. Further experiments are needed to fully discard the possibility that RANK in other organs might be affecting our observations in the primary tumors, but current data do not show very dramatic differences

in tumor growth or immune infiltration. A tendency to lower PD1 expression within the CD4 T cell compartment upon RANK depletion in the hosts' K8+ cells could suggest a minor systemic contribution to tumor growth. However, these data on RANK depletion in tumor-bearing hosts should be validated in further experiments, especially since the tendency goes in the opposite direction in RANK<sup>ΔK8</sup> primary tumors, which show higher PD1 expression in T cells upon RANK depletion when compared to controls.

Some of these observations in immune populations contrast with those reported in the D-BEYOND study (Gómez-Aleza et al., 2020) (Chapter 1), where denosumab treatment increased immune tumor cell infiltration in early breast cancer patients, in particular of T cells and CD8 T cells, while Treg abundance was decreased. With the RANK<sup>ΔK8</sup> models, which might better mimic RANK pathway inhibition in early breast cancer, there were no differences in total immune infiltration upon RANK depletion and an opposite tendency in T cell abundance was observed, with lower T cell percentages observed in tumors bearing RANK depletion. An increase in CD8 T cells observed in D-BEYOND was only mirrored with the early depletion protocol, while the Treg decrease was detected solely with the late depletion protocol. The high variability of the primary PyMT tumor models together with the differences of pharmacologically inhibiting RANK pathway vs. a genetic loss of RANK protein might have affected the results, while the differences between early and late RANK depletion highlight that RANK pathway can have a highly dynamic role affecting immune infiltrates at different timepoints.

It is also noteworthy that most of the observations for changes in immune infiltration for RANK<sup>ΔK8</sup> tumors compared to controls do not mirror those observed for RANK<sup>-/-</sup> tumor transplants. For instance, RANK<sup>ΔK8</sup> primary tumors show no differences in terms of total immune infiltration, lymphocyte, or TAN enrichment. Again, the differences for immune responses for the primary tumor and tumor-transplant settings could be affecting the results. Tumor transplants consist of cell populations which can already establish a pro-angiogenic microenvironment, which enables faster growth and better access for immune infiltration, and also affects the type of immune cells recruited to the tumor (Guerin et al., 2020). For instance, tumor transplants from the MMTV-PyMT model have a faster monocyte influx rate than primary tumors (Franklin et al., 2014). In other spontaneous tumorigenic models, it has been described that in contrast to tumor transplants, T cells from primary tumors are often tolerogenic due to having co-evolved with tumor cells (Anders et al., 2017). Considering these differences between the models, together with the timing of RANK depletion, it might

not be possible to fully compare both results. In primary tumors, T cell infiltration is lower after RANK depletion under both depletion protocols, opposite to the observations with the RANK<sup>+/+</sup> and RANK<sup>-/-</sup> tumor transplants. However, for both models and depletion protocols, the CD4/CD8 ratio is decreased. Lower tumor infiltrating CD4/CD8 ratios have been associated with a good prognosis (Wang et al., 2017) and thus agree with the delayed tumorigenesis observed upon RANK loss. It is worth to highlight that the populations driving the lower ratios vary for the different models and depletion protocols. Both for RANK<sup>-/-</sup> tumor transplants and for an early RANK depletion in primary tumors, a higher CD8 T cell infiltration drives the decrease in CD4/CD8 ratio, while for late RANK depletion in primary tumors it is the lower CD4 T cell infiltration. Tregs are not very abundant in primary tumors and the decrease observed for in RANK<sup>ΔK8</sup> tumors under the late depletion protocol may not be biologically relevant. The increase in PD1 expression within the T cell compartment (equivalent to the observations in RANK<sup>-/-</sup> tumor transplants) might reflect a stronger activation of T cell responses within the RANK<sup>-/-</sup> tumor microenvironment, since PD1 is upregulated in T cells upon encounter with their target antigen (Wei et al., 2018). However, PD1 expression would downregulate T cell activity upon binding PD-L1 expressed by tumor cells or immune cells within the tumor microenvironment (Wei et al., 2018). It is also noteworthy to mention that doxycycline treatment itself has amply been described to affect the immune system (Banck and Forsgren, 1979; Bode et al., 2014; He and Marneros, 2014; Huang et al., 2011; Krakauer and Buckley, 2003; Kuzin et al., 2001; Su et al., 1999, 2014) and, indeed, our model also shows some effects in the tumor immune infiltrates. Tumors from doxycycline-treated control mice show an increase in PD-L1<sup>+</sup> myeloid cells and a decrease in PD1<sup>+</sup> T cells compared to tumors from untreated mice. Also, in the primary tumor setting, RANK expression is strikingly reduced in doxycycline-treated controls when compared to untreated tumors. This would not likely be a direct effect of doxycycline regulating RANK expression in tumor cells, since control tumor transplants in immunodeficient hosts do not show this reduction in RANK expression after having received doxycycline treatment. It could however be the result of changes in the tumor microenvironment, for instance due to a reduction in pro-inflammatory cytokines secreted by infiltrating immune cells (Bode et al., 2014; Huang et al., 2011; Krakauer and Buckley, 2003; Tang et al., 2017). Few information is available regarding RANK expression regulation, with only one publication linking Krüppel-like factor 5 (KLF5) as a direct transcriptional regulator of RANK (Ma et al., 2017), but inflammation in the tumor microenvironment could very well affect the expression of this TNFRSF member.

Given the differences between mouse models and clinical data, it might be advisable to analyze immune infiltration changes with the RANK<sup>ΔK8</sup> model early after RANK depletion to better identify changes directly due to RANK pathway inhibition and avoid longer-term effects which might confound the conclusions.

Beyond changes in the immune system, RANK depletion in tumor cells might have additional systemic effects which could be contributing to primary tumor growth. Several cytokines were altered in the serum of RANK<sup>ΔK8</sup> mice as compared with controls, regardless of whether mice were under the early or late RANK depletion protocol. Downregulation of IGF-I and its transporter proteins (IGFBP-3, -5 and -6) might be both a contributing cause for the decrease in tumorigenesis or a consequence of this observed decrease in tumor burden in RANK<sup>ΔK8</sup> mice. The decrease in the abundance of these proteins could be validated in other models of RANK depletion available in our group (Ubiquitin-cre;RANK<sup>flox/flox</sup>;MMTV-PyMT) and in PDX models of breast cancer treated with RANKL inhibitors. IGF-I has been described to be essential for MG development (Ruan and Kleinberg, 1999), with overexpression of IGF-I during pregnancy/lactation causing MG hypertrophy and failure to recover homeostatic ductal morphology (Hadsell et al., 1996), and overexpression of the receptor (IGF1R) under the MMTV promoter leading to incomplete fat pad invasion and hypertrophic lesions which progress into tumors (Farabaugh et al., 2020; Jones et al., 2007) enriched with K8+K14+ cells (Farabaugh et al., 2020). Interestingly K8+K14+ cells are also more abundant in PyMT tumors with RANK overexpression (Benítez et al., 2021). Importantly, IGF-I blood levels (but not IGFBP-3) were strongly associated with a higher breast cancer risk, in both pre- and postmenopausal women, further highlighting the importance of this pathway in breast cancer (Murphy et al., 2020). IGF-I has been described to decrease OPG and increase RANKL transcription in bone cell lines, and to decrease OPG levels in human serum (Rubin et al., 2002), while IGF-I treatment *in vivo* was described to downregulate RANK expression in pancreatic β-islet cells (although a direct effect was not demonstrated) (Chen et al., 2004). A direct effect between the IGF-I pathway and RANK loss in tumor cells should still be validated, since regulation of serum IGF-I and IGFBPs can be mediated by several hormones, the most important being the Growth Hormone (GH), secreted by the pituitary gland (Laban et al., 2003). In fact, the main source of IGF proteins is the liver, where the epithelial compartment (hepatocytes and cholangiocytes) is K8+ (Ku et al., 2016; Laban et al., 2003), and thus could also undergo RANK depletion and be mediating systemic differences in several serum proteins. IGF-I or IGFBP3 serum level changes upon RANK depletion could be quantified by ELISA and compared between NSG mice bearing RANK<sup>ΔK8</sup>

tumor transplants and C57/Bl6; RANK<sup>ΔK8</sup> hosts bearing PyMT tumor transplant to identify whether RANK status in tumor cells v.s other organs are the source of protein level changes. If validated, serum from denosumab-treated patients from the D-BIOMARK study, currently performed in our group, could be analyzed to validate the relevance of these observations in breast cancer patients. Regardless of the organ where RANK depletion is driving these changes, an indirect effect might be also mediating these observations. For instance, estrogen has been described to regulate IGF-I pathway, with estradiol upregulating IGF1R expression on breast cancer cell lines (Iida et al., 2019) and tamoxifen inhibiting IGF-I production and increasing serum IGFBP-3 levels (Campbell et al., 2001; Huynh et al., 1993).

RANK depletion in other K8+ tissues, and not only luminal MG/tumor RANK depletion, might also be contributing to the different phenotypes seen in this model. K8+ cells are present in the thymic epithelial cells, intestinal/colon epithelia, skin hair follicles, bladder, lung and uterus epithelial cells. in hepatocytes and biliary ducts (Zhang et al., 2012). The role for RANK pathway in T cell development in the thymus (Gardner et al., 2008; Khan et al., 2014; McCarthy et al., 2015; Rossi et al., 2007) as well as for M cell formation in the intestine/colon (Kanaya et al., 2018; Mutoh et al., 2016; Rios et al., 2016) or in the mucosal immunity in the lower airway (Kimura et al., 2019b) might affect the systemic performance of the immune system, with potential effects on the tumor immune response, adding on the effects which might be locally established by depleting RANK in epithelial cells within the tumor microenvironment (luminal untransformed MG epithelium) and tumor cells (Gómez-Aleza et al., 2020). In the lung, RANK has been described to rewire mitochondrial bioenergetics, both in untransformed and tumoral epithelial cells (Rao et al., 2017), a mechanism which could affect the niche of MMTV-PyMT metastatic cells. In the skin, RANK pathway in cells from the hair follicle has been described to be necessary for the proliferation of cells involved in entering into the anagen stage from the hair cycle (Duheron et al., 2011), although the contribution of these described roles for RANK in the skin to our observations in the RANK<sup>ΔK8</sup> models is less clear. Preliminary results with MMTV-PyMT wt tumor cell transplants into syngeneic RANK<sup>ΔK8</sup> hosts suggest that the contribution of RANK deletion in K8 organs other than the tumor cells does not strongly alter tumor latency or growth. However, the number of mice used in these experiments was low and an effect during earlier steps of tumorigenesis cannot be fully discarded.

Besides the importance of considering these organs when interpreting the results obtained with the RANK<sup>ΔK8</sup> mouse model, the implications of these context-dependent roles for RANK

pathway in different organs are of especial relevance when considering the pharmacological inhibition of RANKL in the clinic. Most of the studies evaluating denosumab in solid tumors have been designed to build upon its proven effects on alleviating skeletal-related events and pain (Vadhan-Raj et al., 2012). Late-stage studies evaluating its effects in clinical outcomes revealed no improvement in overall survival or bone-metastasis-free survival in lung cancer (Peters et al., 2020) or early breast cancer (D-CARE) (Coleman et al., 2020), but did however report prolonged BMFS in prostate cancer (NCT00286091, see results section in ClinicalTrials.gov). Result readouts are still pending for other tumor types, such as metastatic RCC (MOSCAR clinical trial, NCT03408652) and bladder cancer (NCT03520231). Additionally, the increasing preclinical evidences regarding the potential of RANK pathway inhibition in immune-oncology (Ahern et al., 2017, 2018; Gómez-Aleza et al., 2020; Khan et al., 2014) support the combination of denosumab with immune checkpoint inhibitors both in immune “cold” and “hot” tumor subtypes. In lung cancer, an ongoing phase 2 study in patients with bone metastases (DENIVOS), will explore combining denosumab and nivolumab (anti-PD-1). In melanoma, there are currently two small exploratory studies evaluating denosumab in combination with checkpoint inhibitors (NCT03161756 and NCT03620019). Although it is still early to know whether these combinations will bring a new clinical perspective to the use of denosumab, and the three studies are performed in immunologically “hot” tumors, our data suggest that the effects of immune checkpoint and RANKL inhibition might have added effects also in tumors not classically responding to immune checkpoint blockade.

Regarding the role of RANK pathway depletion in the RANK<sup>ΔK8</sup> model in lung metastasis, our data confirms previous observations associating loss of RANK with a lower lung mutational burden in RANK<sup>-/-</sup> tumor transplants (Yoldi et al., 2016). However, it is again striking that the phenotype is stronger when depleting RANK late during tumorigenesis (in fact, the differences are only statistically significant for the late and not the early RANK depletion protocols). The high variability of the model could be masking some of the observations, but also the systemic effects of doxycycline could be affecting the results differently depending on the timing of administration. Additionally, RANK expression should be assessed in the metastatic nodules to confirm whether RANK is also not expressed in these metastatic tumor cells, although RANK depletion could have occurred once the tumor cells had already metastasized if they remain K8+. A decrease in lung metastatic burden is observed in doxycycline-treated controls compared with lungs from untreated mice, reinforcing the dramatic systemic effects of doxycycline. Remarkably, analysis of lungs from



immunodeficient hosts bearing RANK<sup>ΔK8</sup> tumors under the fluorescent magnifier revealed that the combination of aRL treatment and tumor RANK loss showed a tendency to have stronger effects than the aRL or tumor RANK depletion alone. RANK depletion in tumor cells induced by doxycycline treatment had a medium effect, while aRL, which would trigger systemic inhibition of RANK pathway, had no reduction in lung tumor burden compared with control lungs. This observation would need to be verified in further experiments. However, if confirmed, it could indicate that RANK could play a RANKL-independent role, at least in the metastatic setting. RANK ligand-independent activation has been reported but only in models of overexpression (Das et al., 2014; Kanazawa and Kudo, 2005; Palafox et al., 2012a). In these models, higher density of receptors in the cell membrane could be leading to a higher affinity during the pre-ligand assembly (Chan, 2007; Kanazawa and Kudo, 2005; Wajant, 2015) of the receptor trimers, which might induce a ligand-independent recruitment of TRAF adaptors. Whether the ligand-independent activation of RANK is possible at physiological levels has not yet been reported.

Another possibility is that blocking RANKL could be liberating OPG, its decoy receptor, which is also known to bind TRAIL (Emery et al., 1998; Infante et al., 2019). Upon binding its target receptors, TRAIL would induce apoptosis, while OPG would inhibit this effect *in vitro* (Emery et al., 1998), a mechanism also described for breast cancer cell lines (Holen et al., 2005; Rachner et al., 2009). Importantly, this protective effect of OPG is blocked when adding RANKL to the culture (Rachner et al., 2009; Zinonos et al., 2011). *In vivo*, however, the anti-apoptotic effect of OPG in breast cancer cell lines implanted in the bone is blocked, even in OPG-overexpressing cell lines, through a mechanism suggested to be mediated by high RANKL levels in the bone microenvironment (Zinonos et al., 2011). It would have been interesting to know whether the inhibition of TRAIL-induced apoptosis would be recovered by treating with aRL in this model. This mechanism would agree with the results seen in the lung metastasis from RANK<sup>ΔK8</sup> transplanted tumors. Metastasis size seems slightly larger when only treating with aRL, which could be due to a reduction of TRAIL-mediated apoptosis in the metastatic niche. RANK depletion in tumor cells would have the combined effect of blocking RANK pathway in tumor cells and increasing TRAIL-mediated apoptosis, by switching the binding equilibrium of OPG-TRAIL towards OPG-RL in order to compensate for the lack of RANK-RL binding. This delicate balance between the interactions of the ligands, decoys and receptors from the RANK and TRAIL pathway could be behind the exacerbated phenotype when combining both RANK depletion and RANKL systemic

inhibition, since RANK depletion could compensate for the decrease in available free-RL which could be affecting OPG-TRAIL equilibrium *in vivo*.

Another putative explanation for the differences seen would be a technical one. Doxycycline needs to be administered together with a high concentration of sucrose in drinking water to compensate for its sour taste (see Methods section). Controls from the transplant experiments in immunodeficient mice should also have received sucrose to compensate for the metabolic effects that this substance could have, but we failed to identify this crucial control for the experiments presented here. This could especially affect results in the tumor transplant models in immunodeficient mice, since the strains chosen spontaneously develop Type I Diabetes at 10-14 weeks of age (King, 2012) (before tumor implantation). Future experiments would compare adding sucrose or not to drinking water in the controls to discard a metabolic effect driving our observations.

Overall, results from the RANK<sup>ΔK8</sup> model confirm previous reports associating RANK pathway to mammary gland tumorigenesis and open the possibility to study RANK depletion at selected stages of primary tumor development where RANK pathway could be playing different context-dependent roles. Additionally, it opens the possibility for evaluating the role of RANK pathway in establishing systemic changes relevant for tumorigenesis and studying the effects of RANK loss in other K8+ tissues.

### Discussion on Chapter 3: RANK pathway in intestinal epithelium.

The TNFRSF proteins are known to have very diverse and context-dependent functions, with complex regulation layers molding their effects on different tissues (Locksley et al., 2001; Medler et al., 2019; Wajant, 2015). RANK pathway is known to play key roles in the bone, the mammary gland, the skin and immune populations (González-Suárez and Sanz-Moreno, 2016; Infante et al., 2019).

RANK protein's remarkably high expression levels on human and murine intestinal and colon epithelia as compared to other organs led to the hypothesis that the pathway could be involved in biological processes other than M cell differentiation (Kanaya et al., 2012; Kimura et al., 2015a, 2020; Knoop et al., 2009; Rios et al., 2016). It was tempting to speculate that so much energy would not be employed to transcribe and translate a protein for the sole purpose of priming the few intestinal epithelial cells which migrate over RANKL-high GALT regions. M cells are a small percentage (10-20%) of FAE (Kimura et al., 2020), which makes them an even scarcer cell population when considering the intestine and colon epithelia as a whole.

However, upon deletion of RANK pathway specifically on intestinal and colon epithelia, there were no evident morphological changes based on H&E or basic stainings. Villin-Cre RANK<sup>flox/flox</sup> intestinal organoid growth and maintenance capacity also remained intact, although they were indeed unresponsive to RANKL-mediated M cell differentiation *in vitro* (de Lau et al., 2012). Interestingly, we observed that a high RANKL concentration, used in previous publications of our group (Yoldi et al., 2016), was actually detrimental for organoid structure maintenance. This organoid disassembly observed after strong RANK activation was highly unexpected, given the described role of the pathway in mammary epithelium survival and proliferation (Beleut et al., 2010; Joshi et al., 2010, 2015b). Gene expression analyses of Wnt and EMT-related genes do not suggest that a stronger activation of the pathway may lead to a direct effect on WNT pathway, essential for intestinal stem cell maintenance (Clevers, 2013), or on EMT programs. This further highlights the differences between RANK pathway on intestinal epithelium versus the mammary gland, where RANKL stimulation has been described to control *Rspo1* expression (Joshi et al., 2015a; Yoldi et al., 2016) and induce EMT (Palafox et al., 2012b).

The gradient of RANK protein expression observed in intestinal epithelium and inferred from microarray data on colon epithelium has not been previously described before, maybe due

to the issues reported for RANK IHC (Infante et al., 2019). This gradient may be a mechanism to avoid differentiation of stem cells or Paneth cells into M cells upon encounter with RL. RANKL is restricted to GALT, which is not directly in contact with intestinal crypts (Kimura et al., 2020; Nagashima et al., 2017). However, under inflammatory conditions, immune infiltration and tertiary immune structures are more abundant. This could cause previously unexposed regions of intestinal epithelium to be in contact with RANKL+ cells such as activated T cells, ILCs or reticular cells (Nagashima et al., 2017). Indeed, villi enterocytes have been demonstrated to differentiate into M cells when exposed to ectopic RL (Kimura et al., 2015a; Knoop et al., 2009). This might be the reason why high RANKL concentration affects organoid integrity after 5 days. At lower concentrations, stem cells and/or their neighboring Paneth cells (source of Wnt ligands (Clevers, 2013; Spit et al., 2018)) may not be stimulated by RANKL, since most of the RANKL molecules would bind to RANK receptors present in more abundant numbers in differentiated enterocytes. It is known that TNFRSF activation often relies on the pre-clustering of receptors. This receptor grouping is induced by proximity and abundance of the receptors in specific membrane regions, increasing their affinity for the ligand (Chan, 2007; Muppidi and Siegel, 2004; Wajant, 2015). Thus, in the scenario of a chemical equilibrium between RANKL and RANK, RANK receptors which are not pre-clustered due to their lower abundance on the cell membrane could only bind RANKL when it is present at high concentrations. Indeed, when intestinal organoids were transiently treated with RANKL, those receiving lower doses were seen to recover some of their branching ability, while those treated with higher doses presented lower viability and remained swollen and without branching, with strong expression of M cell markers. However, it is unclear whether soluble RANKL could be found in the intestine/colon due to the technical difficulty to detect it and differentiate it from membrane-bound form. Despite lack of changes in M cell differentiation were reported with a mouse model expressing an uncleavable version of RANKL (Nagashima et al., 2017), the contribution of the soluble splicing variants of RANKL is unknown and might change in the context of inflammation or cancer.

Further mechanisms to avoid M cell differentiation in the intestinal crypts might be present through OPG upregulation. A recent publication identified M cells as a source of OPG, describing how M cell numbers are regulated in the FAE despite all epithelial cells being in contact with RANKL-expressing cells (Kimura et al., 2020). Indeed, OPG upregulation was observed in our intestinal organoids upon RANKL stimulation, further supporting this regulatory mechanism, although expression levels remained too low to reach statistical

significance. Interestingly, upon Wnt stimulation, OPG levels were remarkably high, reaching a 10-fold upregulation compared to untreated controls. An active Wnt pathway may suppress M cell differentiation through the secretion of OPG, creating yet another crypt-villi gradient to compartmentalize intestinal cell populations (Clevers, 2013; Spit et al., 2018). The high RANKL concentration used in our experimental setting might surpass the physiological levels reached *in vivo*. The OPG levels locally secreted by intestinal organoid subpopulations in contact with Wnt ligands might not be sufficient to inhibit RANKL molecules under these circumstances, thus affecting organoid integrity through differentiation of all cell populations into M cells. Therefore, Wnt pathway might be actively controlling RANK pathway activation through OPG secretion.

Besides activation by RL, RANK has also been described to present ligand-independent signaling and upregulation of NF $\kappa$ B targets when overexpressed (Palafox et al., 2012b). Therefore, it could be possible that the high expression levels of RANK in the intestinal epithelium could present this ligand-independent activity. Driving RANK expression to the intestinal stem-cell compartment with targeted RANK-overexpression mouse models could validate whether the lower expression levels of RANK at the crypt are necessary for epithelial homeostasis and tumor initiation.

As an additional layer of regulation, RANKL has been described to bind to the Lgr4 receptor in osteoclasts (Luo et al., 2016b). Lgr4, together with intestinal stem-cell marker Lgr5, binds R-Spondins and is essential to potentiate Wnt/B-catenin signaling (Carmon et al., 2011). Lgr4 is expressed on intestinal crypts, within the transit-amplifying region and its depletion results in perinatal lethality due to its role in intestinal epithelial cell proliferation and Paneth cell differentiation (Li et al., 2015). We did not observe any changes in any of the genes evaluated in Villin-cre RANK<sup>flox/flox</sup> intestinal organoids treated with RANKL to identify whether the RANKL-Lgr4 pathway might also play a role in the intestine, such as that described in osteoclasts. However, a genome-wide approach would be needed to fully discard the possibility that RANKL signaling through Lgr4 could be activated in the intestine, since the targets that we selected might not be appropriate for this context. Even if this signaling could be detected *in vitro*, the expression restriction of RANKL to the GALT and Lgr4 to the crypts might limit the interaction between these two molecules under homeostatic conditions.

Overall, our data suggest that RANK pathway is limited to prompt M cell differentiation in intestinal epithelium upon the encounter with RANKL in homeostatic conditions. Its broad

expression could then be a mechanism to increase M cell numbers in case of inflammation or other pathogenic conditions which increase the concentration of RANKL-positive cells in the stromal compartment immediately beneath intestinal epithelium (Parnell et al., 2016).

Indeed, administration of bacterial proteins, such as cholera toxin, or inflammatory molecules, such as DSS, induced a significant increase in M cells in both small intestine and colon epithelium (Bennett et al., 2016; Parnell et al., 2016; Wang et al., 2011). RANKL levels on tertiary lymphoid structures have been reported to increase after DSS administration (Parnell et al., 2016), although in this study the increase in colonic M cells was attributed to TNF $\alpha$  signaling through TNFR2 and not to RANK pathway (Parnell et al., 2016).

M cell numbers might be important during inflammation-induced colorectal carcinogenesis. The increased number of M cells, which result in secretion of IgA by B cells, have already been described to protect from colitis induced by DSS (Kanaya et al., 2018). By contrast, Villin-Cre Rank<sup>flox/flox</sup> mice have been described to have defective IgA intestinal production (Rios et al., 2016). However, our data suggest that loss of RANK in intestinal epithelium has no effect on the severity of inflammation-induced colorectal cancer. The high variability of the AOM/DSS model might be detrimental for the observation of subtle effects derived from changes in mucosal immunology reported by others (Kimura et al., 2020; Knoop et al., 2009; Rios et al., 2016). However, these experiments did reveal a previously unknown feature of the adenomas developed after the AOM/DSS carcinogenic protocol. RANK expression was commonly downregulated in adenomas as compared with untransformed colonic epithelium. The RANK-high epithelial patches within the adenomas often inversely correlated with active Wnt signaling, reminiscent of what was observed in normal epithelium, where RANK levels are lower in the crypts. The levels of nuclear  $\beta$ -catenin were not remarkably higher in Villin-Cre Rank<sup>flox/flox</sup> adenomas, thus discarding RANK pathway as a direct modulator of Wnt signaling in colon epithelium.

The most plausible explanation for the inverse correlation would thus be that high RANK expression is a feature of differentiated intestinal epithelial cells. This contrasts with the MMTV-PyMT mouse model, where RANK is greatly upregulated during tumorigenesis compared to normal mammary gland epithelium. In this model, however, RANK expression is markedly higher on earlier stages of tumorigenesis compared to the carcinoma stage (Yoldi et al., 2016). Interestingly, methylation of RANK promoter was reported to be commonly found in gliomas, increasing with the aggressiveness of the tumors (von dem Knesebeck et al., 2012). Whether this is also the case in colorectal carcinomas remains to

be elucidated. Breast cancer data actually point to an opposite direction, since RANK levels correlate with worse prognosis and the most aggressive breast cancer subtype: TNBC (Palafox et al., 2012a; Reyes et al., 2017; Santini et al., 2011). However, given the broad differences observed between intestinal and mammary gland epithelium regarding RANK pathway, the mechanism involved during tumorigenesis might be quite diverse depending on the epithelium of origin.





# CONCLUSIONS



1. RANK pathway in tumor cells from PyMT transplants exerts an immunosuppressive microenvironment, enriched in myeloid cells, neutrophils and macrophages, and with low T cell infiltration, which promotes a faster tumor onset.
2. The microenvironment from RANK-null tumors has less pro-tumorigenic neutrophils, which allows the recruitment of CD8<sup>+</sup> T cells, which are the main mediators of the delayed tumor latency, although tumors finally evade the immune system through the upregulation of immune checkpoints and recruitment of Tregs
3. RANK pathway blockade in tumor cells potentiates the anti-tumor effect of anti-CTLA4 and anti-PD-L1 treatment early and late after tumor transplantation, respectively.
4. Neoadjuvant, single-agent denosumab increased TILs, T cells and CD8 T cell infiltration in early breast cancer tumors from premenopausal women
5. Higher serum sRANKL, intratumoral Tregs or tumor RANK activation were associated with the early BC patients who showed ≥10% TIL increase after denosumab treatment
6. RANK depletion in K8<sup>+</sup> cells delayed primary tumor latency, without affecting tumor growth, with a stronger reduction in tumor and metastatic nodules when RANK is depleted in growing tumors.
7. RANK depletion in primary PyMT tumors results in a reduced T cell infiltration and CD4/CD8 ratio, an increase in PD1 expression in T cells and systemic serum protein level changes including ICAM1 upregulation and downregulation of IGF-I
8. RANK depletion in PyMT tumor transplanted in immunodeficient hosts delays tumor onset and reduces lung metastasis in combination with RANKL inhibitors in a primary-tumor-dependent manner.
9. RANK is highly expressed in intestinal and colon epithelium, with lower expression at the bottom of the crypt, while RANKL expression is restricted to the subepithelial region of the GALT.
10. RANK pathway activation with RANKL is essential for the formation of M cells, with high RANKL levels resulting in intestinal organoid disintegration *in vitro*, maybe due to M-cell differentiation of the intestinal stem cells.
11. RANKL treatment does not alter the expression of WNT- or EMT-related genes but WNT activation might regulate RANK pathway through the induction of *Opg* and *Trail* upregulation

12. RANK loss on the intestinal epithelium or myeloid cells did not affect mouse weight or tumor burden in inflammation-driven colorectal tumorigenesis.
13. RANK expression is downregulated in colon adenomas, as compared to untransformed colon epithelium, with RANKL still restricted to tertiary immune structures, which are increased in the inflamed colon.
14. RANK loss does not result in changes on WNT pathway activation in adenomas but its expression inversely correlates with markers of WNT pathway activation, but its expression inversely correlates with markers of WNT pathway activation.

# **ACKNOWLEDGEMENTS**

(AGRADECIMIENTOS)



Quiero agradecer a la Dr. González por darme la oportunidad de hacer la tesis en su laboratorio y por haberme enseñado tanto, no solo a nivel científico, sino también a nivel personal. La tesis ha sido un período de crecimiento, y no habría sido posible realizarla sin el equipo de grandes científicos y personas que han pasado por el PEBC-6. Quiero agradecer a Sandra, que con su sola presencia llenaba el laboratorio de alegría (y sabiduría, ¡qué haríamos sin esa carpeta de protocolos!), a Jorge, mi primer “profe”, siempre con alguna broma para alegrarte las largas tardes, a Marinaki y Alexandra, mis compañeras de días interminables de experimentos, y Alex-macho, mi confidente, ¡da gusto oírte cuando estás emocionado por algún experimento! También quiero dar las gracias a Ana y EvaT, las postdocs que tanto me han enseñado durante todos estos años, y que me han dado la vida durante el último y triste año de tesis pandémica (que poquitas quedamos en el lab de Barcelona...), junto con Andrea, que es maravilloso hablar contigo, nos haces recordar la valía de lo que hacemos en investigación. Y también, cómo no mencionar a el postdoc chanante y el Hado, Fran y Enrique, bellísimas personas que te alegraban el día pese al estrés que tenían. Y por supuesto, Guille y Maria-Can-I, el equipo inmune, muchas gracias por enseñarme tanto y por hacer de un proyecto tan duro algo llevadero con vuestro buen rollo, bromas y compañerismo, ¡se os echó mucho de menos cuando marchasteis!

Y también, cómo no mencionar al resto de compañeros de ese pasillo mítico que ahora está tan cambiado. Marta, Laura, Adriá-primero y segundo y Joan, gracias por todos los buenos ratos, fue una pena cuando nuestros labos se separaron. Las master, María, Ballenita, Ilaria, Elba y Mikel, ¡qué tiempos aquellos en los que éramos tantos que no teníamos ni sillas para todos! También ese ajetreado pasillo y sala de cultivos, echaré de menos todas las bromas y charlas con vosotros, Paula, Alba, Xec, Vanessa, Pere, Manu, Clara... Demasiados para poner a todo el PEBC. Gracias por todo el buen rollo y las risas. Y por supuesto, mi doctorado habría sido mucho más difícil sin la ayuda de profesionales tan resolutivas, sabias y generosas como Esther y Bea, ¡gracias por todo vuestro apoyo en los largos días de citómetro!

Ahora todo se recuerda con morriña, porque pese a que hacer un doctorado es duro, también sé que es un momento de mi vida que recordaré con mucho cariño. Lo malo se olvida y los buenos momentos con todos vosotros siempre dejarán una sensación de añoranza.

Quiero agradecer a mi familia, por todo su apoyo durante no sólo la tesis, sino durante toda mi vida, haciéndome sentir que no importa lo que me proponga, ellos siempre estarán ahí

para apoyarme y creer en mí. Me hacéis sentir una tranquilidad abrumadora al saber lo mucho que nos queremos. Y por supuesto, también doy las gracias a Marcos, que ha compartido todos estos años conmigo, muchas gracias por ayudarme a crecer y a conocerme mejor, por los increíbles momentos juntos que hacen poner de lado todos los problemas para retomarlos después con energía y aplomo para afrontarlos, por motivarme, escucharme y compartir su ilusión por la ciencia y por tantas otras muchas cosas, ¡gracias!

También quiero dar las gracias a mis amigos de toda la vida, Marina, Moisés, Miguel, Carlos, Vallejo, me siento muy afortunada de teneros en mi vida y sentir que da igual lo lejos que estemos y el tiempo que pase, siempre me sentiré como en casa al estar con vosotros. And of course, my dear Penguins, María, Verito, Dan, Ana peanuts, EleMele, Iratita and Helena, thank you so much for all those moments during the master and the penguin-reunions, hopefully we can see each other soon in a place other than a PC screen!

Por último, cómo no olvidar también agradecer el apoyo a los amigos que me han aguantado todas las quejas y me han alegrado el día con cervezas y compañía durante todos estos años en Barcelona: Luis, Rodrigo, Pancho, Carlos, las Elenas, Almu, María, Ernest, Marc, Sofía, Ernest, Javi, Janire, Jacobo, Barri y Enrique.

¡Muchísimas gracias a todos!



# **BIBLIOGRAPHY**



- Adams, S., Gatti-Mays, M.E., Kalinsky, K., Korde, L.A., Sharon, E., Amiri-Kordestani, L., Bear, H., McArthur, H.L., Frank, E., Perlmutter, J., et al. (2019). Current Landscape of Immunotherapy in Breast Cancer: A Review. *JAMA Oncol.* 5, 1205–1214.
- Ahern, E., Harjunpää, H., Barkauskas, D., Allen, S., Takeda, K., Yagita, H., Wyld, D., Dougall, W.C., Teng, M.W.L., and Smyth, M.J. (2017). Co-administration of RANKL and CTLA4 Antibodies Enhances Lymphocyte-Mediated Antitumor Immunity in Mice. *Clin. Cancer Res.* 23, 5789–5801.
- Ahern, E., Harjunpää, H., O'Donnell, J.S., Allen, S., Dougall, W.C., Teng, M.W.L., and Smyth, M.J. (2018). RANKL blockade improves efficacy of PD1-PD-L1 blockade or dual PD1-PD-L1 and CTLA4 blockade in mouse models of cancer. *Oncoimmunology* 7, e1431088.
- Akiyama, T., Shimo, Y., Yanai, H., Qin, J., Ohshima, D., Maruyama, Y., Asaumi, Y., Kitazawa, J., Takayanagi, H., Penninger, J.M., et al. (2008). The Tumor Necrosis Factor Family Receptors RANK and CD40 Cooperatively Establish the Thymic Medullary Microenvironment and Self-Tolerance. *Immunity* 29, 423–437.
- Allaoui, R., Bergenfelz, C., Mohlin, S., Hagerling, C., Salari, K., Werb, Z., Anderson, R.L., Ethier, S.P., Jirström, K., Pählman, S., et al. (2016). Cancer-associated fibroblast-secreted CXCL16 attracts monocytes to promote stroma activation in triple-negative breast cancers. *Nat. Commun.* 7, 1–14.
- Anders, K., Kershaw, O., Larue, L., Gruber, A.D., and Blankenstein, T. (2017). The immune system prevents recurrence of transplanted but not autochthonous antigenic tumors after oncogene inactivation therapy. *Int. J. Cancer* 141, 2551–2561.
- Anderson, D.M., Maraskovsky, E., Billingsley, W.L., Dougall, W.C., Tometsko, M.E., Roux, E.R., Teepe, M.C., DuBose, R.F., Cosman, D., and Galibert, L. (1997). A homologue of the TNF receptor and its ligand enhance T-cell growth and dendritic-cell function. *Nature* 390, 175–179.
- Andres, A.C., and Strange, R. (1999). Apoptosis in the Estrous and Menstrual Cycles. *J. Mammary Gland Biol. Neoplasia* 4, 221–228.
- Arron, J.R., Vologodskaya, M., Wong, B.R., Naramura, M., Kim, N., Gu, H., and Choi, Y. (2001). A Positive Regulatory Role for Cbl Family Proteins in Tumor Necrosis Factor-related Activation-induced Cytokine (TRANCE) and CD40L-mediated Akt Activation. *J. Biol. Chem.* 276, 30011–30017.
- Asano, T., Okamoto, K., Nakai, Y., Tsutsumi, M., Muro, R., Suematsu, A., Hashimoto, K., Okamura, T., Ehata, S., Nitta, T., et al. (2019). Soluble RANKL is physiologically dispensable but accelerates tumour metastasis to bone. *Nat. Metab.* 1, 868–875.
- Ashcroft, A.J., Cruickshank, S.M., Croucher, P.I., Perry, M.J., Rollinson, S., Lippitt, J.M., Child, J.A., Dunstan, C., Felsburg, P.J., Morgan, G.J., et al. (2003). Colonic dendritic cells, intestinal inflammation, and T cell-mediated bone destruction are modulated by recombinant osteoprotegerin. *Immunity* 19, 849–861.
- Ashkar, S., Weber, G.F., Panoutsakopoulou, V., Sanchirico, M.E., Jansson, M., Zawaideh, S., Rittling, S.R., Denhardt, D.T., Glimcher, M.J., and Cantor, H. (2000). Eta-1 (osteopontin): An early component of type-1 (cell-mediated) immunity. *Science* (80-. ). 287, 860–864.
- Asselin-Labat, M.-L., Vaillant, F., Sheridan, J.M., Pal, B., Wu, D., Simpson, E.R., Yasuda, H., Smyth, G.K., Martin, T.J., Lindeman, G.J., et al. (2010). Control of mammary stem cell function by steroid hormone signalling. *Nature* 465, 798–802.
- Atkins, G.J., Kostakis, P., Vincent, C., Farrugia, A.N., Houchins, J.P., Findlay, D.M., Evdokiou, A., and Zannettino, A.C. (2006). RANK Expression as a Cell Surface Marker of Human Osteoclast Precursors in Peripheral Blood, Bone Marrow, and Giant Cell Tumors of Bone. *J. Bone Miner. Res.*

21, 1339–1349.

Azim, H.A., Peccatori, F.A., Brohée, S., Branstetter, D., Loi, S., Viale, G., Piccart, M., Dougall, W.C., Pruneri, G., and Sotiriou, C. (2015). RANK-ligand (RANKL) expression in young breast cancer patients and during pregnancy. *Breast Cancer Res.* *17*, 24.

Bachmann, M.F., Wong, B.R., Josien, R., Steinman, R.M., Oxenius, A., and Choi, Y. (1999). TRANCE, a Tumor Necrosis Factor Family Member Critical for CD40 Ligand-independent T Helper Cell Activation. *J. Exp. Med.* *189*, 1025–1031.

Baik, S., Sekai, M., Hamazaki, Y., Jenkinson, W.E., and Anderson, G. (2016). Relb acts downstream of medullary thymic epithelial stem cells and is essential for the emergence of RANK(+) medullary epithelial progenitors. *Eur. J. Immunol.* *46*, 857–862.

Banck, G., and Forsgren, A. (1979). Antibiotics and suppression of lymphocyte function in vitro. *Antimicrob. Agents Chemother.* *16*, 554–560.

Bando, J.K., Gilfillan, S., Song, C., McDonald, K.G., Huang, S.C.-C., Newberry, R.D., Kobayashi, Y., Allan, D.S.J., Carlyle, J.R., Cella, M., et al. (2018). The Tumor Necrosis Factor Superfamily Member RANKL Suppresses Effector Cytokine Production in Group 3 Innate Lymphoid Cells. *Immunity* *48*, 1208-1219.e4.

Bates, G.J., Fox, S.B., Han, C., Leek, R.D., Garcia, J.F., Harris, A.L., and Banham, A.H. (2006). Quantification of Regulatory T Cells Enables the Identification of High-Risk Breast Cancer Patients and Those at Risk of Late Relapse. *J. Clin. Oncol.* *24*, 5373–5380.

Baxter, R.C. (2014). IGF binding proteins in cancer: Mechanistic and clinical insights. *Nat. Rev. Cancer* *14*, 329–341.

Beleut, M., Rajaram, R.D., Caikovski, M., Ayyanan, A., Germano, D., Choi, Y., Schneider, P., and Brisken, C. (2010). Two distinct mechanisms underlie progesterone-induced proliferation in the mammary gland. *107*, 2989–2994.

Benítez, S., Cordero, A., Santamaría, P.G., Redondo-Pedraza, J., Rocha, A.S., Collado-Solé, A., Jimenez, M., Sanz-Moreno, A., Yoldi, G., Santos, J.C., et al. (2021). RANK links senescence to stemness in the mammary epithelia, delaying tumor onset but increasing tumor aggressiveness. *Dev. Cell.*

Bennett, K.M., Parnell, E.A., Sanscartier, C., Parks, S., Chen, G., Nair, M.G., and Lo, D.D. (2016). Induction of Colonic M Cells during Intestinal Inflammation. *Am. J. Pathol.* *186*, 1166–1179.

Bertolin, K., and Murphy, B.D. (2014). Reproductive Tract Changes During the Mouse Estrous Cycle. In *The Guide to Investigation of Mouse Pregnancy*, (Elsevier), pp. 85–94.

Bode, C., Diedrich, B., Muenster, S., Hentschel, V., Weisheit, C., Rommelsheim, K., Hoeft, A., Meyer, R., Boehm, O., Knuefermann, P., et al. (2014). Antibiotics regulate the immune response in both presence and absence of lipopolysaccharide through modulation of Toll-like receptors, cytokine production and phagocytosis in vitro. *Int. Immunopharmacol.* *18*, 27–34.

Bolger, A.M., Lohse, M., and Usadel, B. (2014). Trimmomatic: A flexible trimmer for Illumina sequence data. *Bioinformatics* *30*, 2114–2120.

Bonifaci, N., Palafox, M., Pellegrini, P., Osorio, A., Benítez, J., Peterlongo, P., Manoukian, S., Peissel, B., Zaffaroni, D., Roversi, G., et al. (2011). Evidence for a link between TNFRSF11A and risk of breast cancer. *Breast Cancer Res. Treat.* *129*, 947–954.

Böttcher, J.P., Bonavita, E., Chakravarty, P., Blees, H., Cabeza-Cabrerizo, M., Sammiceli, S., Rogers, N.C., Sahai, E., Zelenay, S., and Reis e Sousa, C. (2018). NK Cells Stimulate Recruitment

of cDC1 into the Tumor Microenvironment Promoting Cancer Immune Control. *Cell* 172, 1022-1037.e14.

Boyce, B.F., Xiu, Y., Li, J., Xing, L., and Yao, Z. (2015). NF- $\kappa$ B-Mediated Regulation of Osteoclastogenesis. *Endocrinol. Metab. (Seoul, Korea)* 30, 35–44.

Brandtzaeg, P., Kiyono, H., Pabst, R., and Russell, M.W. (2008). Terminology: nomenclature of mucosa-associated lymphoid tissue. *Mucosal Immunol.* 1, 31–37.

Briskin, C., and Ataca, D. (2015). Endocrine hormones and local signals during the development of the mouse mammary gland. *Wiley Interdiscip. Rev. Dev. Biol.* 4, 181–195.

Broz, M.L., Binnewies, M., Boldajipour, B., Nelson, A.E., Pollack, J.L., Erle, D.J., Barczak, A., Rosenblum, M.D., Daud, A., Barber, D.L., et al. (2014). Dissecting the Tumor Myeloid Compartment Reveals Rare Activating Antigen-Presenting Cells Critical for T Cell Immunity. *Cancer Cell* 26, 638–652.

Buchbinder, E.I., and Desai, A. (2016). CTLA-4 and PD-1 pathways similarities, differences, and implications of their inhibition. *Am. J. Clin. Oncol. Cancer Clin. Trials* 39, 98–106.

Buisseret, L., Garaud, S., De Wind, A., Van den Eynden, G., Boisson, A., Solinas, C., Gu-Trantien, C., Naveaux, C., Lodewyckx, J.N., Duvillier, H., et al. (2017). Tumor-infiltrating lymphocyte composition, organization and PD-1/PD-11 expression are linked in breast cancer. *Oncoimmunology* 6.

Cairns, L., and Curigliano, G. (2016). Highlights from the 38th SABCS annual meeting, 8th – 12th December 2015, San Antonio, USA. *Ecancermedalscience* 10, 618.

Camara, A., Cordeiro, O.G., Alloush, F., Sponsel, J., Chypre, M., Onder, L., Asano, K., Tanaka, M., Yagita, H., Ludewig, B., et al. (2019). Lymph Node Mesenchymal and Endothelial Stromal Cells Cooperate via the RANK-RANKL Cytokine Axis to Shape the Sinusoidal Macrophage Niche. *Immunity* 50, 1467-1481.e6.

Campbell, M.J., Woodside, J. V., Secker-Walker, J., Titcomb, A., and Learthem, A.J.C. (2001). IGF status is altered by tamoxifen in patients with breast cancer. *J. Clin. Pathol. - Mol. Pathol.* 54, 307–310.

Carmon, K.S., Gong, X., Lin, Q., Thomas, A., and Liu, Q. (2011). R-spondins function as ligands of the orphan receptors LGR4 and LGR5 to regulate Wnt/ $\beta$ -catenin signaling. *Proc. Natl. Acad. Sci. U. S. A.* 108, 11452–11457.

Casbon, A.-J., Reynaud, D., Park, C., Khuc, E., Gan, D.D., Schepers, K., Passegué, E., and Werb, Z. (2015). Invasive breast cancer reprograms early myeloid differentiation in the bone marrow to generate immunosuppressive neutrophils. *Proc. Natl. Acad. Sci. U. S. A.* 112, E566.

Cenci, S., Weitzmann, M.N., Roggia, C., Namba, N., Novack, D., Woodring, J., and Pacifici, R. (2000). Estrogen deficiency induces bone loss by enhancing T-cell production of TNF- $\alpha$ . *J. Clin. Invest.* 106, 1229–1237.

Centonze, A., Lin, S., Tika, E., Sifrim, A., Fioramonti, M., Malfait, M., Song, Y., Wuidart, A., Van Herck, J., Dannau, A., et al. (2020). Heterotypic cell–cell communication regulates glandular stem cell multipotency. *Nature* 584, 608–613.

Chaisson, M.L., Branstetter, D.G., Derry, J.M., Armstrong, A.P., Tometsko, M.E., Takeda, K., Akira, S., and Dougall, W.C. (2004). Osteoclast Differentiation Is Impaired in the Absence of Inhibitor of  $\kappa$ B Kinase  $\alpha$ . *J. Biol. Chem.* 279, 54841–54848.

Chan, F.K.-M. (2007). Three is better than one: pre-ligand receptor assembly in the regulation of

TNF receptor signaling. *Cytokine* 37, 101–107.

Chan, F.K.-M., Chun, H.J., Zheng, L., Siegel, R.M., Bui, K.L., and Lenardo, M.J. (2000). A Domain in TNF Receptors That Mediates Ligand-Independent Receptor Assembly and Signaling. *Science* (80-. ). 288, 2351–2354.

Chang, J., Wang, Z., Tang, E., Fan, Z., McCauley, L., Franceschi, R., Guan, K., Krebsbach, P.H., and Wang, C.-Y. (2009). Inhibition of osteoblastic bone formation by nuclear factor-kappaB. *Nat. Med.* 15, 682–689.

Chen, N.J., Huang, M.W., Hsieh, S.L., Davis, J.E., and Siekierka, J.J. (2001). Enhanced secretion of IFN-gamma by activated Th1 cells occurs via reverse signaling through TNF-related activation-induced cytokine. *J. Immunol.* 166, 270–276.

Chen, W., Salojin, K. V., Mi, Q.-S., Grattan, M., Meagher, T.C., Zucker, P., and Delovitch, T.L. (2004). Insulin-Like Growth Factor (IGF)-I/IGF-Binding Protein-3 Complex: Therapeutic Efficacy and Mechanism of Protection against Type 1 Diabetes. *Endocrinology* 145, 627–638.

Chino, T., Draves, K.E., and Clark, E.A. (2009). Regulation of dendritic cell survival and cytokine production by osteoprotegerin. *J. Leukoc. Biol.* 86, 933–940.

Clausen, B.E., Burkhardt, C., Reith, W., Renkawitz, R., and Förster, I. (1999). Conditional gene targeting in macrophages and granulocytes using LysMcre mice. *Transgenic Res.* 8, 265–277.

Clevers, H. (2013). The intestinal crypt, a prototype stem cell compartment. *Cell* 154, 274–284.

Coates, A.S., Winer, E.P., Goldhirsch, A., Gelber, R.D., Gnant, M., Piccart-Gebhart, M.J., Thürlimann, B., Senn, H.J., André, F., Baselga, J., et al. (2015). Tailoring therapies-improving the management of early breast cancer: St Gallen International Expert Consensus on the Primary Therapy of Early Breast Cancer 2015. *Ann. Oncol.* 26, 1533–1546.

Coffelt, S.B., Kersten, K., Doornebal, C.W., Weiden, J., Vrijland, K., Hau, C.S., Versteegen, N.J.M., Ciampricotti, M., Hawinkels, L.J.A.C., Jonkers, J., et al. (2015). IL-17-producing  $\gamma\delta$  T cells and neutrophils conspire to promote breast cancer metastasis. *Nature* 522, 345–348.

Coffelt, S.B., Wellenstein, M.D., and De Visser, K.E. (2016). Neutrophils in cancer: Neutral no more. *Nat. Rev. Cancer* 16, 431–446.

Coleman, R., Finkelstein, D.M., Barrios, C., Martin, M., Iwata, H., Hegg, R., Glaspy, J., Periañez, A.M., Tonkin, K., Deleu, I., et al. (2020). Adjuvant denosumab in early breast cancer (D-CARE): an international, multicentre, randomised, controlled, phase 3 trial. *Lancet Oncol.* 21, 60–72.

Coleman, R.E., Finkelstein, D., Barrios, C.H., Martin, M., Iwata, H., Glaspy, J.A., Zhou, Y., Jandial, D., and Chan, A. (2018). Adjuvant denosumab in early breast cancer: First results from the international multicenter randomized phase III placebo controlled D-CARE study. *J. Clin. Oncol.* 36, 501–501.

Cordeiro, O.G., Chypre, M., Brouard, N., Rauber, S., Alloush, F., Romera-Hernandez, M., Bénézech, C., Li, Z., Eckly, A., Coles, M.C., et al. (2016). Integrin-Alpha IIb Identifies Murine Lymph Node Lymphatic Endothelial Cells Responsive to RANKL. *PLoS One* 11, e0151848.

Cordero, A., Pellegrini, P., Sanz-Moreno, A., Trinidad, E.M., Serra-Musach, J., Deshpande, C., Dougall, W.C., Pujana, M.A., and González-Suárez, E. (2016). Rankl Impairs Lactogenic Differentiation Through Inhibition of the Prolactin/Stat5 Pathway at Midgestation. *Stem Cells* 34, 1027–1039.

Cortes, J., Cescon, D.W., Rugo, H.S., Nowecki, Z., Im, S.-A., Yusof, M.M., Gallardo, C., Lipatov, O., Barrios, C.H., Holgado, E., et al. (2020). KEYNOTE-355: Randomized, double-blind, phase III study

of pembrolizumab + chemotherapy versus placebo + chemotherapy for previously untreated locally recurrent inoperable or metastatic triple-negative breast cancer. *J. Clin. Oncol.* 38, 1000–1000.

Cowan, J.E., Parnell, S.M., Nakamura, K., Caamano, J.H., Lane, P.J.L., Jenkinson, E.J., Jenkinson, W.E., and Anderson, G. (2013). The thymic medulla is required for Foxp3<sup>+</sup> regulatory but not conventional CD4<sup>+</sup> thymocyte development. *J. Exp. Med.* 210, 675–681.

Cremer, I., Dieu-Nosjean, M.-C., Maréchal, S., Dezutter-Dambuyant, C., Goddard, S., Adams, D., Winter, N., Menetrier-Caux, C., Sautès-Fridman, C., Fridman, W.H., et al. (2002). Long-lived immature dendritic cells mediated by TRANCE-RANK interaction. *Blood* 100, 3646–3655.

van Dam, P.A., Verhoeven, Y., Trinh, X.B., Wouters, A., Lardon, F., Prenen, H., Smits, E., Baldewijns, M., and Lammens, M. (2019). RANK/RANKL signaling inhibition may improve the effectiveness of checkpoint blockade in cancer treatment. *Crit. Rev. Oncol. Hematol.* 133, 85–91.

Darnay, B.G., Haridas, V., Ni, J., Moore, P.A., and Aggarwal, B.B. (1998). Characterization of the Intracellular Domain of Receptor Activator of NF- $\kappa$ B (RANK). *J. Biol. Chem.* 273, 20551–20555.

Darnay, B.G., Ni, J., Moore, P.A., and Aggarwal, B.B. (1999). Activation of NF- $\kappa$ B by RANK Requires Tumor Necrosis Factor Receptor-associated Factor (TRAF) 6 and NF- $\kappa$ B-inducing Kinase. *J. Biol. Chem.* 274, 7724–7731.

Das, S., Sepahi, I., Duthie, A., Clark, S., and Crockett, J.C. (2014). RANK receptor oligomerisation in the regulation of NF $\kappa$ B signalling. *J. Mol. Endocrinol.* 53, 81.

Davie, S.A., Maglione, J.E., Manner, C.K., Young, D., Cardiff, R.D., MacLeod, C.L., and Ellies, L.G. (2007). Effects of FVB/NJ and C57Bl/6J strain backgrounds on mammary tumor phenotype in inducible nitric oxide synthase deficient mice. *Transgenic Res.* 16, 193.

Davis, F.M., Lloyd-Lewis, B., Harris, O.B., Kozar, S., Winton, D.J., Muresan, L., and Watson, C.J. (2016). Single-cell lineage tracing in the mammary gland reveals stochastic clonal dispersion of stem/progenitor cell progeny. *Nat. Commun.* 7, 13053.

DeNardo, D.G., and Coussens, L.M. (2007). Inflammation and breast cancer. Balancing immune response: Crosstalk between adaptive and innate immune cells during breast cancer progression. *Breast Cancer Res.* 9.

DeNardo, D.G., Barreto, J.B., Andreu, P., Vasquez, L., Tawfik, D., Kolhatkar, N., and Coussens, L.M. (2009). CD4<sup>+</sup> T Cells Regulate Pulmonary Metastasis of Mammary Carcinomas by Enhancing Protumor Properties of Macrophages. *Cancer Cell* 16, 91–102.

Denkert, C., von Minckwitz, G., Darb-Esfahani, S., Lederer, B., Heppner, B.I., Weber, K.E., Budczies, J., Huober, J., Klauschen, F., Furlanetto, J., et al. (2018). Tumour-infiltrating lymphocytes and prognosis in different subtypes of breast cancer: a pooled analysis of 3771 patients treated with neoadjuvant therapy. *Lancet Oncol.* 19, 40–50.

Dieci, M.V., Guarneri, V., Bisagni, G., Tosi, A., Musolino, A., Spazzapan, S., Moretti, G., Vernaci, G.M., Giarratano, T., Lo Mele, M., et al. (2020). 162MO Neoadjuvant chemotherapy and immunotherapy in Luminal B BC: Results of the phase II GIADA trial. *Ann. Oncol.* 31, S304–S305.

Ding, H., and Wu, T. (2018). Insulin-like growth factor binding proteins in autoimmune diseases. *Front. Endocrinol. (Lausanne)*. 9, 499.

Dobin, A., Davis, C.A., Schlesinger, F., Drenkow, J., Zaleski, C., Jha, S., Batut, P., Chaisson, M., and Gingeras, T.R. (2013). STAR: ultrafast universal RNA-seq aligner. *Bioinformatics* 29, 15–21.

Dougall, W.C., Glaccum, M., Charrier, K., Rohrbach, K., Brasel, K., De Smedt, T., Daro, E., Smith, J., Tometsko, M.E., Maliszewski, C.R., et al. (1999a). RANK is essential for osteoclast and lymph

node development. *Genes Dev.* 13, 2412–2424.

Dougall, W.C., Glaccum, M., Charrier, K., Rohrbach, K., Brasel, K., De Smedt, T., Daro, E., Smith, J., Tometsko, M.E., Maliszewski, C.R., et al. (1999b). RANK is essential for osteoclast and lymph node development. *Genes Dev.* 13, 2412–2424.

Dufour, J.H., Dziejman, M., Liu, M.T., Leung, J.H., Lane, T.E., and Luster, A.D. (2002). IFN- $\gamma$ -Inducible Protein 10 (IP-10; CXCL10)-Deficient Mice Reveal a Role for IP-10 in Effector T Cell Generation and Trafficking. *J. Immunol.* 168, 3195–3204.

Duheron, V., Hess, E., Duval, M., Decossas, M., Castaneda, B., Klopper, J.E., Amoasii, L., Barbaroux, J.-B., Williams, I.R., Yagita, H., et al. (2011). Receptor activator of NF- $\kappa$ B (RANK) stimulates the proliferation of epithelial cells of the epidermo-pilosebaceous unit. *Proc. Natl. Acad. Sci.* 108, 5342–5347.

Eberl, G., Marmon, S., Sunshine, M.-J., Rennert, P.D., Choi, Y., and Littman, D.R. (2004). An essential function for the nuclear receptor ROR $\gamma$ t in the generation of fetal lymphoid tissue inducer cells. *Nat. Immunol.* 5, 64–73.

Eberl, G., Di Santo, J.P., and Vivier, E. (2015). The brave new world of innate lymphoid cells. *Nat. Immunol.* 16, 1–5.

Ellis, M.J., Suman, V.J., Hoog, J., Lin, L., Snider, J., Prat, A., Parker, J.S., Luo, J., DeSchryver, K., Allred, D.C., et al. (2011). Randomized phase II neoadjuvant comparison between letrozole, anastrozole, and exemestane for postmenopausal women with estrogen receptor-rich stage 2 to 3 breast cancer: Clinical and biomarker outcomes and predictive value of the baseline PAM50-based int. *J. Clin. Oncol.* 29, 2342–2349.

Emens, L.A., Cruz, C., Eder, J.P., Braiteh, F., Chung, C., Tolaney, S.M., Kuter, I., Nanda, R., Cassier, P.A., Delord, J.P., et al. (2019). Long-term Clinical Outcomes and Biomarker Analyses of Atezolizumab Therapy for Patients with Metastatic Triple-Negative Breast Cancer: A Phase 1 Study. *JAMA Oncol.* 5, 74–82.

Emens, L.A., Adams, S., Barrios, C.H., Dieras, V.C., Iwata, H., Loi, S., Rugo, H.S., Schneeweiss, A., Winer, E.P., Patel, S., et al. (2020). LBA16 IMpassion130: Final OS analysis from the pivotal phase III study of atezolizumab + nab-paclitaxel vs placebo + nab-paclitaxel in previously untreated locally advanced or metastatic triple-negative breast cancer. *Ann. Oncol.* 31, S1148.

Emery, J.G., McDonnell, P., Burke, M.B., Deen, K.C., Lyn, S., Silverman, C., Dul, E., Appelbaum, E.R., Eichman, C., DiPrinzio, R., et al. (1998). Osteoprotegerin is a receptor for the cytotoxic ligand TRAIL. *J. Biol. Chem.* 273, 14363–14367.

Engelhardt, J.J., Boldajipour, B., Beemiller, P., Pandurangi, P., Sorensen, C., Werb, Z., Egeblad, M., and Krummel, M.F. (2012). Marginating Dendritic Cells of the Tumor Microenvironment Cross-Present Tumor Antigens and Stably Engage Tumor-Specific T Cells. *Cancer Cell* 21, 402–417.

Fang, P., Li, X., Dai, J., Cole, L., Camacho, J.A., Zhang, Y., Ji, Y., Wang, J., Yang, X.-F., and Wang, H. (2018). Immune cell subset differentiation and tissue inflammation. *J. Hematol. Oncol.* 11, 97.

Farabaugh, S.M., Litzenger, B.C., Elangovan, A., Pecar, G., Walheim, L., Atkinson, J.M., and Lee, A. V. (2020). IGF1R constitutive activation expands luminal progenitors and influences lineage differentiation during breast tumorigenesis. *Dev. Biol.* 463, 77–87.

Fata, J.E., Kong, Y.Y., Li, J., Sasaki, T., Irie-Sasaki, J., Moorehead, R.A., Elliott, R., Scully, S., Voura, E.B., Lacey, D.L., et al. (2000a). The osteoclast differentiation factor osteoprotegerin-ligand is essential for mammary gland development. *Cell* 103, 41–50.



- Fata, J.E., Kong, Y.-Y., Li, J., Sasaki, T., Irie-Sasaki, J., Moorehead, R.A., Elliott, R., Scully, S., Voura, E.B., Lacey, D.L., et al. (2000b). The Osteoclast Differentiation Factor Osteoprotegerin-Ligand Is Essential for Mammary Gland Development. *Cell* 103, 41–50.
- Fata, J.E., Chaudhary, V., and Khokha, R. (2001). Cellular Turnover in the Mammary Gland Is Correlated with Systemic Levels of Progesterone and Not 17 $\beta$ -Estradiol During the Estrous Cycle. *Biol. Reprod.* 65, 680–688.
- Fearon, E.R. (2011). Molecular genetics of colorectal cancer. *Annu. Rev. Pathol.* 6, 479–507.
- De Filippo, K., Henderson, R.B., Laschinger, M., and Hogg, N. (2008). Neutrophil Chemokines KC and Macrophage-Inflammatory Protein-2 Are Newly Synthesized by Tissue Macrophages Using Distinct TLR Signaling Pathways. *J. Immunol.* 180, 4308–4315.
- Fluck, M.M., and Schaffhausen, B.S. (2009). Lessons in Signaling and Tumorigenesis from Polyomavirus Middle T Antigen. *Microbiol. Mol. Biol. Rev.* 73, 542.
- Franklin, R.A., Liao, W., Sarkar, A., Kim, M. V., Bivona, M.R., Liu, K., Pamer, E.G., and Li, M.O. (2014). The cellular and molecular origin of tumor-associated macrophages. *Science* (80- ). 344, 921–925.
- Franzoi, M.A., Romano, E., and Piccart, M. (2021). Immunotherapy for early breast cancer: too soon, too superficial, or just right? *Ann. Oncol.* 32.
- Franzoso, G., Carlson, L., Xing, L., Poljak, L., Shores, E.W., Brown, K.D., Leonardi, A., Tran, T., Boyce, B.F., and Siebenlist, U. (1997). Requirement for NF-kappaB in osteoclast and B-cell development. *Genes Dev.* 11, 3482–3496.
- Fridlender, Z.G., Sun, J., Kim, S., Kapoor, V., Cheng, G., Ling, L., Worthen, G.S., and Albelda, S.M. (2009). Polarization of Tumor-Associated Neutrophil Phenotype by TGF- $\beta$ : “N1” versus “N2” TAN. *Cancer Cell* 16, 183–194.
- Fu, N.Y., Nolan, E., Lindeman, G.J., and Visvader, J.E. (2020). Stem Cells and the Differentiation Hierarchy in Mammary Gland Development. *Physiol. Rev.* 100, 489–523.
- Fujimura, T., Kambayashi, Y., Furudate, S., Asano, M., Kakizaki, A., and Aiba, S. (2015). Receptor Activator of NF- $\kappa$ B Ligand Promotes the Production of CCL17 from RANK<sup>+</sup> M2 Macrophages. *J. Invest. Dermatol.* 135, 2884–2887.
- Fujimura, T., Kambayashi, Y., Furudate, S., Kakizaki, A., Hidaka, T., Asano, M., and Aiba, S. (2016). Receptor activator of nuclear factor kappa-B ligand (RANKL)/RANK signaling promotes cancer-related inflammation through M2 macrophages. *Exp. Dermatol.* 25, 397–399.
- Furuya, Y., Inagaki, A., Khan, M., Mori, K., Penninger, J.M., Nakamura, M., Udagawa, N., Aoki, K., Ohya, K., Uchida, K., et al. (2013). Stimulation of bone formation in cortical bone of mice treated with a receptor activator of nuclear Factor-B Ligand (RANKL)-binding peptide that possesses osteoclastogenesis inhibitory activity. *J. Biol. Chem.* 288, 5562–5571.
- Gardner, J.M., Devoss, J.J., Friedman, R.S., Wong, D.J., Tan, Y.X., Zhou, X., Johannes, K.P., Su, M.A., Chang, H.Y., Krummel, M.F., et al. (2008). Deletional tolerance mediated by extrathymic Aire-expressing cells. *Science* 321, 843–847.
- Gatti-Mays, M.E., Balko, J.M., Gameiro, S.R., Bear, H.D., Prabhakaran, S., Fukui, J., Disis, M.L., Nanda, R., Gulley, J.L., Kalinsky, K., et al. (2019). If we build it they will come: targeting the immune response to breast cancer. *Npj Breast Cancer* 5, 37.
- Germano, G., Lamba, S., Rospo, G., Barault, L., Magri, A., Maione, F., Russo, M., Crisafulli, G., Bartolini, A., Lerda, G., et al. (2017). Inactivation of DNA repair triggers neoantigen generation and

impairs tumour growth. *Nature* 552, 116–120.

Glass, D.A., Bialek, P., Ahn, J.D., Starbuck, M., Patel, M.S., Clevers, H., Taketo, M.M., Long, F., McMahon, A.P., Lang, R.A., et al. (2005). Canonical Wnt Signaling in Differentiated Osteoblasts Controls Osteoclast Differentiation. *Dev. Cell* 8, 751–764.

Gnant, M., Pfeiler, G., Dubsy, P.C., Hubalek, M., Greil, R., Jakesz, R., Wette, V., Balic, M., Haslbauer, F., Melbinger, E., et al. (2015). Adjuvant denosumab in breast cancer (ABCSCG-18): a multicentre, randomised, double-blind, placebo-controlled trial. *Lancet* 386, 433–443.

Gnant, M., Pfeiler, G., Steger, G.G., Egle, D., Greil, R., Fitzal, F., Wette, V., Balic, M., Haslbauer, F., Melbinger-Zeinitzer, E., et al. (2019). Adjuvant denosumab in postmenopausal patients with hormone receptor-positive breast cancer (ABCSCG-18): disease-free survival results from a randomised, double-blind, placebo-controlled, phase 3 trial. *Lancet. Oncol.* 20, 339–351.

Goldhirsch, A., Wood, W.C., Coates, A.S., Gelber, R.D., Thürlimann, B., Senn, H.-J., and Panel members, P. (2011). Strategies for subtypes—dealing with the diversity of breast cancer: highlights of the St. Gallen International Expert Consensus on the Primary Therapy of Early Breast Cancer 2011. *Ann. Oncol. Off. J. Eur. Soc. Med. Oncol.* 22, 1736–1747.

Gómez-Aleza, C., Nguyen, B., Yoldi, G., Ciscar, M., Barranco, A., Hernández-Jiménez, E., Maetens, M., Salgado, R., Zafeirolou, M., Pellegrini, P., et al. (2020). Inhibition of RANK signaling in breast cancer induces an anti-tumor immune response orchestrated by CD8<sup>+</sup> T cells. *Nat. Commun.* 11, 1–18.

Gonzalez-Suarez, E., Branstetter, D., Armstrong, A., Dinh, H., Blumberg, H., and Dougall, W.C. (2007). RANK Overexpression in Transgenic Mice with Mouse Mammary Tumor Virus Promoter-Controlled RANK Increases Proliferation and Impairs Alveolar Differentiation in the Mammary Epithelia and Disrupts Lumen Formation in Cultured Epithelial Acini. *Mol. Cell. Biol.* 27.

Gonzalez-Suarez, E., Jacob, A.P., Jones, J., Miller, R., Roudier-Meyer, M.P., Erwert, R., Pinkas, J., Branstetter, D., and Dougall, W.C. (2010). RANK ligand mediates progestin-induced mammary epithelial proliferation and carcinogenesis. *Nature* 468, 103–107.

González-Suárez, E., and Sanz-Moreno, A. (2016). RANK as a therapeutic target in cancer. *FEBS J.* 283, 2018–2033.

Gonzalez, H., Hagerling, C., and Werb, Z. (2018). Roles of the immune system in cancer: from tumor initiation to metastatic progression. *Genes Dev.* 32, 1267–1284.

Granot, Z., Henke, E., Comen, E.A., King, T.A., Norton, L., and Benezra, R. (2011). Tumor Entrained Neutrophils Inhibit Seeding in the Premetastatic Lung. *Cancer Cell* 20, 300–314.

Green, E.A., Choi, Y., and Flavell, R.A. (2002). Pancreatic lymph node-derived CD4(+)CD25(+) Treg cells: highly potent regulators of diabetes that require TRANCE-RANK signals. *Immunity* 16, 183–191.

Greten, F.R., Eckmann, L., Greten, T.F., Park, J.M., Li, Z.W., Egan, L.J., Kagnoff, M.F., and Karin, M. (2004). IKK $\beta$  links inflammation and tumorigenesis in a mouse model of colitis-associated cancer. *Cell* 118, 285–296.

Griffith, J.W., Sokol, C.L., and Luster, A.D. (2014). Chemokines and Chemokine Receptors: Positioning Cells for Host Defense and Immunity. *Annu. Rev. Immunol.* 32, 659–702.

Gröne, J., Lenze, D., Jurinovic, V., Hummel, M., Seidel, H., Leder, G., Beckmann, G., Sommer, A., Grützmann, R., Pilarsky, C., et al. (2011). Molecular profiles and clinical outcome of stage UICC II colon cancer patients. *Int. J. Colorectal Dis.* 26, 847–858.

- Gross, E.T.E., Han, S., Vemu, P., Peinado, C.D., Marsala, M., Ellies, L.G., and Bui, J.D. (2017). Immunosurveillance and immunoediting in MMTV-PyMT-induced mammary oncogenesis. *Oncoimmunology* 6, e1268310.
- Guerin, M. V., Finisguerra, V., Van den Eynde, B.J., Bercovici, N., and Trautmann, A. (2020). Preclinical murine tumor models: A structural and functional perspective. *Elife* 9.
- Günzburg, W.H., and Salmons, B. (1992). Factors controlling the expression of mouse mammary tumour virus. *Biochem. J.* 283, 625.
- Guo, H., Callaway, J.B., and Ting, J.P.Y. (2015). Inflammasomes: Mechanism of action, role in disease, and therapeutics. *Nat. Med.* 21, 677–687.
- Guy, C.T., Cardiff, R.D., and Muller, W.J. (1992). Induction of mammary tumors by expression of polyomavirus middle T oncogene: a transgenic mouse model for metastatic disease. *Mol. Cell. Biol.* 12, 954–961.
- Hadsell, D.L., Greenberg, N.M., Fligger, J.M., Baumrucker, C.R., and Rosen, J.M. (1996). Targeted expression of des(1-3) human insulin-like growth factor I in transgenic mice influences mammary gland development and IGF-binding protein expression. *Endocrinology* 137, 321–330.
- Hakozaki, A., Yoda, M., Tohmonda, T., Furukawa, M., Hikata, T., Uchikawa, S., Takaishi, H., Matsumoto, M., Chiba, K., Horiuchi, K., et al. (2010). Receptor Activator of NF- $\kappa$ B (RANK) Ligand Induces Ectodomain Shedding of RANK in Murine RAW264.7 Macrophages. *J. Immunol.* 184, 2442–2448.
- Haljasorg, U., Bichele, R., Saare, M., Guha, M., Maslovskaja, J., Könd, K., Remm, A., Pihlap, M., Tomson, L., Kisand, K., et al. (2015). A highly conserved NF- $\kappa$ B-responsive enhancer is critical for thymic expression of Aire in mice. *Eur. J. Immunol.* 45, 3246–3256.
- Hanada, R., Leibbrandt, A., Hanada, T., Kitaoka, S., Furuyashiki, T., Fujihara, H., Trichereau, J., Paolino, M., Qadri, F., Plehm, R., et al. (2009). Central control of fever and female body temperature by RANKL/RANK. *Nature* 462, 505–509.
- Hanahan, D., and Coussens, L.M. (2012). Accessories to the crime: functions of cells recruited to the tumor microenvironment. *Cancer Cell* 21, 309–322.
- Hanahan, D., Weinberg, R.A.R.A. a, Adams, J.M., Cory, S., Aguirre-Ghiso, J.A., Ahmed, Z., Bicknell, R., Al-Hajj, M., Wicha, M.S., Benito-Hernandez, A., et al. (2011). Hallmarks of cancer: the next generation. *Cell* 144, 646–674.
- Hanna, R.N., Cekic, C., Sag, D., Tacke, R., Thomas, G.D., Nowyhed, H., Herrley, E., Rasquinha, N., McArdle, S., Wu, R., et al. (2015). Patrolling monocytes control tumor metastasis to the lung. *Science* 350, 985–990.
- Hartman, H.B., Hu, X., Tyler, K.X., Dalal, C.K., and Lazar, M.A. (2002). Mechanisms regulating adipocyte expression of resistin. *J. Biol. Chem.* 277, 19754–19761.
- He, L., and Marneros, A.G. (2014). Doxycycline inhibits polarization of macrophages to the proangiogenic M2-type and subsequent neovascularization. *J. Biol. Chem.* 289, 8019–8028.
- Hess, E., Duheron, V., Decossas, M., Lézot, F., Berdal, A., Chea, S., Golub, R., Bosisio, M.R., Bridal, S.L., Choi, Y., et al. (2012). RANKL Induces Organized Lymph Node Growth by Stromal Cell Proliferation. *J. Immunol.* 188, 1245–1254.
- Hikita, A., Yana, I., Wakeyama, H., Nakamura, M., Kadono, Y., Oshima, Y., Nakamura, K., Seiki, M., and Tanaka, S. (2006). Negative Regulation of Osteoclastogenesis by Ectodomain Shedding of Receptor Activator of NF- $\kappa$ B Ligand. *J. Biol. Chem.* 281, 36846–36855.

Hikosaka, Y., Nitta, T., Ohigashi, I., Yano, K., Ishimaru, N., Hayashi, Y., Matsumoto, M., Matsuo, K., Penninger, J.M., Takayanagi, H., et al. (2008a). The Cytokine RANKL Produced by Positively Selected Thymocytes Fosters Medullary Thymic Epithelial Cells that Express Autoimmune Regulator. *Immunity* 29, 438–450.

Hikosaka, Y., Nitta, T., Ohigashi, I., Yano, K., Ishimaru, N., Hayashi, Y., Matsumoto, M., Matsuo, K., Penninger, J.M., Takayanagi, H., et al. (2008b). The cytokine RANKL produced by positively selected thymocytes fosters medullary thymic epithelial cells that express autoimmune regulator. *Immunity* 29, 438–450.

Hodi, F.S., O'Day, S.J., McDermott, D.F., Weber, R.W., Sosman, J.A., Haanen, J.B., Gonzalez, R., Robert, C., Schadendorf, D., Hassel, J.C., et al. (2010). Improved survival with ipilimumab in patients with metastatic melanoma. *N. Engl. J. Med.* 363, 711–723.

Holen, I., Cross, S.S., Neville-Webbe, H.L., Cross, N.A., Balasubramanian, S.P., Croucher, P.I., Evans, C.A., Lippitt, J.M., Coleman, R.E., and Eaton, C.L. (2005). Osteoprotegerin (OPG) expression by breast cancer cells in vitro and breast tumours in vivo - A role in tumour cell survival? *Breast Cancer Res. Treat.* 92, 207–215.

Honey, K. (2006). CCL3 and CCL4 actively recruit CD8+ T cells. *Nat. Rev. Immunol.* 6, 427–427.

Horimoto, Y., Arakawa, A., Tanabe, M., Sonoue, H., Igari, F., Senuma, K., Tokuda, E., Shimizu, H., Kosaka, T., and Saito, M. (2014). Ki67 expression and the effect of neo-adjuvant chemotherapy on luminal HER2-negative breast cancer. *BMC Cancer* 14, 550.

Huang, Y., Li, R., Chen, X., Zhuo, Y., Jin, R., Qian, X.P., Jiang, Y.Q., Zeng, Z.H., Zhang, Y., and Shao, Q.X. (2011). Doxycycline up-regulates the expression of IL-6 and GM-CSF via MAPK/ERK and NF- $\kappa$ B pathways in mouse thymic epithelial cells. *Int. Immunopharmacol.* 11, 1143–1149.

Hutchinson, K.E., Yost, S.E., Chang, C.W., Johnson, R.M., Carr, A.R., McAdam, P.R., Halligan, D.L., Chang, C.C., Schmolze, D., Liang, J., et al. (2020). Comprehensive profiling of poor-risk paired primary and recurrent triple-negative breast cancers reveals immune phenotype shifts. *Clin. Cancer Res.* 26, 657–668.

Huynh, H.T., Tetenes, E., Wallace, L., and Pollak, M. (1993). In Vivo Inhibition of Insulin-like Growth Factor I Gene Expression by Tamoxifen. *Cancer Res.* 53.

Iida, M., Tsuboi, K., Niwa, T., Ishida, T., and Hayashi, S. (2019). Compensatory role of insulin-like growth factor 1 receptor in estrogen receptor signaling pathway and possible therapeutic target for hormone therapy-resistant breast cancer. *Breast Cancer* 26, 272–281.

Ikebuchi, Y., Aoki, S., Honma, M., Hayashi, M., Sugamori, Y., Khan, M., Kariya, Y., Kato, G., Tabata, Y., Penninger, J.M., et al. (2018). Coupling of bone resorption and formation by RANKL reverse signalling. *Nature* 561, 195–200.

Ikeda, T., Kasai, M., Utsuyama, M., and Hirokawa, K. (2001). Determination of Three Isoforms of the Receptor Activator of Nuclear Factor- $\kappa$ B Ligand and Their Differential Expression in Bone and Thymus<sup>1</sup>. *Endocrinology* 142, 1419–1426.

Infante, M., Fabi, A., Cognetti, F., Gorini, S., Caprio, M., and Fabbri, A. (2019). RANKL/RANK/OPG system beyond bone remodeling: Involvement in breast cancer and clinical perspectives. *J. Exp. Clin. Cancer Res.* 38.

Jimi, E., Kokabu, S., Matsubara, T., Nakatomi, C., Matsuo, K., and Watanabe, S. (2016). NF- $\kappa$ B acts as a multifunctional modulator in bone invasion by oral squamous cell carcinoma. *Oral Sci. Int.* 13, 1–6.

Jones, D.H., Nakashima, T., Sanchez, O.H., Koziaradzki, I., Komarova, S. V., Sarosi, I., Morony, S.,

- Rubin, E., Sarao, R., Hojilla, C. V., et al. (2006). Regulation of cancer cell migration and bone metastasis by RANKL. *Nature* 440, 692–696.
- Jones, R.A., Campbell, C.I., Gunther, E.J., Chodosh, L.A., Petrik, J.J., Khokha, R., and Moorehead, R.A. (2007). Transgenic overexpression of IGF-IR disrupts mammary ductal morphogenesis and induces tumor formation. *Oncogene* 26, 1636–1644.
- Joshi, P.A., Jackson, H.W., Beristain, A.G., Di Grappa, M.A., Mote, P.A., Clarke, C.L., Stingl, J., Waterhouse, P.D., and Khokha, R. (2010). Progesterone induces adult mammary stem cell expansion. *Nature* 465, 803–807.
- Joshi, P.A., Waterhouse, P.D., Kannan, N., Narala, S., Fang, H., Di Grappa, M.A., Jackson, H.W., Penninger, J.M., Eaves, C., and Khokha, R. (2015a). RANK Signaling Amplifies WNT-Responsive Mammary Progenitors through R-SPONDIN1. *Stem Cell Reports* 5, 31–44.
- Joshi, P.A.A., Waterhouse, P.D.D., Kannan, N., Narala, S., Fang, H., Di Grappa, M.A., Jackson, H.W.W., Penninger, J.M.M., Eaves, C., Khokha, R., et al. (2015b). RANK Signaling Amplifies WNT-Responsive Mammary Progenitors through R-SPONDIN1. *Stem Cell Reports* 5, 31–44.
- Josien, R., Wong, B.R., Li, H.L., Steinman, R.M., and Choi, Y. (1999). TRANCE, a TNF family member, is differentially expressed on T cell subsets and induces cytokine production in dendritic cells. *J. Immunol.* 162, 2562–2568.
- Josien, R., Li, H.L., Ingulli, E., Sarma, S., Wong, B.R., Vologodskaya, M., Steinman, R.M., and Choi, Y. (2000). TRANCE, a Tumor Necrosis Factor Family Member, Enhances the Longevity and Adjuvant Properties of Dendritic Cells In Vivo. *J. Exp. Med.* 191, 495–502.
- Ju, J.H., Cho, M.-L., Moon, Y.-M., Oh, H.-J., Park, J.-S., Jhun, J.-Y., Min, S.-Y., Cho, Y.-G., Park, K.-S., Yoon, C.-H., et al. (2008). IL-23 Induces Receptor Activator of NF- $\kappa$ B Ligand Expression on CD4<sup>+</sup> T Cells and Promotes Osteoclastogenesis in an Autoimmune Arthritis Model. *J. Immunol.* 181, 1507–1518.
- Kadono, Y., Okada, F., Perchonock, C., Jang, H.D., Lee, S.Y., Kim, N., and Choi, Y. (2005). Strength of TRAF6 signalling determines osteoclastogenesis. *EMBO Rep.* 6, 171–176.
- Kanamaru, F., Iwai, H., Ikeda, T., Nakajima, A., Ishikawa, I., and Azuma, M. (2004). Expression of membrane-bound and soluble receptor activator of NF- $\kappa$ B ligand (RANKL) in human T cells. *Immunol. Lett.* 94, 239–246.
- Kanaya, T., Hase, K., Takahashi, D., Fukuda, S., Hoshino, K., Sasaki, I., Hemmi, H., Knoop, K.A., Kumar, N., Sato, M., et al. (2012). The Ets transcription factor Spi-B is essential for the differentiation of intestinal microfold cells. *Nat. Immunol.* 13, 729–736.
- Kanaya, T., Sakakibara, S., Jinnohara, T., Hachisuka, M., Tachibana, N., Hidano, S., Kobayashi, T., Kimura, S., Iwanaga, T., Nakagawa, T., et al. (2018). Development of intestinal M cells and follicle-associated epithelium is regulated by TRAF6-mediated NF- $\kappa$ B signaling. *J. Exp. Med.* 215, 501–519.
- Kanazawa, K., and Kudo, A. (2005). Self-Assembled RANK Induces Osteoclastogenesis Ligand-Independently. *J. Bone Miner. Res.* 20, 2053–2060.
- Kanzaki, H., Makihira, S., Suzuki, M., Ishii, T., Movila, A., Hirschfeld, J., Mawardi, H., Lin, X., Han, X., Taubman, M.A., et al. (2016). Soluble RANKL Cleaved from Activated Lymphocytes by TNF- $\alpha$ -Converting Enzyme Contributes to Osteoclastogenesis in Periodontitis. *J. Immunol.* 197, 3871–3883.
- Kaplan, D.H., Shankaran, V., Dighe, A.S., Stockert, E., Aguet, M., Old, L.J., and Schreiber, R.D. (1998). Demonstration of an interferon gamma-dependent tumor surveillance system in

immunocompetent mice. *Proc. Natl. Acad. Sci. U. S. A.* *95*, 7556–7561.

Kargl, J., Busch, S.E., Yang, G.H.Y., Kim, K.H., Hanke, M.L., Metz, H.E., Hubbard, J.J., Lee, S.M., Madtes, D.K., McIntosh, M.W., et al. (2017). Neutrophils dominate the immune cell composition in non-small cell lung cancer. *Nat. Commun.* *8*.

Van Keymeulen, A., Fioramonti, M., Centonze, A., Bouvencourt, G., Achouri, Y., and Blanpain, C. (2017). Lineage-Restricted Mammary Stem Cells Sustain the Development, Homeostasis, and Regeneration of the Estrogen Receptor Positive Lineage. *Cell Rep.* *20*, 1525–1532.

Khan, I.S., Mouchess, M.L., Zhu, M.L., Conley, B., Fasano, K.J., Hou, Y., Fong, L., Su, M.A., and Anderson, M.S. (2014). Enhancement of an anti-tumor immune response by transient blockade of central T cell tolerance. *J. Exp. Med.* *211*, 761–768.

Kim, D., Mebius, R.E., MacMicking, J.D., Jung, S., Cupedo, T., Castellanos, Y., Rho, J., Wong, B.R., Josien, R., Kim, N., et al. (2000). Regulation of Peripheral Lymph Node Genesis by the Tumor Necrosis Factor Family Member Trance. *J. Exp. Med.* *192*, 1467–1478.

Kim, D.H., Park, H.J., Park, H.S., Lee, J.U., Ko, C.M., Gye, M.C., and Choi, J.M. (2019). Estrogen receptor  $\alpha$  in T cells suppresses follicular helper T cell responses and prevents autoimmunity. *Exp. Mol. Med.* *51*, 1–9.

Kimura, S., Yamakami-Kimura, M., Obata, Y., Hase, K., Kitamura, H., Ohno, H., and Iwanaga, T. (2015a). Visualization of the entire differentiation process of murine M cells: suppression of their maturation in cecal patches. *Mucosal Immunol.* *8*, 650–660.

Kimura, S., Kishimoto, A., Mutoh, M., Takashi-Iwanaga, H., and Iwanaga, T. (2015b). GP2-expressing cells in the conjunctiva and tear ducts of mice: identification of a novel type of cells in the squamous stratified epithelium. *Biomed. Res.* *36*, 263–272.

Kimura, S., Kobayashi, N., Nakamura, Y., Kanaya, T., Takahashi, D., Fujiki, R., Mutoh, M., Obata, Y., Iwanaga, T., Nakagawa, T., et al. (2019a). Sox8 is essential for M cell maturation to accelerate IgA response at the early stage after weaning in mice. *J. Exp. Med.* *216*, 831–846.

Kimura, S., Mutoh, M., Hisamoto, M., Saito, H., Takahashi, S., Asakura, T., Ishii, M., Nakamura, Y., Iida, J., Hase, K., et al. (2019b). Airway M Cells Arise in the Lower Airway Due to RANKL Signaling and Reside in the Bronchiolar Epithelium Associated With iBALT in Murine Models of Respiratory Disease. *Front. Immunol.* *10*, 1323.

Kimura, S., Nakamura, Y., Kobayashi, N., Shiroguchi, K., Kawakami, E., Mutoh, M., Takahashi-Iwanaga, H., Yamada, T., Hisamoto, M., Nakamura, M., et al. (2020). Osteoprotegerin-dependent M cell self-regulation balances gut infection and immunity. *Nat. Commun.* *11*, 234.

King, A.J.F. (2012). The use of animal models in diabetes research. *Br. J. Pharmacol.* *166*, 877–894.

Kitamura, T., Fujishita, T., Loetscher, P., Revesz, L., Hashida, H., Kizaka-Kondoh, S., Aoki, M., and Taketo, M.M. (2010). Inactivation of chemokine (C-C motif) receptor 1 (CCR1) suppresses colon cancer liver metastasis by blocking accumulation of immature myeloid cells in amouse model. *Proc. Natl. Acad. Sci. U. S. A.* *107*, 13063–13068.

von dem Knesebeck, A., Felsberg, J., Waha, A., Hartmann, W., Scheffler, B., Glas, M., Hammes, J., Mikeska, T., Yan, P.S., Endl, E., et al. (2012). RANK (TNFRSF11A) is epigenetically inactivated and induces apoptosis in gliomas. *Neoplasia* *14*, 526–534.

Knoop, K.A., Kumar, N., Butler, B.R., Sakthivel, S.K., Taylor, R.T., Nochi, T., Akiba, H., Yagita, H., Kiyono, H., and Williams, I.R. (2009). RANKL is necessary and sufficient to initiate development of antigen-sampling M cells in the intestinal epithelium. *J. Immunol.* *183*, 5738–5747.

Kong, Y.-Y., Yoshida, H., Sarosi, I., Tan, H.-L., Timms, E., Capparelli, C., Morony, S., Oliveira-dos-Santos, A.J., Van, G., Itie, A., et al. (1999). OPGL is a key regulator of osteoclastogenesis, lymphocyte development and lymph-node organogenesis. *Nature* 397, 315–323.

Krakauer, T., and Buckley, M. (2003). Doxycycline Is Anti-Inflammatory and Inhibits Staphylococcal Exotoxin-Induced Cytokines and Chemokines. *Antimicrob. Agents Chemother.* 47, 3630–3633.

Ku, N.O., Strnad, P., Bantel, H., and Omary, M.B. (2016). Keratins: Biomarkers and modulators of apoptotic and necrotic cell death in the liver. *Hepatology* 64, 966–976.

Kuehnemuth, B., Piseddu, I., Wiedemann, G.M., Lauseker, M., Kuhn, C., Hofmann, S., Schmoeckel, E., Endres, S., Mayr, D., Jeschke, U., et al. (2018). CCL1 is a major regulatory T cell attracting factor in human breast cancer. *BMC Cancer* 18.

Kummel, S., Wimberger, P., Von Minckwitz, G., Nekljudova, V., Denkert, C., Just, M., Hanusch, C., Stoetzer, O.J., Huober, J.B., Hofmann, M., et al. (2018). Investigating denosumab as an add-on neoadjuvant treatment for RANK/L-positive or RANK/L-negative primary breast cancer and two different nab-paclitaxel schedules: 2x2 factorial design (GeparX)—An interim safety analysis. *J. Clin. Oncol.* 36, 569–569.

Kuzin, I.I., Snyder, J.E., Ugine, G.D., Wu, D., Lee, S., Bushnell, T., Insel, R.A., Young, F.M., and Bottaro, A. (2001). Tetracyclines inhibit activated B cell function. *Int. Immunol.* 13, 921–931.

Laban, C., Bustin, S.A., and Jenkins, P.J. (2003). The GH-IGF-I axis and breast cancer. *Trends Endocrinol. Metab.* 14, 28–34.

Lang, I., Füllsack, S., Wyzgol, A., Fick, A., Trebing, J., Arana, J.A.C., Schäfer, V., Weisenberger, D., and Wajant, H. (2016). Binding Studies of TNF Receptor Superfamily (TNFRSF) Receptors on Intact Cells. *J. Biol. Chem.* 291, 5022–5037.

Lasry, A., Zinger, A., and Ben-Neriah, Y. (2016). Inflammatory networks underlying colorectal cancer. *Nat. Immunol.* 17, 230–240.

de Lau, W., Kujala, P., Schneeberger, K., Middendorp, S., Li, V.S.W., Barker, N., Martens, A., Hofhuis, F., DeKoter, R.P., Peters, P.J., et al. (2012). Peyer's patch M cells derived from Lgr5(+) stem cells require SpiB and are induced by RankL in cultured "miniguts". *Mol. Cell. Biol.* 32, 3639–3647.

LeBien, T.W., and Tedder, T.F. (2008). B lymphocytes: how they develop and function. *Blood* 112, 1570–1580.

Li, B., Zhang, S., Huang, N., Chen, H., Wang, P., Yang, J., and Li, Z. (2019). CCL9/CCR1 induces myeloid-derived suppressor cell recruitment to the spleen in a murine H22 orthotopic hepatoma model. *Oncol. Rep.* 41, 608–618.

Li, Z., Zhang, W., and Mulholland, M.W. (2015). LGR4 and Its Role in Intestinal Protection and Energy Metabolism. *Front. Endocrinol. (Lausanne)* 6.

Liao, Y., Smyth, G.K., and Shi, W. (2014). FeatureCounts: An efficient general purpose program for assigning sequence reads to genomic features. *Bioinformatics* 30, 923–930.

Liberzon, A., Birger, C., Thorvaldsdóttir, H., Ghandi, M., Mesirov, J.P., and Tamayo, P. (2015). The Molecular Signatures Database Hallmark Gene Set Collection. *Cell Syst.* 1, 417–425.

Lin, E.Y., Nguyen, A. V., Russell, R.G., and Pollard, J.W. (2001). Colony-Stimulating Factor 1 Promotes Progression of Mammary Tumors to Malignancy. *J. Exp. Med.* 193, 727.

Lin, E.Y., Jones, J.G., Li, P., Zhu, L., Whitney, K.D., Muller, W.J., and Pollard, J.W. (2003).

Progression to Malignancy in the Polyoma Middle T Oncoprotein Mouse Breast Cancer Model Provides a Reliable Model for Human Diseases. *Am. J. Pathol.* *163*, 2113–2126.

Liu, S., Foulkes, W.D., Leung, S., Gao, D., Lau, S., Kos, Z., and Nielsen, T.O. (2014). Prognostic significance of FOXP3+ tumor-infiltrating lymphocytes in breast cancer depends on estrogen receptor and human epidermal growth factor receptor-2 expression status and concurrent cytotoxic T-cell infiltration. *Breast Cancer Res.* *16*, 432.

Locksley, R.M., Killeen, N., and Lenardo, M.J. (2001). The TNF and TNF receptor superfamilies: integrating mammalian biology. *Cell* *104*, 487–501.

Lohela, M., Casbon, A.-J., Olow, A., Bonham, L., Branstetter, D., Weng, N., Smith, J., and Werb, Z. (2014). Intravital imaging reveals distinct responses of depleting dynamic tumor-associated macrophage and dendritic cell subpopulations. *Proc. Natl. Acad. Sci.* *111*, E5086–E5095.

Loi, S., Drubay, D., Adams, S., Pruneri, G., Francis, P.A., Lacroix-Triki, M., Joensuu, H., Dieci, M.V., Badve, S., Demaria, S., et al. (2019). Tumor-Infiltrating Lymphocytes and Prognosis: A Pooled Individual Patient Analysis of Early-Stage Triple-Negative Breast Cancers. *J. Clin. Oncol.* *37*, 559–569.

López-Knowles, E., Gao, Q., Cheang, M.C.U., Morden, J., Parker, J., Martin, L.-A., Pinhel, I., McNeill, F., Hills, M., Detre, S., et al. (2016). Heterogeneity in global gene expression profiles between biopsy specimens taken peri-surgically from primary ER-positive breast carcinomas. *Breast Cancer Res.* *18*, 39.

Losser, K., Mehling, A., Loeser, S., Apelt, J., Kuhn, A., Grabbe, S., Schwarz, T., Penninger, J.M., and Beissert, S. (2006). Epidermal RANKL controls regulatory T-cell numbers via activation of dendritic cells. *Nat. Med.* *12*, 1372–1379.

Love, M.I., Huber, W., and Anders, S. (2014). Moderated estimation of fold change and dispersion for RNA-seq data with DESeq2. *Genome Biol.* *15*, 550.

Luci, C., Reynders, A., Ivanov, I.I., Cognet, C., Chiche, L., Chasson, L., Hardwigsen, J., Anguiano, E., Banchereau, J., Chaussabel, D., et al. (2009). Influence of the transcription factor ROR $\gamma$ t on the development of NKp46+ cell populations in gut and skin. *Nat. Immunol.* *10*, 75–82.

Luen, S.J., Salgado, R., Fox, S., Savas, P., Eng-Wong, J., Clark, E., Kiermaier, A., Swain, S.M., Baselga, J., Michiels, S., et al. (2017). Tumour-infiltrating lymphocytes in advanced HER2-positive breast cancer treated with pertuzumab or placebo in addition to trastuzumab and docetaxel: a retrospective analysis of the CLEOPATRA study. *Lancet Oncol.* *18*, 52–62.

Luo, J., Yang, Z., Ma, Y., Yue, Z., Lin, H., Qu, G., Huang, J., Dai, W., Li, C., Zheng, C., et al. (2016a). LGR4 is a receptor for RANKL and negatively regulates osteoclast differentiation and bone resorption. *Nat. Med.* *22*, 539–546.

Luo, J., Yang, Z., Ma, Y., Yue, Z., Lin, H., Qu, G., Huang, J., Dai, W., Li, C., Zheng, C., et al. (2016b). LGR4 is a receptor for RANKL and negatively regulates osteoclast differentiation and bone resorption. *Nat. Med.* *22*, 539–546.

Luo, W., Friedman, M.S., Shedden, K., Hankenson, K.D., and Woolf, P.J. (2009). GAGE: generally applicable gene set enrichment for pathway analysis. *BMC Bioinformatics* *10*, 161.

Ma, D., Chang, L.-Y., Zhao, S., Zhao, J.-J., Xiong, Y.-J., Cao, F.-Y., Yuan, L., Zhang, Q., Wang, X.-Y., Geng, M.-L., et al. (2017). KLF5 promotes cervical cancer proliferation, migration and invasion in a manner partly dependent on TNFRSF11a expression. *Sci. Rep.* *7*, 15683.

Ma, Q., Liang, M., Wu, Y., Ding, N., Duan, L., Yu, T., Bai, Y., Kang, F., Dong, S., Xu, J., et al. (2019). Mature osteoclast-derived apoptotic bodies promote osteogenic differentiation via RANKL-



mediated reverse signaling. *J. Biol. Chem.* 294, 11240–11247.

Maglione, J.E., Moghanaki, D., Young, L.J.T., Manner, C.K., Ellies, L.G., Joseph, S.O., Nicholson, B., Cardiff, R.D., and MacLeod, C.L. (2001). Transgenic Polyoma middle-T mice model premalignant mammary disease. *Cancer Res.* 61, 8298–8305.

Marazioti, A., Kairi, C.A., Spella, M., Giannou, A.D., Magkouta, S., Giopanou, I., Papaleonidopoulos, V., Kalomenidis, I., Snyder, L.A., Kardamakis, D., et al. (2013). Beneficial Impact of CCL2 and CCL12 Neutralization on Experimental Malignant Pleural Effusion. *PLoS One* 8, e71207.

Mardis, E.R. (2019). Neoantigens and genome instability: impact on immunogenomic phenotypes and immunotherapy response. *Genome Med.* 11, 71.

Maruyama, K., Takada, Y., Ray, N., Kishimoto, Y., Penninger, J.M., Yasuda, H., and Matsuo, K. (2006). Receptor Activator of NF- $\kappa$ B Ligand and Osteoprotegerin Regulate Proinflammatory Cytokine Production in Mice. *J. Immunol.* 177, 3799–3805.

Maruyama, K., Kawagoe, T., Kondo, T., Akira, S., and Takeuchi, O. (2012). TRAF Family Member-associated NF- $\kappa$ B Activator (TANK) Is a Negative Regulator of Osteoclastogenesis and Bone Formation. *J. Biol. Chem.* 287, 29114–29124.

Matsumura, S., Wang, B., Kawashima, N., Braunstein, S., Badura, M., Cameron, T.O., Babb, J.S., Schneider, R.J., Formenti, S.C., Dustin, M.L., et al. (2008). Radiation-Induced CXCL16 Release by Breast Cancer Cells Attracts Effector T Cells. *J. Immunol.* 181, 3099–3107.

McCarthy, N.I., Cowan, J.E., Nakamura, K., Bacon, A., Baik, S., White, A.J., Parnell, S.M., Jenkinson, E.J., Jenkinson, W.E., and Anderson, G. (2015). Osteoprotegerin-Mediated Homeostasis of Rank<sup>+</sup> Thymic Epithelial Cells Does Not Limit Foxp3<sup>+</sup> Regulatory T Cell Development. *J. Immunol.* 195, 2675–2682.

Medler, J., Nelke, J., Weisenberger, D., Steinfatt, T., Rothaug, M., Berr, S., Hünig, T., Beilhack, A., and Wajant, H. (2019). TNFRSF receptor-specific antibody fusion proteins with targeting controlled Fc $\gamma$ R-independent agonistic activity. *Cell Death Dis.* 10, 224.

Meng, Y.-H., Zhou, W.-J., Jin, L.-P., Liu, L.-B., Chang, K.-K., Mei, J., Li, H., Wang, J., Li, D.-J., and Li, M.-Q. (2017). RANKL-mediated harmonious dialogue between fetus and mother guarantees smooth gestation by inducing decidual M2 macrophage polarization. *Cell Death Dis.* 8, e3105.

Merlos-Suárez, A., Barriga, F.M., Jung, P., Iglesias, M., Céspedes, M.V., Rossell, D., Sevillano, M., Hernando-Momblona, X., da Silva-Diz, V., Muñoz, P., et al. (2011). The intestinal stem cell signature identifies colorectal cancer stem cells and predicts disease relapse. *Cell Stem Cell* 8, 511–524.

Michaeli, J., Shaul, M.E., Mishalian, I., Hovav, A.-H., Levy, L., Zolotriov, L., Granot, Z., and Fridlender, Z.G. (2017). Tumor-associated neutrophils induce apoptosis of non-activated CD8 T-cells in a TNF $\alpha$  and NO-dependent mechanism, promoting a tumor-supportive environment. *Oncoimmunology* 6, e1356965.

Mittendorf, E.A., Philips, A. V., Meric-Bernstam, F., Qiao, N., Wu, Y., Harrington, S., Su, X., Wang, Y., Gonzalez-Angulo, A.M., Akcakanat, A., et al. (2014). PD-L1 expression in triple-negative breast cancer. *Cancer Immunol. Res.* 2, 361–370.

Mizukami, J., Takaesu, G., Akatsuka, H., Sakurai, H., Ninomiya-Tsuji, J., Matsumoto, K., and Sakurai, N. (2002). Receptor activator of NF- $\kappa$ B ligand (RANKL) activates TAK1 mitogen-activated protein kinase kinase through a signaling complex containing RANK, TAB2, and TRAF6. *Mol. Cell. Biol.* 22, 992–1000.

Mohammed, H., Russell, I.A., Stark, R., Rueda, O.M., Hickey, T.E., Tarulli, G.A., Serandour, A.A.A., Birrell, S.N., Bruna, A., Saadi, A., et al. (2015). Progesterone receptor modulates ER $\alpha$  action in breast cancer. *Nature* 523, 313–317.

Moschen, A.R., Kaser, A., Enrich, B., Ludwiczek, O., Gabriel, M., Obrist, P., Wolf, A.M., and Tilg, H. (2005). The RANKL/OPG system is activated in inflammatory bowel disease and relates to the state of bone loss. *Gut* 54, 479–487.

Mueller, C.G., and Hess, E. (2012). Emerging Functions of RANKL in Lymphoid Tissues. *Front. Immunol.* 3, 261.

Mueller, A., Meiser, A., McDonagh, E.M., Fox, J.M., Petit, S.J., Xanthou, G., Williams, T.J., and Pease, J.E. (2008). CXCL4-induced migration of activated T lymphocytes is mediated by the chemokine receptor CXCR3. *J. Leukoc. Biol.* 83, 875–882.

Muntasell, A., Rojo, F., Servitja, S., Rubio-Perez, C., Cabo, M., Tamborero, D., Costa-García, M., Martínez-García, M., Menéndez, S., Vazquez, I., et al. (2019). NK Cell Infiltrates and HLA Class I Expression in Primary HER2<sup>+</sup> Breast Cancer Predict and Uncouple Pathological Response and Disease-free Survival. *Clin. Cancer Res.* 25, 1535–1545.

Muppidi, J.R., and Siegel, R.M. (2004). Ligand-independent redistribution of Fas (CD95) into lipid rafts mediates clonotypic T cell death. *Nat. Immunol.* 5, 182–189.

Murphy, N., Knuppel, A., Papadimitriou, N., Martin, R.M., Tsilidis, K.K., Smith-Byrne, K., Fensom, G., Perez-Cornago, A., Travis, R.C., Key, T.J., et al. (2020). Insulin-like growth factor-1, insulin-like growth factor-binding protein-3, and breast cancer risk: observational and Mendelian randomization analyses with ~430 000 women. *Ann. Oncol.* 31, 641–649.

Mutoh, M., Kimura, S., Takahashi-Iwanaga, H., Hisamoto, M., Iwanaga, T., and Iida, J. (2016). RANKL regulates differentiation of microfold cells in mouse nasopharynx-associated lymphoid tissue (NALT). *Cell Tissue Res.* 364, 175–184.

Nagashima, K., Sawa, S., Nitta, T., Tsutsumi, M., Okamura, T., Penninger, J.M., Nakashima, T., and Takayanagi, H. (2017). Identification of subepithelial mesenchymal cells that induce IgA and diversify gut microbiota. *Nat. Immunol.* 18, 675–682.

Nakamura, E.S., Koizumi, K., Kobayashi, M., Saitoh, Y., Arita, Y., Nakayama, T., Sakurai, H., Yoshie, O., and Saiki, I. (2006). RANKL-induced CCL22/macrophage-derived chemokine produced from osteoclasts potentially promotes the bone metastasis of lung cancer expressing its receptor CCR4. *Clin. Exp. Metastasis* 23, 9–18.

Nakashima, T., Hayashi, M., Fukunaga, T., Kurata, K., Oh-Hora, M., Feng, J.Q., Bonewald, L.F., Kodama, T., Wutz, A., Wagner, E.F., et al. (2011). Evidence for osteocyte regulation of bone homeostasis through RANKL expression. *Nat. Med.* 17, 1231–1234.

Nelson, C.A., Warren, J.T., Wang, M.W.-H., Teitelbaum, S.L., and Fremont, D.H. (2012). RANKL Employs Distinct Binding Modes to Engage RANK and the Osteoprotegerin Decoy Receptor. *Structure* 20, 1971–1982.

Newman, A.M., Liu, C.L., Green, M.R., Gentles, A.J., Feng, W., Xu, Y., Hoang, C.D., Diehn, M., and Alizadeh, A.A. (2015a). Robust enumeration of cell subsets from tissue expression profiles. *Nat. Methods* 12, 453–457.

Newman, A.M., Liu, C.L., Green, M.R., Gentles, A.J., Feng, W., Xu, Y., Hoang, C.D., Diehn, M., and Alizadeh, A.A. (2015b). Robust enumeration of cell subsets from tissue expression profiles. *Nat. Methods* 12, 453–457.

Nicolás-Ávila, J.Á., Adrover, J.M., and Hidalgo, A. (2017). Neutrophils in Homeostasis, Immunity,

and Cancer. *Immunity* 46, 15–28.

Nolan, E., Vaillant, F., Branstetter, D., Pal, B., Giner, G., Whitehead, L., Lok, S.W., Mann, G.B., Rohrbach, K., Huang, L.Y., et al. (2016). RANK ligand as a potential target for breast cancer prevention in BRCA1-mutation carriers. *Nat. Med.* 22, 933–939.

Novack, D.V., Yin, L., Hagen-Stapleton, A., Schreiber, R.D., Goeddel, D. V., Ross, F.P., and Teitelbaum, S.L. (2003). The I $\kappa$ B Function of NF- $\kappa$ B p100 Controls Stimulated Osteoclastogenesis. *J. Exp. Med.* 198, 771.

Oliveira, S.H.P., Canetti, C., Ribeiro, R.A., and Cunha, F.Q. (2008). Neutrophil migration induced by IL-1 $\beta$  depends upon LTB<sub>4</sub> released by macrophages and upon TNF- $\alpha$  and IL-1 $\beta$  released by mast cells. *Inflammation* 31, 36–46.

Onder, L., Mörbe, U., Pikor, N., Novkovic, M., Cheng, H.-W., Hehlhans, T., Pfeffer, K., Becher, B., Waisman, A., Rüllicke, T., et al. (2017). Lymphatic Endothelial Cells Control Initiation of Lymph Node Organogenesis. *Immunity* 47, 80-92.e4.

Owen, D., and Chaff, J.E. (2018). Immunotherapy in surgically resectable non-small cell lung cancer. *J. Thorac. Dis.* 10, S404–S411.

Palafox, M., Ferrer, I., Pellegrini, P., Vila, S., Hernandez-Ortega, S., Urruticoechea, A., Climent, F., Soler, M.T., Muñoz, P., Viñals, F., et al. (2012a). RANK induces epithelial-mesenchymal transition and stemness in human mammary epithelial cells and promotes tumorigenesis and metastasis. *Cancer Res.* 72, 2879–2888.

Palafox, M., Ferrer, I., Pellegrini, P., Vila, S., Hernandez-Ortega, S., Urruticoechea, A., Climent, F., Soler, M.T., Munoz, P., Vinals, F., et al. (2012b). RANK Induces Epithelial-Mesenchymal Transition and Stemness in Human Mammary Epithelial Cells and Promotes Tumorigenesis and Metastasis. *Cancer Res.* 72, 2879–2888.

Papanastasiou, A.D., Sirinian, C., and Kalofonos, H.P. (2012). Identification of novel human receptor activator of nuclear factor- $\kappa$ B isoforms generated through alternative splicing: implications in breast cancer cell survival and migration. *Breast Cancer Res.* 14, R112.

Park, H.S., Lee, A., Chae, B.J., Bae, J.-S., Song, B.J., and Jung, S.S. (2014). Expression of receptor activator of nuclear factor kappa-B as a poor prognostic marker in breast cancer. *J. Surg. Oncol.* 110, 807–812.

Parnell, E.A., Walch, E.M., and Lo, D.D. (2016). Inducible Colonic M Cells Are Dependent on TNFR2 but Not Lt $\beta$ r, Identifying Distinct Signalling Requirements for Constitutive Versus Inducible M Cells. *J. Crohn's Colitis* 11, jjw212.

Paul, S., and Lal, G. (2017). The Molecular Mechanism of Natural Killer Cells Function and Its Importance in Cancer Immunotherapy. *Front. Immunol.* 8, 1124.

Pellegrini, P., Cordero, A., Gallego, M.I., Dougall, W.C., Purificación, M., Pujana, M.A., Gonzalez-Suarez, E., William, D.C., Muñoz, P., Purificación, M., et al. (2013). Constitutive activation of RANK disrupts mammary cell fate leading to tumorigenesis. *Stem Cells* 31, 1954–1965.

Perl, A.-K.T., Wert, S.E., Nagy, A., Lobe, C.G., and Whitsett, J.A. (2002). Early restriction of peripheral and proximal cell lineages during formation of the lung. *Proc. Natl. Acad. Sci. U. S. A.* 99, 10482–10487.

Perlot, T., and Penninger, J.M. (2012). Development and function of murine B cells lacking RANK. *J. Immunol.* 188, 1201–1205.

Peters, S., Danson, S., Hasan, B., Dafni, U., Reinmuth, N., Majem, M., Tournoy, K.G., Mark, M.T.,

- Pless, M., Cobo, M., et al. (2020). A Randomized Open-Label Phase III Trial Evaluating the Addition of Denosumab to Standard First-Line Treatment in Advanced NSCLC: The European Thoracic Oncology Platform (ETOP) and European Organisation for Research and Treatment of Cancer (EORTC) SPLENDOUR Trial. *J. Thorac. Oncol.* *15*, 1647–1656.
- Pfützner, B.M., Branstetter, D., Loibl, S., Denkert, C., Lederer, B., Schmitt, W.D., Dombrowski, F., Werner, M., Rüdiger, T., Dougall, W.C., et al. (2014). RANK expression as a prognostic and predictive marker in breast cancer. *Breast Cancer Res. Treat.* *145*, 307–315.
- Poubelle, P.E., Chakravarti, A., Fernandes, M.J., Doiron, K., and Marceau, A.-A. (2007). Differential expression of RANK, RANK-L, and osteoprotegerin by synovial fluid neutrophils from patients with rheumatoid arthritis and by healthy human blood neutrophils. *Arthritis Res. Ther.* *9*, R25.
- Qian, B.-Z., Li, J., Zhang, H., Kitamura, T., Zhang, J., Campion, L.R., Kaiser, E.A., Snyder, L.A., and Pollard, J.W. (2011). CCL2 recruits inflammatory monocytes to facilitate breast-tumour metastasis. *Nature* *475*, 222–225.
- Rachner, T.D., Benad, P., Rauner, M., Goettsch, C., Singh, S.K., Schoppet, M., and Hofbauer, L.C. (2009). Osteoprotegerin production by breast cancer cells is suppressed by dexamethasone and confers resistance against TRAIL-induced apoptosis. *J. Cell. Biochem.* *108*, 106–116.
- Rachner, T.D., Kasimir-Bauer, S., Göbel, A., Erdmann, K., Hoffmann, O., Browne, A., Wimberger, P., Rauner, M., Hofbauer, L.C., Kimmig, R., et al. (2019). Prognostic Value of RANKL/OPG Serum Levels and Disseminated Tumor Cells in Nonmetastatic Breast Cancer. *Clin. Cancer Res.* *25*, 1369–1378.
- Rakha, E.A., and Green, A.R. (2017). Molecular classification of breast cancer: what the pathologist needs to know. *Pathology* *49*, 111–119.
- Ramos, C.D.L. (2005). MIP-1 [CCL3] acting on the CCR1 receptor mediates neutrophil migration in immune inflammation via sequential release of TNF- and LTB4. *J. Leukoc. Biol.* *78*, 167–177.
- Rao, S., Sigl, V., Wimmer, R.A., Novatchkova, M., Jais, A., Wagner, G., Handschuh, S., Uribealago, I., Hagelkruys, A., Kozieradzki, I., et al. (2017). RANK rewires energy homeostasis in lung cancer cells and drives primary lung cancer. *Genes Dev.* *31*, 2099–2111.
- Reilly, M.P., Taylor, S.M., Hartman, N.K., Arepally, G.M., Sachais, B.S., Cines, D.B., Poncz, M., and McKenzie, S.E. (2001). Heparin-induced thrombocytopenia/thrombosis in a transgenic mouse model requires human platelet factor 4 and platelet activation through FcγRIIA. *Blood* *98*, 2442–2447.
- Rennhack, J.P., To, B., Swiatnicki, M., Dulak, C., Ogrodzinski, M.P., Zhang, Y., Li, C., Bylett, E., Ross, C., Szczepanek, K., et al. (2019). Integrated analyses of murine breast cancer models reveal critical parallels with human disease. *Nat. Commun.* *10*, 3261.
- Reyes, M.E., Fujii, T., Branstetter, D., Krishnamurthy, S., Masuda, H., Wang, X., Reuben, J.M., Woodward, W.A., Edwards, B.J., Hortobagyi, G.N., et al. (2017). Poor prognosis of patients with triple-negative breast cancer can be stratified by RANK and RANKL dual expression. *Breast Cancer Res. Treat.* *164*, 57–67.
- Riegel, A., Maurer, T., Prior, B., Stegmaier, S., Heppert, V., Wagner, C., and Hänsch, G.M. (2012). Human polymorphonuclear neutrophils express RANK and are activated by its ligand, RANKL. *Eur. J. Immunol.* *42*, 975–981.
- Rios, D., Wood, M.B., Li, J., Chassaing, B., Gewirtz, A.T., and Williams, I.R. (2016). Antigen sampling by intestinal M cells is the principal pathway initiating mucosal IgA production to commensal enteric bacteria. *Mucosal Immunol.* *9*, 907–916.

- Rizvi, N.A., Hellmann, M.D., Snyder, A., Kvistborg, P., Makarov, V., Havel, J.J., Lee, W., Yuan, J., Wong, P., Ho, T.S., et al. (2015). Mutational landscape determines sensitivity to PD-1 blockade in non-small cell lung cancer. *Science* (80-. ). *348*, 124–128.
- Roberts, N.A., White, A.J., Jenkinson, W.E., Turchinovich, G., Nakamura, K., Withers, D.R., McConnell, F.M., Desanti, G.E., Benezech, C., Parnell, S.M., et al. (2012). Rank Signaling Links the Development of Invariant  $\gamma\delta$  T Cell Progenitors and Aire+ Medullary Epithelium. *Immunity* *36*, 427–437.
- Robinson, M.D., and Oshlack, A. (2010). A scaling normalization method for differential expression analysis of RNA-seq data. *Genome Biol.* *11*, R25.
- Robinson, M.D., McCarthy, D.J., and Smyth, G.K. (2009). edgeR: A Bioconductor package for differential expression analysis of digital gene expression data. *Bioinformatics* *26*, 139–140.
- Rossi, S.W., Kim, M.-Y., Leibbrandt, A., Parnell, S.M., Jenkinson, W.E., Glanville, S.H., McConnell, F.M., Scott, H.S., Penninger, J.M., Jenkinson, E.J., et al. (2007). RANK signals from CD4+3<sup>+</sup> inducer cells regulate development of Aire-expressing epithelial cells in the thymic medulla. *J. Exp. Med.* *204*, 1267–1272.
- Ruan, W., and Kleinberg, D.L. (1999). Insulin-like growth factor I is essential for terminal end bud formation and ductal morphogenesis during mammary development. *Endocrinology* *140*, 5075–5081.
- Rubin, J., Ackert-Bicknell, C.L., Zhu, L., Fan, X., Murphy, T.C., Nanes, M.S., Marcus, R., Holloway, L., Beamer, W.G., and Rosen, C.J. (2002). IGF-I regulates osteoprotegerin (OPG) and receptor activator of nuclear factor- $\kappa$ B ligand in vitro and OPG in vivo. *J. Clin. Endocrinol. Metab.* *87*, 4273–4279.
- Ruocco, M.G., Maeda, S., Park, J.M., Lawrence, T., Hsu, L.-C., Cao, Y., Schett, G., Wagner, E.F., and Karin, M. (2005). I $\kappa$ B kinase (IKK) $\beta$ , but not IKK $\alpha$ , is a critical mediator of osteoclast survival and is required for inflammation-induced bone loss. *J. Exp. Med.* *201*, 1677.
- Russnes, H.G., Lingjærde, O.C., Børresen-Dale, A.-L., and Caldas, C. (2017). Breast Cancer Molecular Stratification: From Intrinsic Subtypes to Integrative Clusters. *Am. J. Pathol.* *187*, 2152–2162.
- Ryckman, C., Vandal, K., Rouleau, P., Talbot, M., and Tessier, P.A. (2003). Proinflammatory Activities of S100: Proteins S100A8, S100A9, and S100A8/A9 Induce Neutrophil Chemotaxis and Adhesion. *J. Immunol.* *170*, 3233–3242.
- Salgado, R., and Loi, S. (2018). Tumour infiltrating lymphocytes in breast cancer: increasing clinical relevance. *Lancet Oncol.* *19*, 3–5.
- Salgado, R., Denkert, C., Demaria, S., Sirtaine, N., Klauschen, F., Pruneri, G., Wienert, S., Van den Eynden, G., Baehner, F.L., Penault-Llorca, F., et al. (2015). The evaluation of tumor-infiltrating lymphocytes (TILs) in breast cancer: recommendations by an International TILs Working Group 2014. *Ann. Oncol.* *26*, 259–271.
- Santini, D., Schiavon, G., Vincenzi, B., Gaeta, L., Pantano, F., Russo, A., Ortega, C., Porta, C., Galluzzo, S., Armento, G., et al. (2011). Receptor Activator of NF- $\kappa$ B (RANK) Expression in Primary Tumors Associates with Bone Metastasis Occurrence in Breast Cancer Patients. *PLoS One* *6*, e19234.
- Sato, K., Suematsu, A., Okamoto, K., Yamaguchi, A., Morishita, Y., Kadono, Y., Tanaka, S., Kodama, T., Akira, S., Iwakura, Y., et al. (2006). Th17 functions as an osteoclastogenic helper T cell subset that links T cell activation and bone destruction. *J. Exp. Med.* *203*, 2673–2682.

Savas, P., Salgado, R., Denkert, C., Sotiriou, C., Darcy, P.K., Smyth, M.J., and Loi, S. (2016). Clinical relevance of host immunity in breast cancer: From TILs to the clinic. *Nat. Rev. Clin. Oncol.* *13*, 228–241.

Sawa, S., Cherrier, M., Lochner, M., Satoh-Takayama, N., Fehling, H.J., Langa, F., Santo, J.P. Di, and Eberl, G. (2010). Lineage Relationship Analysis of ROR $\gamma$ t<sup>+</sup> Innate Lymphoid Cells. *Science* (80-. ). *330*, 665–669.

Scheele, C.L.G.J., Hannezo, E., Muraro, M.J., Zomer, A., Langedijk, N.S.M., van Oudenaarden, A., Simons, B.D., and van Rheenen, J. (2017). Identity and dynamics of mammary stem cells during branching morphogenesis. *Nature* *542*, 313–317.

Schmiedel, B.J., Nuebling, T., Steinbacher, J., Malinowska, A., Wende, C.M., Azuma, M., Schneider, P., Grosse-Hovest, L., and Salih, H.R. (2013). Receptor Activator for NF- $\kappa$ B Ligand in Acute Myeloid Leukemia: Expression, Function, and Modulation of NK Cell Immunosurveillance. *J. Immunol.* *190*, 821–831.

Schramek, D., Leibbrandt, A., Sigl, V., Kenner, L., Pospisilik, J.A., Lee, H.J., Hanada, R., Joshi, P.A., Aliprantis, A., Glimcher, L., et al. (2010). Osteoclast differentiation factor RANKL controls development of progesterin-driven mammary cancer. *Nature* *468*, 98–102.

Schwitalla, S., Ziegler, P.K., Horst, D., Becker, V., Kerle, I., Begus-Nahrman, Y., Lechel, A., Rudolph, K.L., Langer, R., Slotta-Huspenina, J., et al. (2013). Loss of p53 in Enterocytes Generates an Inflammatory Microenvironment Enabling Invasion and Lymph Node Metastasis of Carcinogen-Induced Colorectal Tumors. *Cancer Cell* *23*, 93–106.

Secchiero, P., Corallini, F., Barbarotto, E., Melloni, E., di Iasio, M.G., Tiribelli, M., and Zauli, G. (2006). Role of the RANKL/RANK system in the induction of interleukin-8 (IL-8) in B chronic lymphocytic leukemia (B-CLL) cells. *J. Cell. Physiol.* *207*, 158–164.

Shaked, H., Hofseth, L.J., Chumanevich, A., Chumanevich, A.A., Wang, J., Wang, Y., Taniguchi, K., Guma, M., Shenouda, S., Clevers, H., et al. (2012). Chronic epithelial NF- $\kappa$ B activation accelerates APC loss and intestinal tumor initiation through iNOS up-regulation. *Proc. Natl. Acad. Sci. U. S. A.* *109*, 14007–14012.

Shankaran, V., Ikeda, H., Bruce, A.T., White, J.M., Swanson, P.E., Old, L.J., and Schreiber, R.D. (2001). IFN $\gamma$  and lymphocytes prevent primary tumour development and shape tumour immunogenicity. *Nature* *410*, 1107–1111.

Shaul, M.E., and Fridlender, Z.G. (2018). Cancer-related circulating and tumor-associated neutrophils – subtypes, sources and function. *FEBS J.* *285*, 4316–4342.

Shimamura, M., Nakagami, H., Osako, M.K., Kurinami, H., Koriyama, H., Zhengda, P., Tomioka, H., Tenma, A., Wakayama, K., and Morishita, R. (2014). OPG/RANKL/RANK axis is a critical inflammatory signaling system in ischemic brain in mice. *Proc. Natl. Acad. Sci.* *111*, 8191–8196.

Sigl, V., Owusu-Boaitey, K., Joshi, P.A., Kavirayani, A., Wirnsberger, G., Novatchkova, M., Kozieradzki, I., Schramek, D., Edokobi, N., Hersl, J., et al. (2016). RANKL/RANK control Brca1 mutation-driven mammary tumors. *Cell Res.* *26*, 761–774.

Silberstein, G.B., Van Horn, K., Hrabeta-Robinson, E., and Compton, J. (2006). Estrogen-triggered delays in mammary gland gene expression during the estrous cycle: Evidence for a novel timing system. *J. Endocrinol.* *190*, 225–239.

Simonet, W.S., Lacey, D.L., Dunstan, C.R., Kelley, M., Chang, M.S., Lüthy, R., Nguyen, H.Q., Wooden, S., Bennett, L., Boone, T., et al. (1997). Osteoprotegerin: a novel secreted protein involved in the regulation of bone density. *Cell* *89*, 309–319.

- Sirinian, C., Papanastasiou, A.D., Schizas, M., Spella, M., Stathopoulos, G.T., Repanti, M., Zarkadis, I.K., King, T.A., and Kalofonos, H.P. (2018). RANK-c attenuates aggressive properties of ER-negative breast cancer by inhibiting NF- $\kappa$ B activation and EGFR signaling. *Oncogene* 37, 5101–5114.
- Sleeman, K.E., Kendrick, H., Robertson, D., Isacke, C.M., Ashworth, A., and Smalley, M.J. (2007). Dissociation of estrogen receptor expression and in vivo stem cell activity in the mammary gland. *J. Cell Biol.* 176, 19–26.
- Smith-Garvin, J.E., Koretzky, G.A., and Jordan, M.S. (2009). T Cell Activation. *Annu. Rev. Immunol.* 27, 591–619.
- Spit, M., Koo, B.-K., and Maurice, M.M. (2018). Tales from the crypt: intestinal niche signals in tissue renewal, plasticity and cancer. *Open Biol.* 8, 180120.
- Spranger, S., Spaapen, R.M., Zha, Y., Williams, J., Meng, Y., Ha, T.T., and Gajewski, T.F. (2013). Up-regulation of PD-L1, IDO, and T(regs) in the melanoma tumor microenvironment is driven by CD8(+) T cells. *Sci. Transl. Med.* 5, 200ra116.
- Srivastava, S., Matsuda, M., Hou, Z., Bailey, J.P., Kitazawa, R., Herbst, M.P., and Horseman, N.D. (2003). Receptor Activator of NF- $\kappa$ B Ligand Induction via Jak2 and Stat5a in Mammary Epithelial Cells. *J. Biol. Chem.* 278, 46171–46178.
- Steppan, C.M., Bailey, S.T., Bhat, S., Brown, E.J., Banerjee, R.R., Wright, C.M., Patel, H.R., Ahima, R.S., and Lazar, M.A. (2001). The hormone resistin links obesity to diabetes. *Nature* 409, 307–312.
- Su, H., Morrison, R., Messer, R., Whitmire, W., Hughes, S., and Caldwell, H.D. (1999). The Effect of Doxycycline Treatment on the Development of Protective Immunity in a Murine Model of Chlamydial Genital Infection. *J. Infect. Dis.* 180, 1252–1258.
- Su, W., Wan, Q., Han, L., Huang, J., Chen, X., Chen, G., Zheng, S.G., and Liang, D. (2014). Doxycycline exerts multiple anti-allergy effects to attenuate murine allergic conjunctivitis and systemic anaphylaxis. *Biochem. Pharmacol.* 91, 359–368.
- Supiot, S., Gouraud, W., Campion, L., Jezéquel, P., Buecher, B., Charrier, J., Heymann, M.F., Mahé, M.A., Rio, E., and Chérel, M. (2013). Early dynamic transcriptomic changes during preoperative radiotherapy in patients with rectal cancer: A feasibility study. *World J. Gastroenterol.* 19, 3249–3254.
- Swann, J.B., Vesely, M.D., Silva, A., Sharkey, J., Akira, S., Schreiber, R.D., and Smyth, M.J. (2008a). Demonstration of inflammation-induced cancer and cancer immunoediting during primary tumorigenesis. *Proc. Natl. Acad. Sci. U. S. A.* 105, 652–656.
- Swann, J.B., Vesely, M.D., Silva, A., Sharkey, J., Akira, S., Schreiber, R.D., and Smyth, M.J. (2008b). Demonstration of inflammation-induced cancer and cancer immunoediting during primary tumorigenesis. *Proc. Natl. Acad. Sci.* 105, 652–656.
- Szekely, B., Bossuyt, V., Li, X., Wali, V.B., Patwardhan, G.A., Frederick, C., Silber, A., Park, T., Harigopal, M., Pelekanou, V., et al. (2018). Immunological differences between primary and metastatic breast cancer. *Ann. Oncol.* 29, 2232–2239.
- Tait Wojno, E.D., Hunter, C.A., and Stumhofer, J.S. (2019). The Immunobiology of the Interleukin-12 Family: Room for Discovery. *Immunity* 50, 851–870.
- Takayanagi, H., Ogasawara, K., Hida, S., Chiba, T., Murata, S., Sato, K., Takaoka, A., Yokochi, T., Oda, H., Tanaka, K., et al. (2000). T-cell-mediated regulation of osteoclastogenesis by signalling cross-talk between RANKL and IFN- $\gamma$ . *Nature* 408, 600–605.

- Tan, W., Zhang, W., Strasner, A., Grivennikov, S., Cheng, J.Q., Hoffman, R.M., and Karin, M. (2011). Tumour-infiltrating regulatory T cells stimulate mammary cancer metastasis through RANKL–RANK signalling. *Nature* 470, 548–553.
- Tanaka, T., Kohno, H., Suzuki, R., Yamada, Y., Sugie, S., and Mori, H. (2003). A novel inflammation-related mouse colon carcinogenesis model induced by azoxymethane and dextran sodium sulfate. *Cancer Sci.* 94, 965–973.
- Tang, X., Wang, X., Zhao, Y.Y., Curtis, J.M., and Brindley, D.N. (2017). Doxycycline attenuates breast cancer related inflammation by decreasing plasma lysophosphatidate concentrations and inhibiting NF- $\kappa$ B activation. *Mol. Cancer* 16, 1–13.
- Tanos, T., Sflomos, G., Echeverria, P.C., Ayyanan, A., Gutierrez, M., Delaloye, J.-F., Raffoul, W., Fiche, M., Dougall, W., Schneider, P., et al. (2013a). Progesterone/RANKL Is a Major Regulatory Axis in the Human Breast. *Sci. Transl. Med.* 5, 182ra55-182ra55.
- Tanos, T., Sflomos, G., Echeverria, P.C., Ayyanan, A., Gutierrez, M., Delaloye, J.J.-F., Raffoul, W., Fiche, M., Dougall, W., Schneider, P., et al. (2013b). Progesterone/RANKL is a major regulatory axis in the human breast. *Sci. Transl. Med.* 5.
- Taube, J.M., Anders, R.A., Young, G.D., Xu, H., Sharma, R., McMiller, T.L., Chen, S., Klein, A.P., Pardoll, D.M., Topalian, S.L., et al. (2012). Colocalization of Inflammatory Response with B7-H1 Expression in Human Melanocytic Lesions Supports an Adaptive Resistance Mechanism of Immune Escape. *Sci. Transl. Med.* 4, 127ra37-127ra37.
- Taylor, C.R., Branstetter, D., Manna, E., Dougall, W.C., Bussiere, J., and Johnson, C.W. (2017). Distribution of RANK and RANK Ligand in Normal Human Tissues as Determined by an Optimized Immunohistochemical Method. *Appl. Immunohistochem. Mol. Morphol.* 25, 299–307.
- Theoleyre, S., Wittrant, Y., Tat, S.K., Fortun, Y., Redini, F., and Heymann, D. (2004). The molecular triad OPG/RANK/RANKL: involvement in the orchestration of pathophysiological bone remodeling. *Cytokine Growth Factor Rev.* 15, 457–475.
- Thorsson, V., Gibbs, D.L., Brown, S.D., Wolf, D., Bortone, D.S., Ou Yang, T.-H., Porta-Pardo, E., Gao, G.F., Plaisier, C.L., Eddy, J.A., et al. (2018). The Immune Landscape of Cancer. *Immunity* 48, 812-830.e14.
- Tolaney, S.M., Barroso-Sousa, R., Keenan, T., Li, T., Trippa, L., Vaz-Luis, I., Wulf, G., Spring, L., Sinclair, N.F., Andrews, C., et al. (2020). Effect of Eribulin with or without Pembrolizumab on Progression-Free Survival for Patients with Hormone Receptor-Positive, ERBB2-Negative Metastatic Breast Cancer: A Randomized Clinical Trial. *JAMA Oncol.* 6, 1598–1605.
- Tsubaki, M., Komai, M., Fujimoto, S., Itoh, T., Imano, M., Sakamoto, K., Shimaoka, H., Takeda, T., Ogawa, N., Mashimo, K., et al. (2013). Activation of NF- $\kappa$ B by the RANKL/RANK system up-regulates snail and twist expressions and induces epithelial-to-mesenchymal transition in mammary tumor cell lines. *J. Exp. Clin. Cancer Res.* 32, 62.
- Tsutsui, M., Hirase, R., Miyamura, S., Nagayasu, K., Nakagawa, T., Mori, Y., Shirakawa, H., and Kaneko, S. (2018). TRPM2 exacerbates central nervous system inflammation in experimental autoimmune encephalomyelitis by increasing production of CXCL2 chemokines. *J. Neurosci.* 38, 8484–8495.
- Vadhan-Raj, S., Von Moos, R., Fallowfield, L.J., Patrick, D.L., Goldwasser, F., Cleeland, C.S., Henry, D.H., Novello, S., Hungria, V., Qian, Y., et al. (2012). Clinical benefit in patients with metastatic bone disease: Results of a phase 3 study of denosumab versus zoledronic acid. *Ann. Oncol.* 23, 3045–3051.
- Vesely, M.D., Kershaw, M.H., Schreiber, R.D., and Smyth, M.J. (2011). Natural Innate and Adaptive



Immunity to Cancer. *Annu. Rev. Immunol.* 29, 235–271.

Vila-Caballer, M., González-Granado, J.M., Zorita, V., Abu Nabah, Y.N., Silvestre-Roig, C., del Monte-Monge, A., Molina-Sánchez, P., Ait-Oufella, H., Andrés-Manzano, M.J., Sanz, M.J., et al. (2019). Disruption of the CCL1-CCR8 axis inhibits vascular Treg recruitment and function and promotes atherosclerosis in mice. *J. Mol. Cell. Cardiol.* 132, 154–163.

Wacleche, V.S., Cattin, A., Goulet, J.-P., Gauchat, D., Gosselin, A., Cleret-Buhot, A., Zhang, Y., Tremblay, C.L., Routy, J.-P., and Ancuta, P. (2018). CD16+ monocytes give rise to CD103+RALDH2+TCF4+ dendritic cells with unique transcriptional and immunological features. *Blood Adv.* 2, 2862.

Wada, T., Nakashima, T., Hiroshi, N., and Penninger, J.M. (2006). RANKL–RANK signaling in osteoclastogenesis and bone disease. *Trends Mol. Med.* 12, 17–25.

Wajant, H. (2015). Principles of antibody-mediated TNF receptor activation. *Cell Death Differ.* 22, 1727–1741.

Walsh, M.C., and Choi, Y. (2014). Biology of the RANKL-RANK-OPG System in Immunity, Bone, and Beyond. *Front. Immunol.* 5, 511.

Wang, H., Zhang, Q., Kong, H., Zeng, Y., Hao, M., Yu, T., Peng, J., Xu, Z., Chen, J., and Shi, H. (2014). Monocyte chemotactic protein-1 expression as a prognostic biomarker in patients with solid tumor: A meta analysis. *Int. J. Clin. Exp. Pathol.* 7, 3876–3886.

Wang, J., Gusti, V., Saraswati, A., and Lo, D.D. (2011). Convergent and divergent development among M cell lineages in mouse mucosal epithelium. *J. Immunol.* 187, 5277–5285.

Wang, K., Shen, T., Siegal, G.P., and Wei, S. (2017). The CD4/CD8 ratio of tumor-infiltrating lymphocytes at the tumor-host interface has prognostic value in triple-negative breast cancer. *Hum. Pathol.* 69, 110–117.

Wang, R., Zhang, L., Zhang, X., Moreno, J., Celluzzi, C., Tondravi, M., and Shi, Y. (2002). Regulation of activation-induced receptor activator of NF- $\kappa$ B ligand (RANKL) expression in T cells. *Eur. J. Immunol.* 32, 1090–1098.

Watson, J.K., Rulands, S., Wilkinson, A.C., Wuidart, A., Ousset, M., Van Keymeulen, A., Göttgens, B., Blanpain, C., Simons, B.D., and Rawlins, E.L. (2015). Clonal Dynamics Reveal Two Distinct Populations of Basal Cells in Slow-Turnover Airway Epithelium. *Cell Rep.* 12, 90–101.

Wculek, S.K., and Malanchi, I. (2015). Neutrophils support lung colonization of metastasis-initiating breast cancer cells. *Nature* 528, 413–417.

Wei, S.C., Duffy, C.R., and Allison, J.P. (2018). Fundamental Mechanisms of Immune Checkpoint Blockade Therapy. *Cancer Discov.* 8, 1069–1086.

Wei, Y., Zhan, Y., Chen, P., Liu, Z., Zhang, H., Liu, D., Zhang, J., Yu, M., Mo, W., Zhang, J., et al. (2017). Heterologous expression, purification and function of the extracellular domain of human RANK. *BMC Biotechnol.* 17, 87.

Williams, I.R., and Owen, R.L. (2015). Chapter 13 - M Cells: Specialized Antigen Sampling Cells in the Follicle-Associated Epithelium. J. Mestecky, W. Strober, M.W. Russell, B.L. Kelsall, H. Cheroutre, and B.N.B.T.-M.I. (Fourth E. Lambrecht, eds. (Boston: Academic Press), pp. 211–229.

Wong, B.R., Rho, J., Arron, J., Robinson, E., Orlinick, J., Chao, M., Kalachikov, S., Cayani, E., Bartlett, F.S., Frankel, W.N., et al. (1997a). TRANCE is a novel ligand of the tumor necrosis factor receptor family that activates c-Jun N-terminal kinase in T cells. *J. Biol. Chem.* 272, 25190–25194.

- Wong, B.R., Josien, R., Lee, S.Y., Sauter, B., Li, H.-L., Steinman, R.M., and Choi, Y. (1997b). TRANCE (Tumor Necrosis Factor [TNF]-related Activation-induced Cytokine), a New TNF Family Member Predominantly Expressed in T cells, Is a Dendritic Cell-specific Survival Factor. *J. Exp. Med.* *186*, 2075–2080.
- Wong, B.R., Besser, D., Kim, N., Arron, J.R., Vologodskaja, M., Hanafusa, H., and Choi, Y. (1999). TRANCE, a TNF family member, activates Akt/PKB through a signaling complex involving TRAF6 and c-Src. *Mol. Cell* *4*, 1041–1049.
- Wuyts, A., Haelens, A., Proost, P., Lenaerts, J.P., Conings, R., Opdenakker, G., and Van Damme, J. (1996). Identification of mouse granulocyte chemotactic protein-2 from fibroblasts and epithelial cells. Functional comparison with natural KC and macrophage inflammatory protein-2. *J. Immunol.* *157*.
- Xiong, J., Cawley, K., Piemontese, M., Fujiwara, Y., Zhao, H., Goellner, J.J., and O'Brien, C.A. (2018). Soluble RANKL contributes to osteoclast formation in adult mice but not ovariectomy-induced bone loss. *Nat. Commun.* *9*.
- Xiu, Y., Xu, H., Zhao, C., Li, J., Morita, Y., Yao, Z., Xing, L., and Boyce, B.F. (2014). Chloroquine reduces osteoclastogenesis in murine osteoporosis by preventing TRAF3 degradation. *J. Clin. Invest.* *124*, 297.
- Yee, D., Demichele, A.M., Yau, C., Isaacs, C., Symmans, W.F., Albain, K.S., Chen, Y.Y., Krings, G., Wei, S., Harada, S., et al. (2020). Association of Event-Free and Distant Recurrence-Free Survival with Individual-Level Pathologic Complete Response in Neoadjuvant Treatment of Stages 2 and 3 Breast Cancer: Three-Year Follow-up Analysis for the I-SPY2 Adaptively Randomized Clinical Trial. *JAMA Oncol.* *6*, 1355–1362.
- Yersal, O., and Barutca, S. (2014). Biological subtypes of breast cancer: Prognostic and therapeutic implications. *World J. Clin. Oncol.* *5*, 412–424.
- Yoldi, G. (2018). RANK signaling in mammary spontaneous tumorigenesis and tumor-stromal crosstalk. University of Barcelona.
- Yoldi, G., Pellegrini, P., Trinidad, E.M., Cordero, A., Gomez-Miragaya, J., Serra-Musach, J., Dougall, W.C., Munoz, P., Pujana, M.-A.M.-A., Planelles, L., et al. (2016). RANK Signaling Blockade Reduces Breast Cancer Recurrence by Inducing Tumor Cell Differentiation. *Cancer Res.* *76*, 5857–5869.
- Yoshida, H., Naito, A., Inoue, J.-I., Satoh, M., Santee-Cooper, S.M., Ware, C.F., Togawa, A., Nishikawa, S., and Nishikawa, S.-I. (2002). Different cytokines induce surface lymphotoxin-alpha on IL-7 receptor-alpha cells that differentially engender lymph nodes and Peyer's patches. *Immunity* *17*, 823–833.
- Yoshioka, T., Hosoda, M., Yamamoto, M., Taguchi, K., Hatanaka, K.C., Takakuwa, E., Hatanaka, Y., Matsuno, Y., and Yamashita, H. (2015). Prognostic significance of pathologic complete response and Ki67 expression after neoadjuvant chemotherapy in breast cancer. *Breast Cancer* *22*, 185–191.
- Youn, J.-I., Nagaraj, S., Collazo, M., and Gabrilovich, D.I. (2008). Subsets of Myeloid-Derived Suppressor Cells in Tumor-Bearing Mice. *J. Immunol.* *181*, 5791–5802.
- Ze-Yi, Z., Boon-Huat, B., Swee-Eng, A., and Valerie, C.-L.L. (2005). A Novel Antiestrogenic Mechanism in Progesterone Receptor-transfected Breast Cancer Cells. *J. Biol. Chem.* *280*, 17480–17487.
- Zeng, B., Shi, S., Ashworth, G., Dong, C., Liu, J., and Xing, F. (2019). ILC3 function as a double-edged sword in inflammatory bowel diseases. *Cell Death Dis.* *10*, 315.

Zhang, L., Zhang, B., Han, S.J., Shore, A.N., Rosen, J.M., Demayo, F.J., and Xin, L. (2012). Targeting CreER(T2) expression to keratin 8-expressing murine simple epithelia using bacterial artificial chromosome transgenesis. *Transgenic Res.* 21, 1117–1123.

Zhang, S., Wang, X., Li, G., Chong, Y., Zhang, J., Guo, X., Li, B., and Bi, Z. (2017). Osteoclast regulation of osteoblasts via RANK-RANKL reverse signal transduction in vitro. *Mol. Med. Rep.* 16, 3994–4000.

Zinonos, I., Labrinidis, A., Lee, M., Liapis, V., Hay, S., Ponomarev, V., Diamond, P., Findlay, D.M., Zannettino, A.C.W., and Evdokiou, A. (2011). Anticancer efficacy of Apo2L/TRAIL is retained in the presence of high and biologically active concentrations of osteoprotegerin in vivo. *J. Bone Miner. Res.* 26, 630–643.